ENAMEL RESEARCH: MECHANISMS AND CHARACTERIZATION

EDITED BY: Bernhard Ganss and Megan K. Pugach
PUBLISHED IN: Frontiers in Physiology

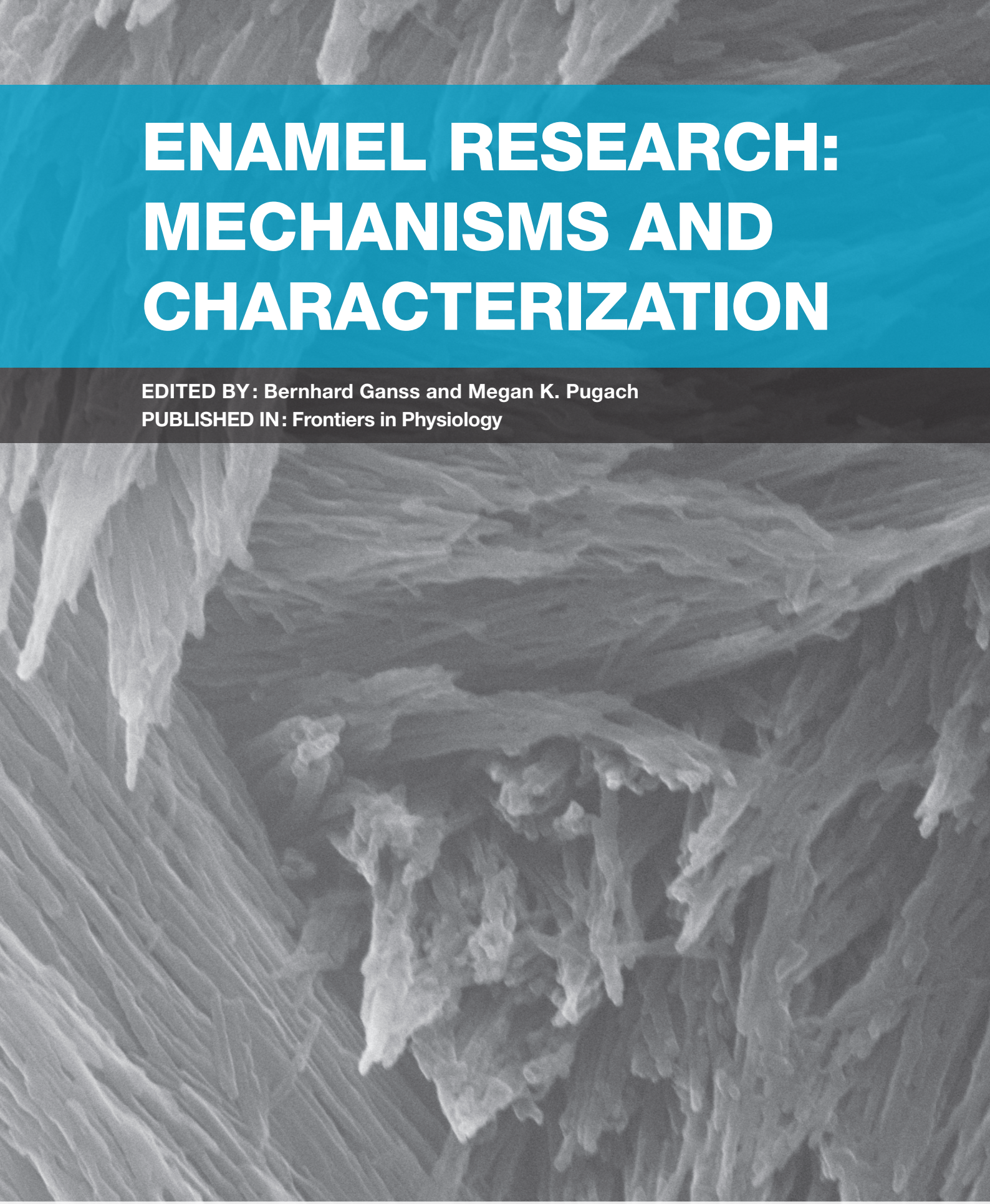

frontiers Research Topics

frontiers

ISSN 1664-8714
ISBN 978-2-88945-019-0
DOI 10.3389/978-2-88945-019-0

About Frontiers

Frontiers is more than just an open-access publisher of scholarly articles: it is a pioneering approach to the world of academia, radically improving the way scholarly research is managed. The grand vision of Frontiers is a world where all people have an equal opportunity to seek, share and generate knowledge. Frontiers provides immediate and permanent online open access to all its publications, but this alone is not enough to realize our grand goals.

Frontiers Journal Series

The Frontiers Journal Series is a multi-tier and interdisciplinary set of open-access, online journals, promising a paradigm shift from the current review, selection and dissemination processes in academic publishing. All Frontiers journals are driven by researchers for researchers; therefore, they constitute a service to the scholarly community. At the same time, the Frontiers Journal Series operates on a revolutionary invention, the tiered publishing system, initially addressing specific communities of scholars, and gradually climbing up to broader public understanding, thus serving the interests of the lay society, too.

Dedication to Quality

Each Frontiers article is a landmark of the highest quality, thanks to genuinely collaborative interactions between authors and review editors, who include some of the world's best academicians. Research must be certified by peers before entering a stream of knowledge that may eventually reach the public - and shape society; therefore, Frontiers only applies the most rigorous and unbiased reviews.
Frontiers revolutionizes research publishing by freely delivering the most outstanding research, evaluated with no bias from both the academic and social point of view.
By applying the most advanced information technologies, Frontiers is catapulting scholarly publishing into a new generation.

What are Frontiers Research Topics?

Frontiers Research Topics are very popular trademarks of the Frontiers Journals Series: they are collections of at least ten articles, all centered on a particular subject. With their unique mix of varied contributions from Original Research to Review Articles, Frontiers Research Topics unify the most influential researchers, the latest key findings and historical advances in a hot research area! Find out more on how to host your own Frontiers Research Topic or contribute to one as an author by contacting the Frontiers Editorial Office: **researchtopics@frontiersin.org**

ENAMEL RESEARCH: MECHANISMS AND CHARACTERIZATION

Topic Editors:
Bernhard Ganss, University of Toronto, Canada
Megan K. Pugach, The Forsyth Institute, USA

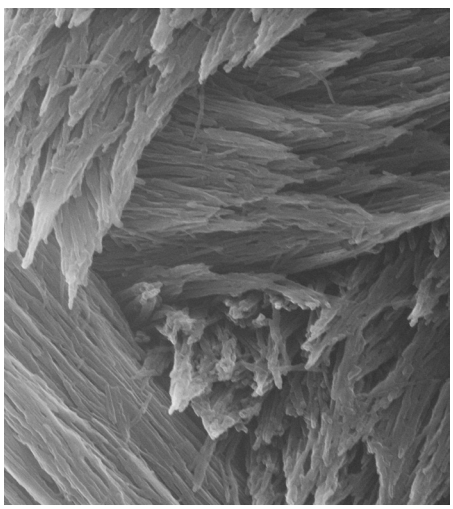

Tooth enamel crystallites are organized into bundles and arranged to minimize crack propagation. The sample is mature enamel from a mouse incisor, embedded, cut in parasagittal plane, polished, etched, and imaged without coating. Field of view 3µm. Image taken on a Zeiss Orion™ Helium Ion microscope, Peabody, MA.
Image courtesy of Felicitas Bidlack, PhD, Forsyth Institute, Cambridge, MA.
Image taken from: Bidlack FB, Huynh C, Marshman J and Goetze B (2014) Helium ion microscopy of enamel crystallites and extracellular tooth enamel matrix. Front. Physiol. 5:395.
doi: 10.3389/fphys.2014.00395

The rodent incisor is a good model system to study the molecular and cellular events that are involved in enamel biomineralization. Incisors in rodents continuously erupt during their lifespan, thus allowing the study of all stages of enamel synthesis, deposition, mineralization and maturation in the same tissue section. This model system has provided invaluable insight into the specifics of enamel formation as a basis to understand human pathologies such as amelogenesis imperfect. Furthermore, the rodent incisor allows exploration and understanding of some of the most fundamental mechanisms that govern biomineralization. Enamel is the most mineralized, hardest tissue in the body. It is formed within a unique organic matrix that, unlike other hard tissues such as bone and dentin, does not contain collagen. The formation

of enamel can be divided into two main stages: the secretory and maturation stage. During the secretory stage, a highly ordered arrangement of hydroxyapatite crystals is formed under the influence of structural matrix proteins such as amelogenin, ameloblastin and enamelin. During the maturation stage, the organic matrix is removed and hydroxyapatite crystals expand to ultimately yield a functional hard structure consisting of over 96% mineral. Research efforts over the past decades have mainly focused on the secretory stage, providing novel insights into the concept of biomineralization. However, the events that occur during the maturation stage have not been yet explored in detail, likely because the physiological roles of the enamel-forming ameloblasts are more diverse and complex at this stage. Mature ameloblasts are involved in the regulation of calcium transport in large amounts, phosphate and protein fragments in and out of the maturing enamel and provide regulatory mechanisms for the control of the pH. In recent years, increased efforts have been dedicated towards defining the molecular events during enamel maturation. The development of an ever-increasing number of transgenic animal models has clearly demonstrated the essential roles of matrix and non-matrix proteins during enamel formation. Multiple traditional and modern analytical techniques are applied for the characterization of enamel in these animals. The need for this Research Topic therefore stems from new information that has been generated on molecular events during the enamel maturation stage and the development and application of highly advanced analytical techniques to characterize dental enamel. The benefits and limitations of these techniques need to be reviewed and their application standardized for valid comparative studies.

Citation: Ganss, B., Pugach, M. K., eds. (2016). Enamel Research: Mechanisms and Characterization. Lausanne: Frontiers Media. doi: 10.3389/978-2-88945-019-0

Table of Contents

Section 3: Methodological Advances in Enamel Analyses and Translation

frontiers in Physiology

EDITORIAL
published: 09 September 2016
doi: 10.3389/fphys.2016.00374

Editorial: Enamel Research: Mechanisms and Characterization

Bernhard Ganss[1*†] *and Megan Pugach-Gordon*[2†]

[1] *Mineralized Tissue Lab, Dentistry - Matrix Dynamics Group, University of Toronto, Toronto, ON, Canada,* [2] *Department of Mineralized Tissue Biology, The Forsyth Institute, Harvard School of Dental Medicine, Cambridge, MA, USA*

Keywords: enamel maturation, physiology, mineralized tissue, amelogenin, structural biology

The Editorial on the Research Topic

Enamel Research: Mechanisms and Characterization

The idea to compile the present collection of articles on the topic on dental enamel formation and maturation was born in the course of a discussion over a glass of wine during the 11th International Conference on the Chemistry and Biology of Mineralized Tissues (ICCBMT) in Lake Geneva, Wisconsin in November 2013. Both of us felt that several issues specific to the mineralization of enamel deserved further exploration, and thus motivated, we approached the supportive editorial team at Frontiers. Over the course of the coming months a total of 15 scientists with a passion for enamel agreed to contribute to what is now compiled as an e-book. Although it may seem a long time since its conception, this publication addresses some very important and contemporary aspects of enamel biology and comes as a timely prelude to the upcoming Conferences, *Enamel 9* in Harrogate (UK) in October/November 2016 and the 12th *ICCBMT* in May/June 2017 in Potsdam (Germany).

A number of prominent enamel researchers have made this e-book what it is today. We have somewhat arbitrarily grouped all contributions into three parts. The first part describes and discusses general concepts and limitations of current approaches to understanding enamel biology. Robinson's Introduction provides an excellent historical review of multiple events occurring during the enamel maturation stage and their relationships to enamel dysplasias, while the article by Ganss and Abbarin highlights the role of recently identified proteins beyond the enamel maturation stage. Pugach and Gibson address the benefits and limitations of mouse models to study enamel development, and Goldberg et al. stress the importance of comparative studies between mouse molars and incisors to appreciate the full complexity of enamel development. Sarkar et al. draw comparative conclusions between two of the very few available ameloblast-like cell lines. Babajko et al. describe the role of the transcription factor MSX2 in ameloblasts and highlight its functional analogies with other mineralized tissues.

The second part focuses on individual aspects of enamel proteins and their processing during the formation and mineralization of enamel. The role of specific regions within the most prominent enamel protein, amelogenin, is discussed in two different articles, by Lu et al., as well as Gopinathan et al.. Both relate to hydroxyapatite binding properties and the control of biomineralization. Mazumder et al. discuss the functional relevance of interactions between ameloblastin and amelogenin for enamel mineralization. Margolis et al. highlight the role and importance of mineralization inhibitors in enamel formation and maturation. The next two articles, authored by Zhu et al., as well as Bartlett and Simmer, highlight the roles of MMP20 and particularly KLK4 as amelogenin-processing enzymes *in vitro* and *in vivo*.

Edited by:
Thimios Mitsiadis, University of Zurich, Switzerland

Reviewed by:
Pierfrancesco Pagella, University of Zurich, Switzerland
Giovanna Orsini, Marche Polytechnic University, Italy

****Correspondence:***
Bernhard Ganss
b.ganss@utoronto.ca

† These authors have contributed equally to this work.

Specialty section:
This article was submitted to Craniofacial Biology, a section of the journal Frontiers in Physiology

Received: *31 May 2016*
Accepted: *12 August 2016*
Published: *09 September 2016*

Citation:
Ganss B and Pugach-Gordon M (2016) Editorial: Enamel Research: Mechanisms and Characterization. Front. Physiol. 7:374. doi: 10.3389/fphys.2016.00374

The third part focuses on recent methodological advances in the analysis of the enamel structure at the nanoscale. Gordon and Joester describe the distribution of magnesium, carbonate and organic material within mature enamel and its possible functional significance, while Bidlack et al. present the use of helium ion microscopy to delineate the three-dimensional organization of enamel mineral and organic matrix. Last, but certainly not least, the article by Lelli et al. provides a translational perspective on toothpaste additives geared toward remineralizing enamel.

This e-book will be most beneficial for researchers in the area of biomineralization, emphasizing biological concepts, technical developments and some remaining controversies. Altogether we believe that this collage of articles focusing on enamel highlights some of the current perspectives, advances, and challenges in this fascinating research area on an extraordinary natural bioceramic material that keeps us all captivated. It is our hope that this publication will contribute to perpetuating this fascination with enamel in students at all levels of education and in various disciplines.

Our special thanks go to all our contributors who have willingly agreed to take on the extra work for this e-book. We also thank the entire editorial team at the Frontiers office who have patiently guided us along the way.

AUTHOR CONTRIBUTIONS

All authors listed, have made substantial, direct and intellectual contribution to the work, and approved it for publication.

FUNDING

Canadian Institutes of Health Research (CIHR) Grant MOP-119310 National Science and Engineering Research Council (NSERC) of Canada Grant RGPIN403292-11.

Conflict of Interest Statement: The authors declare that the research was conducted in the absence of any commercial or financial relationships that could be construed as a potential conflict of interest.

frontiers in
PHYSIOLOGY

REVIEW ARTICLE
published: 08 October 2014
doi: 10.3389/fphys.2014.00388

Enamel maturation: a brief background with implications for some enamel dysplasias

Colin Robinson*

Department of Oral Biology, The Dental Institute, University of Leeds, Leeds, UK

Edited by:
Bernhard Ganss, University of Toronto, Canada

Reviewed by:
Giovanna Orsini, Polytechnic University of Marche, Italy
Carolyn Gibson, University of Pennsylvania, USA

****Correspondence:***
Colin Robinson, Department of Oral Biology, The Dental Institute, University of Leeds, Clarendon Way, Leeds, LS2 9LU, UK
e-mail: c.robinson@leeds.ac.uk

The maturation stage of enamel development begins once the final tissue thickness has been laid down. Maturation includes an initial transitional pre-stage during which morphology and function of the enamel organ cells change. When this is complete, maturation proper begins. Fully functional maturation stage cells are concerned with final proteolytic degradation and removal of secretory matrix components which are replaced by tissue fluid. Crystals, initiated during the secretory stage, then grow replacing the tissue fluid. Crystals grow in both width and thickness until crystals abut each other occupying most of the tissue volume i.e. full maturation. If this is not complete at eruption, a further post eruptive maturation can occur via mineral ions from the saliva. During maturation calcium and phosphate enter the tissue to facilitate crystal growth. Whether transport is entirely active or not is unclear. Ion transport is also not unidirectional and phosphate, for example, can diffuse out again especially during transition and early maturation. Fluoride and magnesium, selectively taken up at this stage can also diffuse both in an out of the tissue. Crystal growth can be compromised by excessive fluoride and by ingress of other exogenous molecules such as albumin and tetracycline. This may be exacerbated by the relatively long duration of this stage, 10 days or so in a rat incisor and up to several years in human teeth rendering this stage particularly vulnerable to ingress of foreign materials, incompletely mature enamel being the result.

Keywords: enamel maturation, matrix protein loss, Porosity, uptake of foreign materials, enamel dysplasias

DEFINITION OF MATURATION STAGE

There is a very extensive literature on enamel development. With regard to the maturation stage there is a considerable amount of contemporary work dealing with cell physiology of the enamel organ and the molecular biology of the enamel matrix, but less so with the chemistry of the tissue. The following is intended to provide a brief basic background for this developmental stage with particular focus on tissue chemistry.

Enamel development has been divided into a series of consecutive stages based on tissue structure, histology of adjacent enamel organ cells and enamel chemistry (Warshawsky et al., 1981; Boyde, 1989; Robinson et al., 1995; Smith and Nanci, 1995).

Two stages can be most easily discerned. These are the secretory stage and the maturation stage. The secretory stage essentially entails the secretion of matrix and the initial mineral phase and can be considered complete when full thickness of the tissue has been laid down (Skobe, 1976).

This is followed by a maturation stage during which final matrix removal occurs and final mineral content is acquired. Final mineralization is probably completed post eruption, a phase not mediated by cells of the enamel organ (Robinson et al., 1997; Smith, 1998).

Between secretion and maturation there is a so called transition stage (Warshawsky and Smith, 1974; Robinson et al., 1981a). Since this appears to occur at or after major amelogenin secretion, it is included here essentially as an early phase of maturation. Many changes characteristic of maturation begin in transition and occur across the boundary between transition and maturation proper.

While these stages are fairly discrete, overlap with respect to certain functions does occur and will be mentioned where appropriate. While cellular, histological and chemical changes are similar in all species so far examined, the duration of this phase varies greatly from species to species.

HISTOLOGY OF THE ENAMEL ORGAN

After final enamel thickness has been achieved, enamel organ histology changes dramatically as the tissue moves into the transition stage (Warshawsky et al., 1981; Smith and Nanci, 1995).

TRANSITION

The transition stage involves reduction of the stratum intermedium to a single cell layer while fenestrated capillaries invade the enamel organ to approach the stratum intermedium layer (Garant and Gillespie, 2005).

The ameloblasts themselves, tall columnar cells about 70 μm in height reduce in height by about half. In addition, the long Tomes process through which the enamel secreted is reduced and is eventually lost (Reith, 1970). Internal structure of the ameloblasts also reorganizes. In brief, the nucleus takes up a more central position and the hitherto dense linearly arranged endoplasmic reticulum acquires a more disordered appearance.

A comparison of histology with the appearance and chemistry of adjacent enamel has indicated that ameloblast shortening is complete at the beginning of maturation proper (Robinson et al., 1981a).

MATURATION

Maturation ameloblasts, now about 50% shorter than secretory cells, develop a rhythmic cyclic change in the membrane structure facing the enamel, from a smooth to a ruffled border (Josephsen and Fejerskov, 1977; Sasaki, 1984). This modulates in such a way that waves of ruffled membrane sweep along the maturing enamel toward the mature tissue. Cell-cell contacts also modulate. Ruffled bordered cells connect via tight junctions at the enamel surface. After loss of the ruffled border the tight junction is also lost (Inai et al., 2008). The result of these changes is that, particularly at the junction between transition and maturation proper, there is relatively free diffusible access to the enamel surface passing between ruffle ended cells then laterally between smooth ended cells into the enamel (Takano and Ozawa, 1984). This access has considerable implications for the access of foreign materials such as fluoride (Weatherell et al., 1975, 1977) and plasma proteins (Strawich and Glimcher, 1989; Robinson et al., 1992) into the tissue (see below) (see also Hammarström, 1967).

These morphological alterations reflect dramatically changed ameloblast function once the full thickness of the tissue has been laid down.

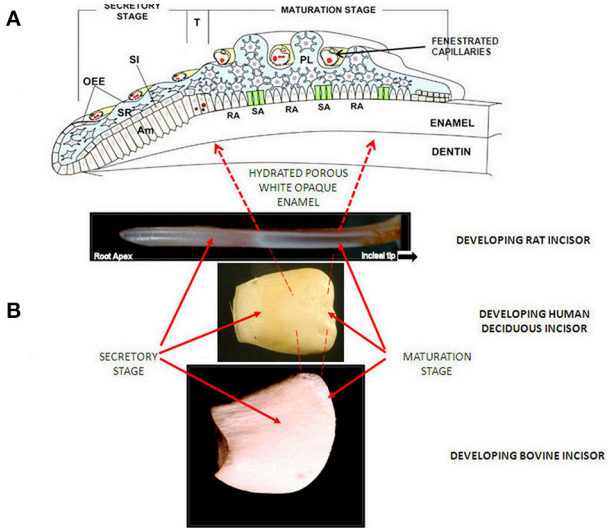

FIGURE 1 | (A) Diagram of enamel organ at each stage of development. OEE; Outer Enamel Epithelium, SI; Stratum Intermedium, SR; Stellate Reticululm, Am; ameloblasts. T; Transition Stage, RA; Ruffle Ended ameloblasts, SA; Smooth Ended ameloblasts, P; papillary layer. With permission, modified from: Josephsen et al. (2010). *Am. J. Physiol. Cell Physiol.* 1299–1307. **(B)** Images of developing incisors from rat, human and cow, showing appearance (after drying) and position of secretory and maturation sages.

CHEMISTRY OF ENAMEL

TRANSITION/MATURATION

During transition, secretion of partially mineralized matrix stops as the surface limit of the tissue is reached and the processes associated with final mineral uptake begin.

ORGANIC MATRIX

Primary amelogenin ceases to appear at this stage (Robinson et al., 1983; Nanci et al., 1998; Wakida et al., 1999), and the enamel no longer increases in thickness. It is presumed that other matrix components, ameloblastin, enamelin, follow the same pattern. While there is evidence that some structural matrix proteins continue to be secreted during maturation (Smith and Nanci, 1996) the amounts appear to be barely detectable and their function, if any at this stage, is unknown. More obviously dramatic loss of organic matrix becomes apparent at this stage with about half of the matrix removed half way through maturation (**Figure 3C**).

Importantly, matrix degradation products are replaced by fluid at transition/maturation (Hiller et al., 1975; Robinson et al., 1988) producing highly hydrated and porous tissue. After tooth extraction and some drying out, the porosity of the maturation stage is seen as a characteristic white opaque zone. (**Figures 1B**, **3A**).

Preceding matrix protein loss, proteolytic degradation occurs apparently following a two stage pattern. During secretion, an orchestrated degradation to specific components occurs via the enzyme MMP20, particularly of amelogenin (Brookes et al., 1995; Lu et al., 2008). During transition/maturation a second degradation phase begins mediated by the serine protease Kallikrein 4 (Lu et al., 2008). During this stage, the peptides produced by MMP20 are further degraded, much more completely. Kallikrein 4 activity initially appears at the end of the secretory stage but becomes most effective during transition and maturation. This results in the formation of small peptides and amino acids most of which disappear from the tissue (Brookes et al., 1995).

Small peptides and amino acids are presumably removed by the ameloblasts/enamel organ. Whether they diffuse out of the tissue or are removed actively is not clear. There is an argument that ruffle ended cells may carry out this function, because small organic molecules have been identified in ruffle ended cells. There is an intact basal lamina between these cells and the enamel so that any diffusion would be by lateral movement between smooth ended cells (Smith, 1998). Organic material remaining in maturing/mature tissue comprises an abundance of glycine and one or two tripetides (Glimcher et al., 1964; Weidmann and Hamm, 1965).

The amino acids and peptide fragments which remain are most likely bound to enamel crystals, for example, aspartate via anionic binding to crystals or glycine, the most dominant mature enamel species, which seems to fit into a spiral groove on apatite crystal surfaces (Montel et al., 1981). Some insoluble material (tuft protein) also appears to be retained at prism boundaries at greatest concentrations near the enamel-dentine junction. Recent studies suggest that this may be cross linked, possibly a protection of the enamel dentine junction from Kallikrein 4. Its origins remain obscure but may comprise residual enamel peptides which have become crosslinked (Robinson et al., 1975; Robinson and Hudson, 2011). Whether this crosslinking occurs specifically during maturation is not known.

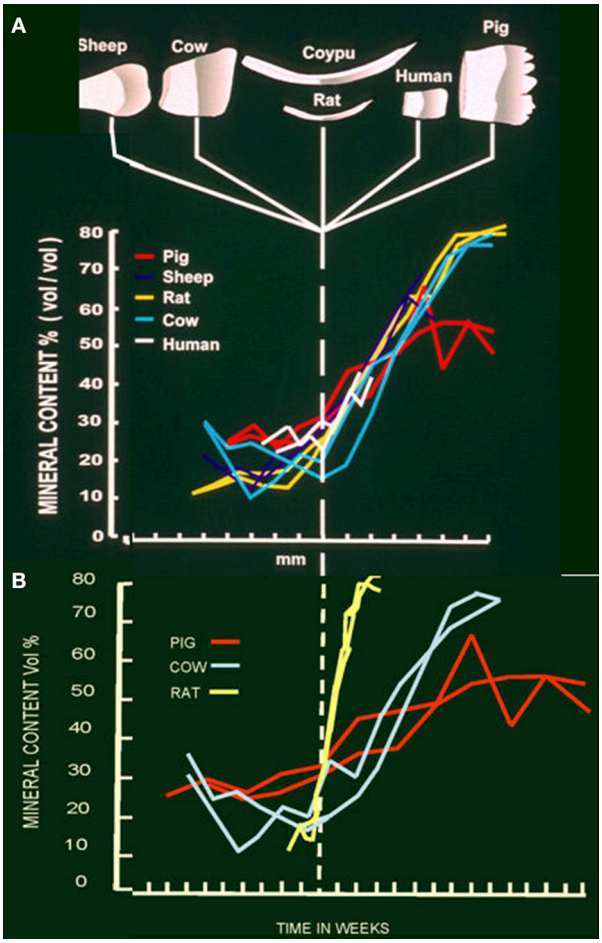

FIGURE 2 | (A) Mineral content at each stage of development in developing teeth of sheep, cow, coypu, rat, human and pig. Steep increase in mineral content can be seen at the beginning of the maturation stage in each species. **(B)** Mineral content of developing teeth from pig, cow and rat in relation to duration of each stage. Maximum mineral content is achieved in about 2 weeks in the rat, 10 weeks in the cow and a minimum of about 13 weeks in the pig.

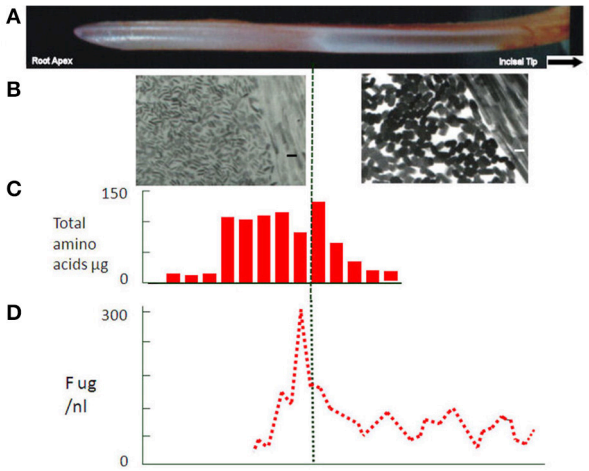

FIGURE 3 | (A) Rat incisor showing secretory and white opaque maturation stages. In rat, enamel. **(B)** Electron micrographs of apatite crystals at secretory and maturation stages in the rat incisor at the same magnification (size bars = 30 nm). Much larger, growing crystals (~30 nm in width) can be seen in the maturation stage tissue. **(C)** Protein expressed as total amino acid content at each developmental stage of the rat incisor. Dramatic fall in protein content can be seen in the maturation stage. **(D)** Fluoride content at each stage of development of rat incisor enamel. Peak concentrations can be seen across the boundary between transition and maturation stages. The peak indicates some loss of free fluoride during the maturation stage.

MINERAL UPTAKE AND CRYSTAL GROWTH

As we move into the maturation stage proper, mineral ion uptake i.e., calcium and phosphate, increases and crystal growth in width and thickness accelerates (**Figures 2A**, **3B**) (Nylen et al., 1963; Robinson et al., 1974; Hiller et al., 1975). This builds on some slower crystal growth in the enamel interior, which occurs during secretion.

Removal of matrix protein seems to be a prerequisite for crystal growth (Robinson et al., 1995) presumably, providing access of mineral ions to the growing crystals. Initial removal of proteins in interior, i.e., first formed, enamel would result in maturation growth accelerating from inside to outside. This would prevent sealing of the surface by rapid growth of surface crystals as ions enter from the ameloblast layer and probably reflects the sequence of protein removal from crystal surfaces.

Increase in crystal volume gradually displaces the fluid which had replaced the organic matrix and the tissue becomes much less hydrated, less porous and harder. The outer edge is the last part of the tissue to mature often erupting before completing leaving a white porous surface.

ROUTE OF MINERAL IONS

Mineral access to the enamel is extremely rapid (Robinson et al., 1974) and there has been considerable discussion as to whether this is an entirely active process. Recently evidence has been presented for specific ion transporters in the ameloblast membrane (Josephsen et al., 2010). The extent to which these are responsible for crystal growth is not yet determined. Active transport into the tissue may occur, regulating the access of ions and to some extent controlling the rate of crystal growth i.e., maturation. The simplest route, however, would be diffusion into the maturing tissue down a concentration gradient generated by growing crystals. Both mechanisms are not mutually exclusive.

pH AND MATURATION

There is an apparent drop in pH during maturation from about 7 to 6.5 (Sasaki, 1991). This has been attributed to growth of apatite crystals which would remove hydroxyl ions from the immediate environment. This prompted the suggestion that carbonic anhydrase, present during maturation in ruffle bordered cells, was needed to buffer the increasing amounts of acid produced as crystals grew (Smith et al., 2006). Since the pH does in fact fall, buffering is not complete. Alternatively, the duration of maturation, i.e., 2 weeks for the rat incisor, months in the cow and years in human teeth (**Figure 2B**) would seem to provide sufficient time for protons to diffuse out of the enamel and/or other buffers to

diffuse in, phosphate, for example, is freely exchangeable with the circulation (Robinson et al., 1974) at this stage.

Since the pH drop has been specifically associated with ruffle ended ameloblasts, an alternative view is possible. It may be that protons are pumped into the enamel at this stage (Damkier et al., 2014) in order to generate a relatively low pH. The resulting protonation of crystal surfaces (Robinson et al., 2006) and perhaps residual peptides may facilitate removal of peptides from crystals thus promoting crystal growth. On the other hand such protonation could be a direct means of controlling the rate of crystal growth.

UPTAKE OF EXTRANEOUS MATERIALS WITH IMPLICATIONS FOR ENAMEL DYSPLASIAS

It is clear that not only are calcium and phosphate taken up by the enamel during maturation but uptake of other materials also occurs. This is most likely facilitated by the high porosity and levels of hydration. Also penetration between ruffle ended ameloblast and lateral diffusion around smooth ended ameloblasts can occur. The close proximity of fenestrated capillaries to the stratum intermedium will in addition facilitate access to the circulation.

PHOSPHATE

This access was indicated by investigations using radioactive phosphate. Radioactive phosphate ions entered the enamel very shortly after injection. Two peaks of uptake were observed, one in early maturation which persisted and was presumably related to crystal growth. A second peak at the transition/maturation junction decreased, over a period of about 10 min probably reflecting blood levels of radioactive phosphate ions. It is presumed that this radioactive phosphate diffused out of the enamel as blood levels decreased (Robinson et al., 1974). This indicated that ions and possibly other materials could diffuse into and out of the enamel across the transition/maturation junction. A number of other components appear to behave in this way.

MAGNESIUM

Magnesium concentrations also show some indication of selective uptake at transition/early maturation followed by a loss. It is not clear what effect this may have, but magnesium can inhibit crystal growth, is often associated with fluoride (see below) and may affect enzyme activity (Hiller et al., 1975; Robinson et al., 1984).

FLUORIDE

Selective fluoride uptake at this stage is of particular interest because of its effect on ameloblasts, enamel structure and dental caries. A peak of fluoride can be seen in transition and early maturation (Weatherell et al., 1975, 1977) (**Figure 3D**). Some of this fluoride is incorporated into the growing crystals but a substantial amount is clearly free and can, like phosphate, diffuse back out of the enamel. This free fluoride ion has become an important aspect of the development of fluorosis. Fluoride has been shown to affect F actin assembly in ameloblasts (Li et al., 2005). This is the likely explanation for the effect of fluoride on the modulation between ruffled and smooth ended maturation ameloblasts (denBesten et al., 1985) with a consequent effect on enamel maturation. Changes in the exposure time to ameloblasts providing calcium and phosphate or removing protein could lead to delayed crystal growth generating the porous immature appearance of fluorotic tissue.

With regard to fluoride incorporation into crystals at this stage, elevated fluoride can inhibit crystal growth by lowering surface energy. In addition, fluoride renders it more difficult to protonate (Robinson et al., 2006) the crystal surface possibly affecting removal of protective protein also affecting crystal growth rate.

CARBONATE

Interestingly, carbonate, high in the mineral during early development, does not increase during early maturation suggesting that it is likely a reflection of local metabolic CO_2 production rather than serum bicarbonate. The high carbonate in the interior of mature enamel may, however, reflect the composition of the earliest formed mineral (Hiller et al., 1975) and the gradient of carbonate concentration seen in mature tissue (Weatherell et al., 1968). A similar argument can be made for the magnesium gradient in mature enamel (Robinson et al., 1981b).

ALBUMIN

Other materials can also be incorporated into the tissue at this stage. Of particular interest is albumin. Albumin at low levels has been reported to occur in secretory and especially maturing enamel (Strawich and Glimcher, 1989; Robinson et al., 1992). The latter may be due to the permeability of the ameloblast layer at this stage and the close proximity of fenestrated capillaries (Garant and Gillespie, 2005) as well as the porous nature of the enamel (**Figure 1A**). While this has been attributed by some to serum contamination, sufficient evidence exists that some albumin is present and in fact shows evidence of degradation due to enamel enzymes. One property of albumin pertinent to maturation is its ability to inhibit crystal growth (Garnett and Dieppe, 1990). This raised the possibility that leakage of albumin into maturing enamel, where crystals no longer are protected by endogenous matrix proteins, causes delayed maturation.

This may explain some types of idiopathic hypomaturation (white opaque hypoplasia) associated with, for example, physical trauma to the developing enamel (Tarján et al., 2002) or with some diseases of childhood. Under these circumstances hyperaemia can occur leading to leakage of albumin (and possibly other serum proteins) on to the growing crystals. Detection of albumin in such lesions has supported this view, for example, Kirkham et al. (2000).

TETRACYCLINE

The absence of defined lines in enamel after injection of tetracycline and its location at transition/maturation reflects the diffusion of tetracycline throughout the porous enamel of the early maturation stage (Hammarström, 1967). Uptake presumably occurs via the permeable ameloblast layer. This offers an explanation for tetracycline staining throughout enamel of children taking the antibiotic during the period of tooth development particularly maturation

SUMMARY

The maturation stage of enamel development comprises a secondary stage of mineral deposition during which apatite crystals, stage grow in width and thickness to replace fluid which had replaced the degraded protein matrix. The timescale for the maturation process is hugely variable dependent on species, from 2 weeks to several years. 90–95% of the tissue volume is finally occupied by apatite crystals. As a result of changes in the enamel organ and the porosity of maturing enamel extraneous materials can enter the tissue at this stage. Depending on the materials themselves and the duration of exposure, this can lead to delayed maturation and the eruption of white opaque dysplastic tissue. Enamel maturation is not only an important stage with regard to tissue development but also a very sensitive one in terms of hypomineralised enamel dysplasias.

REFERENCES

Boyde, A. (1989). "Enamel," in *Handbook of Microscopic Anatomy*, Vol. V/6: Teeth, eds A. Oksche and L. Vollrath (Berlin: Springer-Verlag), 309–473.

Brookes, S. J., Robinson, C., Kirkham, J., and Bonass, W. A. (1995). Biochemistry and molecular biology of amelogenin proteins of developing dental enamel. *Arch. Oral Biol.* 40, 1–14.

Damkier, H. H., Josephsen, K., Takano, Y., Zahn, D., Fejerskov, O., and Frische, S. (2014). Fluctuations in surface pH of maturing rat incisor enamel are a result of cycles of H+-secretion by ameloblasts and variations in enamel buffer characteristics. *Bone* 60, 227–234. doi: 10.1016/j.bone.2013.12.018

Garant, P. R., and Gillespie, R. (2005). The presence of fenestrated capillaries in the papillary layer of the enamel organ. *Anat. Rec.* 163, 71–79. doi: 10.1002/ar.1091630109

Garnett, J., and Dieppe, P. (1990). The effects of serum and human albumin on calcium hydroxyapatite crystal growth. *Biochem. J.* 266, 863–868.

Glimcher, M. J., Friberg, U. A., and Levine, P. T. (1964). The isolation and amino acid composition of the enamel proteins of erupted bovine teeth. *Biochem. J.* 93, 202.

Hammarström, L. (1967). Different localization of tetracycline and simultaneously injected radiocalcium in developing enamel. *Calcif. Tissue Res.* 1, 229–242.

Hiller, C. R., Robinson, C., and Weatherell, J. A. (1975). Variations in the composition of developing rat incisor enamel. *Calcif. Tissue Res.* 18, 1–12.

Inai, T., Sengoku, A., Hirose, E., Iida, H., and Shibata, Y. (2008). Differential expression of the tight junction proteins, claudin-1, claudin-4, occludin, ZO-1, and PAR3, in the ameloblasts of rat upper incisors. *Anat. Rec.* 5, 577–585. doi: 10.1002/ar.20683

Josephsen, K., and Fejerskov, O. (1977). Ameloblast modulation in the maturation zone of the rat incisor enamel organ a light and electron microscopic study. *J. Anat.* 12, 45–70.

Josephsen, K., Takano, Y., Frische, S., Praetorius, J., Nielsen, S., Aoba, T., et al. (2010). Ion transporters in secretory and cyclically modulating ameloblasts: a new hypothesis for cellular control of preeruptive enamel maturation. *Am. J. Physiol. Cell Physiol.* 229, 1299–1307. doi: 10.1152/ajpcell.00218.2010

Kirkham, J., Robinson, C., Strafford, S. M., Shore, R. C., Bonass, W. A., Brookes, S. J., et al. (2000). The chemical composition of tooth enamel in junctional epidermolysis bullosa. *Arch Oral Biol.* 45, 377–386. doi: 10.1016/S0003-9969(00)00003-0

Li, Y., Decker, S., Yuan, Z. A., Denbesten, P. K., Aragon, M. A., Jordan-Sciutto, K., et al. (2005). Effects of sodium fluoride on the actin cytoskeleton of murine ameloblasts. *Arch. Oral Biol.* 50, 681–688. doi: 10.1016/j.archoralbio.2004.11.021

Lu, Y., Papagerakis, P., Yamakoshi, Y., Hu, J. C.-C., Bartlett, J. D., and Simmer, J. P. (2008). Functions of KLK4 and MMP-20 in dental enamel formation. *Biol. Chem.* 389, 695–700. doi: 10.1515/BC.2008.080

Montel, G., Bonel, G., Heughebaert, J. C., Trombe, J. C., and Rey, C. (1981). New concepts in the composition, crystallisation and growth of the mineral component of calcified tissues. *J. Cryst. Growth* 53, 74–99.

Nanci, A., Zalzal, S., Lavoie, P., Kunikata, M., Chen, W., Krebsbach, P. H., et al. (1998). Comparative immunochemical analyses of the developmental expression and distribution of ameloblastin and amelogenin in rat incisors. *J. Histochem. Cytochem.* 46, 911–934.

Nylen, M. U., Eanes, E. D., and Omnell, K.-Å. (1963). Crystal growth in rat enamel. *J. Cell Biol.* 18, 109–123.

denBesten, P. K., Crenshaw, M. A., and Wilson, M. H. (1985). Changes in the fluoride-induced modulation of maturation stage ameloblasts of rats. *J. Dent. Res.* 64, 1365–1370.

Reith, E. J. (1970). The stages of amelogenesis as observed in molar teeth of young rats. *J. Ultrastruct. Res.* 30, 111–151.

Robinson, C., Atkinson, P. J., and Briggs, H. D. (1981a). Histology of enamel organ and chemical composition of adjacent enamel in rat incisors. *Calcif. Tissue Int.* 33, 513–520.

Robinson, C., Briggs, H. D., Kirkham, J., and Atkinson, P. J. (1983). Changes in the incisor enamel protein components of rat during tooth development. *Arch. Oral Biol.* 28, 993–1000.

Robinson, C., Brookes, S. J., Bonass, W. A., Shore, R. C., and Kirkham, J. (1997). Enamel maturation in dental enamel. *Ciba Found. Symp.* 205, 156–174.

Robinson, C., Hallsworth, A. S., and Kirkham, J. (1984). Distribution and uptake of magnesium by developing deciduous bovine incisor enamel. *Arch. Oral Biol.* 29, 479–482.

Robinson, C., Hiller, C. R., and Weatherell, J. A. (1974). Uptake of ^{32}P – labelled phosphate into developing rat incisor enamel. *Calcif. Tissue Res.* 15, 143–152.

Robinson, C., and Hudson, J. (2011). Tuft protein: protein cross–linking in enamel development. *Eur. J. Oral Sci.* 119, 50–54. doi: 10.1111/j.1600-0722.2011.00906.x

Robinson, C., Kirkham, J., Brookes, S. J., Bonass, W. A., and Shore, R. C. (1995). The chemistry of enamel development. *Int. J. Dev. Biol.* 39, 145–152.

Robinson, C., Kirkham, J., Brookes, S. J., and Shore, R. C. (1992). The role of albumin in developing rodent dental enamel: a possible explanation for white spot hypoplasia. *J. Dent Res.* 7, 1270–1274.

Robinson, C., Kirkham, J., and Hallsworth, A. S. (1988). Volume distribution and concentration of protein, mineral and water in developing bovine enamel. *Arch. Oral Biol.* 33, 159–162.

Robinson, C., Lowe, N. R., and Weatherell, J. A. (1975). Amino acid distribution and origin of "tuft" protein in human and bovine dental enamel. *Arch. Oral Biol.* 20, 29–42.

Robinson, C., Weatherell, J. A., and Hallsworth, A. S. (1981b). Distribution of magnesium in mature human enamel. *Caries Res.* 15, 70–77.

Robinson, C., Yamamoto, K., Connell, S. D., Kirkham, J., Nakagaki, H., and Smith, A. D. (2006). The effects of fluoride on the nanostructure and surface pK of enamel crystals. an atomic force microscopy study of human and rat enamel. *Eur. J. Oral Sci.* 114, 1–10. doi: 10.1111/j.1600-0722.2006.00275.x

Sasaki, S. (1991). Cyclical changes in pH in bovine developing enamel as sequential bands. *Arch. Oral Biol.* 36, 227–231.

Sasaki, T. (1984). Endocytotic pathways at the ruffled borders of rat maturation ameloblasts. *Histochemistry* 80, 263–268.

Skobe, Z. (1976). The secretory stage of amelogenesis in rat mandibular incisor teeth observed by scanning electron microscopy. *Calcif. Tissue Res.* 21, 83–103.

Smith, C. E. (1998). Cellular and chemical events during enamel maturation. *Crit. Rev. Oral Bio. Med.* 9, 128–161.

Smith, C. E., and Nanci, A. (1995). Overview of morphological changes in enamel organ cells associated with major events in amelogenesis. *Int. J. Dev. Biol.* 39, 153–161.

Smith, C. E., and Nanci, A. (1996). Protein dynamics of amelogenesis. *Anat. Rec.* 245, 186–207.

Smith, C. E., Nanci, A., and Moffatt, P. (2006). Evidence by signal peptide trap technology for the expression of carbonic anhydrase 6 in rat incisor enamel organs. *Eur. J. Oral Sci.* 114, Suppl. s1, 147–153. doi: 10.1111/j.1600-0722.2006.00273.x

Strawich, E., and Glimcher, M. J. (1989). Major "enamelin" protein in enamel of developing bovine teeth is albumin. *Connect. Tissue. Res.* 22, 111–121.

Takano, Y., and Ozawa, H. (1984). "Autoradiographic and tracer experiments on the exit route for the resorbed organic matrix of the enamel," in *Tooth Enamel* 4,

eds R. W. Fearnhead and S. Suga (Amsterdam: Elsevier; New York, NY: Oxford). 271–275.

Tarján, I. N., Rózsa, Y., Tanikawa, N., Wakamatsu, S., and Tanase, S. (2002). The influx of serum albumin to enamel matrix in rat incisors after trauma. *Calcif. Tissue Int.* 71, 349–355. doi: 10.1007/s00223-001-2121-8

Wakida, K., Amizuka, N., Murakami, C., Satoda, T., Fukae, M., Simmer, J. P., et al. (1999). Maturation ameloblasts of the porcine tooth germ do not express amelogenin. *Histochem. Cell Biol.* 111, 297–303.

Warshawsky, H., Josephsen, K., Thylstrup, A., and Fejerskov, O. (1981). The development of enamel structure in rat incisors as compared to the teeth of monkey and man. *Anat. Rec.* 4, 371–399.

Warshawsky, H., and Smith, C. E. (1974). Morphological classification of rat incisor ameloblasts. *Anat. Rec.* 179, 423–446.

Weatherell, J. A., Deutsch, D., Robinson, C., and Hallsworth, A. S. (1975). Fluoride concentrations in developing enamel. *Nature* 256, 230–232.

Weatherell, J. A., Deutsch, D., Robinson, C., and Hallsworth, A. S. (1977). Assimilation of fluoride by enamel throughout the life of the tooth. *Caries Res.* 11, 85–115.

Weatherell, J. A., Robinson, C., and Hiller, C. R. (1968). Distribution of carbonate in thin sections of dental enamel. *Caries Res.* 2, 1–9.

Weidmann, S. M., and Hamm, S. M. (1965). "Studies on the enamel matrix of mature teeth," in *Tooth Enamel*, eds M. V. Stack and R. W. Fearnhead (Bristol: John Wright and Sons Bristol), 83–90.

Conflict of Interest Statement: The author declares that the research was conducted in the absence of any commercial or financial relationships that could be construed as a potential conflict of interest.

Received: 11 June 2014; paper pending published: 02 July 2014; accepted: 19 September 2014; published online: 08 October 2014.

*Citation: Robinson C (2014) Enamel maturation: a brief background with implications for some enamel dysplasias. Front. Physiol. **5**:388. doi: 10.3389/fphys.2014.00388 This article was submitted to Craniofacial Biology, a section of the journal Frontiers in Physiology.*

frontiers in PHYSIOLOGY

HYPOTHESIS AND THEORY ARTICLE
published: 19 September 2014
doi: 10.3389/fphys.2014.00359

Comparative studies between mice molars and incisors are required to draw an overview of enamel structural complexity

***Michel Goldberg*[1,2]*, *O. Kellermann*[1,2], *S. Dimitrova-Nakov*[1,2], *Y. Harichane*[1,2] and *A. Baudry*[1,2]**

[1] *INSERM UMR-S 1124, Cellules Souches, Signalisation et Prions, Paris, France*
[2] *Université Paris Descartes, Sorbonne Paris Cité, UMR-S 1124, Paris, France*

Edited by:
Bernhard Ganss, University of Toronto, Canada

Reviewed by:
Amel Gritli-Linde, University of Gothenburg, Sweden
Ariane Berdal, UMRS 872 INSERM University Paris-Diderot, France

***Correspondence:**
Michel Goldberg, INSERM UMR-S 1124 & Université Paris Descartes, 45 rue des Saints Pères- 75270 Paris, Cedex 06, France
e-mail: michel.goldberg@parisdescartes.fr; mgoldod@gmail.com

In the field of dentistry, the murine incisor has long been considered as an outstanding model to study amelogenesis. However, it clearly appears that enamel from wild type mouse incisors and molars presents several structural differences. In incisor, exclusively radial enamel is observed. In molars, enamel displays a high level of complexity since the inner part is lamellar whereas the outer enamel shows radial and tangential structures. Recently, the serotonin 2B receptor (5-HT_{2B}R) was shown to be involved in ameloblast function and enamel mineralization. The incisors from $5HT_{2B}$R knockout (KO) mice exhibit mineralization defects mostly in the outer maturation zone and porous matrix network in the inner zone. In the molars, the mutation affects both secretory and maturation stages of amelogenesis since pronounced alterations concern overall enamel structures. Molars from $5HT_{2B}$R KO mice display reduction in enamel thickness, alterations of inner enamel architecture including defects in Hunter-Schreger Bands arrangements, and altered maturation of the outer radial enamel. Differences of enamel structure were also observed between incisor and molar from other KO mice depleted for genes encoding enamel extracellular matrix proteins. Thus, upon mutation, enamel analysis based exclusively on incisor defects would be biased. In view of the functional relationship between enamel structure and tooth morphogenesis, identification of molecular actors involved in amelogenesis requires comparative studies between mice molars and incisors.

Keywords: incisor, molar, serotonin receptor, Hunter-Schreger bands, maturation, gene deletion

INTRODUCTION

In humans, two renewals of the dentition through life occur corresponding to diphyodonty (Whitlock and Richman, 2013). Successive deciduous and permanent sets of teeth with limited growth are formed. The presence of tooth bud adjacent to the deciduous teeth allows building the permanent teeth. Thus, postnatal tooth formation occurs, implying that enamel organ participates to the crown formation of the nascent teeth. Although the mechanisms underlying enamel formation during embryogenesis have been partly elucidated (Laugel-Haushalter et al., 2013), almost nothing is known concerning the signals promoting enamel bud differentiation of the permanent teeth. The thickness and the mechanical properties of permanent vs, deciduous tooth differ indicating that the enamel mineralized microstructures built by ameloblasts depends on tooth identity. Conversely, monophyodont teeth corresponding to one single tooth generation characterizes rodents. Thus, the use of rodent models is dealing with deciduous teeth. We remind that in rodent, molars have limited growth whereas incisors are continuously growing teeth. The rodent represents an exception since ameloblasts do not disappear throughout life ensuring permanent formation of enamel on the labial surface of incisor.

Enamel covers dentin and dental pulp in the crown of the tooth. It is the hardest tissue in the body due to the high mineral content (96%) and a very little protein level (less than 1% organic material). The root is recovered by cementum that participates to the tooth attachment to bone. Dentin and dental pulp derive from neural crest while enamel originates from neuroectoderm. Enamel is the only epithelial derived calcified tissue in vertebrates. This avascular tissue is formed during tooth development by ameloblasts, which are lost after deciduous or permanent tooth eruption.

In mammals, enamel structures display different levels of complexity (Koenigswald and Clemens, 1992). The assembly of hydroxyapatite monocrystals along the so-called Burgers vectors and circuit leads to the formation of individual crystallites (Arends and Jongebloed, 1979). Bundles of crystallites are packed in rods or interrod enamel. Rods contribute to the three-dimensional organization of enamel, either as linear structures, or forming sophisticated spatial constructions characterized as Hunter-Schreger (HS) bands (Osborn, 1990; Risnes, 1990).

ENAMEL STRUCTURAL DIFFERENCES BETWEEN INCISORS AND MOLARS FROM WILD TYPE (WT) MOUSE

In rodent, three-dimensional arrangement of enamel types, named schmelzmuster, are well characterized. The C-type schmelzmuster of molar is related to a basal ring of lamellar enamel. This C-type is not present in the incisor. The P-type

corresponds to radial enamel found in the outer area of molars and predominant in the incisors. The S-type formed by thick HS bands is mostly identified in molars (Koenigswald, 2004).

In rats and mice, the occurrence of a large diastema between the incisor and molar is at the origin of the absence of canine and premolars. A stem cell niche associated with the basal lamina is present in molar and is very active in growing incisor. The absence of stem cells has been reported in diastema area (Lesot and Brook, 2009). The crown of rodent molar is protected by enamel while the root, as in human, is covered by cementum. Of note, in rodent incisor, the presence of enamel restricted to the labial side fulfills biomechanical requirement. The newly formed enamel slides in the bony socket. The lingual root-like part including both the cementum and alveolo-dental ligament (Steinfort et al., 1989) ensures the insertion of the continuous erupted incisor.

Most laboratories have worked on rodent incisor since they exploited the dynamics of enamel formation of the continuously growing incisor (Leblond and Warshawsky, 1979). The advantage of the incisor model is that all the spatio-temporal steps occurring during amelogenesis are clearly identified. Initiation of enamel formation is recognized in the apical zone called the zone of presecretion where polarized ameloblasts are facing the pulp. Then, dentin starts to be formed. Signals exchanges between odontoblasts and ameloblasts occur and epithelio-mesenchymal interactions ensure the differentiation of ameloblast in tooth secretory cells. Enamel extracellular matrix proteins are secreted forming a network for mineral deposition. Radial rods and interrod enamel are formed first in the inner enamel and then in the outer enamel concomitant with the backward migration of ameloblasts. Mineralization occurs at the border between the translucent zone and the chalky enamel, a zone where both hydroxyapatite deposition and crystal nucleation occur. The extensive mineralization of enamel involves the post-secretory step. Ameloblasts that are forming a thin layer of outer enamel secrete proteases such as the metalloprotease MMP20 and kallikrein 4 (KLK4) (Smith et al., 2011) which degrade the organic matrix and reduce ECM content from 20 to 0.4–0.6% (in weight). As mineral crystals grow most of the cleaved peptides are removed. This leads to final enamel maturation that spatially takes place prior eruption. In rodents, the grinding activity leads to incisor abrasion that is compensated by continuous tooth eruption. In the incisor, enamel displays a uniserial lamellar pattern of prisms in the inner enamel, whereas radial prisms are parallel in the outer enamel (Moinichen et al., 1996) (**Figure 1A**). Tightly packed bundles of crystallites form rods and interrod enamel (**Figure 1C**).

In rodents, the enamel of molar displays a multifaceted rod pattern with more variable structures than in the incisor. In the molar, four characteristics are noted: (1) decussation of rods observed in the inner third and absent in the upper ridges and in the bottom of grooves, (2) a feather-like rod organization

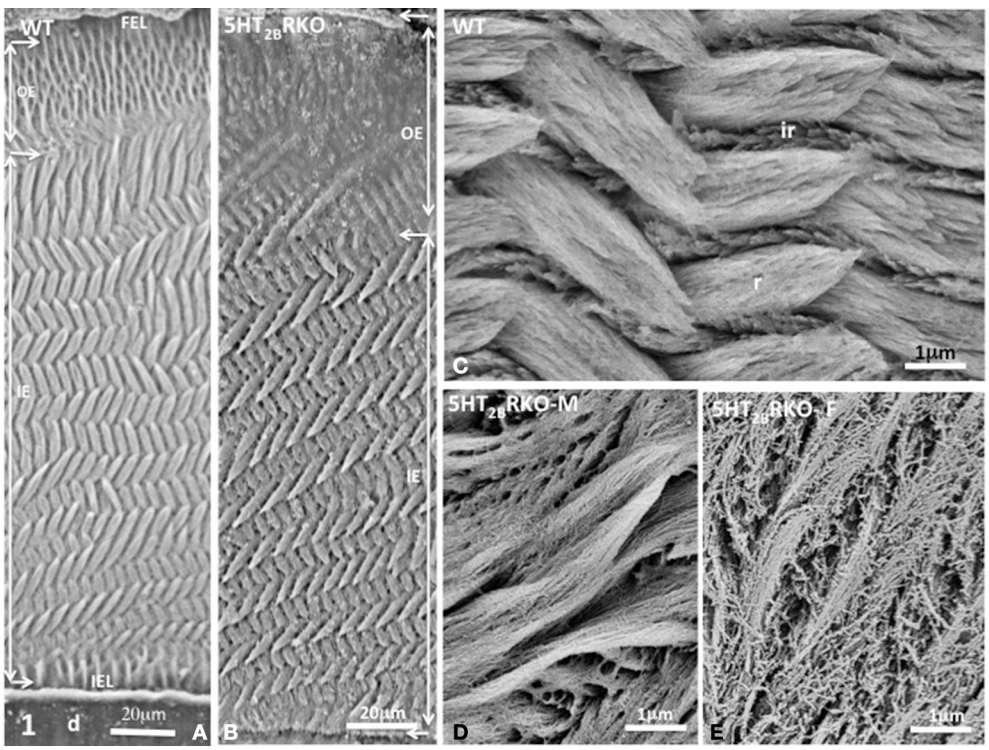

FIGURE 1 | (A) Transverse section of Wild Type (WT) incisor. D, dentin; IEL, inner enamel layer; IE, inner enamel; OE, outer enamel; FEL, final enamel layer. The lamellar pattern is mostly detectable in the inner enamel. **(B)** Transverse section of the incisor of $5HT_{2B}R$ KO mice. The outer enamel (OE) is more resistant to acid etching than the inner enamel (IE), suggesting residual accumulation of the extracellular matrix. **(C)** In the WT mouse, crystallites are tightly packed inside rods (r) or in interrod enamel (ir). **(D)** In the male mutant mouse ($5HT_{2B}R$ KO-M), porosities appear in rods and interrods where crystallites are less densely packed. **(E)** In the female KO ($5HT_{2B}R$ KO-F) the porous appearance is increased. Intercrystallite spaces are enlarged.

also forms lamellar enamel in the inner third (**Figure 2A**), (3) all rods seen in the outer enamel are radial [right angle to the surface (**Figures 2A,C**)] and/or exhibit the same oblique orientation tangential to enamel surface (**Figure 2C**) (Koenigswald and Clemens, 1992), (4) incremental lines with a regular periodicity constitute the superficial aprismatic enamel (Lyngstadaas et al., 1998). Enamel organization is strongly dependent on the zone investigated (Risnes, 1979). A strong link may be established between regional variations of enamel structure and the rod-interrod scaffold, which allows strain resistance (**Figures 2–4**). The predominant structure consists in several waves of rod decussation in the inner enamel and in rods which are radial in outer enamel (Lyngstadaas et al., 1998) (**Figure 2A**).

In addition, HS bands increase the architectural complexity. Two to three rods form a helix due to the cervical translocation of some of the rods in the transverse plane of the tooth (Osborn, 1990). HS bands result from anti-parallel orientation of diazones (dz) (transversely cut rods) and parazones (pz) (longitudinally cut rods) in the lamellar inner enamel (IE) (**Figure 2C**). Enamel architecture is based on the continuity of spirally arranged rows at least in the inner third of dental enamel (Hirota, 1982). The double-coiled helix tends to enlarge gradually the volume of enamel, leading to its thickening by helicoidal growth. HS bands represent a plywood structure that further enhances the axial compression strength below the cusp (**Figure 3A**). HS bands visualized in the lateral aspects of molar (**Figures 4A,B**) also contribute to lateral resistance. HS bands are undetectable in the outer enamel and instead paralleled radial rods are present in the deep part of occlusal groves (**Figures 3B,C**).

These differences in enamel organization between mice incisor and molars imply that the genetic intrinsic program governing ameloblast differentiation involves distinct mechanisms during embryogenesis (molar) vs. post-natal life (incisor). Generation of knockout mice displaying differential defects between incisors and molars may shed light on new actors implicated in amelogenesis.

DIFFERENTIAL STRUCTURAL ENAMEL ALTERATIONS BETWEEN INCISORS AND MOLARS IN 5HT$_{2B}$R KNOCKOUT MICE

Recently, the serotonin 2B receptor (5-HT$_{2B}$R) was shown to be involved in ameloblast function and enamel mineralization. We may remind that during embryogenesis, serotonin (5-HT) contributes to the differentiation of neuroectodermal, neural crest, and mesodermal derivatives (Moiseiwitsch and Lauder, 1995; Gaspar et al., 2003). In addition, 5-HT$_{2B}$R is present in the first branchial arch where tooth buds form (Choi et al., 1997; Lauder et al., 2000). In adult, this receptor controls tissue non-specific

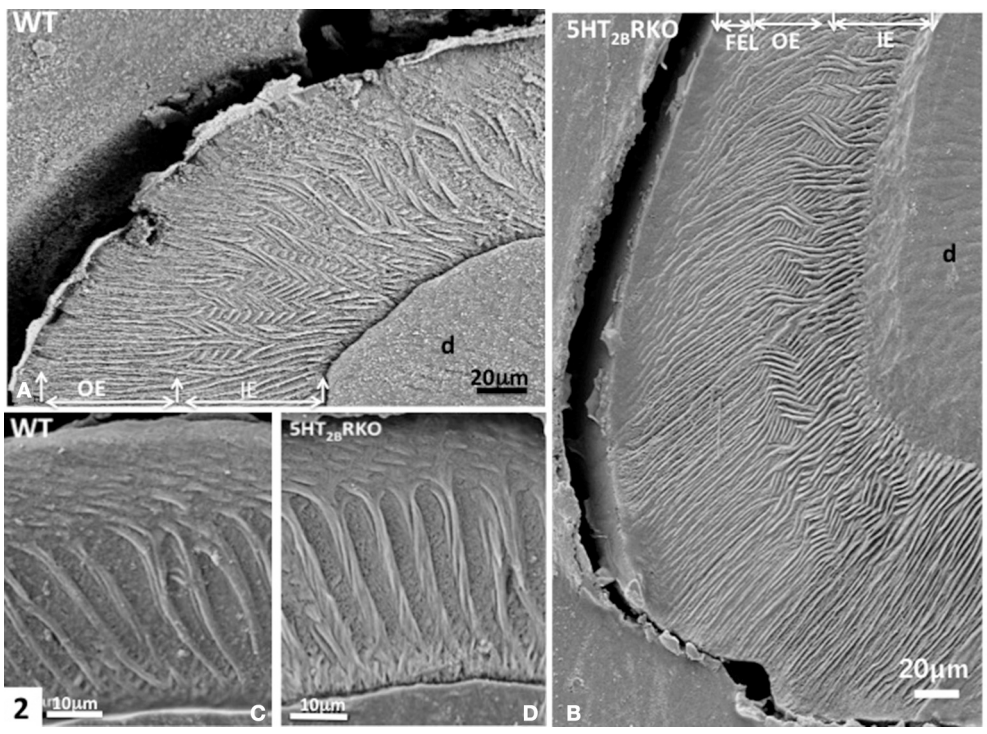

FIGURE 2 | (A) WT molar. In the inner enamel (IE), a feather-like structure is observed, whereas in the outer enamel (OE) radial rods are perpendicular to the enamel surface. D, dentin. **(B)** In the molar of 5HT$_{2B}$R KO mice, rod bending and decussation are seen in the inner enamel (IE), whereas in the outer enamel (OE) radial rods are parallel and perpendicular to the outer final enamel layer (FEL) The Hunter-Schreger Bands are barely detectable. **(C)** WT enamel molar. Hunter-Schreger bands are located in the inner enamel, whereas oblique and radial rods are mostly detected in the outer enamel. **(D)** In the 5HT$_{2B}$R KO mice, twisted and thicker rods contribute to the formation of Hunter-Schreger Bands, which are located in the inner enamel. Along the dentino-enamel junction a thin layer of aprismatic enamel is detected.

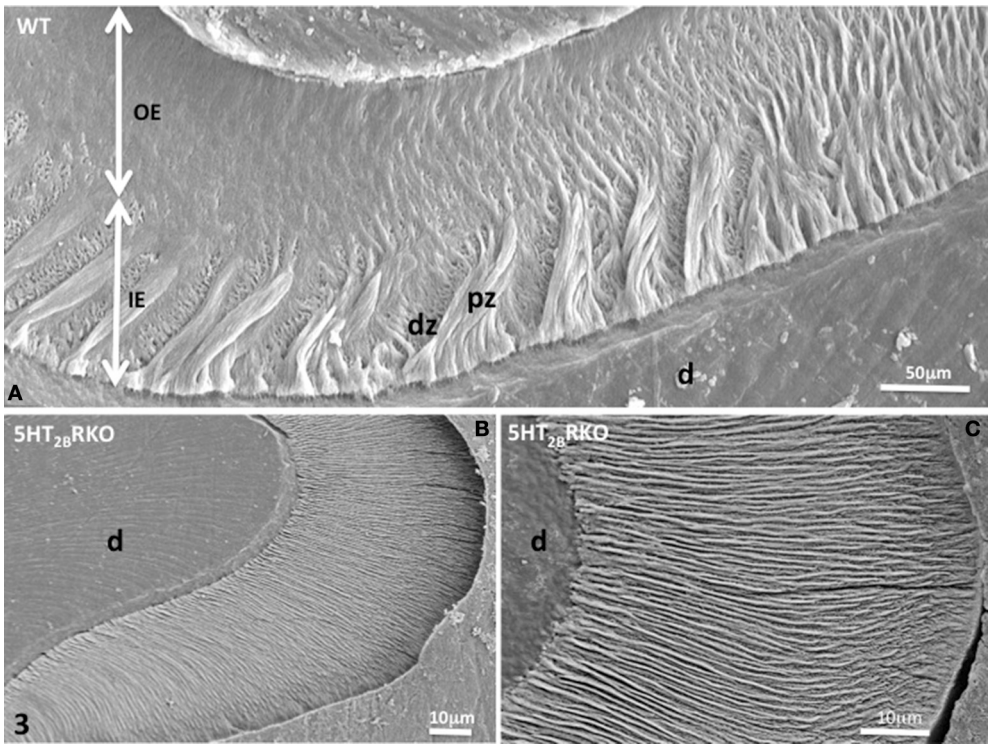

FIGURE 3 | (A) WT molar enamel. In a grove between two cusps, large diazones (dz) and parazones (pz) occupy the inner enamel (IE) near the dentino-enamel junction. Radial rods are located in the outer enamel (OE). **(B)** $5HT_{2B}R$ KO molar rod enamel is continuous and has a radial appearance. **(C)** Radial enamel at the tip of a cusp. d, dentin.

alkaline phosphatase (TNAP) activity (Baudry et al., 2010), and thereby bone mineralization (Collet et al., 2008). Inactivation of the $5HT_{2B}R$ [$5HT_{2B}R$ knockout (KO) mice] disturbs enamel formation (Harichane et al., 2011; Dimitrova-Nakov et al., 2014).

In $5HT_{2B}R$ KO incisor, the outer enamel (OE) is thicker than in WT and has an amorphous appearance (**Figure 1B**) revealing anomalies in post-secretory ameloblast functions. We used a 1.3% nitric acid treatment for three periods of 5 s (Risnes, 1990) that permits limited demineralization at the surface section thus allowing to still visualize mineral structures. The inner enamel (IE) of $5HT_{2B}R$ KO mice displays a series of decussation more accentuated than in WT with minor but significant changes in orientation of rods (r) and interrods (ir) (**Figures 1B,C**). At higher magnification, porosities are observed in the enamel structure of $5HT_{2B}R$ KO mice with a sexual dimorphism. In $5HT_{2B}R$ KO male, the crystallites are thinner and less densely packed (**Figure 1D**), whereas in $5HT_{2B}R$ KO female (**Figure 1E**), the porosities are more pronounced with unpacked crystallites, and swollen inter crystallites void spaces. Such sexual dimorphism was also noted for bone defects in $5HT_{2B}R$ KO mice (Collet et al., 2008).

In molar, $5HT_{2B}R$ depletion affects overall enamel structures. The thickness of enamel in $5HT_{2B}R$ KO mice is decreased possibly due to the observed defects of enamel organization/mineralization and/or the increase in occlusal surface abrasion in enamel-free areas. Interestingly, HS bands almost disappear in the upper part of the cusp. Conversely, HS bands are thicker in the proximal parts of the teeth involving the self-association of additional rods, exhibiting a twisted appearance (**Figures 4C,D**). Near the tip of the cusp, the feather-like structure normally formed by rods and inter-rods is no more observed. Instead, after a series of bendings in the inner enamel, rods and interrod enamel follow radial orientation in the outer enamel (**Figure 2B**). These results indicate that the absence of $5HT_{2B}R$ alters the withdrawal and the wavy route of secretory ameloblasts.

Near the crests of the cusps, closest to the enamel surface, the post-secretory functions of maturing ameloblasts contribute to the formation of a final enamel layer, which is aprismatic, and resulting from ECM re-internalization (**Figures 3B,C**, **4C,D**).

Nearby the top of the cusps, rods and interrod enamel follow radial direction, without noticeable difference between the inner and outer enamel (**Figures 3B,C**).

In the proximal enamel extending from the cervical zone to the top of the cusp, the inner enamel (IE) is formed alternatively by thick parazones and thinner diazones forming a plywood structure, a three-dimensional scaffold allowing better resistance to axial pressures excerpted on the crown (**Figures 4C,D**). The outer enamel is formed by parallel alignment of rods, and covered by a thin aprismatic outer layer (OE) (**Figures 4A,B**). A similar architecture of enamel structures is seen in matched areas of WT and $5HT_{2B}R$ KO molars, but at higher magnification the whole enamel appears to be more porous in absence of $5HT_{2B}R$ (**Figures 4C,D**).

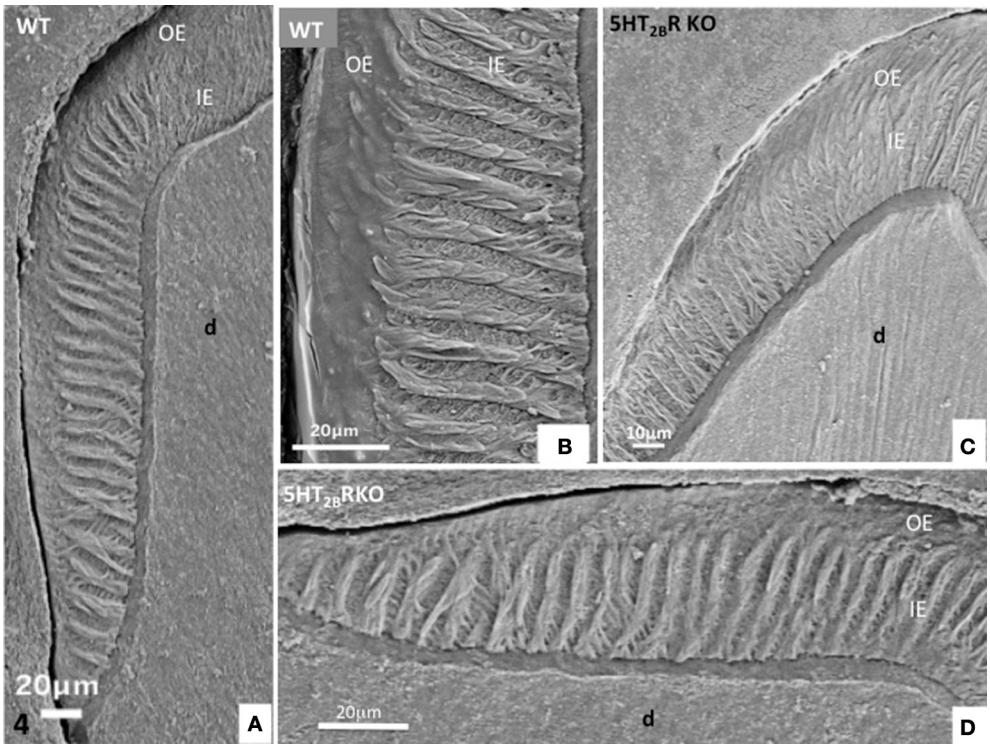

FIGURE 4 | (A,B) Lateral aspect of WT enamel molar. Hunter-Schreger bands occupy the inner enamel (IE) whereas the outer enamel (OE) displays an amorphous appearance. **(C,D)** In the molar of $5HT_{2B}R$ KO mice, alternatively diazones and parazones occupy two third of the inner enamel which looks more porous compared to WT.

LESSONS FROM INCISORS AND MOLARS STRUCTURAL ANALYSIS IN KNOCKOUT MOUSE MODELS

Mice KO for genes encoding proteins known to be present in enamel matrix all exhibit alterations in molar and incisor enamel as compared to WT. In the case of periostin, postnatal defects in incisors and molars predominantly concern dentin (enormous increase at 5 months). Minor alterations are observed in enamel probably resulting from impaired mechanical response (Ma et al., 2011). For ameloblastin and enamelin, enamel of incisor and molar are extremely thin and irregular with a rough surface (Smith et al., 2009; Chun et al., 2010).

Amelogenin is the most abundant enamel matrix protein (90%) and is essential for amelogenesis. Amelogenin-deficient mice display an amelogenesis imperfecta phenotype (Gibson et al., 2001). The amelogenin KO incisors appear as abnormal teeth with chalky-white discoloration, longitudinal furrows, and broken tips. At an ultrastructural level, the characteristic prism pattern is completely absent. The amelogenin KO molar cusps are abraded and the disorganized hypoplastic aprismatic enamel display reduced thickness.

Enamel matrix proteinases suck as KLK4 and MMP20 are secreted in tooth enamel matrix during the maturation stage of amelogenesis. They have a role in the degradation of matrix proteins to promote the export of the cleaved forms from the hardening enamel. In mice lacking KLK4, the incisor enamel has a normal thickness and no change in its overall organization in terms of rod/inter-rod structure. The developmental defect in the enamel rods is restricted to the first formed inner enamel near the dentino-enamel junction. Thinner and structurally abnormal incisor enamel is observed in MMP20 KO mice. As concern molar, both $KLK4^{-/-}$ and $MMP20^{-/-}$ display occlusal attrition (Smith et al., 2011).

The Na^{+}-independent anion exchanger 2 (Ae2) is associated to the basolateral membrane of ameloblasts and is involved in the pH regulation during the maturation phase of amelogenesis. Ae2 maintains low pH in enamel layer in order to catalyze proteins hydrolysis and/or to drive the mineralization process. In Ae2 KO mice, the decrease in mineral content and the presence of high organic matrix level in incisors and molars suggest that in the absence of Ae2, mineral ion transport as well as protein resorption are impaired. These changes are more pronounced in incisors, which in addition, lacks the typical yellow-orange enamel pigmentation normally observed in the WT incisor. Consistent with the loss of mineral, $Ae2^{-/-}$ erupted molars exhibit severe abrasion and the occlusal surface is almost devoid of enamel (Lyaruu et al., 2008).

Ameloblasts express αvβ6 integrins which (i) mediate cell matrix adhesion and thereby may have a role in the backward migration of ameloblasts in molars or cell translation in incisors, (ii) trigger signaling pathways that regulate the cell cycle, shape and motility as well as the mechanical status of extracellular matrix. In $Itgb6^{-/-}$ incisors, the enamel prism organization was completely lost. Further, incisors are abnormally white in absence of αvβ6 integrins. $Itgb6^{-/-}$ molar have also hypomineralized

enamel as inferred by extensive wear at their occlusal surfaces and much faster rate of attrition compared to WT molars (Mohazab et al., 2013).

CONCLUSION

Although enamel mineral composition does not vary much between incisors and molars, enamel microstructural complexity in term of three-dimensional organization of rods and interrods is specific of each tooth type. This well organization structure of enamel is though to be controlled by enamel matrix proteins and proteolytic enzymes whose depletion promotes different degree of enamel hypoplasia. Of note, in all the KO mice described here, enamel is still formed. The more severe phenotype is observed in amelogenin KO mice that mimicks the human amelogenesis imperfecta. As described above, defects related to genetic depletion may have differential effects on molar vs. incisor. They mostly affect the optimal hydroxyapatite crystal growth in the enamel maturation zone and not during the initial forming steps of amelogenesis.

REFERENCES

Arends, J., and Jongebloed, W. L. (1979). Ultrastructural studies of synthetic apatite crystals. *J. Dent. Res.* 58, 837–843. doi: 10.1177/00220345790580023601

Baudry, A., Bitard, J., Mouillet-Richard, S., Locker, M., Poliard, A., Launay, J. M., et al. (2010). Serotonergic 5-HT(2B) receptor controls tissue-nonspecific alkaline phosphatase activity in osteoblasts via eicosanoids and phosphatidylinositol-specific phospholipase C. *J. Biol. Chem.* 285, 26066–26073. doi: 10.1074/jbc.M109.073791

Choi, D. S., Ward, S. J., Messaddeq, N., Launay, J. M., and Maroteaux, L. (1997). 5-HT2B receptor-mediated serotonin morphogenetic functions in mouse cranial neural crest and myocardiac cells. *Development* 124, 1745–1755.

Chun, Y. H., Lu, Y., Hu, Y., Krebsbach, P. H., Yamada, Y., Hu, J. C., et al. (2010). Transgenic rescue of enamel phenotype in Ambn null mice. *J. Dent. Res.* 89, 1414–1420. doi: 10.1177/0022034510379223

Collet, C., Schiltz, C., Geoffroy, V., Maroteaux, L., Launay, J. M., and de Vernejoul, M. C. (2008). The serotonin 5-HT2B receptor controls bone mass via osteoblast recruitment and proliferation. *FASEB J.* 22, 418–427. doi: 10.1096/fj.07-9209com

Dimitrova-Nakov, S., Baudry, A., Harichane, Y., Collet, C., Marchadier, A., Kellermann, O., et al. (2014). Deletion of serotonin 2B receptor provokes structural alterations of mouse dental tissues. *Calcif. Tissue Int.* 94, 293–300. doi: 10.1007/s00223-013-9810-y

Gaspar, P., Cases, O., and Maroteaux, L. (2003). The developmental role of serotonin: news from mouse molecular genetics. *Nat. Rev. Neurosci.* 4, 1002–1012. doi: 10.1038/nrn1256

Gibson, C. W., Yuan, Z. A., Hall, B., Longenecker, G., Chen, E., Thyagarajan, T., et al. (2001). Amelogenin-deficient mice display an amelogenesis imperfecta phenotype. *J. Biol. Chem.* 276, 31871–31875. doi: 10.1074/jbc.M104624200

Harichane, Y., Dimitrova-Nakov, S., Marchadier, A., Collet, C., Baudry, A., Vidal, C., et al. (2011). Enamel alterations in serotonin 2B receptor knockout mice. *Eur. J. Oral. Sci.* 119(Suppl. 1), 177–184. doi: 10.1111/j.1600-0722.2011.00908.x

Hirota, F. (1982). Prism arrangement in human cusp enamel deduced by X-ray diffraction. *Arch. Oral Biol.* 27, 931–937. doi: 10.1016/0003-9969(82)90099-1

Koenigswald, W. V. (2004). Enamel microstructure of rodent molars, classification, and parallelisms, with a note on the systematic affiliation of the enigmatic eocene rodent *Protoptychus*. *J. Mamm. Evol.* 11, 127–142. doi: 10.1023/B:JOMM.0000041192.79808.52

Koenigswald, W. V., and Clemens, W. A. (1992). Levels of complexity in the microstructure of mammalian enamel and their application in studies of systematics. *Scanning Microsc.* 6, 195–217.

Lauder, J. M., Wilkie, M. B., Wu, C., and Singh, S. (2000). Expression of 5-HT(2A), 5-HT(2B) and 5-HT(2C) receptors in the mouse embryo. *Int. J. Dev. Neurosci.* 18, 653–662. doi: 10.1016/S0736-5748(00)00032-0

Laugel-Haushalter, V., Paschaki, M., Thibault-Carpentier, C., Dembele, D., Dolle, P., and Bloch-Zupan, A. (2013). Molars and incisors: show your microarray IDs. *BMC Res. Notes* 6:113. doi: 10.1186/1756-0500-6-113

Leblond, C. P., and Warshawsky, H. (1979). Dynamics of enamel formation in the rat incisor tooth. *J. Dent. Res.* 58, 950–975. doi: 10.1177/00220345790580024901

Lesot, H., and Brook, A. H. (2009). Epithelial histogenesis during tooth development. *Arch. Oral Biol.* 54(Suppl. 1), S25–S33. doi: 10.1016/j.archoralbio.2008.05.019

Lyaruu, D. M., Bronckers, A. L., Mulder, L., Mardones, P., Medina, J. F., Kellokumpu, S., et al. (2008). The anion exchanger Ae2 is required for enamel maturation in mouse teeth. *Matrix Biol.* 27, 119–127. doi: 10.1016/j.matbio.2007.09.006

Lyngstadaas, S. P., Moinichen, C. B., and Risnes, S. (1998). Crown morphology, enamel distribution, and enamel structure in mouse molars. *Anat. Rec.* 250, 268–280.

Ma, D., Zhang, R., Sun, Y., Rios, H. F., Haruyama, N., Han, X., et al. (2011). A novel role of periostin in postnatal tooth formation and mineralization. *J. Biol. Chem.* 286, 4302–4309. doi: 10.1074/jbc.M110.140202

Mohazab, L., Koivisto, L., Jiang, G., Kytomaki, L., Haapasalo, M., Owen, G. R., et al. (2013). Critical role for alphavbeta6 integrin in enamel biomineralization. *J. Cell Sci.* 126, 732–744. doi: 10.1242/jcs.112599

Moinichen, C. B., Lyngstadaas, S. P., and Risnes, S. (1996). Morphological characteristics of mouse incisor enamel. *J. Anat.* 189(pt 2), 325–333.

Moiseiwitsch, J. R., and Lauder, J. M. (1995). Serotonin regulates mouse cranial neural crest migration. *Proc. Natl. Acad. Sci. U.S.A.* 92, 7182–7186. doi: 10.1073/pnas.92.16.7182

Osborn, J. W. (1990). A 3-dimensional model to describe the relation between prism directions, parazones and diazones, and the Hunter-Schreger bands in human tooth enamel. *Arch. Oral Biol.* 35, 869–878. doi: 10.1016/0003-9969(90)90065-I

Risnes, S. (1979). A scanning electron microscope study of aberrations in the prism pattern of rat incisor inner enamel. *Am. J. Anat.* 154, 419–436. doi: 10.1002/aja.1001540307

Risnes, S. (1990). Structural characteristics of staircase-type Retzius lines in human dental enamel analyzed by scanning electron microscopy. *Anat. Rec.* 226, 135–146. doi: 10.1002/ar.1092260203

Smith, C. E., Richardson, A. S., Hu, Y., Bartlett, J. D., Hu, J. C., and Simmer, J. P. (2011). Effect of kallikrein 4 loss on enamel mineralization: comparison with mice lacking matrix metalloproteinase 20. *J. Biol. Chem.* 286, 18149–18160. doi: 10.1074/jbc.M110.194258

Smith, C. E., Wazen, R., Hu, Y., Zalzal, S. F., Nanci, A., Simmer, J. P., et al. (2009). Consequences for enamel development and mineralization resulting from loss of function of ameloblastin or enamelin. *Eur. J. Oral Sci.* 117, 485–497. doi: 10.1111/j.1600-0722.2009.00666.x

Steinfort, J., van den Bos, T., and Beertsen, W. (1989). Differences between enamel-related and cementum-related dentin in the rat incisor with special emphasis on the phosphoproteins. *J. Biol. Chem.* 264, 2840–2845.

Whitlock, J. A., and Richman, J. M. (2013). Biology of tooth replacement in amniotes. *Int. J. Oral Sci.* 5, 66–70. doi: 10.1038/ijos.2013.36

Conflict of Interest Statement: The authors declare that the research was conducted in the absence of any commercial or financial relationships that could be construed as a potential conflict of interest.

Received: 01 July 2014; paper pending published: 21 July 2014; accepted: 02 September 2014; published online: 19 September 2014.

*Citation: Goldberg M, Kellermann O, Dimitrova-Nakov S, Harichane Y and Baudry A (2014) Comparative studies between mice molars and incisors are required to draw an overview of enamel structural complexity. Front. Physiol. **5**:359. doi: 10.3389/fphys.2014.00359*

This article was submitted to Craniofacial Biology, a section of the journal Frontiers in Physiology.

frontiers in
PHYSIOLOGY

MINI REVIEW ARTICLE
published: 25 September 2014
doi: 10.3389/fphys.2014.00371

Maturation and beyond: proteins in the developmental continuum from enamel epithelium to junctional epithelium

Bernhard Ganss* and Nastaran Abbarin

Matrix Dynamics Group, Mineralized Tissue Lab, Faculty of Dentistry, University of Toronto, Toronto, ON, Canada

Edited by:
Megan Pugach-Gordon, The Forsyth Institute, USA

Reviewed by:
Michael Lansdell Paine, University of Southern California, USA
Wu Li, University of California at San Francisco, USA

****Correspondence:***
Bernhard Ganss, Matrix Dynamics Group, Faculty of Dentistry, University of Toronto, 150 College Street, Room 235, Toronto, ON M5S 3E2, Canada
e-mail: b.ganss@utoronto.ca

Enamel, covering the surface of teeth, is the hardest substance in mammals. It is designed to last a lifetime in spite of severe environmental challenges. Enamel is formed in a biomineralization process that is essentially divided into secretory and maturation stages. While the molecular events of enamel formation during the secretory stage have been elucidated to some extent, the mechanisms of enamel maturation are less defined, and little is known about the molecules present beyond the maturation stage. Several genes, all located within the secreted calcium-binding phosphoprotein (SCPP) gene cluster, were recently shown to be expressed during the developmental continuum from maturation stage ameloblasts to junctional epithelium (JE). This review introduces four such genes and their protein products, and presents our current state of knowledge on their roles, primarily in enamel formation and JE biology. The discovery of these proteins, and a more detailed analysis of their biological functions, will likely contribute to a more thorough understanding of the molecular mechanisms of enamel maturation and dentogingival attachment.

Keywords: enamel, maturation stage, junctional epithelium, protein identification, SCPP gene cluster

Enamel is a formidable bioceramic designed to withstand enormous mechanical forces for decades while being subjected to constant changes in temperature, pH and microbial challenges, all that without the ability to regenerate. Thus, the secretory stage of enamel formation has been studied extensively to shed light on the mechanism of enamel formation, which is directly related to three major structural proteins, namely amelogenin (AMEL), ameloblastin (AMBN) and enamelin (ENAM) and two proteases, matrix metalloproteinase (MMP)-20 and kallikrein (KLK)-4. The individual roles of these and other proteins have been studied in great detail *in vitro* and *in vivo* using transgenic mouse models, and we are now beginning to understand the principles of the complex molecular control mechanisms for enamel biomineralization (Moradian-Oldak, 2012). During the following maturation stage the enamel mineral accumulates at the expense of the organic matrix components. Recently some significant progress has been made toward identifying key mechanisms and molecules in this process (Smith, 1998; Simmer et al., 2010; Lacruz et al., 2012a; Damkier et al., 2014). The developmental continuum of ameloblasts beyond the maturation stage, however, has only been described on a histological level, albeit in great detail, and the reader is referred to several excellent reviews on this topic (Schroeder, 1969, 1996; Schroeder and Listgarten, 1997; Bosshardt and Lang, 2005). As teeth erupt into the oral cavity, the reduced enamel epithelium fuses with the oral epithelium and is slowly converted into junctional epithelium (JE) in a coronal-to-apical direction during and after tooth eruption. The JE ultimately provides the "seal" around teeth and is therefore of critical importance to prevent invasion of oral microorganisms, but the molecular composition of the JE attachment apparatus to the mineralized tooth surface remains poorly defined. This short review focuses on four recently identified genes, Amelotin (AMTN), Odontogenic, Ameloblast-Associated (ODAM), Follicular Dendritic Cell Secreted Protein (FDCSP), and Secreted Calcium-binding Phosphoprotein (SCPP), rich in Proline and Glutamine (SCPPPQ1), and briefly summarizes our current state of knowledge regarding their role in enamel and the JE.

DISCOVERY

AMTN was originally discovered as an enamel-specific gene by differential display analysis of mRNA expression from dental tissues in mice (Iwasaki et al., 2005). An expressed fragment of AMTN was also found as EO-063 in a signal trap screening approach in rat enamel (Moffatt et al., 2006a). ODAM was initially identified as the major protein component in the amyloid deposits of calcifying epithelial odontogenic (Pindborg) tumors (Solomon et al., 2003) and was named APin (for Amyloid in Pindborg tumors). It was also found as EO-009 in the signal trap screening approach mentioned above (Moffatt et al., 2006a) in rat incisor enamel. Due to its high expression in enamel-associated epithelia (Park et al., 2007; Moffatt et al., 2008) it has been renamed ODAM. FDCSP was originally discovered as a secreted protein in follicular dendritic cells (Marshall et al., 2002) and continues to be of great interest in immune cell regulation (Hou et al., 2014). Its relevance to this review comes from its expression in the

JE (see below). SCPPPQ1 has been identified as a novel gene in the SCPP gene cluster in mammals (Kawasaki et al., 2011), characterized by its high content of proline and glutamine (PQ). The SCPP and enamel gene clusters are located in close proximity.

GENOMIC LOCALIZATION, ORGANIZATION, AND PROTEIN CHARACTERISTICS

The genomic location of *AMTN, ODAM, FDCSP*, and *SCPPPQ1* contains clusters for genes involved in milk (e.g., caseins), saliva (e.g., statherins), enamel (e.g., *AMBN, ENAM*), and bone (small integrin-binding ligand N-linked glycoproteins, SIBLING family) and their evolutionary and functional aspects have been extensively reviewed (Huq et al., 2005; Kawasaki and Weiss, 2008; Kawasaki, 2011; Kawasaki et al., 2011; Staines et al., 2012). The more recently discovered *AMTN*, *ODAM*, *FDCSP*, and *SCPPPQ1* genes are located within this cluster in the proximal-to-distal sequence *ODAM*, *FDCSP*, *AMTN*, *SCPPPQ1* and this sequence appears to be conserved in mammalian genomes. **Figure 1** shows a schematic map of the mouse chromosome 5 and the relative location of genes of interest. **Table 1** summarizes genomic organization, protein characteristics, expression and possible functions for the four proteins discussed here. Data for the human orthologs are similar unless indicated otherwise.

All four proteins contain an N-terminal signal sequence and have either been shown (Iwasaki et al., 2005; Moffatt et al., 2008) or are expected to be secreted. The *Amtn* gene consists of nine exons and the mature, secreted AMTN protein (after cleavage of the N-terminal signal sequence) is 20.4 kDa in size with a pI of 5.88. It is rich in proline, leucine, threonine, glutamine, and glycine and is predicted to be modified by serine, threonine and tyrosine phosphorylation and O-glycosylation. AMTN expression seems to be restricted to maturation stage ameloblasts and the JE, although the application of increasingly sensitive techniques has shown *Amtn* transcripts in calvaria-derived osteoblasts (Atsawasuwan et al., 2013). Whether this low level expression has any functional implication *in vivo* remains to be determined. The *Odam* gene consists of 12 exons and the protein is 28.3 kDa in size with a pI of 4.83. It is rich in glutamine and proline and predicted to be phosphorylated at multiple serine and threonine residues and O-glycosylated at multiple positions. ODAM expression is highest in maturation stage ameloblasts and JE, but present in other tissues including nasal and salivary glands (Moffatt et al., 2008), indicating a broader biological role. The *Fdcsp* gene consists of five exons and its product is a small (8.0 kDa), very

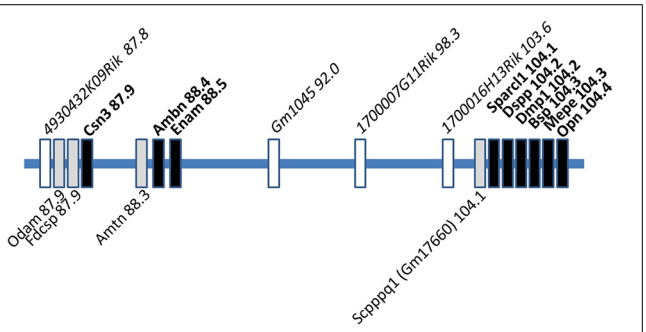

FIGURE 1 | Schematic presentation of the SCPP gene cluster on the long arm of mouse chromosome 5. The relative position of the genes is indicated as distance in Mb from the centromere. Well-characterized genes are indicated by black boxes and their names above the central line in bold, uncharacterized genes by white boxes with their names above the central line in italics. The four genes reviewed here are shown below the central line.

Table 1 | Summary of genes of interest, their designation, genomic organization, protein characteristics expression profile, and possible functions.

Gene name	Odontogenic, ameloblast-associated	Follicular dendritic cell secreted protein	Amelotin	Secretory calcium-binding phosphoprotein, rich in proline and glutamine
Abbreviation and alternate designations	ODAM (APin)	FDCSP (C4orf7; human)	AMTN	SCPPPQ1 (Gm17660; mouse)
Genomic organization	12 exons	5 exons	9 exons	10 exons
Protein characteristics	28.3 kDa, pI 4.83 PQ rich P-Ser, p-Thr O-gly	8.0 kDa, pI 4.46 P rich P-Ser, p-Thr O-gly	20.4 kDa, pI 5.88 PLTQG rich P-Ser, p-Thr, p-Tyr O-gly	8.3 kDa, pI 4.68 PL rich P-Ser
Predominant expression	Maturation ameloblasts, junctional epithelium Nasal and salivary glands, oral epithelial tumors	Tonsils, lymph nodes, junctional epithelium	Maturation ameloblasts, junctional epithelium	Maturation stage ameloblasts
Possible functions	Multifunctional matricellular protein, Regulation of MMP-20	Regulation of inflammation in the JE	Induction of mineralization, cell attachment	Unknown

Note that phosphorylations of serine (p-Ser), threonine (p-Thr), and tyrosine (p-Tyr) as well as O-glycosylations are predicted in silico, not experimentally proven.

proline-rich polypeptide with a pI of 4.46. It is predicted to be phosphorylated at serine and threonine residues, and possibly O-glycosylated. FDCSP is predominantly expressed in tissues related to the immune system including tonsils and lymph nodes, but also in tooth supporting structures such as the JE (Shinomura et al., 2008) and periodontal ligament (Nakamura et al., 2005). Its expression in ameloblasts has not been reported. The *SCPPPQ1* gene (annotated as *Gm17660* in the mouse) consists of 10 exons and the protein is 8.3 kDa in size with a pI of 4.68, rich in proline and leucine. The protein is predicted to be phosphorylated at two serine residues at the N-terminus, but not glycosylated. All four proteins are predicted by *in silico* analyses to be intrinsically disordered, a characteristic shared with other known mineralization regulators in the SCPP gene cluster. None of the four proteins contain integrin-binding "RGD" motifs or N-glycosylation sites.

ROLES IN ENAMEL FORMATION

AMTN has been identified by differential display analysis of mRNA expression from dental tissues (Iwasaki et al., 2005) and is, based on lack of expression in other tissues, considered to be specific to the ameloblast lineage. Evolutionary analyses have provided further evidence for AMTN as an enamel-specific protein (Gasse et al., 2012). The expression of mouse amelotin was found by several independent groups to be rapidly and dramatically upregulated in ameloblasts at the transition from secretory to maturation stage, and this expression profile is very different from that of the more established enamel proteins AMEL, AMBN, and ENAM (Moffatt et al., 2006b; Trueb et al., 2007; Somogyi-Ganss et al., 2012). In contrast, a single report using non-affinity-purified antibodies has shown Amtn expression in secretory stage enamel matrix of the mouse (Gao et al., 2010). The secreted AMTN protein accumulates at the interface between cells and enamel mineral and appears to be part of the specialized basal lamina-like layer that reappears at the onset of the maturation stage (Dos Santos Neves et al., 2012; Somogyi-Ganss et al., 2012). This restricted and specific localization of AMTN suggests functional roles in cell adhesion and/or surface enamel mineralization. Since AMTN can form multimeric aggregates in solution (Holcroft and Ganss, 2011) it is also possible that it is part of a basal lamina-like structure that may be involved in transport control in and out of the maturing enamel. We have described a simple cell adhesion experiment where bacterially produced, recombinant (and therefore lacking post-translational modifications) AMTN did not mediate any cell attachment (Somogyi-Ganss et al., 2012). However, since AMTN is predicted to contain P-serine and potentially O-glycosylations, these modifications may alter the adhesive properties of the protein. It may also be possible that AMTN requires other interacting proteins to mediate cell adhesion, and in this context it is particularly interesting that AMTN has been shown to interact with ODAM (Holcroft and Ganss, 2011). More detailed protein interaction studies are underway to determine whether other proteins bind to AMTN and/or ODAM in a multimeric complex that may mediate cell attachment. It is currently not known whether AMTN plays any role in controlling the transport of ions and/or protein fragments in and out of the maturing enamel. Preliminary experiments in our lab have failed to detect any significant differences in staining pattern of incisal enamel with pH sensitive dyes between wild type and AMTN KO mice. This indicates that the naturally occurring proton transport during enamel maturation is not fundamentally altered. It would be interesting to probe the potential role of AMTN in ion transport by comparing the distribution of fluoride that is supplied in the drinking water (Lyaruu et al., 2014) in wild type and AMTN-deficient mice in light of dental fluorosis as a clinical problem. The expression of AMTN coincides with the establishment of the dense, highly mineralized, aprismatic surface enamel layer (Moinichen et al., 1996) and it is conceivable that the protein is involved in the establishment of this layer. We have recently reported transgenic mice engineered to overexpress AMTN under the AMEL gene promoter (Lacruz et al., 2012b). These mice express AMTN not only at higher amounts, but also earlier during amelogenesis and as a result show a hypoplastic yet densely mineralized irregular enamel layer that does not show any organized rod and interrod microstructure, indicating that AMTN may have an accelerating role in the controlled mineralization of hydroxyapatite. We have recently developed AMTN-deficient animals, and it will be interesting to determine their phenotype with particular attention to the mineralization of the surface enamel mineral structure and density.

ODAM is expressed in a pattern very similar to AMTN during enamel formation. The first published report that indicated an involvement of ODAM in enamel formation showed high expression during amelogenesis in the rat incisor (Park et al., 2007) using immunohistochemistry and *in situ* hybridization. The authors further postulated that ODAM could exert its function during enamel formation and mineralization by modulating the expression of the enamel protease MMP-20. The onset of ODAM expression is slightly earlier (late secretory stage) than AMTN, but both proteins are localized in the basal lamina-like layer at the ameloblast-enamel interface. There appears to be a subtle difference in ODAM/AMTN localization with ODAM closer to the cell surface and AMTN closer to the enamel surface (Dos Santos Neves et al., 2012), but whether this bears any functional significance is not known. ODAM KO mice have not been described in the literature to date. Further studies on the molecular mechanism of ODAM-mediated regulation of enamel mineralization have postulated that an intracellular form of ODAM is phosphorylated by the bone morphogenetic protein receptor type IB (BMPR-IB)-mediated action of BMP-2 and thus modulates the signaling pathways involved in ameloblast differentiation (Lee et al., 2012a). The same group has further shown that intracellular ODAM cooperates with the runt domain transcription factor Runx2 and thus regulates the expression of MMP-20. This modulation of MMP-20 by ODAM was interpreted as a mechanism by which enamel matrix maturation is regulated by ODAM (Lee et al., 2010). While the notion of an intracellular form of ODAM is interesting and not unprecedented—as shown for the SIBLING protein osteopontin (OPN) (Zohar et al., 1997, 2000)—it remains to be explained how and why the ODAM protein is retained or accumulates in the cytoplasm and the nucleus of ameloblasts *in vivo* and in culture. Presumably it is the intracellular/nuclear form of ODAM that is involved in MMP-20 regulation, but details of this process also remain to be determined. These findings contrast the identification of ODAM from rat ameloblasts by a

signal trap screening approach (Moffatt et al., 2006a), which is designed to target secreted proteins. Interestingly, a direct inductive effect on dentin mineralization was observed when recombinant ODAM protein was applied to odontoblast cells in culture and in a dental pulp capping experiments in rats *in vivo* (Yang et al., 2010), but whether a similar effect would be observed in enamel is currently unexplored.

The expression profiles of SCPPPQ1 and FDCSP during enamel formation have not yet been detailed in published work, but SCPPPQ1 has been identified as EO-463 by screening for secreted proteins in rat enamel (Moffatt et al., 2006a) and the expression of SCPPPQ1 has been demonstrated in the basal lamina-like layer of late maturation stage ameloblasts (Wazen et al., 2013). Knockout animals for FDCSP have been developed (Hou et al., 2014), but no phenotype related to teeth has been reported, even though FDCSP apparently binds to hydroxyapatite (Shinomura et al., 2008). A knockout for SCPPPQ1 has not been published. Thus, the expression profiles and potential role(s) for these two proteins in enamel formation remain to be elucidated.

ROLES IN THE JUNCTIONAL EPITHELIUM

AMTN protein is continuously detected at the ameloblast-enamel interface from the maturation through the reduced enamel epithelium to the JE in mice (Somogyi-Ganss et al., 2012) and rats (Moffatt et al., 2006b; Nishio et al., 2013). The localization of AMTN in the JE is restricted to the cell/mineral interface, while ODAM is localized in a pericellular fashion in the JE. In this context it is interesting to note that the presence of AMTN during formation of the primary JE has only been detected by immunohistochemistry, but not by *in situ* hybridization, which either indicates insufficient sensitivity of the technique to detect low abundance Amtn mRNA transcripts, or that the AMTN protein found in the JE is residual from production by the reduced enamel epithelium (Sawada et al., 2013). Regardless, both AMTN and ODAM are re-expressed in the JE after gingivectomy and regain their normal expression pattern after the gingival tissue has regenerated (Nishio et al., 2010a). Notably, ODAM expression is induced in epithelial rests of Malassez (ERM) after experimental periodontal detachment and ODAM is re-expressed during orthodontic tooth movement (Nishio et al., 2010b; Jue et al., 2013), indicating that ODAM may play a role in periodontal regeneration. However, the work to date is largely descriptive and functional studies have not been published. Aside from its role in the immune system, a growing body of literature indicates the involvement of FDCSP in the dentogingival attachment apparatus. The specific pericellular expression of FDCSP in the PDL (Nakamura et al., 2005) and the JE (Shinomura et al., 2008) has been described earlier, followed by the observation that periodontal pathogen-derived lipopolysaccharide (LPS) leads to rapid loss of FDCSP expression in an experimental rat model (Oshiro et al., 2012). Exposure of periodontal ligament cells to FDCSP in culture resulted in increased cell proliferation and suppression of mineralization-associated gene expression (Wei et al., 2011), possibly indicating a role for FDCSP in maintaining these cells in a fibroblastic state that allows them to rapidly respond to traumatic events. Overexpression of FDCSP in PDL cells by viral transfection also reduced the level of osteogenic gene expression (Xiang et al., 2013a,b), presumably stabilizing a fibroblastic phenotype. In a ligature-induced model of periodontitis in rats the expression of FDCSP was significantly decreased during the establishment of periodontal attachment loss, while interleukin 17 (IL-17) and the RANKL/OPG ratio were up regulated, indicating a state of acute inflammation and increased bone resorption, respectively. This suggests a possible role for FDCSP in mediating the inflammatory responses to periodontal pathogens in the JE, and ties back to the documented immunmodulatory role of FDCSP (Al-Alwan et al., 2007; Hou et al., 2014).

A recently published *in vitro* model system for junctional, sulcular and gingival epithelium formation has used ODAM and FDCSP expression to delineate the JE (Dabija-Wolter et al., 2013). Further support for a potential role of the four genes described here in periodontal health was provided in a recent report that linked regions in the enamel gene cluster to periodontitis susceptibility by QTL analysis (Shusterman et al., 2013).

ROLES IN TUMORS

In addition to the potential functions in enamel and the JE, there has been some interest in the expression of these enamel gene cluster proteins in cancers. For ODAM this was expected, since it was initially discovered in Pindborg tumors (Solomon et al., 2003; Murphy et al., 2008). ODAM has further been found in other types of lung and breast tumors of epithelial origin and has been suggested as a prognostic marker for such neoplasms (Kestler et al., 2008), particularly human breast cancer (Siddiqui et al., 2009). Other descriptive work focusing on the expression of enamel proteins has confirmed the expression of ODAM and AMTN in certain types of odontogenic tumors (Ren et al., 2011; Crivelini et al., 2012), often associated with sites of mineral deposition (Stolf et al., 2013). ODAM expression has further been described in odontoblasts, osteoblasts and various cancer cells (Lee et al., 2012b). The first study looking at functional aspects of the expression of ODAM in tumors has shown that it can inhibit tumorigenic characteristics in the human breast cancer cell line MDA-MB-231 *in vitro* and the transplantation of ODAM-expressing tumor cells into mice lead to significantly reduced tumor growth and their inability to metastasize, compared to control cells that did not express ODAM (Kestler et al., 2011). Further dissection of the molecular pathways affected by ODAM revealed that it can act through elevation of the tumor suppressor phosphatase and tensin homolog (PTEN) and inhibition of the apoptosis-blocking PI3 kinase/AKT pathway (Foster et al., 2013). One published report indicates that FDCSP (designated C4orf7 at the time) can modulate cytoskeletal actin dynamics, thereby promoting migration and invasion of ovarian cancer cells (Wang et al., 2010)

OTHER GENES WITHIN THE SCPP GENE CLUSTER

In addition to the enamel and SIBLING gene cluster, which contain genes involved in mineralized tissue formation, other calcium binding phosphoproteins are found in this genomic region. These include the casein genes, salivary protein genes (statherin etc.), but also a number of uncharacterized annotated genes. The issue of poor and incomplete annotation makes it difficult to predict the existence and function of additional genes in this cluster.

For example, the mouse genome contains a gene annotated as 4930432K09Rik in the ensembl genome browser (http://www.ensembl.org), which codes for a predicted protein of 344 and 352 amino acids from two alternatively spliced transcripts, just upstream of the ODAM gene. A presumptive human ortholog, annotated as C4orf40, has significant sequence similarity with parts of 4930432K09Rik, but encodes a protein of only 219 amino acids. Both C4orf40 and 4930432K09Rik predicted proteins contain a well-conserved N-terminal signal sequence, are mildly acidic (pI 4.82 and 5.30, respectively), proline-rich and contain multiple predicted serine, threonine and tyrosine phosphorylation as well as O-glycosylation sites. Similarly, other uncharacterized, protein-coding genes are currently annotated in the human genome as C4orf26, C4orf22, C4orf36, and in the mouse genome as Gm1045, 1700007G11Rik, and 1700016H13Rik, all within the enamel/SIBLING gene cluster. C4orf26 has recently been described as a candidate gene for *amelogenesis imperfecta*, and the protein apparently possesses hydroxyapatite nucleation and growth activity (Parry et al., 2012). Interestingly, the FDCSP gene is not annotated as such in the mouse genome in both the ensembl (http://www.ensembl.org/index.html) and UCSC (https://genome.ucsc.edu/) genome browsers, even though the genomic organization (Marshall et al., 2002) and even knockout animals (Hou et al., 2014) have been described. Clearly, much work remains to be done to discover and understand the biology of additional proteins coded by other genes in the SCPP gene cluster.

In conclusion, the SCPP gene cluster contains multiple genes that have been studied to various extents in the context of mineralized tissue. AMTN, ODAM, FDCSP, and SCPPPQ1 have been added to the more established enamel and SIBLING genes, and other genes await characterization. The expression of AMTN, ODAM, and FDCSP has emphasized the developmental continuum from the reduced enamel epithelium to the JE on a molecular level and may become instrumental in understanding the molecular details of the dentogingival attachment apparatus.

REFERENCES

Al-Alwan, M., Du, Q., Hou, S., Nashed, B., Fan, Y., Yang, X., et al. (2007). Follicular dendritic cell secreted protein (FDC-SP) regulates germinal center and antibody responses. *J. Immunol.* 178, 7859–7867. doi: 10.4049/jimmunol.178.12.7859

Atsawasuwan, P., Lu, X., Ito, Y., Chen, Y., Gopinathan, G., Evans, C. A., et al. (2013). Expression and function of enamel-related gene products in calvarial development. *J. Dent. Res.* 92, 622–628. doi: 10.1177/0022034513487906

Bosshardt, D. D., and Lang, N. P. (2005). The junctional epithelium: from health to disease. *J. Dent. Res.* 84, 9–20. doi: 10.1177/154405910508400102

Crivelini, M. M., Felipini, R. C., Miyahara, G. I., and de Sousa, S. C. (2012). Expression of odontogenic ameloblast-associated protein, amelotin, ameloblastin, and amelogenin in odontogenic tumors: immunohistochemical analysis and pathogenetic considerations. *J. Oral Pathol. Med.* 41, 272–280. doi: 10.1111/j.1600-0714.2011.01079.x

Dabija-Wolter, G., Bakken, V., Cimpan, M. R., Johannessen, A. C., and Costea, D. E. (2013). *In vitro* reconstruction of human junctional and sulcular epithelium. *J. Oral Pathol. Med.* 42, 396–404. doi: 10.1111/jop.12005

Damkier, H. H., Josephsen, K., Takano, Y., Zahn, D., Fejerskov, O., and Frische, S. (2014). Fluctuations in surface pH of maturing rat incisor enamel are a result of cycles of H(+)-secretion by ameloblasts and variations in enamel buffer characteristics. *Bone* 60, 227–234. doi: 10.1016/j.bone.2013.12.018

Dos Santos Neves, J., Wazen, R. M., Kuroda, S., Francis Zalzal, S., Moffatt, P., and Nanci, A. (2012). Odontogenic ameloblast-associated and amelotin are novel basal lamina components. *Histochem. Cell Biol.* 137, 329–338. doi: 10.1007/s00418-011-0901-4

Foster, J. S., Fish, L. M., Phipps, J. E., Bruker, C. T., Lewis, J. M., Bell, J. L., et al. (2013). Odontogenic ameloblast-associated protein (ODAM) inhibits growth and migration of human melanoma cells and elicits PTEN elevation and inactivation of PI3K/AKT signaling. *BMC Cancer* 13:227. doi: 10.1186/1471-2407-13-227

Gao, Y., Wang, W., Sun, Y., Zhang, J., Li, D., Wei, Y., et al. (2010). Distribution of amelotin in mouse tooth development. *Anat. Rec.* 293, 135–140. doi: 10.1002/ar.21022

Gasse, B., Silvent, J., and Sire, J. Y. (2012). Evolutionary analysis suggests that AMTN is enamel-specific and a candidate for AI. *J. Dent. Res.* 91, 1085–1089. doi: 10.1177/0022034512460551

Holcroft, J., and Ganss, B. (2011). Identification of amelotin- and ODAM-interacting enamel matrix proteins using the yeast two-hybrid system. *Eur. J. Oral Sci.* 119(Suppl. 1), 301–306. doi: 10.1111/j.1600-0722.2011.00870.x

Hou, S., Landego, I., Jayachandran, N., Miller, A., Gibson, I. W., Ambrose, C., et al. (2014). Follicular dendritic cell secreted protein FDC-SP controls IgA production. *Mucosal Immunol.* 7, 948–957. doi: 10.1038/mi.2013.113

Huq, N. L., Cross, K. J., Ung, M., and Reynolds, E. C. (2005). A review of protein structure and gene organisation for proteins associated with mineralised tissue and calcium phosphate stabilisation encoded on human chromosome 4. *Arch. Oral Biol.* 50, 599–609. doi: 10.1016/j.archoralbio.2004.12.009

Iwasaki, K., Bajenova, E., Somogyi-Ganss, E., Miller, M., Nguyen, V., Nourkeyhani, H., et al. (2005). Amelotin–a novel secreted, ameloblast-specific protein. *J. Dent. Res.* 84, 1127–1132. doi: 10.1177/154405910508401207

Jue, S. S., Kim, J. Y., Na, S. H., Jeon, K. D., Bang, H. J., Park, J. H., et al. (2013). Localization of ODAM, PCNA, and CK14 in regenerating junctional epithelium during orthodontic tooth movement in rats. *Angle Orthod.* 84, 534–540. doi: 10.2319/051613-378.1

Kawasaki, K. (2011). The SCPP gene family and the complexity of hard tissues in vertebrates. *Cells Tissues Organs* 194, 108–112. doi: 10.1159/000324225

Kawasaki, K., Lafont, A. G., and Sire, J. Y. (2011). The evolution of milk casein genes from tooth genes before the origin of mammals. *Mol. Biol. Evol.* 28, 2053–2061. doi: 10.1093/molbev/msr020

Kawasaki, K., and Weiss, K. M. (2008). SCPP gene evolution and the dental mineralization continuum. *J. Dent. Res.* 87, 520–531. doi: 10.1177/154405910808700608

Kestler, D. P., Foster, J. S., Bruker, C. T., Prenshaw, J. W., Kennel, S. J., Wall, J. S., et al. (2011). ODAM expression inhibits human breast cancer tumorigenesis. *Breast Cancer* 5, 73–85. doi: 10.4137/BCBCR.S6859

Kestler, D. P., Foster, J. S., Macy, S. D., Murphy, C. L., Weiss, D. T., and Solomon, A. (2008). Expression of odontogenic ameloblast-associated protein (ODAM) in dental and other epithelial neoplasms. *Mol. Med.* 14, 318–326. doi: 10.2119/2008-00010.Kestler

Lacruz, R. S., Nakayama, Y., Holcroft, J., Nguyen, V., Somogyi-Ganss, E., Snead, M. L., et al. (2012b). Targeted overexpression of amelotin disrupts the microstructure of dental enamel. *PLoS ONE* 7:e35200. doi: 10.1371/journal.pone.0035200

Lacruz, R. S., Smith, C. E., Moffatt, P., Chang, E. H., Bromage, T. G., Bringas, P. Jr., et al. (2012a). Requirements for ion and solute transport, and pH regulation during enamel maturation. *J. Cell. Physiol.* 227, 1776–1785. doi: 10.1002/jcp.22911

Lee, H. K., Lee, D. S., Ryoo, H. M., Park, J. T., Park, S. J., Bae, H. S., et al. (2010). The odontogenic ameloblast-associated protein (ODAM) cooperates with RUNX2 and modulates enamel mineralization via regulation of MMP-20. *J. Cell. Biochem.* 111, 755–767. doi: 10.1002/jcb.22766

Lee, H. K., Park, J. T., Cho, Y. S., Bae, H. S., Cho, M. I., and Park, J. C. (2012a). Odontogenic ameloblasts-associated protein (ODAM), via phosphorylation by bone morphogenetic protein receptor type IB (BMPR-IB), is implicated in ameloblast differentiation. *J. Cell. Biochem.* 113, 1754–1765. doi: 10.1002/jcb.24047

Lee, H. K., Park, S. J., Oh, H. J., Kim, J. W., Bae, H. S., and Park, J. C. (2012b). Expression pattern, subcellular localization, and functional implications of ODAM in ameloblasts, odontoblasts, osteoblasts, and various cancer cells. *Gene Expr. Patterns* 12, 102–108. doi: 10.1016/j.gep.2012.02.002

Lyaruu, D. M., Medina, J. F., Sarvide, S., Bervoets, T. J., Everts, V., Denbesten, P., et al. (2014). Barrier formation: potential molecular mechanism of enamel fluorosis. *J. Dent. Res.* 93, 96–102. doi: 10.1177/0022034513510944

Marshall, A. J., Du, Q., Draves, K. E., Shikishima, Y., HayGlass, K. T., and Clark, E. A. (2002). FDC-SP, a novel secreted protein expressed by follicular dendritic cells. *J. Immunol.* 169, 2381–2389. doi: 10.4049/jimmunol.169.5.2381

Moffatt, P., Smith, C. E., Sooknanan, R., St-Arnaud, R., and Nanci, A. (2006a). Identification of secreted and membrane proteins in the rat incisor enamel organ using a signal-trap screening approach. *Eur. J. Oral Sci.* 114(Suppl. 1), 139–146. discussion: 64–65, 380–381. doi: 10.1111/j.1600-0722.2006.00318.x

Moffatt, P., Smith, C. E., St-Arnaud, R., and Nanci, A. (2008). Characterization of Apin, a secreted protein highly expressed in tooth-associated epithelia. *J. Cell. Biochem.* 103, 941–956. doi: 10.1002/jcb.21465

Moffatt, P., Smith, C. E., St-Arnaud, R., Simmons, D., Wright, J. T., and Nanci, A. (2006b). Cloning of rat amelotin and localization of the protein to the basal lamina of maturation stage ameloblasts and junctional epithelium. *Biochem. J.* 399, 37–46. doi: 10.1042/BJ20060662

Moinichen, C. B., Lyngstadaas, S. P., and Risnes, S. (1996). Morphological characteristics of mouse incisor enamel. *J. Anat.* 189(pt 2), 325–333.

Moradian-Oldak, J. (2012). Protein-mediated enamel mineralization. *Front. Biosci.* 17, 1996–2023. doi: 10.2741/4034

Murphy, C. L., Kestler, D. P., Foster, J. S., Wang, S., Macy, S. D., Kennel, S. J., et al. (2008). Odontogenic ameloblast-associated protein nature of the amyloid found in calcifying epithelial odontogenic tumors and unerupted tooth follicles. *Amyloid* 15, 89–95. doi: 10.1080/13506120802005965

Nakamura, S., Terashima, T., Yoshida, T., Iseki, S., Takano, Y., Ishikawa, I., et al. (2005). Identification of genes preferentially expressed in periodontal ligament: specific expression of a novel secreted protein, FDC-SP. *Biochem. Biophys. Res. Commun.* 338, 1197–1203. doi: 10.1016/j.bbrc.2005.10.076

Nishio, C., Wazen, R., Kuroda, S., Moffatt, P., and Nanci, A. (2010a). Expression pattern of odontogenic ameloblast-associated and amelotin during formation and regeneration of the junctional epithelium. *Eur. Cell Mater.* 20, 393–402. doi: 10.1111/j.1600-0765.2010.01288.x

Nishio, C., Wazen, R., Kuroda, S., Moffatt, P., and Nanci, A. (2010b). Disruption of periodontal integrity induces expression of apin by epithelial cell rests of Malassez. *J. Periodontal Res.* 45, 709–713. doi: 10.1111/j.1600-0765.2010.01288.x

Nishio, C., Wazen, R., Moffatt, P., and Nanci, A. (2013). Expression of odontogenic ameloblast-associated and amelotin proteins in the junctional epithelium. *Periodontology 2000* 63, 59–66. doi: 10.1111/prd.12031

Oshiro, A., Iseki, S., Miyauchi, M., Terashima, T., Kawaguchi, Y., Ikeda, Y., et al. (2012). Lipopolysaccharide induces rapid loss of follicular dendritic cell-secreted protein in the junctional epithelium. *J. Periodontal Res.* 47, 689–694. doi: 10.1111/j.1600-0765.2012.01482.x

Park, J. C., Park, J. T., Son, H. H., Kim, H. J., Jeong, M. J., Lee, C. S., et al. (2007). The amyloid protein APin is highly expressed during enamel mineralization and maturation in rat incisors. *Eur. J. Oral Sci.* 115, 153–160. doi: 10.1111/j.1600-0722.2007.00435.x

Parry, D. A., Brookes, S. J., Logan, C. V., Poulter, J. A., El-Sayed, W., Al-Bahlani, S., et al. (2012). Mutations in C4orf26, encoding a peptide with *in vitro* hydroxyapatite crystal nucleation and growth activity, cause amelogenesis imperfecta. *Am. J. Hum. Genet.* 91, 565–571. doi: 10.1016/j.ajhg.2012.07.020

Ren, C., Diniz, M. G., Piazza, C., Amm, H. M., Rollins, D. L., Rivera, H., et al. (2011). Differential enamel and osteogenic gene expression profiles in odontogenic tumors. *Cells Tissues Organs* 194, 296–301. doi: 10.1159/000324759

Sawada, T., Yamazaki, T., Shibayama, K., Kumazawa, K., Yamaguchi, Y., and Ohshima, M. (2013). Expression and localization of laminin 5, laminin 10, type IV collagen, and amelotin in adult murine gingiva. *J. Mol. Histol.* 45, 293–302. doi: 10.1007/s10735-013-9559-7

Schroeder, H. (1996). The junctional epithelium: origin, structure and significance. *Schweiz. Monatsschr. Zahnmed.* 106, 155–167.

Schroeder, H. E. (1969). Ultrastructure of the junctional epithelium of the human gingiva. *Helv. Odontol. Acta* 13, 65–83.

Schroeder, H. E., and Listgarten, M. A. (1997). The gingival tissues: the architecture of periodontal protection. *Periodontology 2000* 13, 91–120. doi: 10.1111/j.1600-0757.1997.tb00097.x

Shinomura, T., Nakamura, S., Ito, K., Shirasawa, S., Hook, M., and Kimura, J. H. (2008). Adsorption of follicular dendritic cell-secreted protein (FDC-SP) onto mineral deposits. Application of a new stable gene expression system. *J. Biol. Chem.* 283, 33658–33664. doi: 10.1074/jbc.M800719200

Shusterman, A., Durrant, C., Mott, R., Polak, D., Schaefer, A., Weiss, E. I., et al. (2013). Host susceptibility to periodontitis: mapping murine genomic regions. *J. Dent. Res.* 92, 438–443. doi: 10.1177/0022034513484039

Siddiqui, S., Bruker, C. T., Kestler, D. P., Foster, J. S., Gray, K. D., Solomon, A., et al. (2009). Odontogenic ameloblast associated protein as a novel biomarker for human breast cancer. *Am. Surgeon* 75, 769–775. discussion: 75.

Simmer, J. P., Papagerakis, P., Smith, C. E., Fisher, D. C., Rountrey, A. N., Zheng, L., et al. (2010). Regulation of dental enamel shape and hardness. *J. Dent. Res.* 89, 1024–1038. doi: 10.1177/0022034510375829

Smith, C. E. (1998). Cellular and chemical events during enamel maturation. *Crit. Rev. Oral Biol. Med.* 9, 128–161.

Solomon, A., Murphy, C. L., Weaver, K., Weiss, D. T., Hrncic, R., Eulitz, M., et al. (2003). Calcifying epithelial odontogenic (Pindborg) tumor-associated amyloid consists of a novel human protein. *J. Lab. Clin. Med.* 142, 348–355. doi: 10.1016/S0022-2143(03)00149-5

Somogyi-Ganss, E., Nakayama, Y., Iwasaki, K., Nakano, Y., Stolf, D., McKee, M. D., et al. (2012). Comparative temporospatial expression profiling of murine amelotin protein during amelogenesis. *Cells Tissues Organs* 195, 535–549. doi: 10.1159/000329255

Staines, K. A., MacRae, V. E., and Farquharson, C. (2012). The importance of the SIBLING family of proteins on skeletal mineralisation and bone remodelling. *J. Endocrinol.* 214, 241–255. doi: 10.1530/JOE-12-0143

Stolf, D. P., Lee, T.-Y., Bradley, G., and Ganss, B. (2013). Evaluation of amelotin expression in benign odontogenic tumors. *J. Interdiscipl. Histopathol.* 1, 236–245. doi: 10.5455/jihp.20130506045106

Trueb, B., Taeschler, S., Schild, C., and Lang, N. P. (2007). Expression of phosphoproteins and amelotin in teeth. *Int. J. Mol. Med.* 19, 49–54. doi: 10.3892/ijmm.19.1.49

Wang, C., Zhou, L., Li, S., Wei, J., Wang, W., Zhou, T., et al. (2010). C4orf7 contributes to ovarian cancer metastasis by promoting cancer cell migration and invasion. *Oncol. Rep.* 24, 933–939. doi: 10.3892/or_00000939

Wazen, R. M., Dos Santos Neves, J., Moffatt, P., and Nanci, A. (2013). "SCPPPQ is a component of the basal lamina associated with maturation stage ameloblasts," in *11th International Conference on Tooth Morphogenesis and Differentiation*, eds L. Viriot, F. Bleicher, and V. Laudet (La Londe le Maures).

Wei, N., Yu, H., Yang, S., Yang, X., Yuan, Q., Man, Y., et al. (2011). Effect of FDC-SP on the phenotype expression of cultured periodontal ligament cells. *Arch. Med. Sci.* 7, 235–241. doi: 10.5114/aoms.2011.22073

Xiang, L., Ma, L., He, Y., Wei, N., and Gong, P. (2013a). Transfection with follicular dendritic cell secreted protein to affect phenotype expression of human periodontal ligament cells. *J. Cell. Biochem.* 115, 940–948. doi: 10.1002/jcb.24736

Xiang, L., Ma, L., He, Y., Wei, N., and Gong, P. (2013b). Osteogenic differentiation of human periodontal ligament cells after transfection with recombinant lentiviral vector containing follicular dendritic cell secreted protein. *J. Periodontal Res.* 49, 554–562. doi: 10.1111/jre.12135

Yang, I. S., Lee, D. S., Park, J. T., Kim, H. J., Son, H. H., and Park, J. C. (2010). Tertiary dentin formation after direct pulp capping with odontogenic ameloblast-associated protein in rat teeth. *J. Endod.* 36, 1956–1962. doi: 10.1016/j.joen.2010.08.052

Zohar, R., Lee, W., Arora, P., Cheifetz, S., McCulloch, C., and Sodek, J. (1997). Single cell analysis of intracellular osteopontin in osteogenic cultures of fetal rat calvarial cells. *J. Cell. Physiol.* 170, 88–100.

Zohar, R., Suzuki, N., Suzuki, K., Arora, P., Glogauer, M., McCulloch, C. A., et al. (2000). Intracellular osteopontin is an integral component of the CD44-ERM complex involved in cell migration. *J. Cell. Physiol.* 184, 118–130. doi: 10.1002/(SICI)1097-4652(200007)184:1<118::AID-JCP13>3.0.CO;2-Y

Conflict of Interest Statement: The authors declare that the research was conducted in the absence of any commercial or financial relationships that could be construed as a potential conflict of interest.

Received: 04 August 2014; paper pending published: 16 August 2014; accepted: 08 September 2014; published online: 25 September 2014.

*Citation: Ganss B and Abbarin N (2014) Maturation and beyond: proteins in the developmental continuum from enamel epithelium to junctional epithelium. Front. Physiol. **5**:371. doi: 10.3389/fphys.2014.00371*

This article was submitted to Craniofacial Biology, a section of the journal Frontiers in Physiology.

frontiers in
PHYSIOLOGY

REVIEW ARTICLE
published: 17 September 2014
doi: 10.3389/fphys.2014.00313

Analysis of enamel development using murine model systems: approaches and limitations

Megan K. Pugach[1]* and Carolyn W. Gibson[2]

[1] *Department of Mineralized Tissue Biology, The Forsyth Institute, Harvard School of Dental Medicine, Harvard University, Cambridge, MA, USA*
[2] *Department of Anatomy and Cell Biology, School of Dental Medicine, University of Pennsylvania, Philadelphia, PA, USA*

Edited by:
Bernhard Ganss, University of Toronto, Canada

Reviewed by:
Harald Osmundsen, University of Oslo, Norway
Catherine Chaussain, Université Paris Descartes Paris Cité, France

****Correspondence:***
Megan K. Pugach, Department of Mineralized Tissue Biology, Harvard School of Dental Medicine, The Forsyth Institute, 245 First Street, Cambridge, MA 02142, USA
e-mail: mpugach@forsyth.org

A primary goal of enamel research is to understand and potentially treat or prevent enamel defects related to amelogenesis imperfecta (AI). Rodents are ideal models to assist our understanding of how enamel is formed because they are easily genetically modified, and their continuously erupting incisors display all stages of enamel development and mineralization. While numerous methods have been developed to generate and analyze genetically modified rodent enamel, it is crucial to understand the limitations and challenges associated with these methods in order to draw appropriate conclusions that can be applied translationally, to AI patient care. We have highlighted methods involved in generating and analyzing rodent enamel and potential approaches to overcoming limitations of these methods: (1) generating transgenic, knockout, and knockin mouse models, and (2) analyzing rodent enamel mineral density and functional properties (structure and mechanics) of mature enamel. There is a need for a standardized workflow to analyze enamel phenotypes in rodent models so that investigators can compare data from different studies. These methods include analyses of gene and protein expression, developing enamel histology, enamel pigment, degree of mineralization, enamel structure, and mechanical properties. Standardization of these methods with regard to stage of enamel development and sample preparation is crucial, and ideally investigators can use correlative and complementary techniques with the understanding that developing mouse enamel is dynamic and complex.

Keywords: enamel development, transgenic, knockout, knockin, amelogenin, mineralization

INTRODUCTION

Because murine teeth have significant similarities to those of humans, murine models have been generated to study effects of deleting or altering specific protein coding genes, followed by detailed phenotypic evaluation. Mice are ideal for this purpose as their genetics have been well characterized and gene transfer technology is highly developed. The focus will be on genes encoding enamel proteins which have significant homology to those of humans, including secreted proteins amelogenin, ameloblastin, enamelin, proteases MMP20 (matrix metalloproteinase 20) and KLK4 (kallikrein 4) and cell-associated proteins ODAM (odontogenic ameloblast-associated protein) and AMTN (amelotin) (see **Table 1** for list of abbreviations) (Hu et al., 2005; Wright et al., 2009; Holcroft and Ganss, 2011; Dos Santos Neves et al., 2012; Bartlett, 2013).

Enamel phenotypes from rodents with genetically modified enamel genes have been analyzed using a wide range of methods to report and compare the physical properties of enamel such as mineral density, structure, mechanical integrity, and color. Mineral density of mouse enamel has been measured by microcomputed tomography (μCT) (Schmitz et al., 2014), backscattered scanning electron microscopy (BSE) (Smith et al., 2011b), and ashing (heating) (Smith et al., 2011a). Enamel structure has been analyzed by a variety of microscopy techniques and magnifications, but the most appropriate microscopy and magnification depends heavily on the structural information (i.e., enamel rods, enamel crystallites, enamel proteins) and stage of enamel development of interest to the investigator. Enamel mechanical integrity from genetically modified mice has been measured by microhardness (Sharma et al., 2011; Lacruz et al., 2012; Kweon et al., 2013) and nanoindentation (Fong et al., 2003; Li et al., 2008; Pugach et al., 2013). It is critical to understand the limitations of these techniques so that they can be utilized correlatively to complement each other, and so investigators can share and compare data from different rodent models, in an effort to more completely understand enamel formation and mineralization.

GENERATION OF MICE WITH GENETICALLY MODIFIED ENAMEL GENES

TRANSGENIC MICE

A transgene can be generated on a plasmid in such a way that the regulatory region that directs tissue specificity is inserted upstream of a protein coding region for expression in that tissue. This plasmid is injected into fertilized mouse eggs and then the eggs are re-implanted into a foster mother mouse (Doyle

Table 1 | List of Abbreviations.

MMP20	Matrix metalloproteinase-20
KLK4	Kallikrein-related petidase 4
ODAM	Odontogenic ameloblast-associated protein
AMTN	Amelotin
AMELX	Amelogenin
M180	Murine 180 amino acid amelogenin
LRAP	Leucine rich amelogenin peptide
TRAP	Tyrosine rich amelogenin peptide
M180ΔA-FLAG	Amelogenin with engineered N-terminal changes and reporter
M180ΔB-FLAG	Amelogenin with engineered C-terminal changes and reporter
CTRNC	Transgene with the C-terminus of amelogenin (M180) deleted
DSPP	Dentin sialophosphoprotein
FAM20C	Family with sequence similarity 20 gene
ENAM	Enamelin
AMBN	Ameloblastin
KO	Knockout or null mutation, designated −/− (+/− is heterozygous gene)
WT	Wild-type
PCR	Polymerase chain reaction
Cre-Lox	System to generate site specific recombinations in DNA
K14	Keratin-14 gene promoter
LacZ	Gene encoding beta-galactosidase
E18.5	Mouse at embryonic age day 18.5
AI	Amelogenesis imperfecta
HA	Hydroxyapatite
Tg	Transgene
SEM	Scanning electron microscopy
BSE	Backscattered SEM
FESEM	Field-emission SEM
TEM	Transmission electron microscopy
μCT	Micro-computed tomography
VOI	Volume-of-interest
RGB	Red, green and blue
WIC	Whiteness index
CIE	International Commission on Illumination
LAB	Color space where L is lightness, a is red/green and b is yellow/blue
ICC	Immunocytochemistry

et al., 2012). This DNA will insert randomly into the genome so that it must contain sufficient regulatory material to direct expression without major influence by the site of insertion. The DNA can insert in multiple copies as well as in multiple locations in the genome, and frequently higher copy number leads to higher expression of the transgenic protein. However, if the DNA inserts into a required gene, a secondary phenotype may be observed unrelated to the transgenic protein. For this reason, at least three independent transgenic pups are generally analyzed to avoid problems related to site of insertion. An advantage is that this approach may allow low, medium, and high levels of transgene expression to be studied, but in the presence of expression by the endogenous gene.

A simple model system involves a transgenic mouse that expresses a detectable reporter protein to indicate where a specific gene regulatory sequence is active, such as was done for the amelogenin gene promoter (Chen et al., 1994). Transgenic reporters have included β-galactosidase, luciferase, human growth hormone, and thymidine kinase (Al-Shawi et al., 1988; Dilella et al., 1988; Sweetser et al., 1988; Theopold and Kohler, 1990).

Another common strategy is to generate a transgenic mouse that overexpresses a normal protein in the endogenous tissue such as amelogenin, LRAP or TRAP (small amelogenins), ameloblastin, enamelin, MMP20, amelotin, DSPP (Paine et al., 2003, 2004, 2005; Gibson et al., 2007; Lacruz et al., 2012; Stahl et al., 2013; Hu et al., 2014; Shin et al., 2014). It is also possible to express a transgene more broadly so that the transgenic protein is expressed in a tissue different from or in addition to the endogenous, e.g., by use of the K14 promoter (Atsawasuwan et al., 2013). Overexpression of a transgene with a mutation or deletion to interfere with the function of the endogenous protein in a dominant negative strategy has been used followed by phenotypic analysis in order to better understand protein function (Dunglas et al., 2002; Gibson et al., 2007; Pugach et al., 2010; Chen et al., 2011).

Transgenes are relatively unlikely to cause a lethal event, but lack of detectable transgenic expression, or expression in unexpected tissues are both common. These observations related to expression can be confusing but may lead to new ideas concerning where the gene is normally expressed, additional functions during development, or gene motif requirements for accurate tissue specific and level of expression. Transgene overexpression may not however accurately reflect the human condition.

Transgene expression levels

A problem in use of transgenic mice is difficulty in replicating the level of expression of the endogenous gene. In the case of amelogenins, since there is one primary RNA transcript but many amelogenin mRNAs, the appropriate expression level for an individual protein is cause for debate as it is not clear whether matching the endogenous level is possible. In rescue experiments, the high expression level of one of the amelogenin transgenes can rescue the phenotype when mated with amelogenin null mice, but the low expressor is unable to rescue significantly. Various levels of transgene expression have allowed determination of the amount of protein that either damages the normal phenotype or rescues the null phenotype (Li et al., 2008; Chun et al., 2010; Shin et al., 2014).

KNOCKOUT MOUSE MODELS

A "knockout" is a term for a mouse with a single mutated gene so that no protein is expressed, also referred to as a "null" mutation (Mansour et al., 1988). A null mutation can provide relatively straight forward means to understand consequences of lack of a particular protein. If the result is a lethal event, this approach can still provide information on when protein function begins to be important, and tissues impacted by lack of the protein. Loss of a structural protein in a mineralized tissue may lead to an obvious defect, or to a defect that becomes apparent in the presence of a stressor. Mutations in enamel proteins frequently lead

to enamel that is chalky in appearance and subject to attrition. This knockout approach can be designed to duplicate human pathology by deletion of a structural protein or enzyme predicted to be important.

In the simplest situation, a plasmid vector that includes antibiotic selection cassettes is generated to contain a segment of the gene of interest with an engineered mutation such as a deletion or stop codon to prevent expression. This plasmid is introduced into cultured embryonic stem cells followed by chemical or antibiotic selection *in vitro*. Clones that grow are tested to determine whether the engineered gene has replaced the endogenous gene. Clones that seem perfect by Southern blot and PCR of genomic DNA are transferred into blastocysts and the recombinant structure is implanted into a surrogate female mouse (Doyle et al., 2012). The pups that are born are tested by PCR using DNA isolated from tail tissue to determine the presence of the mutation in individual pups. Positive mice are mated with wild-type mice to ascertain that the mutation can be passed on to offspring, and has been inserted correctly into the mouse genome. Individual strains can be developed from positive mice; usually several mouse strains are evaluated phenotypically for effects of the deleted gene.

Several problems can be encountered using this approach. The amelogenin null mouse was generated by deletion of parts of exon 2 and intron 2, and exon 2 containing the start sequence in present in all cDNAs sequenced to date (Gibson et al., 2001). This deletion allowed amelogenin RNA to be produced that lacked exon 2, but was not translated.

The ameloblastin KO originally reported (Fukumoto et al., 2004) was actually a partial deletion leading to expression of truncated protein (Wazen et al., 2009). A different kind of problem is associated with the MMP20 KO as the KO enamel delaminates from dentin so that it is difficult to study the enamel structure (Caterina et al., 2002).

RESCUE EXPERIMENTS

In addition to direct analysis, transgenic and null mice can be mated together to perform phenotypic rescue experiments. An example is rescue of the amelogenin null hypoplastic phenotype by single amelogenin proteins. Although there are more than 15 amelogenin mRNAs, this rescue required only one or two transgenes for significant improvement of the enamel layer (Li et al., 2008; Gibson et al., 2011). As mentioned above, transgene expression level is also critical for efficient rescue for ameloblastin, enamelin, and MMP20 null mice (Chun et al., 2010; Hu et al., 2014; Shin et al., 2014).

SECONDARY PHENOTYPES FROM WHOLE-BODY GENE DELETION

The above strategy is useful when ablation of a protein does not constitute a lethal event. In that case, other strategies such as Cre-lox mediated tissue specific deletions can be attempted. Unexpected phenotypes may develop in a tissue that was not previously known to express the deleted gene.

An unexpected phenotype can also be observed when a null mutation is moved to a mouse with a different genetic background. Most null mutations are generated in mice with mixed background but then are transferred by repeated mating and screening to C57Bl/6 or another inbred strain in order to reduce phenotypic heterogeneity. Many examples have been reported where inbred mice have a phenotype different from that in the original mixed background strain. Phenotypic heterogeneity of the incisors can be easily observed within a group of adult amelogenin null mice with mixed genetic backgrounds (**Figure 1**). For example, when MMP20 or amelogenin null mutations were moved to a different genetic background, the enamel phenotype was altered (Li et al., 2014; Bartlett, personal communication).

The above limitations could be seen as supplying new knowledge difficult to obtain by other means, such as *in vitro* experiments. However, an important consideration is the expense of maintaining colonies of mice, especially those having small or infrequent litters, or those with lethal outcomes. When mating efficiency is reduced in null mice, they can be maintained as heterozygotes (+/−) and then mated together to produce +/+, +/−, and −/− offspring, that is the controls are generated within the litter.

Cre-lox TISSUE SPECIFIC DELETIONS

To generate a tissue specific targeted gene deletion using the Cre-lox system, two mice are required (Doyle et al., 2012). One mouse will have a transgene that expresses the Cre-recombinase under control of a tissue specific promoter. That mouse is mated to a mouse with LOX-P sites inserted within the gene of interest in

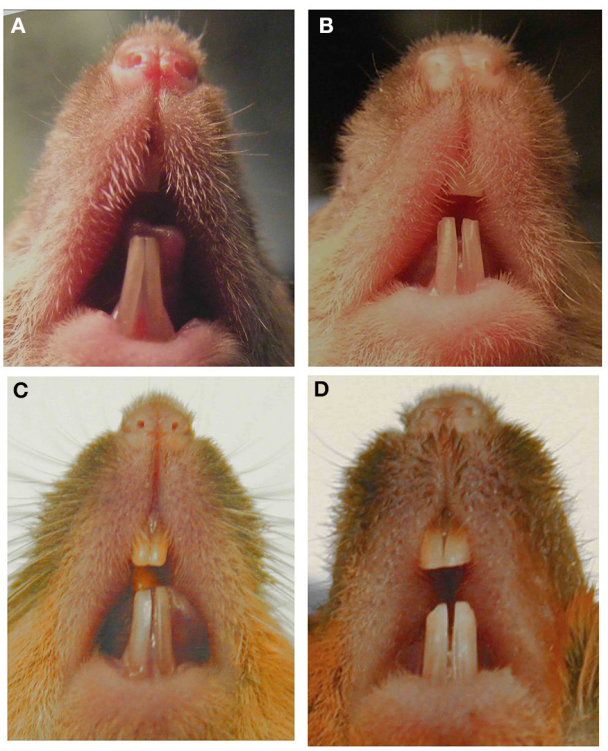

FIGURE 1 | Images of murine incisors from Amelx null mice. Null mice with mixed genetic background and phenotypic variability in **(A)** 7-week male, **(B)** 8-week male, **(C)** 6-month male, **(D)** 6-month female. This figure was originally published in Li et al. (2014).

such a way that deletion of the gene segment between LOX-P sites will lead to a tissue specific null mutation in the offspring that have both Cre and LOX-P genes. This strategy may avoid lethality as the Cre recombinase, under control of a tissue specific promoter, may be expressed later in development and in only the target tissues.

Using the Cre-lox approach, a deletion was generated in the ARHGAP6 gene which also removed the amelogenin gene localized to an ARHGAP6 intron, leading to an enamel defect (Prakash et al., 2005). A mouse that expressed the Cre recombinase under control of the Amelogenin regulatory sequences was mated with mice with a floxed TGFβ receptor II gene to generate enamel pathology due to deletion of receptor activity (Cho et al., 2013). Mice with the K14 promoter regulated Cre recombinase were mated to floxed Rac1 mice leading to ameloblast cell changes and enamel defects (Huang et al., 2011). K14-Cre was also used to delete FAM20C, again leading to enamel defects (Wang et al., 2013).

KNOCK-IN APPROACHES

This strategy is similar to that used for a knock-out mouse, except the vector does not contain a deletion to generate a null mouse. Instead the knock-in vector replaces the endogenous gene with a gene segment with a mutation in a region of interest of the translated protein or with a reporter gene. This mouse will express a mutated protein or reporter in place of the wild-type protein.

N- or C-terminal coding regions of the amelogenin gene were removed in a knock-in model that addressed function of domains of the amelogenin protein (Zhu et al., 2006). The enamelin gene was replaced by the LacZ gene to generate a knock-in mouse with enamel defects (Hu et al., 2008). A similar approach was used for a knock-in of the KLK4 gene (Simmer et al., 2009). This approach allows detection of tissue specific gene expression while generating a null mutation in the gene of interest.

ANALYSIS OF GENETICALLY MODIFIED RODENT ENAMEL

MINERAL CONTENT

The mineral content of wild-type rodent enamel has been reported to range from 86.2% (by volume) (Angmar et al., 1963) to 95.06% (by volume) (Schmitz et al., 2014), values that depend greatly on the enamel composition model used. Rodent enamel has a very broad range of mineral content, both during development (molars) and in continuously erupting incisors. When enamel is affected by genetically altering enamel genes in rodents, mineralization defects are common. However, assessment of degree of mineralization in poorly mineralized enamel is technically challenging. Hydroxyapatite (HA) content in enamel can be quantified through direct and indirect methods.

The most direct method to measure the mineral density of enamel is to perform the ashing technique, wherein adult rodent incisors are microdissected. Enamel is lifted off the dentin in 1-mm wide strips from secretory (apical) through maturation stages (incisal) with a scalpel blade (**Figure 2A**). The weight of each strip is measured before and after heating (ashing) to determine the relative mineral and organic content (Smith et al., 2005, 2009). The erupted portions of WT incisors are fully mineralized and thus too hard to cut with a scalpel blade and therefore not analyzed. Ashing has been used to determine mineral density in normal and genetically altered mice with mineralization defects: Enam$^{-/-}$, Ambn^{-}, Mmp20^{-}, and KLK4$^{-/-}$ (Smith et al., 2011b). While ashing is the most direct and accurate method to determine mineral density, it is destructive, time-consuming and lacks of reproducibility (Smith et al., 2011a; Schmitz et al., 2014). Furthermore, ashing requires advanced technical expertise to process the enamel strips.

Backscattered SEM (BSE) can also be used to quantitate mineralization of rodent enamel, either for visualization of enamel surface mineralization (Smith et al., 2009) or for investigating internal enamel mineralization in cross-section (Bronckers et al., 2013; Hu et al., 2014; Lyaruu et al., 2014). BSE relies on the linear relationship between the intensity of the BSE signal and the atomic number of a compound. Mineral densities are derived from the gray level of the BSE micrograph. Four-level color mapping has been used to aid visualization of mineral density differences across the thickness of rodent enamel (Smith et al., 2011b). For the most accurate assessment of mineral density, BSE should be used in combination with either μCT or ashing (Schmitz et al., 2014).

Micro-computed tomography (μCT) is a non-destructive method that utilizes differences in x-ray intensity before and after passing through an object (**Figure 2E**). Validity of enamel density measurements depends on calibration with hydroxyapatite (HA) standards (phantoms) (Schweizer et al., 2007), and the μCT has limitations in terms of the range of mineral densities it can detect. For example, μCT cannot be used to analyze secretory-stage enamel because of the similarities in densities between dentin and partially mineralized enamel. The lower range (secretory stage, hypoplastic, or hypomature enamel) of mineral densities are therefore not detectable. Ashing has been shown to be a more reliable method to analyze enamel with low mineral content (Schmitz et al., 2014). The upper range (over 1.2 g/cm^3) of enamel mineralization must be extrapolated when using the Scanco μCT instrument, which is calibrated using HA phantoms between 0 and 1.2 g/cm^3. μCT results correspond well to direct measurements by ashing and BSE (Schmitz et al., 2014).

μCT-based mineral density values of developing WT mouse incisor enamel range from 0.7 to 2.97 g HA/cm^3, using phantoms with a broad range of densities (Schweizer et al., 2007) and the Skyscan μCT instrument. Fully mineralized WT incisor enamel measured using a Scanco μCT instrument was 2.7 g HA/cm^3, a relative value (Bronckers et al., 2013; Lyaruu et al., 2014). It is important to note that interaction with the x-ray beam can change the sample properties (beam-hardening), which can greatly influence μCT measurements of mineral density (Burghardt et al., 2008; Fajardo et al., 2009; Hamba et al., 2012). Furthermore, manual contouring of volumes-of-interest (VOIs) for μCT can lead to inter- and intra-operator error. Therefore, enamel volume measurements are sensitive to user error and should be performed by a single operator (Schmitz et al., 2014). When reporting enamel mineral density values, it is important to understand the limitation of the method used and whether the reported values are relative or absolute.

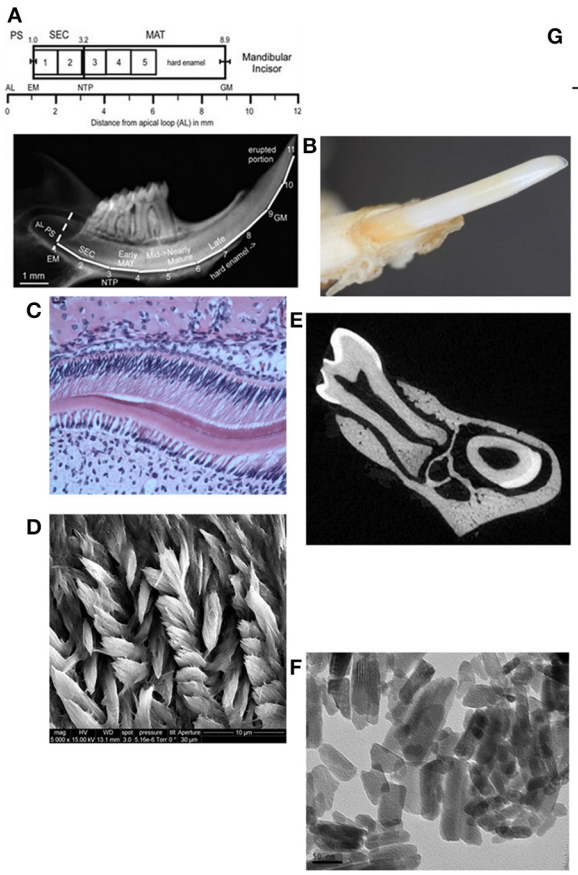

G Scale	Properties measured	Methods
Macro ~1-10 mm	Mineral density	Ashing: *excludes erupted enamel*
	Pigment	Color analysis: *excludes unerupted enamel*
Micro ~1-50 μm	Mineral density	Backscattered SEM μCT: *limited detection range*
	Prism structure, cells & proteins	Microscopy: light & SEM Histology Immunolocalization
	Mechanical properties	Microindentation
Nano ~50-100 nm	Crystal structure, cells & proteins	TEM Colloidal gold ICC Field emission SEM Helium Ion Microscopy
	Mechanical properties	Nanoindentation
	Elemental mapping	Energy dispersive x-ray analysis Atom probe tomography

FIGURE 2 | Summary of methods for analyzing genetically modified rodent enamel. (A–F) Representative images of WT mouse enamel analyzed by different methods are shown, with the corresponding table **(G)** in which methods are separated according to scale (mm, μm, and nm) and enamel properties of interest to analyze and compare mutant enamel with WT: mineral density, pigment, structure of prisms and crystals, cells, proteins, mechanical properties and elemental mapping. Within the macro scale (~1–10 mm) of enamel analysis **(A)** mineral density can be determined by enamel ashing. The representative 1-mm strips of mandibular incisor enamel dissected and processed for ashing are shown below the locations of stages of enamel development on mouse incisors in relation to molars (from Smith et al., 2011a). Note that ashing cannot be performed on highly mineralized and erupted enamel (after strip #5 or 6 mm from the apical loop). AL, apical loop; EM, start of enamel matrix formation; PS, presecretory stage; SEC, secretory stage; MAT, maturation stage; NTP, no Tomes' processes in ameloblasts; GM, gingival margin. **(B)** Pigment analysis of adult erupted WT incisor enamel using CIELAB color channels following high-resolution photography. Within the micro scale (~1–50 μm) of enamel analysis, there is a wide range of microscopy methods utilized to investigate enamel prism structure, ameloblasts and enamel proteins, including **(C)** light microscopy to analyze H&E stained paraffin sections of developing WT mouse molar enamel, and **(D)** SEM to analyze enamel prism structure. **(E)** μCT can be used to determine mineral density. Within the nano scale (50–100 nm), **(F)** TEM can be used to analyze enamel crystals, and additional high-resolution microscopy methods can be used to analyze the relationships between enamel prisms and the organic matrix (enamel proteins). Nanoindentation can be used to determine mechanical properties on a nano-scale, i.e., to measure differences between adjacent enamel prisms. Furthermore, elemental mapping of enamel can give information about the molecules that form enamel crystals **(G)**.

ENAMEL STRUCTURE

Analyzing fully mineralized rodent enamel structure microscopically (other than SEM) is technically challenging due to the high level of mineralization and resulting tissue hardness. Sample preparation issues related to sectioning fully mineralized enamel or decalcification of enamel are well documented (Singhrao et al., 2010; Sun et al., 2012). To assess and compare enamel structure of mutant mice to WT, scanning electron microscopy (SEM) is commonly used. Rodent enamel is extracted, fixed in most cases, then fractured or sectioned before coating with gold and/or palladium for SEM analysis. Fracturing enamel allows visualization of enamel thickness and structure in fixed but otherwise unaltered tissue. Furthermore, fracturing of rodent incisors allows for visualization of enamel at specific developmental landmarks, which is useful to compare mutant enamel to WT. Fractured incisor enamel showed improvements in the rod structure of LRAP/Amelx$^{-/-}$ mice, compared to Amelx$^{-/-}$ incisor enamel which is aprismatic, indicative of partial rescue with the amelogenin splice variant (Gibson et al., 2009). When incisor enamel was fractured from mice overexpressing amelotin, the enamel was thin, with no decussating enamel prisms (Lacruz et al., 2012). Enam$^{+/-}$ incisor enamel had decussating prisms but fractured differently than WT, while Enam$^{-/-}$ incisor enamel was aprismatic (Hu et al., 2014).

To observe the enamel prism structure in more detail, plastic embedding allows for undecalcified samples to be sectioned. Furthermore, analysis of transverse sections through rodent incisors or molars by SEM allows for enamel thickness measurements. Ground sections are created by cutting thick sections (1–2 mm) of plastic embedded teeth and subsequent polishing of the section until the desired section thickness is reached. After the sections are polished, they are acid-etched, often with phosphoric acid to reveal the enamel rod organization by removing a thin layer of mineral from the polished surface (**Figure 2D**). Polished and etched first molar enamel from M180/LRAP/Amelx$^{-/-}$ mice, when observed by SEM, showed that the enamel structure and thickness were similar to WT, and improved over M180/Amelx$^{-/-}$ and LRAP/Amelx$^{-/-}$, indicating complementarity of the transgenes M180 and LRAP in enamel formation (Gibson et al., 2011). Transmission electron microscopy (TEM) can be used to observe enamel crystallite morphology (**Figure 2F**) and requires ultrathin sections of 80–100 nm.

ENAMEL PROTEINS AND AMELOBLASTS

To identify enamel proteins in developing rodent enamel, immunogold labeling has been used. Colloidal gold particles are used to immunodetect to secondary antibodies which are in turn bound to primary antibodies designed to bind a specific protein. Gold is used for its high electron density which increases electron scatter to give high contrast dark spots under SEM or TEM. Mmp20 was localized to the forming outer enamel using electron immunogold staining (Bourd-Boittin et al., 2004). Dual-immunogold labeling has been used to visualize and quantify the presence of amelogenin and ameloblastin in secretory granules, and showed that amelogenin and ameloblastin are almost always packaged together for secretion, suggesting a functional relationship between these two enamel proteins (Zalzal et al., 2008). To understand the spatial localization of amelogenins in relation to the mineral crystallites, immunogold labeling with field emission SEM (FESEM) showed that amelogenins were located along the side faces of the apatite crystals (Du et al., 2009). TEM has also been used to visualize the secretion and localization of amelogenin in Enam$^{-/-}$ mice (Hu et al., 2014).

To determine the distribution of the proteins ODAM and AMTN in maturation stage rodent incisors, postembedding colloidal gold immunocytochemistry showed localization to the basal lamina associated with maturation stage ameloblasts and suggested that the basal lamina is dynamic during the maturation process (Dos Santos Neves et al., 2012). The effects of overexpression of AMTN in cellular morphology of ameloblasts at different stages of enamel formation were observed by TEM (Lacruz et al., 2012).

Paraffin is most frequently used for histological embedding because it has a similar density as most soft tissues. However, mineralized tissues cannot be sectioned properly when embedded in paraffin because calcium and paraffin have different densities. After decalcification of enamel, the mineralized enamel layer is a blank space. Paraffin embedding is suitable for analysis of developing or embryonic enamel, since enamel mineralization takes place around birth, P0 in mice. The timing of mineralization should be considered when deciding which type of histological sections to use. In general, WT enamel tissue does not need decalcification if mice are 3 days postnatal or younger.

Ameloblasts can only be studied in sections of developing enamel (**Figure 2C**), as erupted enamel is acellular. Decalcified tissues can be cut more thinly than calcified tissue, allowing the sections to be studied under a wide range of magnification and microscopy techniques (TEM, environmental SEM, light microscopy, fluorescent microscopy, and confocal microscopy). However, it is extremely difficult to preserve mature enamel in decalcified sections. Decalcification removes the mineralized part of hard tissues, making the histologic examination of enamel less than optimal. Therefore, erupted enamel must be studied in calcified sections.

ENAMEL MECHANICAL PROPERTIES

Mechanical property analysis to determine enamel functionality allows for the best endpoint assessment of enamel performance. Indentation is a non-destructive method to measure mechanical properties of materials and tissues. Generally, either microindentation hardness testing (microhardness) or nanoindentation has been used to determine enamel mechanical properties. Microhardness is measured using a diamond indenter with a specific geometry and makes an indent of about 50 μm into the tissue surface, using loads of up to 2N. The surface area of the indent is used to calculate the hardness value. Microhardness measurements of rodent enamel have suggested that its organic content significantly influences its mechanical properties (Baldassarri et al., 2008). Unfortunately microhardness testing is not optimal for measuring enamel from mice with genetically modified enamel genes, since these mutations often cause a hypoplastic (thin enamel) phenotype. While WT incisor enamel is approximately 100 μm thick, WT molar enamel is only about 50–60 μm thick (Gibson et al., 2011; Pugach et al., 2013). Amelogenin$^{-/-}$ molar enamel is between 10 and 20 μm thick (Gibson et al., 2011; Pugach et al., 2013), which means that the microhardness indentation of 50 μm would extend beyond the KO enamel, making impossible to contain the indent with the enamel tissue. Furthermore, the loads used in microhardness testing may be too high to measure mutant rodent enamel. This problem was encountered when microhardness testing was attempted on incisor enamel from mice overexpressing the AMTN transgene, which was too brittle for measurements to be possible (Lacruz et al., 2012).

Nanoindentation uses small loads and tip sizes, with the indentation area measuring a few microns. The load and depth of penetration of the tip are plotted to create a load-displacement curve, which is used to calculate the mechanical properties: (1) Young's (elastic) modulus, or the elasticity of the material, and (2) hardness as a function of depth, which is slightly different from microhardness. Using a load of 1350 μN which produced an indentation of 3 μm, transgenic mouse enamel lacking the N-terminus of amelogenin (M180ΔA-FLAG) had 22% lower hardness and 24% lower elastic modulus than WT (Fong et al., 2003). Transgenic mouse enamel lacking the C-terminus of amelogenin (M180ΔB-FLAG) had 8% lower hardness and 18% lower

elastic modulus. This decrease in mechanical properties was proposed to be due to defective amelogenin self-assembly due to misassembled nanospheres, compromising the integrity of the organic phase and thus the mechanical integrity. These data confirm the importance of the N- and C-termini of amelogenin in enamel formation (Fong et al., 2003).

Nanoindentation was used to measure mechanical properties of mice overexpressing different transgenes representing amelogenin cleavage products and isoforms in amelogenin null backgrounds. Amelogenin$^{-/-}$ (KO) molar enamel has approximately 60% lower hardness and 58% lower elastic modulus than WT (Li et al., 2008; Pugach et al., 2013). Molar enamel from mice expressing only the most abundant amelogenin isoform (M180/Amelx$^{-/-}$) had similar mechanical properties as WT, indicating rescue from this transgene even though the enamel thickness was not fully restored. Mice lacking the C-terminus of amelogenin (CTRNC/Amelx$^{-/-}$) had 33% lower hardness and 38% lower elastic modulus than WT, again illustrating the importance of the C-terminus (Pugach et al., 2013). Recent nanoindentation data suggests that mice expressing the other abundant isoform, LRAP have molar enamel with 40% lower hardness and 34% lower elastic modulus than WT (**Figure 3**), an improvement over KO, which suggests that while the LRAP transgene was unable to rescue the mechanical properties as well as M180, it does play some role in the final mechanical properties of enamel. When the two transgenes, M180 and LRAP, are expressed in a KO background, the mechanical properties are unsurprisingly similar to WT (**Figure 3**).

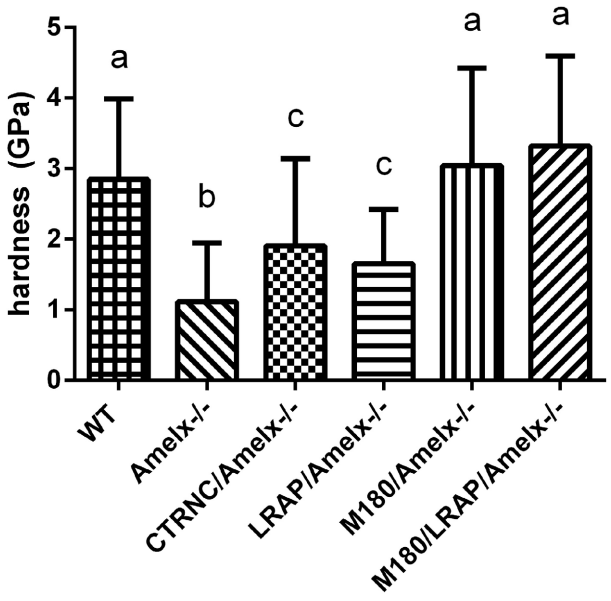

FIGURE 3 | Mouse molar enamel hardness measured by nanoindentation. WT, M180/Amelx$^{-/-}$, and M180/LRAP/Amelx$^{-/-}$ (a) were not different from each other but were significantly harder than CTRNC/Amelx$^{-/-}$ (c), LRAP/Amelx$^{-/-}$ (c) and Amelx$^{-/-}$ (b) enamel ($p < 0.05$). CTRNC/Amelx$^{-/-}$ and LRAP/Amelx$^{-/-}$ (c) were not different from each other but were significantly harder than Amelx$^{-/-}$ enamel ($p < 0.05$).

ENAMEL PIGMENT

Unlike human incisors, rodent incisors have a yellowish pigmentation due to a higher presence of iron in the outer enamel layer (Halse, 1972). It has been suggested that iron incorporation in enamel serves as a strengthening agent to resist cracking and abrasion, and that animals that feed on harder prey may have more iron (Motta, 1987). Many studies in which knockout or transgenic rodents are generated with alterations of enamel genes, loss of incisor pigment has been reported, indicating that iron incorporation is involved in normal enamel formation (Gibson et al., 2001; Paine et al., 2005) (**Figure 2B**). The variability of mouse incisor enamel pigment that is evident in **Figure 4** is the result of mutations to different regions of a single gene, amelogenin, and its isoforms. A recent study confirmed that iron is present in rodent molars in addition to their incisors, indicating the iron is an essential component for rodent enamel formation (Wen and Paine, 2013). It was therefore suggested that iron incorporation may be final refinement for enamel mineralization, providing extra strength and acid resistance. However, the presence of iron is linked to erupting nature of the rodent tooth since there is a significantly higher iron accumulation in incisors compared to molars (Wen and Paine, 2013).

Morphometric measurements of rodent incisor color and whiteness are essential to aid in interpretation of phenotype outcomes caused by genetic alterations of enamel genes. A detailed method to measure rodent incisor color and whiteness has been recommended (Coxon et al., 2012). Incisors are held in black modeling clay and imaged in 2D with an SLR camera using an established image analysis system (Brook et al., 2007) and macro photo lens. Using Adobe Photoshop, red, green, and blue (RGB) outputs were converted to CIELAB color space and whiteness using previously described methods (Guan et al., 2005; Smith et al., 2008).

Quantification of mutant enamel color and whiteness phenotypes using established methods is recommended for aiding in the understanding of the role of enamel proteins in its formation, and can allow for comparisons of mutant rodent models between investigators. The CIELAB or CIE (Kuehni, 1976) L*a*b

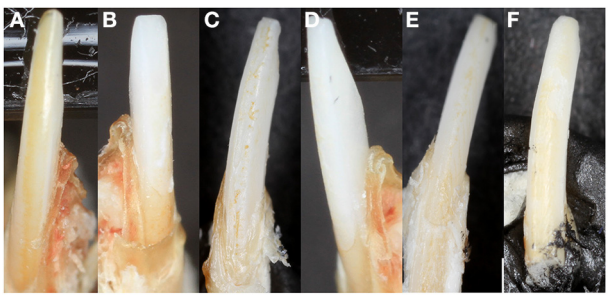

FIGURE 4 | Mouse incisor enamel pigment. (A) WT enamel has a pigment due to iron content, **(B)** Amelx$^{-/-}$ enamel is chalky white, **(C)** CTRNC/Amelx$^{-/-}$ has some improvement in pigment from Amelx$^{-/-}$, **(D)** LRAP/Amelx$^{-/-}$ enamel is chalky white like Amelx$^{-/-}$, **(E)** M180/Amelx$^{-/-}$ enamel has some improvement in pigment from Amelx$^{-/-}$, and **(F)** M180/LRAP/Amelx$^{-/-}$ enamel has significantly more pigment than Amelx$^{-/-}$ enamel.

values are perceptually based: L* is lightness related to physical intensity of a color, a* represents the red-green axis, and b* represents the yellow-blue color axis. The CIE whiteness index (WIC) has been used to describe tooth color for making porcelain veneers and whitening, where white is $L^* = 100$, $a^* = 0$ and $b^* = 0$. Mutant mouse incisor enamel has been measured using this technique and *Amelx* and *Enam* mutant mice had significantly lower yellow/blue (b) values and higher lightness (L) and whiteness (WIC) values than their WT counterparts (Coxon et al., 2012).

Mouse models with genetically modified enamel genes have been generated for the past two decades using a variety of methods including transgenics, knockouts, conditional knockouts, and knockins. These valuable research tools continue to be the most direct way to study enamel formation *in vivo* and Amelogenesis Imperfecta. Investigators have utilized a variety of methods to determine the outcome of generating mutant enamel, to observe mineral content, structure, mechanical properties, pigment, and in the case of developing enamel, ameloblasts (**Figure 2G**). In order for data characterizing enamel phenotypes from mice with mutated enamel genes to be compared to each other, it is necessary to have standardized workflow of analytical methods. Enamel development and mineralization is a dynamic and complex process, and correlating similarly measured data between mouse models could allow for increased understanding of the process of forming this extraordinarily intricate enamel tissue.

ACKNOWLEDGMENTS

Research reported in this publication was supported by the National Institute of Dental and Craniofacial Research of the National Institutes of Health, grants R00DE022624 (Megan K. Pugach) and R01DE011089 (Carolyn W. Gibson).

REFERENCES

Al-Shawi, R., Burke, J., Jones, C. T., Simons, J. P., and Bishop, J. O. (1988). A Mup promoter-thymidine kinase reporter gene shows relaxed tissue-specific expression and confers male sterility upon transgenic mice. *Mol. Cell. Biol.* 8, 4821–4828.

Angmar, B., Carlstrom, D., and Glas, J. E. (1963). Studies on the ultrastructure of dental enamel. IV. The mineralization of normal human enamel. *J. Ultrastruct. Res.* 8, 12–23.

Atsawasuwan, P., Lu, X., Ito, Y., Chen, Y., Gopinathan, G., Evans, C. A., et al. (2013). Expression and function of enamel-related gene products in calvarial development. *J. Dent. Res.* 92, 622–628. doi: 10.1177/0022034513487906

Baldassarri, M., Margolis, H. C., and Beniash, E. (2008). Compositional determinants of mechanical properties of enamel. *J. Dent. Res.* 87, 645–649. doi: 10.1177/154405910808700711

Bartlett, J. D. (2013). Dental Enamel Development: proteinases and their enamel matrix substrates. *ISRN Dent.* 2013:684607. doi: 10.1155/2013/684607

Bourd-Boittin, K., Septier, D., Hall, R., Goldberg, M., and Menashi, S. (2004). Immunolocalization of enamelysin (matrix metalloproteinase-20) in the forming rat incisor. *J. Histochem. Cytochem.* 52, 437–445. doi: 10.1177/002215540405200402

Bronckers, A. L., Gueneli, N., Lullmann-Rauch, R., Schneppenheim, J., Moraru, A. P., Himmerkus, N., et al. (2013). The intramembrane protease SPPL2A is critical for tooth enamel formation. *J. Bone Miner. Res.* 28, 1622–1630. doi: 10.1002/jbmr.1895

Brook, A. H., Smith, R. N., and Lath, D. J. (2007). The clinical measurement of tooth colour and stain. *Int. Dent. J.* 57, 324–330. doi: 10.1111/j.1875-595X.2007.tb00141.x

Burghardt, A. J., Kazakia, G. J., Laib, A., and Majumdar, S. (2008). Quantitative assessment of bone tissue mineralization with polychromatic micro-computed tomography. *Calcif. Tissue Int.* 83, 129–138. doi: 10.1007/s00223-008-9158-x

Caterina, J. J., Skobe, Z., Shi, J., Ding, Y., Simmer, J. P., Birkedal-Hansen, H., et al. (2002). Enamelysin (matrix metalloproteinase 20)-deficient mice display an amelogenesis imperfecta phenotype. *J. Biol. Chem.* 277, 49598–49604. doi: 10.1074/jbc.M209100200

Chen, E., Piddington, R., Decker, S., Park, J., Yuan, Z. A., Abrams, W. R., et al. (1994). Regulation of amelogenin gene expression during tooth development. *Dev. Dyn.* 199, 189–198. doi: 10.1002/aja.1001990304

Chen, X., Li, Y., Alawi, F., Bouchard, J. R., Kulkarni, A. B., and Gibson, C. W. (2011). An amelogenin mutation leads to disruption of the odontogenic apparatus and aberrant expression of Notch1. *J. Oral Pathol. Med.* 40, 235–242. doi: 10.1111/j.1600-0714.2010.00940.x

Cho, A., Haruyama, N., Hall, B., Danton, M. J., Zhang, L., Arany, P., et al. (2013). TGF-ss regulates enamel mineralization and maturation through KLK4 expression. *PLoS ONE* 8:e82267. doi: 10.1371/journal.pone.0082267

Chun, Y. H., Lu, Y., Hu, Y., Krebsbach, P. H., Yamada, Y., Hu, J. C., et al. (2010). Transgenic rescue of enamel phenotype in Ambn null mice. *J. Dent. Res.* 89, 1414–1420. doi: 10.1177/0022034510379223

Coxon, T. L., Brook, A. H., Barron, M. J., and Smith, R. N. (2012). Phenotype-genotype correlations in mouse models of amelogenesis imperfecta caused by Amelx and Enam mutations. *Cells Tissues Organs* 196, 420–430. doi: 10.1159/000336440

Dilella, A. G., Hope, D. A., Chen, H., Trumbauer, M., Schwartz, R. J., and Smith, R. G. (1988). Utility of firefly luciferase as a reporter gene for promoter activity in transgenic mice. *Nucleic Acids Res.* 16, 4159.

Dos Santos Neves, J., Wazen, R. M., Kuroda, S., Francis Zalzal, S., Moffatt, P., and Nanci, A. (2012). Odontogenic ameloblast-associated and amelotin are novel basal lamina components. *Histochem. Cell Biol.* 137, 329–338. doi: 10.1007/s00418-011-0901-4

Doyle, A., McGarry, M. P., Lee, N. A., and Lee, J. J. (2012). The construction of transgenic and gene knockout/knockin mouse models of human disease. *Transgenic Res.* 21, 327–349. doi: 10.1007/s11248-011-9537-3

Du, C., Fan, D., Sun, Z., Fan, Y., Lakshminarayanan, R., and Moradian-Oldak, J. (2009). Immunogold labeling of amelogenin in developing porcine enamel revealed by field emission scanning electron microscopy. *Cells Tissues Organs* 189, 207–211. doi: 10.1159/000151385

Dunglas, C., Septier, D., Paine, M. L., Zhu, D. H., Snead, M. L., and Goldberg, M. (2002). Ultrastructure of forming enamel in mouse bearing a transgene that disrupts the amelogenin self-assembly domains. *Calcif. Tissue Int.* 71, 155–166. doi: 10.1007/s00223-001-2116-5

Fajardo, R. J., Cory, E., Patel, N. D., Nazarian, A., Laib, A., Manoharan, R. K., et al. (2009). Specimen size and porosity can introduce error into microCT-based tissue mineral density measurements. *Bone* 44, 176–184. doi: 10.1016/j.bone.2008.08.118

Fong, H., White, S. N., Paine, M. L., Luo, W., Snead, M. L., and Sarikaya, M. (2003). Enamel structure properties controlled by engineered proteins in transgenic mice. *J. Bone Miner. Res.* 18, 2052–2059. doi: 10.1359/jbmr.2003.18.11.2052

Fukumoto, S., Kiba, T., Hall, B., Iehara, N., Nakamura, T., Longenecker, G., et al. (2004). Ameloblastin is a cell adhesion molecule required for maintaining the differentiation state of ameloblasts. *J. Cell Biol.* 167, 973–983. doi: 10.1083/jcb.200409077

Gibson, C. W., Li, Y., Daly, B., Suggs, C., Yuan, Z. A., Fong, H., et al. (2009). The leucine-rich amelogenin peptide alters the amelogenin null enamel phenotype. *Cells Tissues Organs* 189, 169–174. doi: 10.1159/000151384

Gibson, C. W., Li, Y., Suggs, C., Kuehl, M. A., Pugach, M. K., Kulkarni, A. B., et al. (2011). Rescue of the murine amelogenin null phenotype with two amelogenin transgenes. *Eur. J. Oral. Sci.* 119(Suppl. 1), 70–74. doi: 10.1111/j.1600-0722.2011.00882.x

Gibson, C. W., Yuan, Z. A., Hall, B., Longenecker, G., Chen, E., Thyagarajan, T., et al. (2001). Amelogenin-deficient mice display an amelogenesis imperfecta phenotype. *J. Biol. Chem.* 276, 31871–31875. doi: 10.1074/jbc.M104624200

Gibson, C. W., Yuan, Z. A., Li, Y., Daly, B., Suggs, C., Aragon, M. A., et al. (2007). Transgenic mice that express normal and mutated amelogenins. *J. Dent. Res.* 86, 331–335. doi: 10.1177/154405910708600406

Guan, Y. H., Lath, D. L., Lilley, T. H., Willmot, D. R., Marlow, I., and Brook, A. H. (2005). The measurement of tooth whiteness by image analysis and spectrophotometry: a comparison. *J. Oral Rehabil.* 32, 7–15. doi: 10.1111/j.1365-2842.2004.01340.x

Halse, A. (1972). An electron microprobe investigation of the distribution of iron in rat incisor enamel. *Scand. J. Dent. Res.* 80, 26–39.

Hamba, H., Nikaido, T., Sadr, A., Nakashima, S., and Tagami, J. (2012). Enamel lesion parameter correlations between polychromatic micro-CT and TMR. *J. Dent. Res.* 91, 586–591. doi: 10.1177/0022034512444127

Holcroft, J., and Ganss, B. (2011). Identification of amelotin- and ODAM-interacting enamel matrix proteins using the yeast two-hybrid system. *Eur. J. Oral. Sci.* 119(Suppl. 1), 301–306. doi: 10.1111/j.1600-0722.2011.00870.x

Hu, J. C., Hu, Y., Lu, Y., Smith, C. E., Lertlam, R., Wright, J. T., et al. (2014). Enamelin is critical for ameloblast integrity and enamel ultrastructure formation. *PLoS ONE* 9:e89303. doi: 10.1371/journal.pone.0089303

Hu, J. C., Hu, Y., Smith, C. E., McKee, M. D., Wright, J. T., Yamakoshi, Y., et al. (2008). Enamel defects and ameloblast-specific expression in Enam knock-out/lacz knock-in mice. *J. Biol. Chem.* 283, 10858–10871. doi: 10.1074/jbc.M710565200

Hu, J. C., Yamakoshi, Y., Yamakoshi, F., Krebsbach, P. H., and Simmer, J. P. (2005). Proteomics and genetics of dental enamel. *Cells Tissues Organs* 181, 219–231. doi: 10.1159/000091383

Huang, Z., Kim, J., Lacruz, R. S., Bringas, P. Jr., Glogauer, M., Bromage, T. G., et al. (2011). Epithelial-specific knockout of the Rac1 gene leads to enamel defects. *Eur. J. Oral. Sci.* 119(Suppl. 1), 168–176. doi: 10.1111/j.1600-0722.2011.00904.x

Kuehni, R. G. (1976). Color-tolerance data and the tentative CIE 1976 L a b formula. *J. Opt. Soc. Am.* 66, 497–500.

Kweon, Y. S., Lee, K. E., Ko, J., Hu, J. C., Simmer, J. P., and Kim, J. W. (2013). Effects of Fam83h overexpression on enamel and dentine formation. *Arch. Oral Biol.* 58, 1148–1154. doi: 10.1016/j.archoralbio.2013.03.001

Lacruz, R. S., Nakayama, Y., Holcroft, J., Nguyen, V., Somogyi-Ganss, E., Snead, M. L., et al. (2012). Targeted overexpression of amelotin disrupts the microstructure of dental enamel. *PLoS ONE* 7:e35200. doi: 10.1371/journal.pone.0035200

Li, Y., Konicki, W. S., Wright, J. T., Suggs, C., Xue, H., Kuehl, M. A., et al. (2014). Mouse genetic background influences the dental phenotype. *Cells Tissues Organs*. 198, 448–456. doi: 10.1159/000360157

Li, Y., Suggs, C., Wright, J. T., Yuan, Z. A., Aragon, M., Fong, H., et al. (2008). Partial rescue of the amelogenin null dental enamel phenotype. *J. Biol. Chem.* 283, 15056–15062. doi: 10.1074/jbc.M707992200

Lyaruu, D. M., Medina, J. F., Sarvide, S., Bervoets, T. J., Everts, V., Denbesten, P., et al. (2014). Barrier formation: potential molecular mechanisms of enamel fluorosis. *J. Dent. Res.* 93, 96–102. doi: 10.1177/0022034513510944

Mansour, S. L., Thomas, K. R., and Capecchi, M. R. (1988). Disruption of the proto-oncogene int-2 in mouse embryo-derived stem cells: a general strategy for targeting mutations to non-selectable genes. *Nature* 336, 348–352. doi: 10.1038/336348a0

Motta, P. (1987). A quantitative analysis of ferric iron in butterflyfish teeth (Chaetodontidae Perciformes) and the relationship to feeding ecology. *Can. J. Zool.* 65, 106–112.

Paine, M. L., Luo, W., Wang, H. J., Bringas, P. Jr., Ngan, A. Y., Miklus, V. G., et al. (2005). Dentin sialoprotein and dentin phosphoprotein overexpression during amelogenesis. *J. Biol. Chem.* 280, 31991–31998. doi: 10.1074/jbc.M502991200

Paine, M. L., Wang, H. J., Luo, W., Krebsbach, P. H., and Snead, M. L. (2003). A transgenic animal model resembling amelogenesis imperfecta related to ameloblastin overexpression. *J. Biol. Chem.* 278, 19447–19452. doi: 10.1074/jbc.M300445200

Paine, M. L., Zhu, D. H., Luo, W., and Snead, M. L. (2004). Overexpression of TRAP in the enamel matrix does not alter the enamel structural hierarchy. *Cells Tissues Organs* 176, 7–16. doi: 10.1159/000075023

Prakash, S. K., Gibson, C. W., Wright, J. T., Boyd, C., Cormier, T., Sierra, R., et al. (2005). Tooth enamel defects in mice with a deletion at the Arhgap 6/Amel X locus. *Calcif. Tissue Int.* 77, 23–29. doi: 10.1007/s00223-004-1213-7

Pugach, M. K., Li, Y., Suggs, C., Wright, J. T., Aragon, M. A., Yuan, Z. A., et al. (2010). The amelogenin C-terminus is required for enamel development. *J. Dent. Res.* 89, 165–169. doi: 10.1177/0022034509358392

Pugach, M. K., Suggs, C., Li, Y., Wright, J. T., Kulkarni, A. B., Bartlett, J. D., et al. (2013). M180 amelogenin processed by MMP20 is sufficient for decussating murine enamel. *J. Dent. Res.* 92, 1118–1122. doi: 10.1177/0022034513506444

Schmitz, J. E., Teepe, J. D., Hu, Y., Smith, C. E., Fajardo, R. J., and Chun, Y. H. (2014). Estimating mineral changes in enamel formation by ashing/BSE and microCT. *J. Dent. Res.* 93, 256–262. doi: 10.1177/0022034513520548

Schweizer, S., Hattendorf, B., Schneider, P., Aeschlimann, B., Gauckler, L., Muller, R., et al. (2007). Preparation and characterization of calibration standards for bone density determination by micro-computed tomography. *Analyst* 132, 1040–1045. doi: 10.1039/b703220j

Sharma, R., Tye, C. E., Arun, A., Macdonald, D., Chatterjee, A., Abrazinski, T., et al. (2011). Assessment of dental fluorosis in Mmp20 +/− mice. *J. Dent. Res.* 90, 788–792. doi: 10.1177/0022034511398868

Shin, M., Hu, Y., Tye, C. E., Guan, X., Deagle, C. C., Antone, J. V., et al. (2014). Matrix metalloproteinase-20 over-expression is detrimental to enamel development: a Mus musculus model. *PLoS ONE* 9:e86774. doi: 10.1371/journal.pone.0086774

Simmer, J. P., Hu, Y., Lertlam, R., Yamakoshi, Y., and Hu, J. C. (2009). Hypomaturation enamel defects in Klk4 knockout/LacZ knockin mice. *J. Biol. Chem.* 284, 19110–19121. doi: 10.1074/jbc.M109.013623

Singhrao, S. K., Sloan, A. J., Smith, E. L., and Archer, C. W. (2010). Technical advances in the sectioning of dental tissue and of on-section cross-linked collagen detection in mineralized teeth. *Microsc. Res. Tech.* 73, 741–745. doi: 10.1002/jemt.20815

Smith, C. E., Chong, D. L., Bartlett, J. D., and Margolis, H. C. (2005). Mineral acquisition rates in developing enamel on maxillary and mandibular incisors of rats and mice: implications to extracellular acid loading as apatite crystals mature. *J. Bone Miner. Res.* 20, 240–249. doi: 10.1359/JBMR.041002

Smith, C. E., Hu, Y., Richardson, A. S., Bartlett, J. D., Hu, J. C., and Simmer, J. P. (2011a). Relationships between protein and mineral during enamel development in normal and genetically altered mice. *Eur. J. Oral. Sci.* 119(Suppl. 1), 125–135. doi: 10.1111/j.1600-0722.2011.00871.x

Smith, C. E., Richardson, A. S., Hu, Y., Bartlett, J. D., Hu, J. C., and Simmer, J. P. (2011b). Effect of kallikrein 4 loss on enamel mineralization: comparison with mice lacking matrix metalloproteinase 20. *J. Biol. Chem.* 286, 18149–18160. doi: 10.1074/jbc.M110.194258

Smith, C. E., Wazen, R., Hu, Y., Zalzal, S. F., Nanci, A., Simmer, J. P., et al. (2009). Consequences for enamel development and mineralization resulting from loss of function of ameloblastin or enamelin. *Eur. J. Oral Sci.* 117, 485–497. doi: 10.1111/j.1600-0722.2009.00666.x

Smith, R. N., Collins, L. Z., Naeeni, M., Joiner, A., Philpotts, C. J., Hopkinson, I., et al. (2008). The *in vitro* and *in vivo* validation of a mobile non-contact camera-based digital imaging system for tooth colour measurement. *J. Dent.* 36(Suppl. 1), S15–S20. doi: 10.1016/j.jdent.2008.02.002

Stahl, J., Nakano, Y., Kim, S. O., Gibson, C. W., Le, T., and Denbesten, P. (2013). Leucine rich amelogenin peptide alters ameloblast differentiation *in vivo*. *Matrix Biol.* 32, 432–442. doi: 10.1016/j.matbio.2013.05.004

Sun, J. X., Horst, O. V., Bumgarner, R., Lakely, B., Somerman, M. J., and Zhang, H. (2012). Laser capture microdissection enables cellular and molecular studies of tooth root development. *Int. J. Oral Sci.* 4, 7–13. doi: 10.1038/ijos.2012.15

Sweetser, D. A., Hauft, S. M., Hoppe, P. C., Birkenmeier, E. H., and Gordon, J. I. (1988). Transgenic mice containing intestinal fatty acid-binding protein-human growth hormone fusion genes exhibit correct regional and cell-specific expression of the reporter gene in their small intestine. *Proc. Natl. Acad. Sci. U.S.A.* 85, 9611–9615.

Theopold, U., and Kohler, G. (1990). Partial tolerance in beta-galactosidase-transgenic mice. *Eur. J. Immunol.* 20, 1311–1316. doi: 10.1002/eji.1830200617

Wang, S. K., Aref, P., Hu, Y., Milkovich, R. N., Simmer, J. P., El-Khateeb, M., et al. (2013). FAM20A mutations can cause enamel-renal syndrome (ERS). *PLoS Genet.* 9:e1003302. doi: 10.1371/journal.pgen.1003302

Wazen, R. M., Moffatt, P., Zalzal, S. F., Yamada, Y., and Nanci, A. (2009). A mouse model expressing a truncated form of ameloblastin exhibits dental and junctional epithelium defects. *Matrix Biol.* 28, 292–303. doi: 10.1016/j.matbio.2009.04.004

Wen, X., and Paine, M. L. (2013). Iron deposition and ferritin heavy chain (Fth) localization in rodent teeth. *BMC Res. Notes* 6:1. doi: 10.1186/1756-0500-6-1

Wright, J. T., Hart, T. C., Hart, P. S., Simmons, D., Suggs, C., Daley, B., et al. (2009). Human and mouse enamel phenotypes resulting from mutation or altered expression of AMEL, ENAM, MMP20 and KLK4. *Cells Tissues Organs* 189, 224–229. doi: 10.1159/000151378

Zalzal, S. F., Smith, C. E., and Nanci, A. (2008). Ameloblastin and amelogenin share a common secretory pathway and are co-secreted during

enamel formation. *Matrix Biol.* 27, 352–359. doi: 10.1016/j.matbio.2008.01.003

Zhu, D., Paine, M. L., Luo, W., Bringas, P. Jr., and Snead, M. L. (2006). Altering biomineralization by protein design. *J. Biol. Chem.* 281, 21173–21182. doi: 10.1074/jbc.M510757200

Conflict of Interest Statement: The authors declare that the research was conducted in the absence of any commercial or financial relationships that could be construed as a potential conflict of interest.

Received: 16 June 2014; accepted: 01 August 2014; published online: 17 September 2014.

Citation: Pugach MK and Gibson CW (2014) Analysis of enamel development using murine model systems: approaches and limitations. Front. Physiol. ***5****:313. doi: 10.3389/fphys.2014.00313*

This article was submitted to Craniofacial Biology, a section of the journal Frontiers in Physiology.

frontiers in PHYSIOLOGY

ORIGINAL RESEARCH ARTICLE
published: 25 July 2014
doi: 10.3389/fphys.2014.00277

Comparison of two mouse ameloblast-like cell lines for enamel-specific gene expression

Juni Sarkar[1], Emil J. Simanian[1], Sarah Y. Tuggy[1], John D. Bartlett[2], Malcolm L. Snead[1], Toshihiro Sugiyama[3] and Michael L. Paine[1]*

[1] Center for Craniofacial Molecular Biology, Division of Biomedical Sciences, Herman Ostrow School of Dentistry of USC, University of Southern California, Los Angeles, CA, USA
[2] Department of Mineralized Tissue Biology, The Forsyth Institute, Cambridge, MA, USA
[3] Department of Biochemistry, Akita University Graduate School of Medicine, Hondo, Akita, Japan

Edited by:
Bernhard Ganss, University of Toronto, Canada

Reviewed by:
Charles Shuler, University of British Columbia Faculty of Dentistry, Canada
Ariane Berdal, UMRS 872 INSERM University Paris-Diderot Team 5, France

***Correspondence:**
Michael L. Paine, Center for Craniofacial Molecular Biology, Division of Biomedical Sciences, Herman Ostrow School of Dentistry of USC, University of Southern California, Los Angeles, CA 90033, USA
e-mail: paine@usc.edu

Ameloblasts are ectoderm-derived cells that produce an extracellular enamel matrix that mineralizes to form enamel. The development and use of immortalized cell lines, with a stable phenotype, is an important contribution to biological studies as it allows for the investigation of molecular activities without the continuous need for animals. In this study we compare the expression profiles of enamel-specific genes in two mouse derived ameloblast-like cell lines: LS8 and ALC cells. Quantitative PCR analysis indicates that, relative to each other, LS8 cells express greater mRNA levels for genes that define secretory-stage activities (*Amelx*, *Ambn*, *Enam*, and *Mmp20*), while ALC express greater mRNA levels for genes that define maturation-stage activities (*Odam* and *Klk4*). Western blot analyses show that Amelx, Ambn, and Odam proteins are detectable in ALC, but not LS8 cells. Unstimulated ALC cells form calcified nodules, while LS8 cells do not. These data provide greater insight as to the suitability of both cell lines to contribute to biological studies on enamel formation and biomineralization, and highlight some of the strengths and weaknesses when relying on enamel epithelial organ-derived cell lines to study molecular activities of amelogenesis.

Keywords: amelogenesis, ameloblast, cell culture, LS8, ALC and biomineralization

INTRODUCTION

Dental enamel, the most highly mineralized and hardest tissue in vertebrates, is comprised of highly organized hydroxyapatite (Hap) crystallites formed by ameloblast cells (Smith, 1998). Dental enamel formation is tightly controlled by ameloblast cells whose differential activities toward enamel formation can be broadly divided into the initial secretory-stage, followed by a maturation-stage (Smith, 1998; Lacruz et al., 2013b). The enamel organ transcriptome for secretory-stage vs. maturation-stage amelogenesis is remarkably different from one another and highlights the changing cellular events orchestrated for each stage of enamel formation (Lacruz et al., 2012c, 2013b). There is a lack of available immortalized ameloblast-derived cell lines and this limits the possibilities to explore in detail the cellular events characteristic of ameloblasts through the different stages of amelogenesis, thus increasing the immediate need for animal experimentation. The few available ameloblast-like cell lines that are under investigation by the research community include mouse LS8 (Chen et al., 1992) and ALC (Nakata et al., 2003), rat HAT-7 (Kawano et al., 2002) and SF2-24 (Arakaki et al., 2012), and porcine PABSo-E (Denbesten et al., 1999) cells. LS8 cells have been used extensively to study amelogenin (*Amelx*) (Zhou and Snead, 2000; Zhou et al., 2000; Xu et al., 2006, 2007a,b) and ameloblastin (*Ambn*) (Dhamija et al., 1999; Dhamija and Krebsbach, 2001) gene promoter activities, and also fluoride uptake mechanisms and related endoplasmic reticulum (ER) stress activities (Kubota et al., 2005). LS8 (Lacruz et al., 2012a) and HAT-7 cells (Zheng et al., 2013) have been used to investigate circadian rhythm gene activities related to enamel formation. When exposed to sonic hedgehog at 100 ng/ml ALC cells are more completely differentiated into ameloblast-lineage cells, as determined by an increase in Amelx and Ambn mRNA levels (Takahashi et al., 2007). PABSo-E cells have been used to study calcium-sensing receptor activities in enamel formation (Mathias et al., 2001). PABSo-E (Duan et al., 2011) and LS8 (Shapiro et al., 2007; Lacruz et al., 2013a) cells have also been used to study endocytotic events in amelogenesis. ALC cells are noted to form calcified nodules when cultured in conditioned Dulbecco's modified Eagle's medium (DMEM) (Nakata et al., 2003), suggesting that ALC cells may be a model more suitable to the study of maturation-stage events of amelogenesis, such as ion transport associated with mineral phase maturation.

In this study we compare the molecular profiles of selected enamel-specific genes, and the ability to form calcified nodules in the two mouse-derived ameloblast-like cells: the Swiss-Webster derived LS8 cells (Chen et al., 1992) and the C57BL/6J derived and

Abbreviations: Actb, beta actin; Gapdh, glyceraldehyde-3-phosphate dehydrogenase; Amelx, amelogenin; Ambn, ameloblastin; Enam, enamelin; Mmp20, matrix metallopeptidase 20; Amtn, amelotin; Odam, odontogenin ameloblast associated; Klk4, kallikrein related-peptidase 4; DMEM, Dulbecco's modified Eagle's medium; PN, post natal; RIPA buffer, radio-immunoprecipitation assay buffer; BCA, bicinchoninic acid; SDS, sodium dodecyl sulfate.

ALC cells (Nakata et al., 2003). This comparative investigation better characterizes both cell lines, and identifies some of the advantages of experimenting with one cell line in preference to the other, to focus studies to ameloblast-specific cellular phenomena such as matrix formation vs. mineral maturation.

MATERIALS AND METHODS

ANIMALS AND TISSUE PREPARATION

Swiss-Webster mice were treated in accordance with Institutional and Federal guidelines. For quantitative real-time PCR and Western blot analysis, the first molars from mice at postnatal (PN) days 3, 6, and 9 were extracted and total RNA and protein recovered for analysis. These three PN time points were chosen to demonstrate the shift in ameloblast gene expression from primarily secretory-stage activities (PN3) to a stage where maturation-stage activities predominate (PN9); and a point midway (PN6) where there is a mixed population of secretory and maturation ameloblasts (Simmer et al., 2009; Hu et al., 2012). For the purpose of this study isolated first molar teeth at the three developmental stages serve as a suitable control, however RNA and protein isolated from these teeth are not only attributed by enamel organ epithelial cells but also non-epithelial cells including odontoblast and pulp cells (Jacques et al., 2014).

CELL CULTURE

The mouse fibroblast cell line NIH3T3 (ATCC Catalog # CRL-1658), and LS8 (Chen et al., 1992) and ALC (Nakata et al., 2003) cells were cultured in DMEM supplemented with 10% heat inactivated fetal bovine serum (FBS), in a 5% CO_2 atmosphere at 37°C.

RNA EXTRACTION AND QUANTITATIVE PCR

Total RNA was extracted from NIH3T3, LS8 and ALC cells, and from first molars of Swiss Webster mice at PN day 3, 6, and 9 using Roche High Pure RNA Extraction Kit (Roche Applied Science, Indianapolis, IN). For cell culture 7-different passages of LS8 ($n = 7$), ALC ($n = 7$), and NIH3T3 ($n = 7$) were used to extract RNA after the cells reached confluency. Extracted RNA was treated with DNAse I to remove all residual genomic DNA. RNA samples were further purified with DNase Inactivation Beads (Cat # AM1907, Ambion, NY, USA) according to the manufacturer's protocol to remove contaminating genomic DNA. 5 μg of total RNA was reverse transcribed to first strand cDNA using a cDNA Synthesis Kit (Takara Bio, Clontech, Mountain View, CA). The cDNA was analyzed using mouse specific Actb (a.k.a. beta actin or β-actin) primers to confirm the absence of contaminating DNA from the isolation process (**Table 1**). The PCR conditions applied were: 94°C for 30 s; 55°C for 30 s; and 72°C for 1 min for 30 cycles. The PCR products were electrophoresed in a 2% agarose gel, stained with ethidium bromide, and visualized under ultraviolet light.

For real-time PCR, mouse specific primers of *Amelx*, *Ambn*, *Enam*, *Mmp20*, *Amtn*, *Odam*, *Klk4*, and *Actb* were used (**Table 1**). PCR was accomplished with iQ SYBRGREEN Supermix (BioRad Laboratories, Hercules, CA) according to the manufacturer's instructions. Expression quantity was analyzed by ABI PRISM 7500 (Applied Biosystems, Grand Island, NY). The PCR conditions were 94°C for 1 min followed by 95°C for 15 s and 62°C for 34 s for 40 cycles. All samples were run in triplicate. All data points were normalized to *Actb*.

WESTERN BLOT ANALYSIS

Total protein was extracted from cell pellets at either 3 or 7 days after passage, and from mouse first molars (maxillary and mandibular) at post natal (PN) days −3, −6, and −9, using ice-cold RIPA lysis buffer (Pierce Biotechnology, Inc., Rockford, IL), supplemented with Halt Protease Inhibitor Cocktail (Thermoscientific, Rockford, IL). For protein extraction from mouse molars, the samples were homogenized manually with a pestle for 40 s. Samples were then cleared by centrifugation and protein concentration quantified using the Bicinchoninic Acid (BCA) assay (Pierce Biotechnology). Ten microgram of total protein from mouse molars and 20 μg of total protein from cell culture were size resolved on denaturing 12% Tris–HCl polyacrylamide gels by SDS gel electrophoresis and transferred to nitrocellulose membranes to detect the enamel proteins. Antibodies used were: mouse-derived anti-Gapdh (GA1R, Thermo Scientific); chicken-derived anti-Amelx (Shapiro et al., 2007); rabbit-derived anti-Ambn (sc-50534, Santa Cruz Biotechnology, Dallas, TX); rabbit-derived anti-Amtn (Lacruz et al., 2012b); and rabbit-derived anti-Odam (Moffatt et al., 2008). Secondary antibodies used were: horseradish peroxidase labeled goat-derived anti-mouse (Cat # 32430, Pierce Biotechnology); goat-derived anti-rabbit (Cat # 32460, Pierce Biotechnology); and rabbit-derived anti-chicken (Cat # 31401, Pierce Biotechnology). Labeled protein bands were detected with an Enhanced ChemiLuminescence (ECL) detection system (Pierce Biotechnology).

ALIZARIN RED S STAINING

5×10^4 cells/well were inoculated in 12 well plates. Cells were fixed with 10% formaldehyde for 20 min and stained with 1%

Table 1 | Primers used in this study.

Gene ID	Forward primer 5′-3′	Reverse primer 5′-3′	Product (bp)
Amelx	GTCACCTCTGCATCCCATG	TTCCCGCTTGGTCTTGTC	136
Ambn	TGAGCCTTGAGACAATGAGAC	AAAGAGTTATGCGGTGGGAG	133
Enam	TATGGTCTTCCACCAAGGAA	TAGGCACACCATCTCCAAAT	181
Mmp20	CACCTCACAAGCCATCTATCC	GAAGCTCCTTTCCCAACATTG	81
Amtn	GCACATACTCTCCCGTTCAC	AAGATTTGGGAGGCTAACGG	144
Odam	TTGACAGCTTTGTAGGCACA	GACCTTCTGTTCTGGAGCAA	197
Klk4	CAACTAAAGAATGGGAAACTGCC	GAGTCCTTTTGGTCCTGTCC	143
Actb	CTGGCACCACACCTTCTACAATG	GATGTCACGCACGATTTCCCTC	382

Alizarin Red S provided in the Osteogenesis Quantification Kit (Millipore, Billerica, MA) for detection of mineral under phase contrast microscope. The cells were evaluated for Alizarin Red stain at 1-, 3-, 7-, 14-, 21-, and 28-days post inoculation.

QUANTITATIVE ANALYSIS OF ALIZARIN RED STAINING

Stained monolayer cells fixed in the above method were detached using 10% acetic acid as described in manufacturer's protocol of the Osteogenesis Quantification Kit (Millipore). Cells were recovered by mechanically scrapping off the well, and the cells recovered into a microcentrifuge tube and vortexed vigorously. Tubes were heated at 85°C for 10 min and stored on ice for 5 min. The cell suspension was cleared of debris by centrifugation at 20,000 × g for 15 min. Four hundred microliter of supernatant was transferred into new microcentrifuge tube and pH was neutralized with 150 μL of 10% ammonium hydroxide. One hundred and fifty microliter of this supernatant was transferred into an opaque walled transparent bottom 96-well plate, and the optical density of the suspension was measured by absorption at 405 nm. Alizarin Red stain incorporated into the cells was quantified using a standard curve generated as per the protocol provided by the manufacturer. A standard plot for Alizaren Red concentration (range = 2.0 mM–0.47 μm) vs. OD_{405} was applied to quantify the unknown samples.

STATISTICAL ANALYSIS

The data were analyzed for statistical significance using Student's *t*-test and values of $p < 0.05$ were considered statistically significant.

RESULTS

ENAMEL-SPECIFIC mRNA EXPRESSION IN LS8, ALC, AND MOUSE MOLARS

Enamel gene-specific primers (**Table 1**) were used to compare mRNA transcript levels in ameloblast-like (LS8 and ALC) cells, and mouse molars (PN days 3, 6, and 9). Messenger RNA expression levels in LS8 and ALC, relative to β-actin, were also compared (**Figure 1A**). Higher mRNA levels for *Amelx*, *Ambn*, *Enam*, and *Mmp20* were noted in LS8 cells, while ALC cells expressed higher mRNA levels for *Odam* and *Klk4*. Expression of *Amtn* in both cell lines was negligible. These expression levels were then compared to mRNA transcripts in mouse first molars isolated at PN3, 6, and 9 (**Figure 1B**). This *in vivo* derived molar data clearly demonstrated a shift from a more dominate secretory function, with high levels of expression for *Amelx*, *Ambn*, *Enam*, and *Mmp20* at PN3, to a more dominant maturation-stage gene expression profile, with the highest levels of *Amtn*, *Odam*, and *Klk4* seen at PN9. The data may indicate that ALC gene expression profiles represent a later stage of gene expression associated with enamel maturation, when compared to the gene expression profiles of LS8 cells that may represent better a secretory function.

ENAMEL-SPECIFIC PROTEIN EXPRESSION IN LS8, ALC, AND MOUSE MOLARS

Western blot analysis for Amelx, Ambn, Amtn, and Odam was performed on protein extracts isolated from NIH3T3, LS8, and ALC cells as described in Materials and Methods and for protein lysates from PN3, 6, and 9 molars (**Figure 2A**). Gapdh was applied as a normalizing control. Suitable antibodies for Western blot analysis of Enam, Mmp20, and Klk4 protein were not immediately available thus their expression profiles were not examined. Unlike the mRNA expression profiles that could be appreciated in both LS8 and ALC cells, protein for Amelx, Ambn, and Odam was evident only in ALC cells (**Figure 2A**). No protein gene expression associated with enamel matrix was detected in LS8 cell lysates, or by the NIH3T3 cells used as a negative control. In the case of the *in vivo* derived molar PN3, 6, and 9 samples, the selected protein expression profiles reflected the levels observed for the mRNA expression profile, with the highest expression levels for Amelx and Ambn apparent at PN3, and the highest levels of Amtn and Odam expression apparent at PN9.

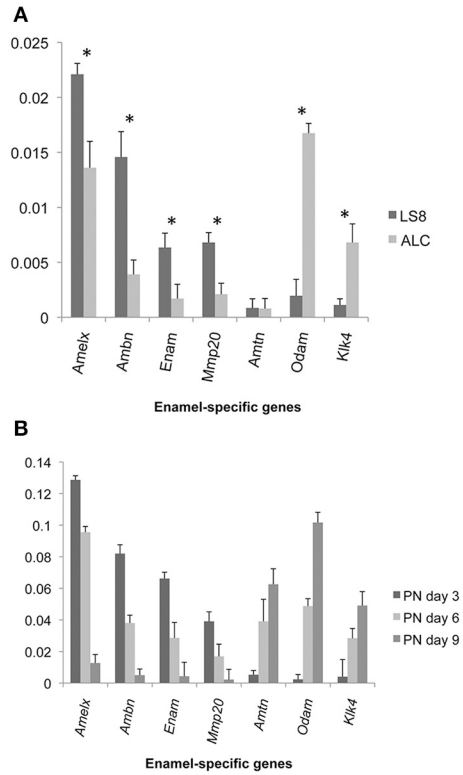

FIGURE 1 | Expression of enamel-specific genes in LS8 and ALC cells, and mice first molars at post natal (PN) days 3, 6, and 9. (A) Results of real-time PCR analyses for LS8 and ALC. The expression of each enamel-specific gene was compared within the two cell lines, and normalized to β-actin. mRNA transcript levels were compared between LS8 and ALC for Amelx, Ambn, Enam, Mmp20, Amtn, Odam, and Klk4. Average expression levels, and standard error of deviation, were calculated from seven independent real-time PCR amplifications (each run in triplicate; $n = 7$). Expression levels relative to Actb expression are graphed. With the exception of Amtn, there was a statistically significant difference in expression ($p < 0.05$) between both cell lines. **(B)** The expression of each gene with the enamel genes is compared from three stages of development; PN3, 6, and 9, and normalized to Actb levels. For each gene examined there were statistically significant (*$p < 0.05$) expression level differences noted between PN3 and PN6, PN3 and PN9, and PN6 and PN9 days. Expression levels relative to Actb expression are graphed.

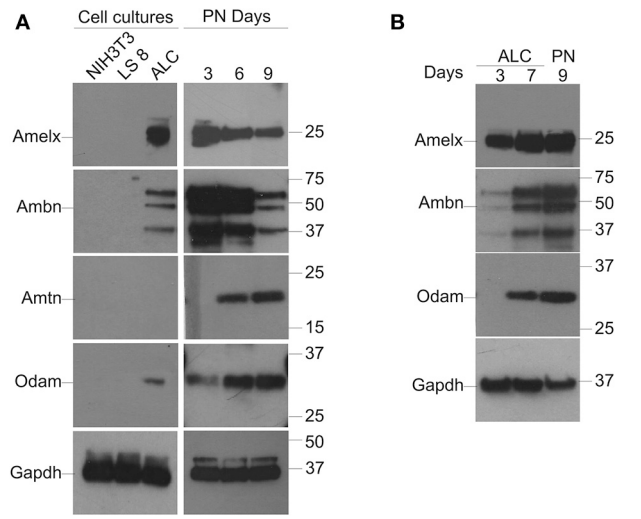

FIGURE 2 | Protein expression in LS8 and ALC cells, and *in vivo* mouse molars. (A) Groupings to left: Western blot analysis of the expression of Amelx, Ambn, and Odam is noted in ALC cells only. LS8 cells did not appear to express the enamel proteins examined. No Amtn expression was noted in either enamel organ cell line. NIH3T3 (fibroblasts) cells are used here as a negative control. All cells cultured for 7 days. Groupings to right: Protein from PN3, 6, and 9 mouse first molars were examined to confirm the suitability of each antibody to assess mouse-derived enamel proteins; and also to illustrate the decreasing levels of Amelx and Amtn from PN3 to PN9, and the increasing levels of Amtn and Odam over the same time course. **(B)** A second series of Western blots were completed with ALC cells isolated at days 3 and 7 after passage, and also from PN9 mouse molars to directly compare protein levels for Amelx, Ambn, and Odam in ALC cells when compared to *in vivo* derived tooth tissues. Glyceraldehyde-3-phosphate dehydrogenase (Gapdh) was used as a loading (normalizing) control.

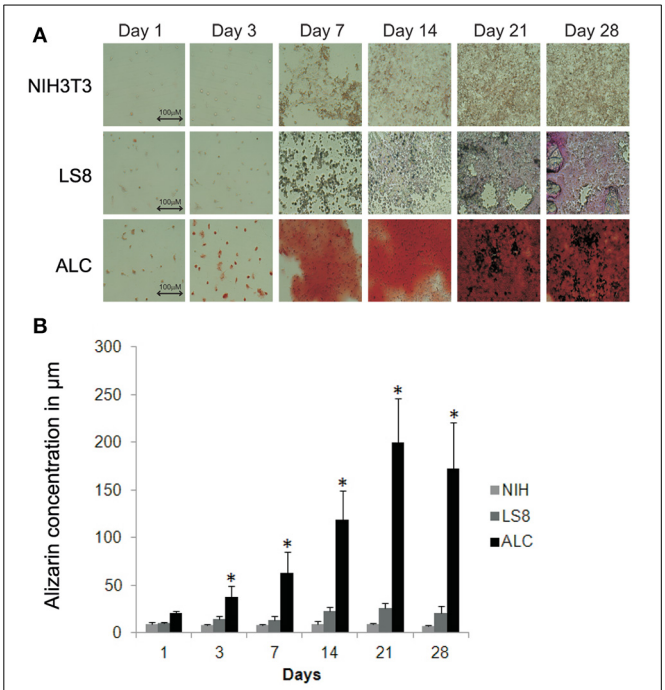

FIGURE 3 | Biomineralization assay for ALC and LS8 cells. (A) Alizarin Red staining was detected at levels significantly higher than background at day 3 post inoculation, and this is characteristic of calcified nodule formation. In ALC cells, stain accumulation increased over a period of 21 days, with no significant change beyond 21-days. Only background level staining was observed in LS8 cells, when compared to NIH3T3 cells (negative control) at day 1 and also over this same time period. Scale bar 100.0 µm. **(B)** Alizarin Red stain in NIH3T3, LS8, and ALC cell culture were quantified using Osteogenesis quantification kit at OD_{405}. Graph shows significant increase in red staining in ALC cells only. Significance indicated by * for $p < 0.05$ for differences in individual cell lines.

A second series of Western blots were performed using protein extracts from ALC cells cultured for 3- and 7-days after passage, alongside protein extracted from PN9 first molars (**Figure 2B**) with Gapdh applied as the normalizing factor. This data suggest that ALC cells show robust levels of Amelx, Ambn, and Odam after 7-days in culture when compared to these same ALC cells cultured for 3-days.

QUANTITATIVE ANALYSIS OF BIOMINERALIZATION ABILITY OF ALC CELLS

LS8 and ALC cells, and NIH3T3 cells (negative control), were compared to assess their abilities to form calcified nodules in a defined culture condition (DMEM supplemented with 10% FBS) without additional growth factors. ALC cells showed positive Alizarin Red S staining, which became apparent at day-3 and increased over the 28-days duration of culture (**Figure 3A**). NIH3T3 cells showed negligible Alizarin Red reactivity, and LS8 cells revealed only modest staining at the end of the 28-days. Alizarin Red S staining was quantified by extrapolating from a standard curve of concentrations measured at 405 nm. Graphical representation of the solubilized Alizarin Red S stain from each cell culture indicated a progressive, and highly significant, increase in calcified nodule formation for ALC cells only, reacting a maximum staining at day 21 (**Figure 3B**).

DISCUSSION

This current study has focused on comparing two mouse ameloblast-like cell lines (LS8 and ALC) with respect to their expression of enamel specific genes as mRNAs and proteins. The purpose of the comparison is to determine if two "well-established" and "widely-studied" ameloblast-like cell lines could be distinguished from each other, and if one line could to be judged as more suitable to study certain molecular aspects of amelogenesis. Based on mRNA gene expression profiles LS8 cells exhibit higher levels of *Amelx*, *Ambn*, and *Enam*, and *Mmp20* mRNAs, while ALC cells show noticeably higher levels of *Amelx*, *Odam*, and *Klk4* mRNAs. Both cell lines show significant levels of *Amelx* transcripts, and as such, both should be suitable to investigate *Amelx* gene transcriptional regulatory activities. These transcriptome profile data also suggest that LS8 cells may be preferable in a study of transcriptional regulation for *Ambn*, *Enam*, or *Mmp20*, while ALC cells may be the more appropriate cell line to study transcriptional activities related to *Odam* and *Klk4*.

From the quantitative PCR analysis we may conclude that, relative to each other, LS8 cells are less differentiated than are the ALC cells because of the higher mRNA levels seen for gene

transcripts related to secretory-stage activities (*Amelx*, *Ambn*, *Enam*, and *Mmp20*). This conclusion is also supported by the fact that ALC cells show higher levels of *Odam* and *Klk4* mRNAs, and also that ALC cells form calcified nodules in culture while LS8 cells do not, and that calcification/mineralization of the enamel matrix is characteristic of the maturation-stage of amelogenesis, *in vivo*. However, our protein analysis presents an alternative body of data which suggests that translational events of the mRNA expressed by LS8 and ALC cells are very different, as Amelx and Ambn (secretory-stage proteins), and Odam (maturation-stage protein) were all detected in ALC cells only.

This study clearly has its limitations and could be further expanded. For example we have been very selective in studying only a small number of enamel-specific genes at the message level (*Amelx*, *Ambn*, *Enam*, *Mmp20*, *Amtn*, *Odam*, and *Klk4*), and from these, only four (Amelx, Ambn, Amtn, and Odam) were investigated at the protein level. Performing a whole genome transcriptome analysis with microarray technology would help to determine if other events that define amelogenesis are apparent in either cell line. A second experiment of value would be to establish if the secretory activities observed in ameloblasts *in vivo* are active in cell culture, and which of these enamel proteins are secreted into the culture medium. For example, even though Amelx protein was not evident from the disrupted LS8 cells, there may be evidence for the protein in the medium. All the enamel proteins studied here are secreted products, so an investigation of ameloblast secretory dynamics would also be of value to better define each of the cell lines' biological characteristics. In any case, this study is the first of its kind to compare two ameloblast-like cell lines side by side.

CONCLUSION

When studying biological phenomenon in health and disease, investigators are limited by the resources they have at hand. Small animal models (e.g., mice and rats) are often used as surrogates for humans, and restrictions are in place to limit animal experiments such that statistically significant data is collected from the most appropriate species using minimal animal numbers. Cell culture allows for experimentation on cells derived from animal sources, and is a valuable tool to investigate many aspects of cell and molecular biology. The use of recovered canonical proteins or recombinant produced proteins assembled in an artificial environment is another alternative to investigate complex biological processes in a systematic manner, *in vitro*. What appears still to remain a limitation to these types of studies is the availability of suitable antibodies for each protein of interest. Finally, while different approaches to study certain biological phenomenon each have their strengths and weaknesses, each offer invaluable insight into biology at the molecular level. Creating a framework of knowledge from *in vitro* cell or protein models permits well-designed and focused studies to be conducted on whole animals to validate outcomes and extend our capacity to mimic Nature.

ACKNOWLEDGMENTS

The authors would like to thank Dr. Bernhard Ganss (University of Toronto) for the antibody against Amtn, and Dr. Antonio Nanci (University of Montreal) for the antibody against Odam. The authors would also like to thank Dr. Saumya Prajapati for expert assistance with animal management. This work was supported by grant DE019629 (Michael L. Paine), DE016276 (John D. Bartlett) and DE013405 (Malcolm L. Snead) from the National Institute of Dental and Craniofacial Research, National Institutes of Health (Michael L. Paine). The authors declare no potential conflicts of interest with respect to the authorship and/or publication of this article.

REFERENCES

Arakaki, M., Ishikawa, M., Nakamura, T., Iwamoto, T., Yamada, A., Fukumoto, E., et al. (2012). Role of epithelial-stem cell interactions during dental cell differentiation. *J. Biol. Chem.* 287, 10590–10601. doi: 10.1074/jbc.M111.285874

Chen, L. S., Couwenhoven, D., Hsu, D., Luo, W., and Snead, M. L. (1992). Maintainance of amelogenin gene expression by transformed epithelial cells of mouse enamel organ. *Arch. Oral Biol.* 37, 771–778. doi: 10.1016/0003-9969(92)90110-T

Denbesten, P. K., Gao, C., Li, W., Mathews, C. H., and Gruenert, D. C. (1999). Development and characterization of an SV40 immortalized porcine ameloblast-like cell line. *Eur. J. Oral Sci.* 107, 276–281. doi: 10.1046/j.0909-8836.1999.eos107407.x

Dhamija, S., and Krebsbach, P. H. (2001). Role of Cbfa1 in ameloblastin gene transcription. *J. Biol. Chem.* 276, 35159–35164. doi: 10.1074/jbc.M010719200

Dhamija, S., Liu, Y., Yamada, Y., Snead, M. L., and Krebsbach, P. H. (1999). Cloning and characterization of the murine ameloblastin promoter. *J. Biol. Chem.* 274, 20738–20743. doi: 10.1074/jbc.274.29.20738

Duan, X., Mao, Y., Wen, X., Yang, T., and Xue, Y. (2011). Excess fluoride interferes with chloride-channel-dependent endocytosis in ameloblasts. *J. Dent. Res.* 90, 175–180. doi: 10.1177/0022034510385687

Hu, P., Lacruz, R. S., Smith, C. E., Smith, S. M., Kurtz, I., and Paine, M. L. (2012). Expression of the sodium/calcium/potassium exchanger, NCKX4, in ameloblasts. *Cells Tissues Organs* 196, 501–509. doi: 10.1159/000337493

Jacques, J., Hotton, D., De La Dure-Molla, M., Petit, S., Asselin, A., Kulkarni, A. B., et al. (2014). Tracking endogenous amelogenin and ameloblastin *in vivo*. *PLoS ONE* 9:e99626. doi: 10.1371/journal.pone.0099626

Kawano, S., Morotomi, T., Toyono, T., Nakamura, N., Uchida, T., Ohishi, M., et al. (2002). Establishment of dental epithelial cell line (HAT-7) and the cell differentiation dependent on Notch signaling pathway. *Connect. Tissue Res.* 43, 409–412. doi: 10.1080/713713488

Kubota, K., Lee, D. H., Tsuchiya, M., Young, C. S., Everett, E. T., Martinez-Mier, E. A., et al. (2005). Fluoride induces endoplasmic reticulum stress in ameloblasts responsible for dental enamel formation. *J. Biol. Chem.* 280, 23194–23202. doi: 10.1074/jbc.M503288200

Lacruz, R. S., Brookes, S. J., Wen, X., Jimenez, J. M., Vikman, S., Hu, P., et al. (2013a). Adaptor protein complex 2-mediated, clathrin-dependent endocytosis, and related gene activities, are a prominent feature during maturation stage amelogenesis. *J. Bone Miner. Res.* 28, 672–687. doi: 10.1002/jbmr.1779

Lacruz, R. S., Hacia, J. G., Bromage, T. G., Boyde, A., Lei, Y., Xu, Y., et al. (2012a). The circadian clock modulates enamel development. *J. Biol. Rhythms* 27, 237–245. doi: 10.1177/0748730412442830

Lacruz, R. S., Nakayama, Y., Holcroft, J., Nguyen, V., Somogyi-Ganss, E., Snead, M. L., et al. (2012b). Targeted overexpression of amelotin disrupts the microstructure of dental enamel. *PLoS ONE* 7:e35200. doi: 10.1371/journal.pone.0035200

Lacruz, R. S., Smith, C. E., Bringasjr, P., Chen, Y. B., Smith, S. M., Snead, M. L., et al. (2012c). Identification of novel candidate genes involved in mineralization of dental enamel by genome-wide transcript profiling. *J. Cell Physiol.* 227, 2264–2275. doi: 10.1002/jcp.22965

Lacruz, R. S., Smith, C. E., Kurtz, I., Hubbard, M. J., and Paine, M. L. (2013b). New paradigms on the transport functions of maturation-stage ameloblasts. *J. Dent. Res.* 92, 122–129. doi: 10.1177/0022034512470954

Mathias, R. S., Mathews, C. H., Machule, C., Gao, D., Li, W., and Denbesten, P. K. (2001). Identification of the calcium-sensing receptor in the developing tooth organ. *J. Bone Miner. Res.* 16, 2238–2244. doi: 10.1359/jbmr.2001.16.12.2238

Moffatt, P., Smith, C. E., St-Arnaud, R., and Nanci, A. (2008). Characterization of Apin, a secreted protein highly expressed in tooth-associated epithelia. *J. Cell. Biochem.* 103, 941–956. doi: 10.1002/jcb.21465

Nakata, A., Kameda, T., Nagai, H., Ikegami, K., Duan, Y., Terada, K., et al. (2003). Establishment and characterization of a spontaneously immortalized mouse ameloblast-lineage cell line. *Biochem. Biophys. Res. Commun.* 308, 834–839. doi: 10.1016/S0006-291X(03)01467-0

Shapiro, J. L., Wen, X., Okamoto, C. T., Wang, H. J., Lyngstadaas, S. P., Goldberg, M., et al. (2007). Cellular uptake of amelogenin, and its localization to CD63, and Lamp1-positive vesicles.. *Cell. Mol. Life Sci.* 64, 244–256. doi: 10.1007/s00018-006-6429-4

Simmer, J. P., Hu, Y., Lertlam, R., Yamakoshi, Y., and Hu, J. C. (2009). Hypomaturation enamel defects in Klk4 knockout/LacZ knockin mice. *J. Biol. Chem.* 284, 19110–19121. doi: 10.1074/jbc.M109.013623

Smith, C. E. (1998). Cellular and chemical events during enamel maturation. *Crit. Rev. Oral Biol. Med.* 9, 128–161. doi: 10.1177/10454411980090020101

Takahashi, S., Kawashima, N., Sakamoto, K., Nakata, A., Kameda, T., Sugiyama, T., et al. (2007). Differentiation of an ameloblast-lineage cell line (ALC) is induced by Sonic hedgehog signaling. *Biochem. Biophys. Res. Commun.* 353, 405–411. doi: 10.1016/j.bbrc.2006.12.053

Xu, Y., Zhou, Y. L., Erickson, R. L., Macdougald, O. A., and Snead, M. L. (2007a). Physical dissection of the CCAAT/enhancer-binding protein alpha in regulating the mouse amelogenin gene. *Biochem. Biophys. Res. Commun.* 354, 56–61. doi: 10.1016/j.bbrc.2006.12.182

Xu, Y., Zhou, Y. L., Gonzalez, F. J., and Snead, M. L. (2007b). CCAAT/enhancer-binding protein delta (C/EBPdelta) maintains amelogenin expression in the absence of C/EBPalpha *in vivo*. *J. Biol. Chem.* 282, 29882–29889. doi: 10.1074/jbc.M702097200

Xu, Y., Zhou, Y. L., Luo, W., Zhu, Q. S., Levy, D., Macdougald, O. A., et al. (2006). NF-Y and CCAAT/enhancer-binding protein alpha synergistically activate the mouse amelogenin gene. *J. Biol. Chem.* 281, 16090–16098. doi: 10.1074/jbc.M510514200

Zheng, L., Seon, Y. J., Mourao, M. A., Schnell, S., Kim, D., Harada, H., et al. (2013). Circadian rhythms regulate amelogenesis. *Bone* 55, 158–165. doi: 10.1016/j.bone.2013.02.011

Zhou, Y. L., Lei, Y., and Snead, M. L. (2000). Functional antagonism between Msx2 and CCAAT/enhancer-binding protein alpha in regulating the mouse amelogenin gene expression is mediated by protein-protein interaction. *J. Biol. Chem.* 275, 29066–29075. doi: 10.1074/jbc.M002031200

Zhou, Y. L., and Snead, M. L. (2000). Identification of CCAAT/enhancer-binding protein alpha as a transactivator of the mouse amelogenin gene. *J. Biol. Chem.* 275, 12273–12280. doi: 10.1074/jbc.275.16.12273

Conflict of Interest Statement: The authors declare that the research was conducted in the absence of any commercial or financial relationships that could be construed as a potential conflict of interest.

Received: 19 May 2014; paper pending published: 20 June 2014; accepted: 07 July 2014; published online: 25 July 2014.

*Citation: Sarkar J, Simanian EJ, Tuggy SY, Bartlett JD, Snead ML, Sugiyama T and Paine ML (2014) Comparison of two mouse ameloblast-like cell lines for enamel-specific gene expression. Front. Physiol. **5**:277. doi: 10.3389/fphys.2014.00277*

This article was submitted to Craniofacial Biology, a section of the journal Frontiers in Physiology.

frontiers in
PHYSIOLOGY

REVIEW ARTICLE
published: 05 January 2015
doi: 10.3389/fphys.2014.00510

MSX2 in ameloblast cell fate and activity

Sylvie Babajko[1,2,3,4]*, Muriel de La Dure-Molla[1,2,3,4,5], Katia Jedeon[1,2,3,4] and Ariane Berdal[1,2,3,4,5]

[1] Laboratory of Molecular Oral Pathophysiology, Centre de Recherche des Cordeliers, Institut National de la Santé et de la Recherche Médicale, UMRS 1138, Paris, France
[2] Laboratory of Molecular Oral Pathophysiology, Centre de Recherche des Cordeliers, Université Paris-Descartes, Paris, France
[3] Laboratory of Molecular Oral Pathophysiology, Centre de Recherche des Cordeliers, Université Pierre et Marie Curie-Paris, Paris, France
[4] Laboratory of Molecular Oral Pathophysiology, Centre de Recherche des Cordeliers, Université Paris-Diderot, Paris, France
[5] Centre de Référence des Maladies Rares de la Face et de la Cavité Buccale MAFACE, Hôpital Rothschild, Paris, France

Edited by:
Bernhard Ganss, University of Toronto, Canada

Reviewed by:
David Clouthier, University of Colorado Anschutz Medical Campus, USA
Colin Robinson, University of Leeds, UK

***Correspondence:**
Sylvie Babajko, Laboratory of Molecular Oral Pathophysiopathology, Centre de Recherche des Cordeliers, Institut National de la Santé et de la Recherche Médicale, UMRS 1138, 15-21 rue de l'Ecole de Médecine, 75270 Paris 06, France
e-mail: sylvie.babajko@crc.jussieu.fr

While many effectors have been identified in enamel matrix and cells via genetic studies, physiological networks underlying their expression levels and thus the natural spectrum of enamel thickness and degree of mineralization are now just emerging. Several transcription factors are candidates for enamel gene expression regulation and thus the control of enamel quality. Some of these factors, such as MSX2, are mainly confined to the dental epithelium. MSX2 homeoprotein controls several stages of the ameloblast life cycle. This chapter introduces MSX2 and its target genes in the ameloblast and provides an overview of knowledge regarding its effects *in vivo* in transgenic mouse models. Currently available *in vitro* data on the role of MSX2 as a transcription factor and its links to other players in ameloblast gene regulation are considered. MSX2 modulations are relevant to the interplay between developmental, hormonal and environmental pathways and *in vivo* investigations, notably in the rodent incisor, have provided insight into dental physiology. Indeed, *in vivo* models are particularly promising for investigating enamel formation and MSX2 function in ameloblast cell fate. MSX2 may be central to the temporal-spatial restriction of enamel protein production by the dental epithelium and thus regulation of enamel quality (thickness and mineralization level) under physiological and pathological conditions. Studies on MSX2 show that amelogenesis is not an isolated process but is part of the more general physiology of coordinated dental-bone complex growth.

Keywords: MSX2, transcription factors, ameloblast, differentiation, enamel, teeth

STRUCTURE AND MOLECULAR MECHANISMS OF MUSCLE SEGMENT HOMEOBOX (Msx) GENES

HOMEOBOX GENES

Msx2 is a member of the family of divergent homeobox-containing genes homologous to the Drosophila *M*uscle *S*egment *H*omeobox (*msh*) gene. Evolution including the duplication of the ancestral *msh* gene, has led to three different genes in mice and two in humans. Homeobox-containing genes share a well-conserved sequence of 183 bp coding for a helix-loop-helix motif of 64 amino acids (Shirasawa et al., 1994). This homeodomain interacts with an A/T-rich DNA sequence thereby conferring transcriptional activity on the proteins carrying it (Gehring et al., 1994). Most homeobox genes are organized in clusters, and this is the case for *HoxA*, *B*, *C*, and *D* genes that control the development of the trunk spatially and temporally. Other homeobox genes, dispersed around the genome and classified as divergent homeogenes also include the *Msx* family which is crucial for the development of the head.

MSX1 AND MSX2 ARE TRANSCRIPTIONAL REGULATORS

The homeodomain of homeogenes *Msx1* and *Msx2* share 98% sequence identity, such that they have similar transcriptional properties (Catron et al., 1996). MSX1 and MSX2 were first reported as transcriptional repressors (Catron et al., 1993, 1995), but their respective activities have not been precisely characterized. They are able to interact with a C/GTAATTG core consensus sequence (Catron et al., 1993). MSX homeoproteins may form either homodimers or heterodimers with other homeoproteins such as those encoded by *Dlx* (Zhang et al., 1997) and *Pax* genes (Bendall et al., 1999; Ogawa et al., 2006). The resulting competition for the same promoter sequence may explain, at least in part, their antagonist regulatory activities (Bendall and Abate-Shen, 2000). In addition to the presumed direct interactions via the homeodomain, their N- and C-terminal domains are able to interact with other proteins and thereby also modulate transcription (Catron et al., 1995; Zhang et al., 1996). MSX2 is able to interact with SP3 (Bei, 2009) and with C/EBPα, notably in ameloblasts (Zhou and Snead, 2000). Such physical interactions between MSX2 and C/EBPα enable switching of cell differentiation, as described for osteogenic/adipogenic differentiation in aortic myofibroblasts (Cheng et al., 2003). Transcriptional repression by MSX (reported for MSX1) is also modulated by interactions that drive the nuclear localization of the proteins, as shown for PIAS-1 (Lee et al., 2006) and H3K27me3 (Wang and Abate-Shen, 2012). These various papers show that the target selectivity of MSX1 and MSX2 and their transcriptional activities

Abbreviations: Bp, Base pairs; IEE, internal enamel epithelium.

are dependent on the nature of the partners they interact with, via binding motifs located outside the homeodomain (Catron et al., 1995; Zhang et al., 1996). The sequence similarity between MSX1 and MSX2 in the N- and C-termini is lower (than in their homeodomains) and this presumably explains the different activities of the two factors. Transcriptional regulations of MSX2 depend on the nature of its partners: the specific combinations involved determine when, where and how the expression of the various MSX2-target genes is modulated.

MSX1 AND 2 PRESENT REDUNDANT AND NON-REDUNDANT FUNCTIONS

MSX functions are significant in morphogenesis in which specific developmental patterns control distinct stages and events. The involvement of MSX in morphogenesis was discovered in work with limb buds and ectodermal appendages such as teeth (Satokata and Maas, 1994; Houzelstein et al., 1997; Satokata et al., 2000). There are now a vast number of human and transgenic mouse gene mutations available (**Table 1**) providing evidence that both MSX1 and MSX2 are essential for skeletal morphogenesis and differentiation. The expression profiles of *Msx* homeobox genes may overlap; there may be redundancy between MSX1 and MSX2 as they display structural conservation, according to anatomical site (Sharpe, 1995). This is the case in limbs (and the resulting appendicular skeleton) but not in craniofacial morphogenesis and differentiation as illustrated by the selective phenotype of *Msx* mutants.

Non-redundant roles of MSX are exemplified in teeth. Both MSX1 and MSX2 are expressed as soon as dental lamina is initiated and their expression continues until the end of tooth formation, but in different areas (Thesleff, 2003). Transgenic mouse models have been used to characterize their respective function in dental development: MSX1 drives early tooth morphogenesis, whereas MSX2 is involved later in development (Bei et al., 2004; Thesleff, 2006). *MSX1* gene mutations are associated with tooth agenesis in both human and mouse species (Vastardis et al., 1996; Houzelstein et al., 1997). *Msx2* null mutants survive and display variable bone and dental phenotypes, especially in areas in which development is driven by epithelial-mesenchymal cell communications (Satokata et al., 2000). The different phenotypes associated with either MSX1 or MSX2 transgenic models strongly indicate that they do not have the same functions in tooth development; their respective molecular actions and partners need to be characterized.

MSX2: A KEY ELEMENT OF THE TRANSCRIPTIONAL NETWORK DETERMINING AMELOBLAST GENE EXPRESSION AND AMELOBLAST LIFE-CYCLE

MSX2, A KEY FACTOR FOR ENAMEL GENE EXPRESSION

A number of studies have investigated the regulation of enamel gene transcription. They have identified a number of factors, including MSX2, controlling the transcription of enamel genes (**Table 2**). The amelogenin gene was the first to be studied because it encodes the most abundant enamel matrix protein. Amelogenin gene repression by MSX2 appears to be indirect through interaction with C/EBPα (**Figure 1**) (Zhou et al., 2000; Xu et al., 2007a). Interaction between MSX2 and C/EBPα abolishes the activating activity of C/EBPα on amelogenin transcription. MSX2/DLX heterodimers may also be involved in modulating amelogenin expression (Lézot et al., 2008). Indeed, DLX2 and DLX3 have been shown to control amelogenin expression (Lézot et al., 2008; Athanassiou-Papaefthymiou et al., 2011). The selective role of each DLX homeoprotein may be influenced by the other DLX family members expressed in ameloblasts (Lézot et al., 2008). MSX2 transcriptional modulations have been documented for other key enamel genes, notably those encoding enamel matrix proteins (enamelin and ameloblastin) and the two main proteases (MMP20 and KLK4) (Berdal et al., 1993; Molla et al., 2010). MSX2 is also able to repress the expression of calbindin-D_{28k}, a vitamin D-dependent calcium-handling protein, by direct interaction with its proximal promoter (Bolaños et al., 2012). Several partners of MSX2 identified in osteoblasts also influence ameloblast gene expression: for example, RUNX2 differentially regulates enamelin and *Klk4* gene expression. Interestingly, its

Table 1 | *MSX* mutations in human and corresponding experimental models.

	Human		Mutant mice	References
	Pathology	**OMIM**	**Phenotype**	
MSX1	Ectodermal dysplasia 3, Witkop type	189500	*Loss of function*_(*Msx1*−/−)	
	Orofacial cleft 5	608874	Tooth agenesis, cleft palate	Satokata and Maas, 1994
	Tooth agenesis, with or without orofacial cleft	106600		Houzelstein et al., 1997
			Gain of function (transgenic mice)	Nassif et al., 2014
			craniofacial bone morphogenesis	
MSX2	Loss of function	168550	*Loss of function* (*Msx2*−/−)	
	Parietal foramina with cleidocranial dysplasia		Bone defects	Satokata et al., 2000
			Tooth	Aïoub et al., 2007
				Molla et al., 2010
	Gain of function	604757	*Gain of function* (transgenic mice)	Liu et al., 1995
	Craniosynostosis, type 2		Premature suture closure,	Shao et al., 2005
			Ectopic cranial bone	
			Cardiovascular calcification	

Table 2 | Transcriptional regulations of the major enamel genes.

Target genes	Transcription factors	References
Amelogenin	Msx2 ↘	Zhou et al., 2000; Xu et al., 2007a
	C/EBPα ↗	Zhou and Snead, 2000
	NF-Y ↗	Xu et al., 2006
	C/EBPΔ ↗	Xu et al., 2007b
	Dlx2 ↗	Lézot et al., 2008
	Dlx2 and FoxJ1 ↗	Venugopalan et al., 2011
	Oct-1 ↘	Xu et al., 2010
	Pitx2 ↗	Li et al., 2013, 2014
	Clock genes ↗	Lacruz et al., 2012a; Zheng et al., 2013
	Runx2 ↘ and Dlx3 ↗	Athanassiou-Papaefthymiou et al., 2011
		Mitsiadis et al., 2008
	Tbx1 ↗	
Ameloblastin	Cbfa1 (Runx2) ↗	Dhamija and Krebsbach, 2001
Enamelin	B-catenin/LEF1 ↗	Tian et al., 2010
	Runx2 ↘ and Dlx3 ↗	Athanassiou-Papaefthymiou et al., 2011
MMP20	Runx2 and ODAM ↗	Lee et al., 2010
	c-Jun (AP1) ↗	Zhang et al., 2007
KLK4	Clock genes ↗	Zheng et al., 2013
	Runx2 ↗ and Dlx3 ↗	Athanassiou-Papaefthymiou et al., 2011
Calbindin D 28k	Msx2 ↘	Bolaños et al., 2012

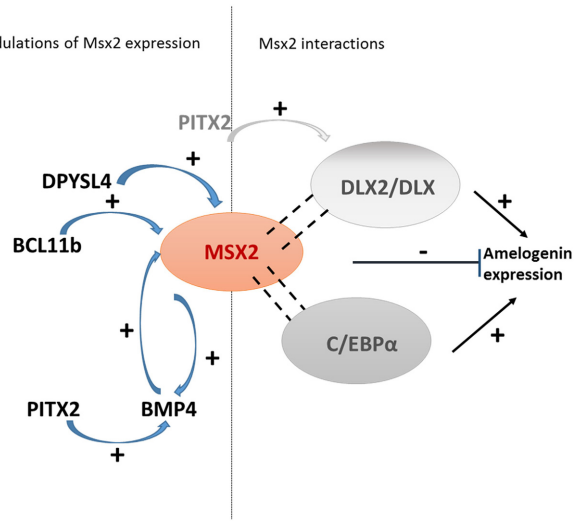

FIGURE 1 | The central role of MSX2 in ameloblast cell fate. *Msx2* expression is controlled by transcription factors involved in ameloblast proliferation. MSX2 modulates the expression of its target genes directly or indirectly by interacting with various partners such as C/EBPα or Dlx (Zhou and Snead, 2000; Lézot et al., 2002, 2008). Thus, it represses the transcriptional activity of the transcription factors that modulate amelogenin expression.

own expression is up-regulated by NR1D1 which expression is also controlled by clock genes (Athanassiou-Papaefthymiou et al., 2011) establishing a complex network of direct and indirect controls by circadian transcription factors. Thus, clock proteins (BMAL1, Clock, PER1, and PER2) may regulate enamel gene expression either directly (Lacruz et al., 2012a; Zheng et al., 2013) or indirectly via NR1D1 and consequently MSX2. *ODAM* expression is also up-regulated by RUNX2, and ODAM increases *Mmp20* expression with its promoter activity (Lee et al., 2010). In view of the relationship between MSX2 and RUNX2, it may be possible that MSX2 also modulates *Mmp20* expression.

In addition, as evidenced in early development, *Msx2* expression itself may be controlled either directly or indirectly via enamel proteins. This was demonstrated by *in vivo* and *in vitro* studies showing a feedback loop between ameloblastin and *Msx2* expression (Fukumoto et al., 2004; Sonoda et al., 2009). However, the best characterized positive feedback loop involving MSX2 and a secreted protein is that operating with BMP4: BMP4 induces *Msx2* expression and in turn, MSX2 controls *Bmp4* (Bei and Maas, 1998) (**Figure 2**). Indeed, the *Msx2* promoter contains a BMP-responsive enhancer element (Brugger et al., 2004) and the *Bmp4* promoter contains an Msx (1 and 2) responsive element (Wang et al., 2011).

Considering the redundancies between *Msx1* and *Msx2*, it is interesting to raise the question of similar expression modulations for *Msx2* compared to those already reported for *Msx1*. Also, the level of Msx1 protein is regulated by its own antisense RNA: the *Msx1* gene is transcribed in both directions producing, in addition to the sense transcript, a long endogenous antisense non-coding RNA (Blin-Wakkach et al., 2001). This RNA is believed to provide fine control of MSX1 homeoprotein quantities during development (Coudert et al., 2005) via post-transcriptional sense RNA decay (Petit et al., 2009) and thus influence MSX1 protein activity (Babajko et al., 2009). Number of *Hox* homeogenes are submitted to bi-directional transcription (Mainguy et al., 2007); similar events that need to be investigated may also control *Msx2* expression.

In conclusion, *Msx2* expression is modulated either directly by various intracellular factors or indirectly by secreted factors, resulting in fined tuned levels of MSX2 that control enamel gene expression and ameloblast cell fate.

Msx2 IS INVOLVED IN CELL PROLIFERATION

MSX2 is present throughout the process of ameloblast differentiation/maturation although its expression decreases during the secretory stage and may modulate enamel gene expression differently depending on the combination of transcription factors present (**Figure 2**). Very few studies report gene expression modulations during the maturation stage (Lacruz et al., 2012b), such that the function of MSX2 during the terminal differentiation of ameloblasts is less clear.

Msx2 is not only expressed in the inner dental epithelium but throughout the entire enamel organ as evidenced in the rodent apical loop (Jiang and Wang, 2010). In *Msx2*−/− mouse dental epithelium, proliferation of stellate reticulum cells and stratum

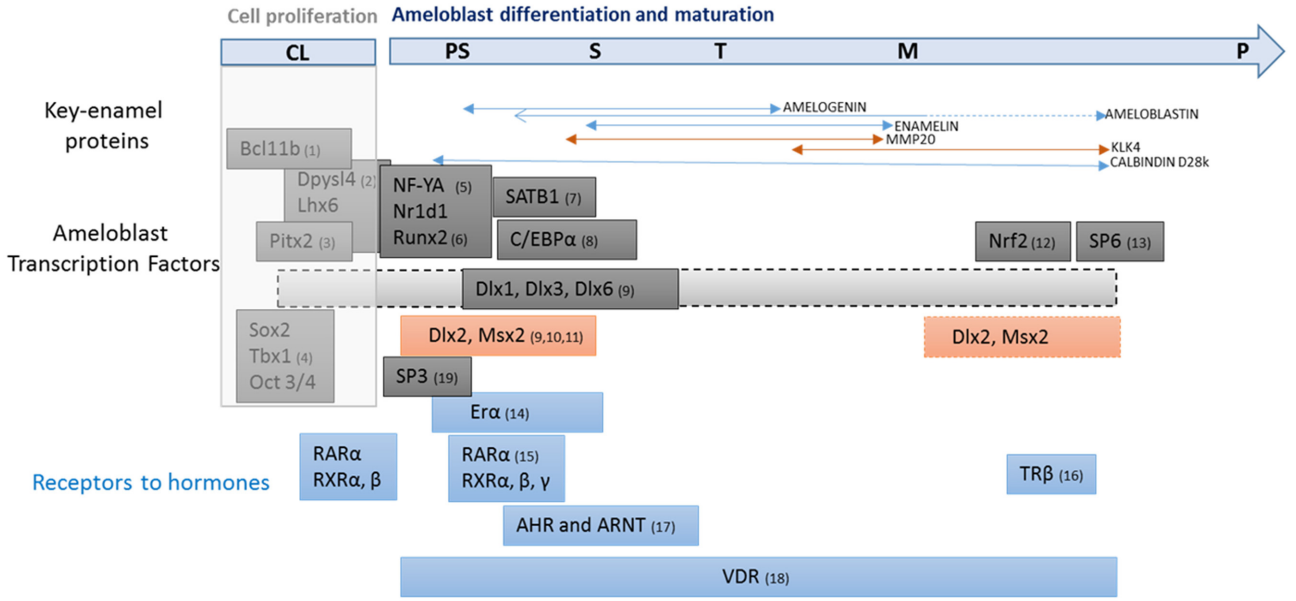

FIGURE 2 | Transcription factors involved in ameloblast proliferation, differentiation and maturation. Transcription factors involved in ameloblast proliferation and differentiation (in black), and hormonal response (in blue). Enamel gene patterns are linked to presecretion, secretion and maturation stages of amelogenesis. The first key-point is the transition from presecretion to secretion stage during which differentiated ameloblasts acquire all the properties required for orderly secretion of enamel proteins (amelogenin, enamelin, amelobastin, and calbindin-D_{28k}). A subsequent key-point for amelogenesis is the second transition from secretion to post-secretion. This event determines final enamel thickness via an abrupt decrease in matrix protein production. Enamel mineral quality is also conditioned by this transition associated with massive cell apoptosis and size reduction. Ameloblasts show an abrupt increase in the production of proteins involved in the mineralization process, including MMP20 and KLK4 proteases, mineral-handling effectors such as Ca-ATPase, alkaline phosphatase, proton pumps, carbonic anhydrase, calbindin-D_{28k}, and tight junction elements which contribute to enamel maturation. The list of up- and down-regulated genes at these two key stages of amelogenesis is emerging from current "omics" studies and most of them have been identified. The challenge now will be to integrate these effectors and their regulators into a model that describes the resulting enamel quality. **CL**, cervical loop; **PS**, pre-secretion; **S**, secretion; **T**, transition; **M**, maturation stages and **P**, pigmentation. (1, Golonzhka et al., 2009; 2, Yasukawa et al., 2013; 3, Cao et al., 2013; 4, Catón et al., 2009; 5, Xu et al., 2007a; 6, Athanassiou-Papaefthymiou et al., 2011; 7, Stahl et al., 2013; 8, Zhou and Snead, 2000; 9, Lézot et al., 2008; 10, Bei et al., 2004; 11, Molla et al., 2010; 12, Yanagawa et al., 2004; 13, Muto et al., 2012; 14, Ferrer et al., 2005; 15, Bloch-Zupan et al., 1994; 16, Lacruz et al., 2012b; 17, Sahlberg et al., 2002; 18, Davideau et al., 1996; 19, Bei, 2009).

intermedium cells increases. At these early stages, *Msx2* expression is induced by the key transcription factors, DPYSl4 and BCL11b (Ctip2), also determinant of cell proliferation (**Figures 1**, **2**) (Golonzhka et al., 2009; Yasukawa et al., 2013). *Msx2* expression and *Dlx2* expression are also indirectly up-regulated by PITX2 via BMP4, which are also expressed in proliferative cells (Venugopalan et al., 2011; Cao et al., 2013) (**Figure 1**). As a result of the various *Msx2* expression modulations by early factors, *Msx2* is expressed in undifferentiated inner enamel epithelial (IEE) cells and down-regulated when ameloblast cells overtly differentiate (Mackenzie et al., 1991, 1992; Maas and Bei, 1997).

LESSONS FROM NON-CONDITIONAL *Msx2* MUTANTS—STRENGTHS AND LIMITATIONS

Most of the data described above result from *in vitro* studies. However, *in vivo* models are also informative about MSX2 function because they include cell-cell communications.

Msx2−/− MOUSE DENTAL PHENOTYPE ILLUSTRATES THE PLEIOTROPIC ROLE PLAYED BY *Msx2*

At this time, several targets have been identified in enamel within their physiological context. Dental morphogenesis in *Msx2*−/− mice is abnormal: cusp generation is affected by enamel knot disorganization (**Figure 3D**) (Bei et al., 2004); defects are observed in the enamel (Molla et al., 2010) and other dental tissues; and roots are malformed with the root epithelium overexpressing enamel proteins, especially amelogenins and ameloblastin. Also, jaw osteoclast activity is decreased locally around the dental follicle; eruption failure and pseudo-odontogenic tumor deviation of the tooth germs culminate in the third mandibular molars (Aïoub et al., 2007). This phenotype is coherent with the pattern of *Msx2* expression in many cells forming the tooth and periodontal bone. Indeed, its expression starts from the very beginning of odontogenesis, first in the ectoderm and mesoderm from the gastrulation stage, and subsequently in neural crest cells and oral epithelium (Bendall and Abate-Shen, 2000). During root formation, *Msx2* is again expressed in epithelial cells (Hertwig root sheath and later epithelial Malassez rests) as well as in dental and periodontal mesenchyme (Yamashiro et al., 2003; Molla et al., 2010). As alveolar bone and tooth development are linked, it is important to note that differentiating and differentiated osteoblasts express *Msx2* (Dodig et al., 1996; Mirzayans et al., 2012). Finally, peridental osteoclasts express *Msx2* and do so with regional gradients related to both dental crown and root growth (Aïoub et al., 2007) (**Figure 3**).

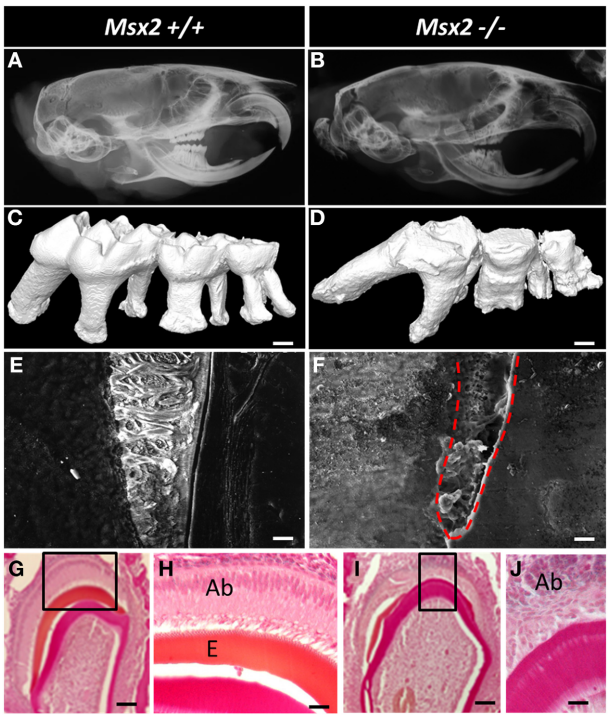

FIGURE 3 | Dental phenotype of *Msx2*−/− mice with reference to wild-type animals (*Msx2*+/+). (A,B) Microradiographs of the whole heads of 3-month old mice showing craniofacial and teeth dysmorphology; indeed craniofacial morphogenesis is under the control of MSX2 (Simon et al., 2014). *Msx2*−/− mutant mice present a non-isometric overall craniofacial size decrease; the teeth exhibit crown and root dysmorphology with altered enamel, enlargement of the pulp cavity, short and curved roots with abnormal orientations, and reduced curvature of the incisor. The third molar showed impaired eruption and the most severe phenotype. **(C,D)** 3D reconstruction of mouse molars revealed the absence of cuspid relief and severe generalized enamel hypoplasia with irregular surface. *Msx2*−/− mice displayed complex radicular morphology (Aïoub et al., 2007). **(E,F)** Scanning electron microscopy of the first molar mandible illustrates a severe reduction in enamel thickness. Enamel in *Msx2*−/− animals shows the absence of enamel prisms, replaced by an amorphous layer (Molla et al., 2010); scale bars: 10 μm. **(G–J)** Histological analysis of mouse molar enamel reveals hypoplastic amelogenesis imperfecta in *Msx2*−/− mice. This feature is related, after a correct ameloblast differentiation process, to a secondary inability of ameloblasts to secrete the enamel matrix which would mineralize. Ameloblast cells in these animals lose their polarization, become rounded and isolated, and finally disappear (Ab, ameloblast; E, enamel —scale bars: **G**, **I**: 100 μm; **H**, **J**: 40 μm).

In summary, all cells associated with the complex formed by tooth and bone express the *Msx2* gene during their lifetime, and do so with exquisitely precise timing and levels. This makes it difficult to directly anticipate MSX2 function in one tissue (*in vivo*) from data obtained *in vitro*. For example, in the periodontal ligament cells, MSX2 prevents osteo-differentiation *in vitro* (Yoshizawa et al., 2004) while bona fide ankylosis is not found in *Msx2*−/− mice (Aïoub et al., 2007). A thorough analysis of MSX2 function in tooth/bone inter-dependent development requires a number of conditional gene mutations or misexpressions in each MSX2-target cell, each corresponding to different restricted temporal windows and finely defined levels of expression. A complementary strategy has been used to rescue osteoclast activity in non-conditional *Msx2*−/− mice by mating *Msx2*−/− mice with a transgenic mouse line overexpressing RANK (Tnfrsf11a), the main osteoclastic-differentiating factor (Castaneda et al., 2013). This allowed the impact of one-cell processes (resorption) on tooth and bone complex formation to be specified and described.

Msx2 CONTROLS MORPHOGENESIS VIA EPITHELIAL *Bmp4* LEVELS AND THE ASSOCIATED DEATH PROGRAM IN ENAMEL KNOT

Early tooth development in *Msx2* null mice is normal, and only a small number of effectors are modified: epithelial *Bmp4* expression decreases whereas expressions of *Fgf4*, the cyclin-dependent kinase (cdk) inhibitor gene p21, and *Shh* are not modified (Bei et al., 2004). Furthermore, *Bmp4* expression is not altered in the mesenchymal compartment. MSX2 intervenes in epithelial-mesenchymal cross-talk, leading to odontogenesis. Mesenchymal BMP4 stimulates *Msx2* and *Cdk* p21 expression in the enamel knot; MSX2 in turn stimulates *Bmp4* expression in epithelial cells. MSX2 *in vitro* cooperates in the BMP4-mediated programmed cell death pathway (Israsena and Kessler, 2002), and *Msx2* overexpression stimulates *Bmp4* increasing apoptosis (Marazzi et al., 1997; Wu et al., 2003). Thus, the regulatory loop initiated by MSX2 is determinant for dental cell signaling and communication and consequently tooth morphogenesis.

ALTERED LAMININ 5α3 PATTERNS AFFECT AMELOBLAST INTEGRITY

In the dental epithelium, laminin 5α3 is expressed in the basal membrane prior to ameloblast differentiation and disappears when cells differentiate (Yoshiba et al., 1998). It has been described as being distributed in a "membrane like" structure localized between the stratum intermedium and ameloblast cell layer. In *Msx2*−/− mice, ameloblasts are able to achieve terminal differentiation but the integrity of their junctional complexes is affected. In the absence of MSX2, the inner dental epithelium presents rounded and detached ameloblasts with loose intercellular junctions (Bei et al., 2004; Molla et al., 2010) (**Figure 4**). Laminin 5α3 expression is lower than in wild-type animals, whereas the expression of E-cadherin, β-catenin, and the integrin subunits α5β5 and α6β4 remains unchanged (Bei et al., 2004; Molla et al., 2010). Thus, the MSX2 target gene laminin 5α3 may control the formation of cell-cell-junctions and thus organization of the ameloblastic layer (Zhou et al., 1999). This possibility is supported by a *LAMA5* gene mutation in the epidermolysis bullosa characterized by skin fragility and enamel dysplasia (Brooks et al., 2008), as a result of the destruction of dermal and dental epithelia, respectively.

PROSPECTS FOR EXPERIMENTAL MODELS—FROM DISCRETE TO CONTINUOUS PARAMETERS OF ENAMEL QUALITY CONTROL

THE PHYSIOLOGICAL CONDITIONS ARE ONLY PARTLY REPRODUCED *IN VITRO*

There have been reported successful *in vitro* promoter studies in ameloblasts (see above) thanks to establishment of cell models that help to decipher molecular mechanisms (Zhou and Snead, 2000; Zhou et al., 2000; Xu et al., 2007a). However,

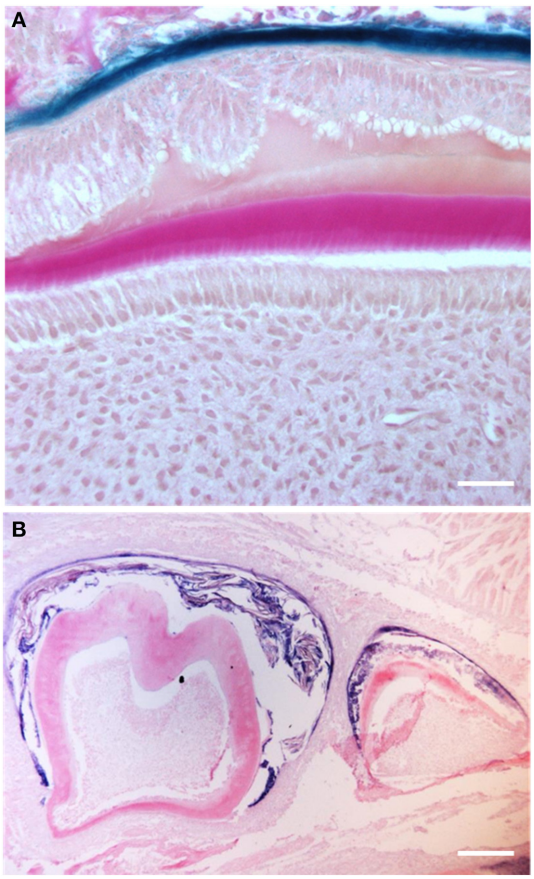

FIGURE 4 | Amelogenin production in 21-day old *Msx2*−/− mice showing ameloblast cell secretory disorders in more detail (Molla et al., 2010). In this condition, the polarity of the entire enamel organ is completely lost. (A) Epithelial cells appear to delaminate losing their orientation and intercellular cohesion (scale bars: 20 μm). **(B)** The apparent level of amelogenin RNA synthesis is uniformly low in the entire enamel organ. The resulting ameloblasts do not produce significant amounts of enamel matrix (scale bars: 100 μm).

the transcriptional program leading to ameloblast activity during enamel presecretion, secretion, and post-secretion is only progressively emerging (Lacruz et al., 2012b; Simmer et al., 2014) (**Figure 2**). Indeed, the spatial and temporal program of enamel formation is not recapitulated in cell cultures. Five factors are more or less reproduced in current cell culture models: (1) Epithelial organization and ameloblast polarity. (2) Signals produced by non ameloblastic cells (enamel knot, stratum intermedium and mesenchymal odontoblasts) which drive ameloblast fate and activity. Indeed, epithelial-mesenchymal interaction has been demonstrated in ameloblasts co-cultured with odontoblasts (Matsumoto et al., 2011). (3) Key stages of presecretion, secretion and post-secretion related to up- and down-regulation of matrix protein levels and protease activities (**Figure 2**). (4) The delicate crystal and prism architecture which requires significant and ordered enamel matrix deposition and biomineralization. (5) An appropriate peridental microenvironment in which bone apposition and resorption rates may influence enamel formation. Indeed, allometric tooth growth is dependent on (and reversely determines) eruption rate (Castaneda et al., 2011, 2013).

THE RODENT INCISOR, AN "*IN VIVO* TEST TUBE" FOR ANALYZING GENE AND ENVIRONMENT INTERACTIONS IN ENAMEL

Various experimental approaches have been developed including organotypic cultures (Bronckers, 1983; Bronckers et al., 2009), primary cultures (DenBesten et al., 2005), and hybrid cell cultures (Matsumoto et al., 2011; Jiang et al., 2014). *In vivo* studies may involve dissections under a microscope which is either manual or, more recently, by laser-capture (Jacques et al., 2014). For growth-limited teeth (three non-renewed molars in rodents), amelogenesis follow-up requires animals of different ages, increasing the sample size required (Onishi et al., 2008). Rodent incisor enamel displays an exceptionally simple structure and is reasonably large. Its continuous growth facilitates the exploration of enamel formation under defined conditions and during defined temporal windows (transgenic mice, environmental, and systemic disturbances) at any animal age (Damkier et al., 2014). The course of amelogenesis is spatially distributed along the longitudinal axis of the tooth. Consequently, extracellular cascades of peptide-peptide and mineral interactions can be sampled along the longitudinal axis of single rodent incisors (Jedeon et al., 2013), and ameloblasts and changing enamel matrix are easily followed (Houari et al., 2014). Protein and mRNA studies are feasible and have included comparisons between incisor samples from test and control conditions in rats (Berdal et al., 1993; Jedeon et al., 2013) and mice (Descroix et al., 2010; Molla et al., 2010).

MSX2 IS A MORPHOGEN FOR ENAMEL, CONTROLLING ITS THICKNESS

The murine incisor "*in vivo* test tube" has been used in studies of MSX2 in differentiated ameloblasts. *Msx2* heterozygous (*Msx2*+/−) mice are a unique model for investigating MSX2 dose effects. Ameloblasts survive and differentiate appropriately in *Msx2*+/− mice (unlike those in *Msx2*−/− mice) and the amounts of *Msx2* mRNA are half those in wild-type mice. Enamel gene studies have revealed a specific overabundance of amelogenin mRNA in *Msx2*+/− mice. The enamel phenotype in *Msx2*+/− mice included increased thickness and, more specifically, a thicker outer prismatic enamel layer and larger prism diameter (Molla et al., 2010; **Figure 5**). This suggests that MSX2 determines enamel thickness *in vivo*. Indeed, a rigorous analysis of the pattern of *Msx2* expression during the secretion stage revealed a inverse relationship between *Msx2* mRNA levels and enamel thickness (Molla et al., 2010) as similarly described for enamel thickness and amelogenin levels (Snead et al., 1988). This is also the case for DLX2 (Lézot et al., 2008) in which an inverse correlation between DLX2 levels and thickness was shown through quantitative measurements of incisors. Also, decreased production of enamel proteins during the enamel maturation stage is associated with a significant up-regulation of *Msx2* (**Figure 5**), in accordance with *in vitro* data showing the MSX2 transcriptional repression of amelogenin expression. On the contrary, ameloblast alterations observed in *Msx2*−/− mice result in deficient enamel protein production (especially amelogenin) and result in hypoplastic enamel without visible prismatic structures (Molla et al., 2010—see **Figure 3F**).

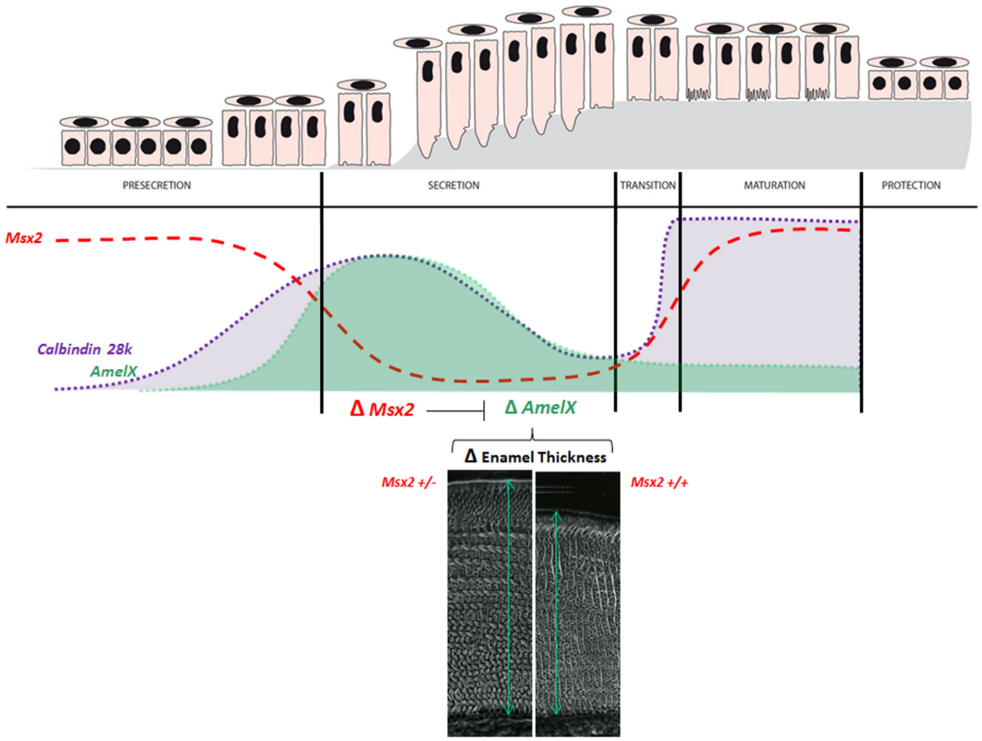

FIGURE 5 | Physiological levels of MSX2 and its target-genes, amelogenin and calbindin-D_{28k}. *Msx2* expression during the ameloblast life-cycle is inversely related to amelogenin abundance. The figure is a compilation of published findings (Molla et al., 2010) and illustrates two significant examples of gene expression level fluctuations (amelogenin—green; and calbindin-D_{28k}—gray) in ameloblasts during amelogenesis and their relationships with *Msx2* expression (red). (1) The presecretion/secretion/maturation sequence. *Msx2* down-regulation is related to down-regulation of amelogenin and calbindin-D_{28k} from the presecretion stage to the secretion stage. (2) During the secretion stage controlling enamel thickness; amelogenin mRNA production in ameloblasts depends on their sites or localization (Snead et al., 1988), leading to the differing thickness of enamel across the tooth. The patterns of *Msx2* and *Dlx2* expression are the converse of that of amelogenin (Lézot et al., 2008). We established that MSX2 indeed contributes to enamel thickness inhibition *in vivo* (Molla et al., 2010). Enamel thickness as determined by scanning electron microscopy in mandible incisor of 3-month old mice is greater under *Msx2* haploinsufficiency than in controls (here *Msx2*+/− compared to wild-type *Msx2*+/+ mice). This Msx2 haploinsufficiency is also associated with overexpression of both amelogenin (Molla et al., 2010) and calbindin-D_{28k} (Bolaños et al., 2012). The relationship between calbindin-D_{28k} and MSX2 is more complex because calbindin-D_{28k} abundance abruptly increases for a second time during the maturation stage. However, the partners of MSX2 at this stage are still unknown and its activity on gene expression has not been extensively investigated.

CONCLUSION

Integrative physiological networks underlying amelogenesis are just emerging. Experimental progress in the field of enamel has mainly been based on gene disrupting strategies to describe developmental circuits which drive enamel formation. However, only precise quantitative and continuous studies allow appropriate analysis of the interplays that determine enamel thickness and quality. This is the case for studies addressing the constitutive regulation of ameloblast activity, illustrated here by the MSX and DLX homeoprotein pathways. They provide clues on how enamel acquires differential thickness depending on its anatomical location. They modulate expression of key genes involved in amelogenesis (Lézot et al., 2002, 2008; Molla et al., 2010; Bolaños et al., 2012). It is thus very likely that these factors are able to transmit effects of many environmental factors, whether regional or systemic (including the availability of calcium, vitamin D, fluoride, or even pollutants) that also affect the final enamel composition and quality (Berdal et al., 1993; Jedeon et al., 2013; Houari et al., 2014).

In summary, the dental cell and enamel system illustrates how MSX homeoproteins may be reiteratively enrolled in a single organ. Throughout the cell life-cycle, cooperation between particular transcription factors in a stage-specific manner controls the expression of a number of genes. Such MSX2-target genes encode growth factors, junctional complexes, matrix proteins, and other proteins involved in enamel mineralization. Consistent with reiterative up- and down-regulations, MSX2 drives particular events; some in early development, some during growth and, finally, some in conditions of homeostasis in adults with the effect decreasing with age. MSX2 is exemplary of the integrative schemes of a single transcription factor making multiple contributions to the physiological or pathological development of complex organs, composed of many cells of different types, as described here in the dental-bone complex.

FUNDING

This work was funded by the University Paris-Diderot, the French National Institute of Health and Medical Research (INSERM) and the National Research Agency (ANR): OSTEODIVERSITY (SVSE 1-2012).

REFERENCES

Aïoub, M., Lézot, F., Molla, M., Castaneda, B., Robert, B., Goubin, G., et al. (2007). Msx2 −/− transgenic mice develop compound amelogenesis imperfecta, dentinogenesis imperfecta and periodental osteopetrosis. *Bone* 41, 851–859. doi: 10.1016/j.bone.2007.07.023

Athanassiou-Papaefthymiou, M., Kim, D., Harbron, L., Papagerakis, S., Schnell, S., Harada, H., et al. (2011). Molecular and circadian controls of ameloblasts. *Eur. J. Oral Sci.* 119(Suppl. 1), 35–40. doi: 10.1111/j.1600-0722.2011.00918.x

Babajko, S., Petit, S., Fernandes, I., Méary, F., LeBihan, J., Pibouin, L., et al. (2009). Msx1 expression regulation by its own antisense RNA: consequence on tooth development and bone regeneration. *Cells Tissues Organs* 189, 115–121. doi: 10.1159/000151748

Bei, M. (2009). Molecular genetics of ameloblast cell lineage. *J. Exp. Zool. B Mol. Dev. Evol.* 312B, 437–444. doi: 10.1002/jez.b.21261

Bei, M., and Maas, R. (1998). FGFs and BMP4 induce both Msx1-independent and Msx1-dependent signaling pathways in early tooth development. *Development* 125, 4325–4333.

Bei, M., Stowell, S., and Maas, R. (2004). Msx2 controls ameloblast terminal differentiation. *Dev. Dyn.* 231, 758–765. doi: 10.1002/dvdy.20182

Bendall, A. J., and Abate-Shen, C. (2000). Roles for Msx and Dlx homeoproteins in vertebrate development. *Gene* 247, 17–31. doi: 10.1016/S0378-1119(00)00081-0

Bendall, A. J., Ding, J., Hu, G., Shen, M. M., and Abate-Shen, C. (1999). Msx1 antagonizes the myogenic activity of Pax3 in migrating limb muscle precursors. *Development* 26, 4965–4976.

Berdal, A., Hotton, D., Pike, J. W., Mathieu, H., and Dupret, J. M. (1993). Cell- and stage-specific expression of vitamin D receptor and calbindin genes in rat incisor: regulation by 1,25-dihydroxyvitamin D3. *Dev. Biol.* 155, 172–179.

Blin-Wakkach, C., Lezot, F., Ghoul-Mazgar, S., Hotton, D., Monteiro, S., Teillaud, C., et al. (2001). Endogenous Msx1 antisense transcript: *in vivo* and *in vitro* evidences, structure, and potential involvement in skeleton development in mammals. *Proc. Natl. Acad. Sci. U.S.A.* 98, 7336–7341. doi: 10.1073/pnas.131497098

Bloch-Zupan, A., Décimo, D., Loriot, M., Mark, M. P., and Ruch, J. V. (1994). Expression of nuclear retinoic acid receptors during mouse odontogenesis. *Differentiation* 57, 195–203. doi: 10.1046/j.1432-0436.1994.5730195.x

Bolaños, A., Hotton, D., Ferbus, D., Loiodice, S., Berdal, A., and Babajko, S. (2012). Regulation of calbindin-D (28k) expression by Msx2 in the dental epithelium. *J. Histochem. Cytochem.* 60, 603–610. doi: 10.1369/0022155412450641

Bronckers, A. L. (1983). Effect of oxygen tension on matrix formation and mineralization in hamster molars during development *in vitro*. *J. Biol. Buccale* 11, 195–207.

Bronckers, A. L., Lyaruu, D. M., and DenBesten, P. K. (2009). The impact of fluoride on ameloblasts and the mechanisms of enamel fluorosis. *J. Dent. Res.* 88, 877–893. doi: 10.1177/0022034509343280

Brooks, J. K., Bare, L. C., Davidson, J., Taylor, L. S., and Wright, J. T. (2008). Junctional epidermolysis bullosa associated with hypoplastic enamel and pervasive failure of tooth eruption: oral rehabilitation with use of an overdenture. *Oral Surg. Oral Med. Oral Pathol. Oral Radiol. Endod.* 105, e24–e28. doi: 10.1016/j.tripleo.2007.12.038

Brugger, S. M., Merrill, A. E., Torres-Vazquez, J., Wu, N., Ting, M. C., Cho, J. Y., et al. (2004). A phylogenetically conserved cis-regulatory module in the Msx2 promoter is sufficient for BMP-dependent transcription in murine and Drosophila embryos. *Development* 131, 5153–5165. doi: 10.1242/dev.01390

Cao, H., Jheon, A., Li, X., Sun, Z., Wang, J., Florez, S., et al. (2013). The Pitx2: miR-200c/141:noggin pathway regulates Bmp signaling and ameloblast differentiation. *Development* 140, 3348–3359. doi: 10.1242/dev.089193

Castaneda, B., Simon, Y., Ferbus, D., Robert, B., Chesneau, J., Mueller, C., et al. (2013). Role of RANKL (TNFSF11)-dependent osteopetrosis in the dental phenotype of Msx2 null mutant mice. *PLoS ONE* 8:e80054. doi: 10.1371/journal.pone.0080054

Castaneda, B., Simon, Y., Jacques, J., Hess, E., Choi, Y. W., Blin-Wakkach, C., et al. (2011). Bone resorption control of tooth eruption and root morphogenesis: involvement of the receptor activator of NF-κB (RANK). *J. Cell. Physiol.* 226, 74–85. doi: 10.1002/jcp.22305

Catón, J., Luder, H. U., Zoupa, M., Bradman, M., Bluteau, G., Tucker, A. S., et al. (2009). Enamel-free teeth: Tbx1 deletion affects amelogenesis in rodent incisors. *Dev. Biol.* 328, 493–505. doi: 10.1016/j.ydbio.2009.02.014

Catron, K. M., Iler, N., and Abate, C. (1993). Nucleotides flanking a conserved TAAT core dictate the DNA binding specificity of three murine homeodomain proteins. *Mol. Cell. Biol.* 13, 2354–2365.

Catron, K. M., Wang, H., Hu, G., Shen, M. M., and Abate-Shen, C. (1996). Comparison of MSX-1 and MSX-2 suggests a molecular basis for functional redundancy. *Mech. Dev.* 55, 185–199.

Catron, K. M., Zhang, H., Marshall, S. C., Inostroza, J. A., Wilson, J. M., and Abate, C. (1995). Transcriptional repression by Msx-1 does not require homeodomain DNA-binding sites. *Mol. Cell. Biol.* 15, 861–871.

Cheng, S. L., Shao, J. S., Charlton-Kachigian, N., Loewy, A. P., and Towler, D. A. (2003). MSX2 promotes osteogenesis and suppresses adipogenic differentiation of multipotent mesenchymal progenitors. *J. Biol. Chem.* 278, 45969–45977. doi: 10.1074/jbc.M306972200

Coudert, A. E., Pibouin, L., Vi-Fane, B., Thomas, B. L., Macdougall, M., Choudhury, A., et al. (2005). Expression and regulation of the Msx1 natural antisense transcript during development. *Nucleic Acids Res.* 33, 5208–5218. doi: 10.1093/nar/gki831

Damkier, H. H., Josephsen, K., Takano, Y., Zahn, D., Fejerskov, O., and Frische, S. (2014). Fluctuations in surface pH of maturing rat incisor enamel are a result of cycles of H(+)-secretion by ameloblasts and variations in enamel buffer characteristics. *Bone* 60, 227–234. doi: 10.1016/j.bone.2013.12.018

Davideau, J. L., Papagerakis, P., Hotton, D., Lezot, F., and Berdal, A. (1996). *In situ* investigation of vitamin D receptor, alkaline phosphatase, and osteocalcin gene expression in oro-facial mineralized tissues. *Endocrinology* 137, 3577–3585.

DenBesten, P. K., Machule, D., Zhang, Y., Yan, Q., and Li, W. (2005). Characterization of human primary enamel organ epithelial cells *in vitro*. *Arch. Oral Biol.* 50, 689–694. doi: 10.1016/j.archoralbio.2004.12.008

Descroix, V., Kato, S., Lézot, F., and Berdal, A. (2010). Physiopathology of dental rickets in vitamin D receptor-ablated mice. *J. Dent. Res.* 89, 1427–1432. doi: 10.1177/0022034510379603

Dhamija, S., and Krebsbach, P. H. (2001). Role of Cbfa1 in ameloblastin gene transcription. *J. Biol. Chem.* 276, 35159–35164. doi: 10.1074/jbc.M101 0719200

Dodig, M., Kronenberg, M. S., Bedalov, A., Kream, B. E., Gronowicz, G., Clark, S. H., et al. (1996). Identification of a TAAT-containing motif required for high level expression of the COL1A1 promoter in differentiated osteoblasts of transgenic mice. *J. Biol. Chem.* 271, 16422–16429.

Ferrer, V. L., Maeda, T., and Kawano, Y. (2005). Characteristic distribution of immunoreaction for estrogen receptor alpha in rat ameloblasts. *Anat. Rec. A Discov. Mol. Cell. Evol. Biol.* 284, 529–536. doi: 10.1002/ar.a.20190

Fukumoto, S., Kiba, T., Hall, B., Iehara, N., Nakamura, T., Longenecker, G., et al. (2004). Ameloblastin is a cell adhesion molecule required for maintaining the differentiation state of ameloblasts. *J. Cell Biol.* 167, 973–983. doi: 10.1083/jcb.200409077

Gehring, W. J., Qian, Y. Q., Billeter, M., Furukubo-Tokunaga, K., Schier, A. F., Resendez-Perez, D., et al. (1994). Homeodomain-DNA recognition. *Cell* 78, 211–223. doi: 10.1016/0092-8674(94)90292-5

Golonzhka, O., Metzger, D., Bornert, J. M., Bay, B. K., Gross, M. K., Kioussi, C., et al. (2009). Ctip2/Bcl11b controls ameloblast formation during mammalian odontogenesis. *Proc. Natl. Acad. Sci. U.S.A.* 106, 4278–4283. doi: 10.1073/pnas.0900568106

Houari, S., Wurtz, T., Ferbus, D., Chateau, D., Desombz, A., Berdal, A., et al. (2014). Asporin and the mineralization process in fluoride-treated rats. *J. Bone Min. Res.* 29, 1446–1455. doi: 10.1002/jbmr.2153

Houzelstein, D., Cohen, A., Buckingham, M. E., and Robert, B. (1997). Insertional mutation of the mouse Msx1 homeobox gene by an nlacZ reporter gene. *Mech. Dev.* 65, 123–133.

Israsena, N., and Kessler, J. A. (2002). Msx2 and p21(CIP1/WAF1) mediate the proapoptotic effects of bone morphogenetic protein-4 on ventricular zone progenitor cells. *J. Neurosci. Res.* 69, 803–809. doi: 10.1002/jnr.10362

Jedeon, K., De la Dure-Molla, M., Brookes, S. J., Loiodice, S., Marciano, C., Kirkham, J., et al. (2013). Enamel defects reflect perinatal exposure to bisphenol A. *Am. J. Pathol.* 183, 108–118. doi: 10.1016/j.ajpath.2013.04.004

Jacques, J., Hotton, D., De la Dure-Molla, M., Kulkarni, A. B., and Gibson, C., Petit, S., et al. (2014). Tracking endogenous amelogenin and ameloblastin *in vivo*. *PLoS ONE* 9:e99626. doi: 10.1371/journal.pone.0099626

Jiang, N., Zhou, J., Chen, M., Schiff, M. D., Lee, C. H., Kong, K., et al. (2014). Postnatal epithelium and mesenchyme stem/progenitor cells in bioengineered amelogenesis and dentinogenesis. *Biomaterials* 35, 2172–2180. doi: 10.1016/j.biomaterials.2013.11.061

Jiang, S. Y., and Wang, J. T. (2010). Msx2 alters the timing of retinal ganglion cells fate commitment and differentiation. *Biochem. Biophys. Res. Commun.* 395, 524–529. doi: 10.1016/j.bbrc.2010.04.058

Lacruz, R. S., Hacia, J. G., Bromage, T. G., Boyde, A., Lei, Y., Xu, Y., et al. (2012a). The circadian clock modulates enamel development. *J. Biol. Rhythms* 27, 237–245. doi: 10.1177/0748730412442830

Lacruz, R. S., Smith, C. E., Bringas, P. Jr., Chen, Y. B., Smith, S. M., Snead, M. L., et al. (2012b). Identification of novel candidate genes involved in mineralization of dental enamel by genome-wide transcript profiling. *J. Cell. Physiol.* 227, 2264–2275. doi: 10.1002/jcp.22965

Lee, H. K., Lee, D. S., Ryoo, H. M., Park, J. T., Park, S. J., Bae, H. S., et al. (2010). The odontogenic ameloblast-associated protein (ODAM) cooperates with RUNX2 and modulates enamel mineralization via regulation of MMP-20. *J. Cell. Biochem.* 111, 755–767. doi: 10.1002/jcb.22766

Lee, H., Quinn, J. C., Prasanth, K. V., Swiss, V. A., Economides, K. D., Camacho, M. M., et al. (2006). PIAS1 confers DNA-binding specificity on the Msx1 homeoprotein. *Genes Dev.* 20, 784–794. doi: 10.1101/gad.1392006

Lézot, F., Descroix, V., Mesbah, M., Hotton, D., Blin, C., Papagerakis, P., et al. (2002). Cross-talk between Msx/Dlx homeobox genes and vitamin D during tooth mineralization. *Connect. Tissue Res.* 43, 509–514. doi: 10.1080/03008200290000583

Lézot, F., Thomas, B., Greene, S. R., Hotton, D., Yuan, Z. A., Castaneda, B., et al. (2008). Physiological implications of DLX homeoproteins in enamel formation. *J. Cell. Physiol.* 216, 688–697. doi: 10.1002/jcp.21448

Li, X., Florez, S., Wang, J., Cao, H., and Amendt, B. A. (2013). Dact2 represses PITX2 transcriptional activation and cell proliferation through Wnt/beta-catenin signaling during odontogenesis. *PLoS ONE* 8:e54868. doi: 10.1371/journal.pone.0054868

Li, X., Venugopalan, S. R., Cao, H., Pinho, F. O., Paine, M. L., Snead, M. L., et al. (2014). A model for the molecular underpinnings of tooth defects in Axenfeld-Rieger syndrome. *Hum. Mol. Genet.* 23, 194–208. doi: 10.1093/hmg/ddt411

Liu, Y. H., Kundu, R., Wu, L., Luo, W., Ignelzi, M. A. Jr., Snead, M. L., et al. (1995). Premature suture closure and ectopic cranial bone in mice expressing Msx2 transgenes in the developing skull. *Proc. Natl. Acad. Sci. U.S.A.* 92, 6137–6141.

Maas, R., and Bei, M. (1997). The genetic control of early tooth development. *Crit. Rev. Oral Biol. Med.* 8, 4–39.

Mackenzie, A., Ferguson, M. W., and Sharpe, P. T. (1992). Expression patterns of the homeobox gene, Hox-8, in the mouse embryo suggest a role in specifying tooth initiation and shape. *Development* 115, 403–420.

Mackenzie, A., Leeming, G. L., Jowett, A. K., Ferguson, M. W., and Sharpe, P. T. (1991). The homeobox gene Hox 7.1 has specific regional and temporal expression patterns during early murine craniofacial embryogenesis, especially tooth development *in vivo* and *in vitro*. *Development* 111, 269–285.

Mainguy, G., Koster, J., Woltering, J., Jansen, H., and Durston, A. (2007). Extensive polycistronism and antisense transcription in the mammalian Hox clusters. *PLoS ONE* 2:e356. doi: 10.1371/journal.pone.0000356

Marazzi, G., Wang, Y., and Sassoon, D. (1997). Msx2 is a transcriptional regulator in the BMP4-mediated programmed cell death pathway. *Dev. Biol.* 186, 127–138.

Matsumoto, A., Harada, H., Saito, M., and Taniguchi, A. (2011). Induction of enamel matrix protein expression in an ameloblast cell line co-cultured with a mesenchymal cell line *in vitro*. *In Vitro Cell. Dev. Biol. Anim.* 47, 39–44. doi: 10.1007/s11626-010-9362-7

Mirzayans, F., Lavy, R., Penner-Chea, J., and Berry, F. B. (2012). Initiation of early osteoblast differentiation events through the direct transcriptional regulation of Msx2 by FOXC1. *PLoS ONE* 7:e49095. doi: 10.1371/journal.pone.0049095

Mitsiadis, T. A., Tucker, A. S., De Bari, C., Cobourne, M. T., and Rice, D. P. (2008). A regulatory relationship between Tbx1 and FGF signaling during tooth morphogenesis and ameloblast lineage determination. *Dev. Biol.* 320, 39–48. doi: 10.1016/j.ydbio.2008.04.006

Molla, M., Descroix, V., Aïoub, M., Simon, S., Castañeda, B., Hotton, D., et al. (2010). Enamel protein regulation and dental and periodontal physiopathology in MSX2 mutant mice. *Am. J. Pathol.* 177, 2516–2526. doi: 10.2353/ajpath.2010.091224

Muto, T., Miyoshi, K., Horiguchi, T., and Noma, T. (2012). Dissection of morphological and metabolic differentiation of ameloblasts via ectopic SP6 expression. *J. Med. Invest.* 59, 59–68. doi: 10.2152/jmi.59.59

Nassif, A., Senussi, I., Méary, F., Loiodice, S., Hotton, D., Robert, B., et al. (2014). Msx1 role in craniofacial bone morphogenesis. *Bone* 66, 96–104. doi: 10.1016/j.bone.2014.06.003

Ogawa, T., Kapadia, H., Feng, J. Q., Raghow, R., Peters, H., and D'Souza, R. N. (2006). Functional consequences of interactions between Pax9 and Msx1 genes in normal and abnormal tooth development. *J. Biol. Chem.* 281, 18363–18369. doi: 10.1074/jbc.M601543200

Onishi, T., Shintani, S., Wakisaka, S., and Ooshima, T. (2008). Relationship of vitamin D with calbindin D9k and D28k expression in ameloblasts. *Arch. Oral Biol.* 53, 117–123. doi: 10.1016/j.archoralbio.2007.09.009

Petit, S., Meary, F., Pibouin, L., Jeanny, J. C., Fernandes, I., Poliard, A., et al. (2009). Autoregulatory loop of Msx1 expression involving its antisense transcripts. *J. Cell. Physiol.* 220, 303–310. doi: 10.1002/jcp.21762

Sahlberg, C., Pohjanvirta, R., Gao, Y., Alaluusua, S., Tuomisto, J., and Lukinmaa, P. L. (2002). Expression of the mediators of dioxin toxicity, aryl hydrocarbon receptor (AHR) and the AHR nuclear translocator (ARNT), is developmentally regulated in mouse teeth. *Int. J. Dev. Biol.* 46, 295–300.

Satokata, I., and Maas, R. (1994). Msx1 deficient mice exhibit cleft palate and abnormalities of craniofacial and tooth development. *Nat. Genet.* 6, 348–356.

Satokata, I., Ma, L., Ohshima, H., Bei, M., Woo, I., Nishizawa, K., et al. (2000). Msx2 deficiency in mice causes pleiotropic defects in bone growth and ectodermal organ formation. *Nat. Genet.* 24, 391–395. doi: 10.1038/74231

Shao, J. S., Cheng, S. L., Pingsterhaus, J. M., Charlton-Kachigian, N., Loewy, A. P., and Towler, D. A. (2005). Msx2 promotes cardiovascular calcification by activating paracrine Wnt signals. *J. Clin. Invest.* 115, 1210–1220. doi: 10.1172/JCI24140

Sharpe, P. T. (1995). Homeobox genes and orofacial development. *Connect. Tissue Res.* 32, 17–25. doi: 10.3109/03008209509013701

Shirasawa, T., Sakamoto, K., and Tkahashi, H. (1994). Molecular cloning and evolutional analysis of a mammalian homologue of the Distal-less 3 (Dlx-3) homeobox gene. *FEBS Lett.* 351, 380–384. doi: 10.1016/0014-5793(94)00896-5

Simmer, J. P., Richardson, A. S., Wang, S. K., Reid, B. M., Bai, Y., Hu, H. et al. (2014). Ameloblast transcriptome changes from secretory to maturation stages. *Connect Tissue Res.* 55(Suppl. 1), 29–32. doi: 10.3109/03008207.2014.923862

Simon, Y., Marchadier, A., Riviere, M. K., Vandamme, K., Koenig, F., Lezot, F., et al. (2014). Cephalometric assessment of craniofacial dysmorphologies in relation with Msx2 mutations in mouse. *Orthod. Craniofac. Res.* 17, 92–105. doi: 10.1111/ocr.12035

Snead, M. L., Luo, W., Lau, E. C., and Slavkin, H. C. (1988). Spatial- and temporal-restricted pattern for amelogenin gene expression during mouse molar tooth organogenesis. *Development* 104, 77–85.

Sonoda, A., Iwamoto, T., Nakamura, T., Fukumoto, E., Yoshizaki, K., Yamada, A., et al. (2009). Critical role of heparin binding domains of ameloblastin for dental epithelium cell adhesion and ameloblastoma proliferation. *J. Biol. Chem.* 284, 27176–27184. doi: 10.1074/jbc.M109.033464

Stahl, J., Nakano, Y., Kim, S. O., Gibson, C. W., Le, T., and DenBesten, P. (2013). Leucine rich amelogenin peptide alters ameloblast differentiation *in vivo*. *Matrix Biol.* 32, 432–442. doi: 10.1016/j.matbio.2013.05.004

Thesleff, I. (2003). Epithelial-mesenchymal signalling regulating tooth morphogenesis. *J. Cell Sci.* 116, 1647–1648. doi: 10.1242/jcs.00410

Thesleff, I. (2006). The genetic basis of tooth development and dental defects. *Am. J. Med. Genet. A* 140, 2530–2535. doi: 10.1002/ajmg.a.31360

Tian, H., Lv, P., Ma, K., Zhou, C., and Gao, X. (2010). Beta-catenin/LEF1 activated enamelin expression in ameloblast-like cells. *Biochem. Biophys. Res. Commun.* 398, 519–524. doi: 10.1016/j.bbrc.2010.06.111

Vastardis, H., Karimbux, N., Guthua, S. W., Seidman, J. G., and Seidman, C. E. (1996). A human MSX1 homeodomain missense mutation causes selective tooth agenesis. *Nat. Genet.* 13, 417–421.

Venugopalan, S. R., Li, X., Amen, M. A., Florez, S., Gutierrez, D., Cao, H., et al. (2011). Hierarchical interactions of homeodomain and forkhead transcription factors in regulating odontogenic gene expression. *J. Biol. Chem.* 286, 21372–21383. doi: 10.1074/jbc.M111.252031

Wang, J., and Abate-Shen, C. (2012). Transcriptional repression by the Msx1 homeoprotein is associated with global redistribution of the H3K27me3 repressive mark to the nuclear periphery. *Nucleus* 3, 155–161. doi: 10.4161/nucl.19477

Wang, Y., Kong, H., Mues, G., and D'Souza, R. (2011). Msx1 mutations: how do they cause tooth agenesis? *J. Dent. Res.* 90, 311–316. doi: 10.1177/0022034510387430

Wu, L. Y., Li, M., Hinton, D. R., Guo, L., Jiang, S., Wang, J. T., et al. (2003). Microphthalmia resulting from MSX2-induced apoptosis in the optic vesicle. *Invest. Ophthalmol. Vis. Sci.* 44, 2404–2412. doi: 10.1167/iovs.02-0317

Xu, L., Matsumoto, A., Sasaki, A., Harada, H., and Taniguchi, A. (2010). Identification of a suppressor element in the amelogenin promoter. *J. Dent. Res.* 89, 246–251. doi: 10.1177/0022034509355144

Xu, Y., Zhou, Y. L., Erickson, R. L., MacDougald, O. A., and Snead, M. L. (2007a). Physical dissection of the CCAAT/enhancer-binding protein alpha in regulating the mouse amelogenin gene. *Biochem. Biophys. Res. Commun.* 354, 56–61. doi: 10.1016/j.bbrc.2006.12.182

Xu, Y., Zhou, Y. L., Gonzalez, F. J., and Snead, M. L. (2007b). CCAAT/enhancer-binding protein delta (C/EBPdelta) maintains amelogenin expression in the absence of C/EBPalpha *in vivo*. *J. Biol. Chem.* 282, 29882–29889. doi: 10.1074/jbc.M702097200

Xu, Y., Zhou, Y. L., Luo, W., Zhu, Q. S., Levy, D., MacDougald, O. A., et al. (2006). NF-Y and CCAAT/enhancer-binding protein alpha synergistically activate the mouse amelogenin gene. *J. Biol. Chem.* 281, 16090–16098. doi: 10.1074/jbc.M510514200

Yamashiro, T., Tummers, M., and Thesleff, I. (2003). Expression of bone morphogenetic proteins and Msx genes during root formation. *J. Dent. Res.* 82, 172–176. doi: 10.1177/154405910308200305

Yanagawa, T., Itoh, K., Uwayama, J., Shibata, Y., Yamaguchi, A., Sano, T., et al. (2004). Nrf2 deficiency causes tooth decolourization due to iron transport disorder in enamel organ. *Genes Cells* 9, 641–651. doi: 10.1111/j.1356-9597.2004.00753.x

Yasukawa, M., Ishida, K., Yuge, Y., Hanaoka, M., Minami, Y., Ogawa, M., et al. (2013). Dpysl4 is involved in tooth germ morphogenesis through growth regulation, polarization and differentiation of dental epithelial cells. *Int. J. Biol. Sci.* 9, 382–390. doi: 10.7150/ijbs.5510

Yoshiba, N., Yoshiba, K., Aberdam, D., Meneguzzi, G., Perrin-Schmitt, F., Stoetzel, C., et al. (1998). Expression and localization of laminin-5 subunits in the mouse incisor. *Cell Tissue Res.* 292, 143–149.

Yoshizawa, T., Takizawa, F., Iizawa, F., Ishibashi, O., Kawashima, H., Matsuda, A., et al. (2004). Homeobox protein MSX2 acts as a molecular defense mechanism for preventing ossification in ligament fibroblasts. *Mol. Cell. Biol.* 24, 3460–3472. doi: 10.1128/MCB.24.8.3460-3472.2004

Zhang, H., Catron, K. M., and Abate-Shen, C. (1996). A role for the Msx-1 homeodomain in transcriptional regulation: residues in the N-terminal arm mediate TATA binding protein interaction and transcriptional repression. *Proc. Natl. Acad. Sci. U.S.A.* 93, 1764–1769.

Zhang, H., Hu, G., Wang, H., Sciavolino, P., Iler, N., Shen, M. M., et al. (1997). Heterodimerization of Msx and Dlx homeoproteins results in functional antagonism. *Mol. Cell. Biol.* 17, 2920–2932.

Zhang, Y., Li, W., Chi, H. S., Chen, J., and Denbesten, P. K. (2007). JNK/c-Jun signaling pathway mediates the fluoride-induced down-regulation of MMP-20 *in vitro*. *Matrix Biol.* 26, 33–641. doi: 10.1016/j.matbio.2007.06.002

Zheng, L., Seon, Y. J., Mourão, M. A., Schnell, S., Kim, D., Harada, H., et al. (2013). Circadian rhythms regulate amelogenesis. *Bone* 55, 158–165. doi: 10.1016/j.bone.2013.02.011

Zhou, H. M., Nichols, A., Wohlwend, A., Bolon, I., and Vassalli, J. D. (1999). Extracellular proteolysis alters tooth development in transgenic mice expressing urokinase-type plasminogen activator in the enamel organ. *Development* 126, 903–912.

Zhou, Y. L., Lei, Y., and Snead, M. L. (2000). Functional antagonism between Msx2 and CCAAT/enhancer-binding protein alpha in regulating the mouse amelogenin gene expression is mediated by protein-protein interaction. *J. Biol. Chem.* 275, 29066–29075. doi: 10.1074/jbc.M002031200

Zhou, Y. L., and Snead, M. L. (2000). Identification of CCAAT/enhancer-binding protein alpha as a transactivator of the mouse amelogenin gene. *J. Biol. Chem.* 275, 12273–12280. doi: 10.1074/jbc.275.16.12273

Conflict of Interest Statement: The authors declare that the research was conducted in the absence of any commercial or financial relationships that could be construed as a potential conflict of interest.

Received: 11 June 2014; accepted: 08 December 2014; published online: 05 January 2015.

Citation: Babajko S, de La Dure-Molla M, Jedeon K and Berdal A (2015) MSX2 in ameloblast cell fate and activity. Front. Physiol. ***5****:510. doi: 10.3389/fphys.2014.00510 This article was submitted to Craniofacial Biology, a section of the journal Frontiers in Physiology.*

frontiers in
PHYSIOLOGY

ORIGINAL RESEARCH ARTICLE
published: 11 July 2014
doi: 10.3389/fphys.2014.00254

The flexible structure of the K24S28 region of Leucine-Rich Amelogenin Protein (LRAP) bound to apatites as a function of surface type, calcium, mutation, and ionic strength

Jun-xia Lu, Sarah D. Burton, Yimin S. Xu, Garry W. Buchko and Wendy J. Shaw*

Fundamental and Computational Sciences Directorate, Pacific Northwest National Laboratory, Richland, WA, USA

Edited by:
Megan Pugach-Gordon, The Forsyth Insitute, USA

Reviewed by:
Javier Catón, King's College London, UK
Seo-Young Kwak, The Forsyth Institute, USA

Correspondence:
Wendy J. Shaw, Fundamental and Computational Sciences Directorate, Pacific Northwest National Laboratory, Richland, WA, USA
e-mail: wendy.shaw@pnnl.gov

Leucine-Rich Amelogenin Protein (LRAP) is a member of the amelogenin family of biomineralization proteins, proteins which play a critical role in enamel formation. Recent studies have revealed the structure and orientation of the N- and C-terminus of LRAP bound to hydroxyapatite (HAP), a surface used as an analog of enamel. The structure of one region, K24 to S28, was found to be sensitive to phosphorylation of S16, the only naturally observed site of serine phosphorylation in LRAP, suggesting that K24S28 may sit at a key region of structural flexibility and play a role in the protein's function. In this work, we investigated the sensitivity of the structure and orientation of this region when bound to HAP as a function of several factors which may vary during enamel formation to influence structure: the ionic strength (0.05, 0.15, 0.2 M), the calcium concentration (0.07 and 0.4 mM), and the surface to which it is binding [HAP and carbonated apatite (CAP), a more direct mimic of enamel]. A naturally occurring mutation found in amelogenin (T21I) was also investigated. The structure in the K24S28 region of the protein was found to be sensitive to these conditions, with the CAP surface and excess Ca^{2+} (8:1 [Ca^{2+}]:[LRAP-K24S28(+P)]) resulting in a tighter helix, while low ionic strength relaxed the helical structure. Higher ionic strength and the point mutation did not result in any structural change in this region. The distance of the backbone of K24 from the surface was most sensitive to excess Ca^{2+} and in the T21I-mutation. Collectively, these data suggest that phosphorylated LRAP is able to accommodate structural changes while maintaining its interaction with the surface, and provides further evidence of the structural sensitivity of the K24S28 region, a sensitivity that may contribute to function in biomineralization.

Keywords: amelogenin, LRAP, secondary structure, biomineralization protein, solid state NMR

INTRODUCTION

Leucine-Rich Amelogenin Protein (LRAP) (Gibson et al., 1991) is a member of the amelogenin family of proteins, proteins which are known to be essential in the formation of enamel (Simmer and Fincham, 1995; Fincham et al., 1999; Margolis et al., 2006). The 59-residue protein is a splice-variant of full-length amelogenin and contains only the N- and the C-terminus (Gibson et al., 1991), regions associated with protein-protein and protein-HAP interactions in the full-length protein (Simmer and Fincham, 1995; Margolis et al., 2006). The role of LRAP in enamel formation is unclear, but it has been demonstrated to control both crystal organization *in vivo* (Gibson et al., 2008) and crystal width *in vitro* (Ravindranath et al., 2007), and may also serve a protein-regulating role (Stahl et al., 2013).

Structural studies of amelogenin have been challenged due to their self-assembly into quaternary structures containing 20–100 monomers called nanospheres (Fincham et al., 1994; Moradian-Oldak et al., 1994, 1995). These complexes, which form under many different conditions, are 500–1000 kDa in size and have never been crystallized, making structure determination using traditional solution-state NMR and X-ray diffraction (XRD) methods difficult. Solution studies at low pH, a condition that stabilizes the monomeric state, suggest amelogenin adopts few elements of canonical secondary structure, characteristic of intrinsically disordered proteins (Tompa, 2002; Uversky, 2002), making detailed structural analysis more complicated (Delak et al., 2009; Zhang et al., 2011; Buchko et al., 2013).

In recent years, solid state NMR (SSNMR) techniques have been extremely valuable for the quantitative structural characterization of biomineralization proteins in general (Drobny et al., 2002, 2003, 2006; Stayton et al., 2003; Goobes et al., 2007), and amelogenins in particular (Shaw et al., 2004, 2008; Shaw and Ferris, 2008; Masica et al., 2011; Lu et al., 2013a,b). Studying proteins bound to surfaces is inherently a solid state problem, and with the use of isotopic labels, SSNMR enables the site-specific investigation of structure, protein-surface interactions, and dynamics. Using such methods, LRAP has been extensively studied bound to hydroxyapatite (HAP), an analog for enamel which is described as carbonated apaptite (Simmer and Fincham, 1995; Fincham et al., 1999; Margolis et al., 2006), in order to identify structural features which may play important roles in binding to enamel (Shaw et al., 2004, 2008; Shaw and Ferris, 2008; Masica

et al., 2011; Lu et al., 2013a,b). Many studies show that LRAP is a good model for the full-length protein (Moradian-Oldak et al., 1998b; Moradian-Oldak, 2001; Shaw et al., 2004, 2008; Le et al., 2006; Tarasevich et al., 2010) with the added advantage that its smaller size (59 residues) allows the incorporation of site-specific isotopic labels via solid phase peptide synthesis (Shaw et al., 2004, 2008; Shaw and Ferris, 2008; Masica et al., 2011; Lu et al., 2013b; Tarasevich et al., 2013). This has enabled quantitative structural studies of LRAP bound to HAP, providing much of the existing molecular level details of amelogenin's interactions with solid surfaces (Shaw et al., 2004, 2008; Shaw and Ferris, 2008; Masica et al., 2011; Lu et al., 2013b; Tarasevich et al., 2013).

Quantitative structural, dynamic, and orientation studies of LRAP bound to HAP include the following regions in the C- and the N-terminus: G8-Y12, L15-V19, V19-L23, K24-S28, L42-A46, A49-T53, and K54-V58 (Shaw et al., 2004, 2008; Shaw and Ferris, 2008; Masica et al., 2011; Lu et al., 2013b). In these pairs the first residue corresponds to a ^{13}C-backbone carbonyl and the second a ^{15}N-backbone amide. Collectively, the data on these LRAP samples bound to HAP represent the most comprehensive study of a biomineralization protein to date. In general, the C-terminus was found to be largely disordered and oriented close enough to the surface to influence mineral growth (5.8–8.0 Å), but at the same time is highly dynamic, suggesting that other regions of the protein may also be close enough to the HAP surface to stabilize interactions (Shaw et al., 2004, 2008; Shaw and Ferris, 2008). Investigations in the N-terminus revealed that this region contained much more helical content. The N-terminus was also similar in distance from or further from the HAP surface than the C-terminus depending on the phosphorylation state, 7.0–9.0 Å for LRAP(−P) and 5.3–7.0 Å for LRAP(+P), still close enough to the HAP surface in both cases to influence mineral growth. The variable distance suggests that in addition to interacting with HAP, the N-terminus may serve a second function such as facilitating protein-protein interactions (Masica et al., 2011). Neutron reflectivity studies bound to COOH-SAMs were also consistent with the N- and C-terminus of LRAP interacting with the surface (Tarasevich et al., 2013).

The only naturally observed site of serine phosphorylation in LRAP is at serine 16. To investigate the potential structural and functional implications of S16 phosphorylation, we recently completed SSNMR structural studies on the N-terminus of S16 phosphorylated LRAP and compared them to unphosphorylated LRAP. Using samples with pairs of site-specific labels (first residue a ^{13}C-backbone carbonyl and the second a ^{15}N-backbone amide), three regions covering the N-terminus, L15V19, V19L23, and K24S28, were studied bound to HAP as a function of solution condition. While some structural and dynamic variations in the L15–L23 region were noted, the most significant differences were observed in the K24S28 region (Lu et al., 2013b) a site 16 residues away from the phosphorylation. The sensitivity of the structure and dynamics of the K24S28 region to phosphorylation suggests that this may be a site with a potentially important role in biomineralization. Indeed, previous modeling studies suggest that K24 is a point at which the protein turns from the surface (Masica et al., 2011). In this work, we more fully investigate the structural and dynamic consequences on S16 phosphorylated LRAP by factors that may vary during enamel development: ionic strength (0.05, 0.15, and 0.2 M), Ca^{2+} concentration, and surface identity [HAP vs. carbonated apatite (CAP)]. A naturally occurring mutation found in full-length amelogenin (T21I) (Ravassipour et al., 2000) which results in malformed enamel was also investigated, due to its proximity to the K24S28 region. The implications of our results on the development of enamel will be considered.

EXPERIMENTAL METHODS

MATERIALS

Labeled amino acids were purchased from Cambridge Isotopes (Andover, MA). Fmoc-protected labeled amino acids were prepared as previously described (Shaw et al., 2008) using standard procedures (Carpino and Han, 1972; Wiejak et al., 1999). The HAP (90 m^2/g) used for binding was made and characterized according to literature preparation (Ebrahimpour et al., 1993) and stored as a slurry (28.9 mg/mL) to maintain the high surface area.

CARBONATED APAPTITE (CAP) SYNTHESIS AND CHARACTERIZATION

Solutions of calcium nitrate (1.18 g in 20 mL water) and sodium dihydrogen phosphate (0.41 g in 20 mL water) contained in dropping funnels were added simultaneously and dropwise at a rate of ca. 1 drop per second to a solution of sodium hydrogen carbonate (0.13 g in 20 mL) previously heated to 60 ± 5°C. The $NaHCO_3$ solution was contained in a three-neck round bottom flask and was stirred magnetically. The pH was maintained at nine throughout the addition. When the addition was complete, the mixture was maintained at pH = 9 with stirring at 60 ± 5°C for 2 h. After the mixture cooled to room temperature it was vacuum filtered using a Büchner funnel and the residue was washed four times with distilled water. The product (0.91 g, 65% yield) was dried in a 120°C oven for 24 h. Powder XRD showed no evidence of calcium carbonate or other impurities. The XRD line pattern of the product was in good agreement with PDF-00-001-1008 HAP. The percent carbonate (5.2%) was determined by Galbraith Laboratories, Knoxville, TN by combustion in oxygen at 1000°C; the surface area was determined by the BET method to be 172 m^2/g. All reagents were ACS reagent grade and distilled water was used throughout.

PROTEIN SYNTHESIS AND PURIFICATION

Site-specifically labeled LRAP-K24S28(+P) was prepared by solid phase peptide synthesis using Fmoc-chemistry by the Protein Chemistry Technology Center, University of Texas, (Dallas, TX). Isotopically labeled backbone carbonyl carbon at K24 (^{13}C') and amide nitrogen at S28 (^{15}N) were introduced in the i and $i + 4$ positions, respectively (**Figure 1**). The T21I-mutant is LRAP-K24S28(+P) prepared with the substitution of threonine at position 21 with an isoleucine. The proteins were purified by reverse phase HPLC using: buffer A, 0.1% trifluoroacetic acid in water; buffer B, 0.1% trifluoroacetic acid in acetonitrile. Both proteins eluted at 54% B. Mass spectroscopy was used to characterize the purity and molecular weight of the proteins. After purification, proteins were lyophilized, and stored until ready for use.

PROTEIN SOLUTIONS

LRAP-K24S28(+P) was bound to HAP under three different conditions and bound to CAP under the "standard condition," while the T21I-mutant was bound to HAP under the "standard condition" (**Table 1**). The "standard condition" is defined as pH = 7.4, *IS* = 0.15 M, and 326 μg/mL (0.047 mM) LRAP. The solution for the standard conditions samples was prepared as follows: a buffer saturated with respect to HAP (Saturated Calcium Phosphate—SCP; the resulting solution has a Ca^{2+} concentration of 0.07 mM) was prepared by stirring excess HAP in a 0.15 M NaCl (pH 7.4) solution, maintaining pH. After 12–24 h, the undissolved HAP was filtered (0.22 μm, Isopore, Millipore). LRAP (16.8 mg) was then dissolved into 50 mL of SCP (326 μg/mL; 0.047 mM) and the pH adjusted to 7.4. For solutions with different ionic strengths, the same procedure was followed, but the NaCl concentration was adjusted to obtain the desired ionic strength (0.05 or 0.2 M). For the solution with eight-times excess calcium added relative to the LRAP concentration, the same procedure was followed, but $CaCl_2$ was added to obtain 0.4 mM [Ca^{2+}], providing a [Ca^{2+}]:[LRAP-K24S28(+P)] of 8:1.

PROTEIN ADSORPTION TO HAP OR CAP

The HAP or CAP was prepared for protein adsorption by washing 54.3 mg of HAP or CAP three times with 10 mL of SCP immediately before adding it to one of the above protein solutions. The mixture was stirred for 3 h at room temperature, centrifuged, and the LRAP-HAP or LRAP-CAP complex washed three times with 5 mL SCP to remove non-specifically bound protein. The amount of protein bound to HAP or CAP was determined by measuring the change in concentration before and after binding and for each wash using ultraviolet absorbance measurements (λ = 277).

The prepared sample was packed into the NMR rotor by first transferring it to a sealed 1 mL pipette tip. The tip was centrifuged for 10 min at 12,000 rpm to remove residual liquid, resulting in a tightly packed hydrated LRAP-HAP/CAP complex. The sealed end was then cut open and the pellet transferred to a 5 mm NMR rotor using a centrifuge. The rotor was placed in an NMR probe and spun at 6–7 kHz to remove the excess water, resulting in a >100% hydrated, surface bound sample. A thin layer of parafilm or a rubber disk was positioned before the rotor's end cap to keep the sample fully hydrated during NMR data collection.

FIGURE 1 | Murine amelogenin amino acid sequence. The primary amino acid sequence of murine amelogenin with the basic and acidic residues colored blue and red, respectively. The splice-variant LRAP is composed of the N-terminal 33 and C-terminal 26 residues, shaded gray. Both full-length amelogenin and LRAP are post-translationally modified by side chain phosphorylation of S16, shaded yellow. The isotopic labels at specific atomic locations and residues are shown with the arrows: K24 ($^{13}C'$) and S28 (^{15}N). In the T21I-mutant the threonine at position 21 is replaced with an isoleucine.

Table 1 | Sample conditions studied and their binding efficiency.

Condition	Binding (±4%)
0.05 M ionic strength	68
0.2 M ionic strength	64
Bound to CAP	55
8-times excess Ca^{2+} (0.4 mM)	66
T21I-mutant	61
Standard conditions*	68*

**Standard conditions previously reported: pH = 7.4, IS = 0.15 M, and 326 μg/mL LRAP (Lu et al., 2013b).*

NMR EXPERIMENTS

All NMR experiments were conducted on a three-channel Chemagnetics Infinity spectrometer (Chemagnetics, Fort Collins, CO) with an Oxford 7.05 T [$\upsilon_0(^1H)$ = 300 MHz] wide-bore magnet, operating at resonance frequencies of $\upsilon_0(^{13}C) = 75.78$ MHz and $\upsilon_0(^{15}N) = 30.54$ MHz. Deconvolution of the 1D-spectra was performed with Mestranova (Mestrelab Research, Escondido, CA). For chemical shift measurements, a double resonance HX magic-angle spinning (MAS), variable temperature Chemagnetics probe was used. For REDOR measurements, a triple resonance HXY MAS, variable-temperature Chemagnetics probe was used. Temperatures in the rotor were calibrated using $^{207}Pb(NO^3)_2$ (Bielecki and Burum, 1995). Chemical shifts were referenced to the adamantane CH peak at 40.26 ppm (Wishart et al., 1995), which was referenced to 2,2-dimethyl-2-silapentane-5-sulfonate (DSS).

REDOR

XY8 phase cycling was applied on both observe (^{13}C) and dephasing channels (^{15}N or ^{31}P) (Gullion and Schaefer, 1989, 1991). For all REDOR experiments, 180° pulses of 13.0–15.0 μs were used for both the observe and dephasing nuclei with a 65 kHz TPPM decoupling field (Bennett et al., 1995) employed during the recoupling and acquisition periods. Both $^{13}C\{^{15}N\}$ and $^{13}C\{^{31}P\}$ REDOR data were obtained for each sample preparation condition (**Table 2**). Data were acquired at −80°C to eliminate contributions due to motion and at a spinning speed of 4 kHz. For $^{13}C\{^{15}N\}$ REDOR, dephasing points were collected at 8, 24, 40, 56, 72, 88, and 104 rotor periods. Between 4096 and 8192 scans were taken for 8, 24, and 40 rotor periods, 8192–10240 scans for 56, 72, and 88 rotor periods, and 16384–20480 scans for 104 rotor periods. For $^{13}C\{^{31}P\}$ REDOR, dephasing points were collected at 8, 24, 40, 56, 72, 88, 104 rotor periods with 4096 scans taken for 8, 24, 40, and 56 rotor periods, and 8192–16384 scans for 72, 88, and 104 rotor periods. All data were collected with a 1 s pulse delay. Each point in the dephasing curve represents the average of at least five repetitions. The REDOR dephasing curves were corrected for the natural abundance background (59 backbone carbonyls and 10 side chain carbonyls, or 41% of the total signal) and were fit by simulations generated using SIMPSON (Bak et al., 2000). The best fit to the closest distance was determined utilizing a chi-squared analysis to provide a quantitative comparison of any given data set to the calculated dephasing curves.

RESULTS

BINDING EFFICIENCY

As shown in **Table 1**, LRAP-K24S28(+P) bound to HAP with similar efficiency under the four conditions varied, where efficiency is the percentage of LRAP bound with respect to the initial amount available. The percent error is estimated based on the binding efficiency of multiple (>15) LRAP(+P) binding results. Slightly lower binding was observed for the high ionic strength condition and the T21I-mutant. Relative to HAP, LRAP-K24S28(+P) bound less efficiently to CAP.

CHEMICAL SHIFT STUDIES

As illustrated in **Figure 2** and **Table 2**, two distinct resonances are observed for the K24 carbonyl resonance in each sample that correspond to two different conformations. As previously described (Lu et al., 2013b), the downfield resonance is most consistent with a helical component of K24, while the upfield resonance is a combination of a β-strand component of K24, but also has contributions from the natural abundance (unlabeled) backbone and side chain carbonyls. A random coil component, if present, would be between the two resonances, but due to spectral overlap, we did not try to fit this separately. The chemical shifts of the helical carbonyl (**Table 2**) ranged from 178.4 to 178.9 ppm, while the upfield carbonyl ranged from 174.8 to 175.3 ppm, in both cases invariant within our experimental error to the varying binding conditions.

Table 2 | ^{13}C′ chemical shifts for K24 in LRAP-K24S28(+P).

LRAP-K24S28(+P) binding condition	Chemical shift (ppm) Downfield resonance (α-helix)	Chemical shift (ppm) Upfield resonance (β-strand/coil/background)
Standard conditions	178.4 ± 0.5	174.8 ± 0.5
IS = 0.05 M	178.9 ± 0.5	175.1 ± 0.5
IS = 0.2 M	178.8 ± 0.5	175.1 ± 0.5
8:1 Ca^{2+}:[LRAP]	178.9 ± 0.5	175.3 ± 0.5
Bound to CAP	178.7 ± 0.5	175.0 ± 0.5
T21I-Mutant	178.6 ± 0.5	174.8 ± 0.5

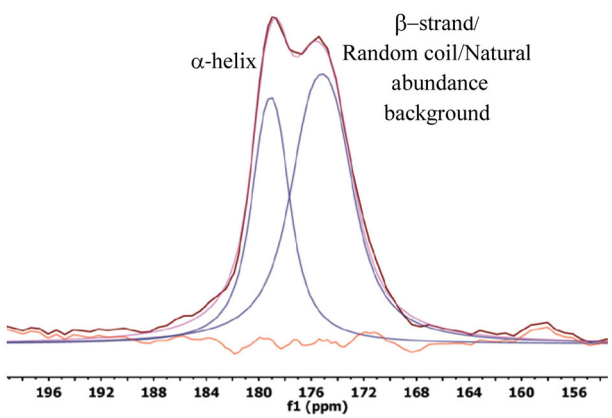

FIGURE 2 | One-dimensional ^{13}C spectrum. Representative spectrum of LRAP-K24S28(+P) bound to HAP, in this case at an ionic strength of 0.05 M. The deconvolution is also shown. The data is shown in pink, the combined fit in maroon, with individual fits in blue. The difference of the fit spectrum and the actual spectrum is shown in orange.

STRUCTURE AS A FUNCTION OF BINDING CONDITION

To gain further insight into the structural motif at K24 to S28, the distance between the ^{13}C backbone carbonyl of K24 and the ^{15}N amide of S28 was measured for each of the complexes using REDOR (**Figure 3**). The distances obtained from the resulting dephasing curves are well-established for regular α-helices (4.2 Å) and β-strands (10.6 Å). The dephasing curve for a random coil structure is obtained by averaging all of the dephasing curves between 4.2 Å and 10.6 Å, at 0.1 Å intervals, yielding an average distance of 5.8 Å. When bound to HAP under standard conditions, LRAP-K24S28(+P) had a significant helical content based on the ^{13}C-^{15}N distance of 4.8 Å. As seen in **Table 3**, this distance is unchanged when bound at an ionic strength of 0.2 M, or for the T21I-mutant bound under standard conditions, indicating a similar content of α-helix for these conditions. When bound at an ionic strength of 0.05 M, the distance lengthens to 5.2 Å (**Figure 3**), indicating a shift to more random coil structures, and suggesting that salt concentration influences structure. Under conditions where the protein is bound to CAP or bound in the presence of 0.4 mM Ca^{2+}, the distance decreases to 4.4 Å (**Figure 3**), a value approaching a canonical α-helix, suggesting that calcium may stabilize helix formation in this region of LRAP.

The dephasing curves can also result from a combination of multiple distinct structures. In the case of dephasing curves consistent with α-helices [e.g., LRAP-K24S28(+P) bound to CAP or bound to HAP in the presence of 0.4 mM calcium], the contribution from structures other than α-helix would be low. However,

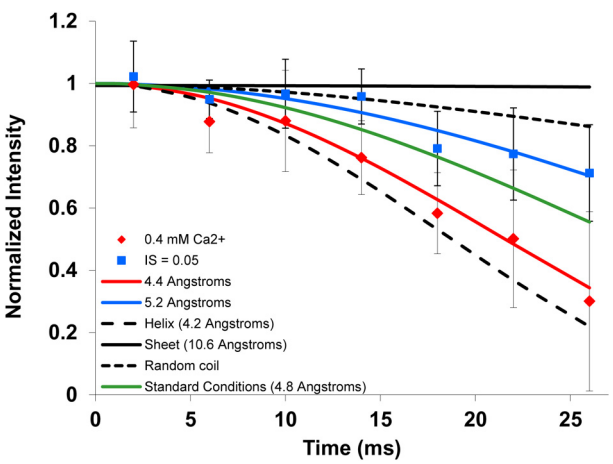

FIGURE 3 | Representative ^{13}C-^{15}N REDOR data and fits. The ^{13}C-^{15}N REDOR data shows that LRAP-K24S28(+P) bound to HAP in the presence of excess Ca^{2+} (red diamonds) had the shortest C-N distance (4.4 Å, nearly helical), while binding at an ionic strength of 0.05 M (blue squares) resulted in a longer C-N distance (5.2 Å) consistent with a looser helix or less helical content at low ionic strength. The simulated dephasing curves for an α-helix (4.2 Å, dashed), β-strand (10.6 Å, solid), random coil (long dash), and the standard conditions (green line) are shown for comparison.

Table 3 | REDOR determined distances for LRAP-K24S28(+P).

LRAP-K24S28(+P) binding condition	$^{13}C(i)$-$^{15}N(i+4)$ distance	^{13}C-^{31P} distance
Standard condition	4.8 ± 0.4 Å	7.5 ± 0.5 Å
IS = 0.05 M	5.2 ± 0.5 Å	8.0 ± 0.5 Å
IS = 0.2 M	4.9 ± 0.4 Å	8.0 ± 0.5 Å
8-times calcium (0.4 mM)	4.4 ± 0.3 Å	8.5 ± 0.5 Å
Bound to CAP	4.4 ± 0.3 Å	7.5 ± 0.5 Å
T21I-Mutant	4.8 ± 0.4 Å	8.5 ± 0.5 Å

for dephasing curves with longer distances which are indicative of structures deviating from a helical structure, contributions from random coil or β-strand structures can be significant. For example, at an ionic strength of 0.05 M, the dephasing curve fits to a single distance of 5.2 Å, but could be fit equally well by some contribution of α-helix, random coil, and/or β-strand. To provide a starting point, deconvolution and integration of the 1D-spectra (**Figure 2**) suggests that ∼60% of this region is in an α-helical structure. This number is based on integrations of 37% α-helix (downfield signal) and 23% other (upfield signal) with the later signal corrected by removing the 40% intensity contribution due to the natural abundance $^{13}C'$ background. This analysis is not quantitative due to potential errors in deconvoluting as well as other possible contributions to the intensity of the resonance attributed to the α-helical component. Fixing the α-helical contribution to 60% resulted in a curve that dephased much faster than the data, regardless of whether the remaining 40% was random coil or β-strand. However, a combination of 40% α-helix, 60% β-strand fits the data well, as does 30% α-helix, 70% random coil. These two options cannot be distinguished, nor can they be distinguished from a combination of all three structures (40% α-helix, 10% random coil, and 50% β-strand) that fit the data. What is clear for the combined chemical shift and REDOR data is that the K24S28 region has a smaller population of α-helical character as a function of low ionic strength.

DISTANCE FROM THE SURFACE AS A FUNCTION OF BINDING CONDITION

The ^{31}P nucleus on the HAP surface provides another handle with which to characterize the HAP-LRAP interface. This is because the distance from the backbone ^{13}C carbonyl to surface ^{31}P can be measured, providing an indication of the orientation of the protein relative to the surface. For instance, if the K24 carbonyl is oriented away from the surface, the $^{13}C'$-^{31}P distance would be long (>12 Å), while a strong interaction in this region would result in a much shorter distance. The shortest distance from the backbone $^{13}C'$ observed for LRAP to date is 5.3 Å (Masica et al., 2011).

Binding under standard conditions resulted in a ^{13}C-^{31}P distance of 7.5 ± 0.5 Å from the nearest ^{31}P on the surface (**Figure 4** and **Table 3**). Binding to CAP and to HAP at an ionic strength of 0.05 or 0.2 M did not result in any ^{13}C-^{31}P distance changes relative to the standard condition outside the error limits of the measurements. The largest ^{13}C-^{31}P distance changes relative to the standard condition were observed for LRAP-K24S28(+P) in the presence of 0.4 mM Ca^{2+} and for the T21I-mutant, which both increased to 8.5 ± 0.5 Å (**Figure 4**). Interestingly, of the latter two conditions, a change in structure was only observed in the presence of excess calcium.

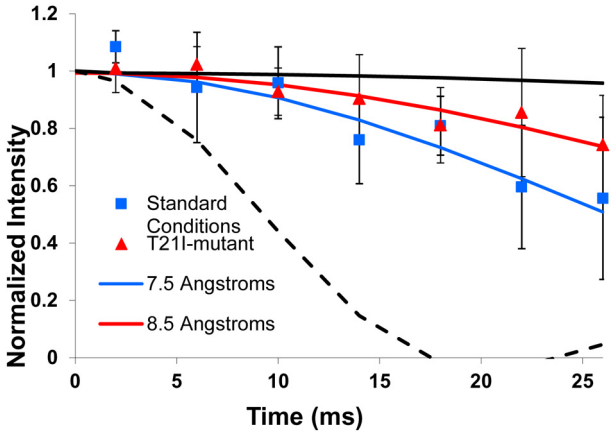

FIGURE 4 | Representative ^{13}C-^{31}P REDOR data and fits. The ^{13}C-^{31}P REDOR data for LRAP-K24S28(+P) under the standard condition (blue squares) and for the T21I-mutant (red triangles) with fits for a distance of 7.5 Å (blue line) and 8.5 Å (red line). The T21I-mutant and the sample prepared in the presence of 0.4 mM Ca^{2+} (not illustrated) showed the largest ^{13}C-^{31}P distance difference relative to the standard condition (∼1 Å). A distance too long to measure (12 Å, solid black line) and the shortest distance measured from a backbone $^{13}C'$ to HAP (5.3 Å, dashed line) are shown for reference.

DISCUSSION

The amelogenin proteins have been classified as intrinsically disordered (Delak et al., 2009), a characterization which implies structural flexibility may be necessary to achieve a particular function (Tompa, 2002; Uversky, 2002). Consistent with a predilection to structural flexibility, both amelogenin and LRAP are dynamic even when they are bound to HAP (Shaw and Ferris, 2008; Shaw et al., 2008; Masica et al., 2011; Lu et al., 2013a,b). Despite the inherent flexibility, specific structured regions have been identified for the surface immobilized protein based on SSNMR REDOR data (Masica et al., 2011; Lu et al., 2013a,b). The LRAP-K24S28(+P)/(−P) has been identified to be an ideal helix when lyophilized from solution. Upon binding to HAP, LRAP(+P) remained helical, while LRAP(−P) became largely unstructured. The observation of structural lability as a function of phosphorylation suggests an important function for this region of the protein.

Protein structure in solution state NMR is often evaluated using ^{13}C, ^{15}N, and ^{1}H chemical shifts. This is because NMR chemical shifts arise from the electron density around the nucleus and differs for each element of secondary structure (α-helix, β-strand, random coil). For the same reasons, chemical shifts can also provide qualitative insight into the structure of proteins immobilized onto surfaces in the solid state. In this case, the unique observation of two resonances for the carbonyl of K24 compared to one resonance for all of the other carbonyls studied for LRAP (Shaw et al., 2004, 2008; Shaw and Ferris, 2008; Masica et al., 2011; Lu et al., 2013a,b) suggests a unique and

important structural feature for this region of the protein. We previously demonstrated that the downfield K24 carbonyl resonance is most consistent with an α-helical conformation, based on the downfield chemical shift expected for a helical carbonyl and the evaluation of REDOR data for this resonance alone (Lu et al., 2013b). That two K24 carbonyl resonances are observed under each of the preparation conditions tested (**Table 2**) suggests that there are common structural features, including a significant amount of helical structure at K24, regardless of the preparation.

In addition to secondary structure, for surface immobilized proteins, differences in chemical shift can also arise from how the protein is associated with the highly charged surface due to alterations of local electron density. Consequently, the chemical shift and intensity measurements for the two K24 carbonyl resonances are qualitative and the interpretations need to be treated with care. The difficulty in quantifying chemical shift information for surface immobilized proteins due to these two contributions emphasizes the need for a more quantitative technique. Dipolar recoupling techniques such as REDOR, which directly measure the distance between two nuclei, provide such quantitation.

The REDOR data under the binding conditions studied here provide further evidence for a structurally flexible region centered around the K24S28 region that may play a functional role. For example, the REDOR data is consistent with an ideal α-helix in this region in the presence of excess Ca^{2+} (8:1 [Ca^{2+}]:[LRAP-K24S28(+P)]), suggesting a significant increase in helical content in this region relative to binding under the standard condition. Associated with this increase in helical character is a 1 Å increase in the K24 carbonyl distance to ^{31}P on the surface. Since soluble free calcium is present *in vivo* in the enamel fluid at similar concentrations to those used in our studies (Aoba and Moreno, 1987), this is a critical observation and suggests the importance of calcium in dictating structure. Previously, small angle X-ray scattering was used to investigate the overall shape of LRAP(+P) and LRAP(−P) in solution as a function of Ca^{2+} concentration. Under Ca^{2+}:[LRAP] ratios similar to ours, significant structural changes were also observed with LRAP(+P) transitioning from an extended to a more globular structure as a function of increasing Ca^{2+} (Le Norcy et al., 2011a). While the X-ray scattering and sedimentation experiments do not have the resolution to identify molecular level structural changes, the microscopic changes observed here using SSNMR are in agreement with the macroscopic changes observed using sedimentation velocity and X-ray scattering and may be providing the first insight into the reasons behind the macroscopic changes. Further comparisons suggest a competition between solubilized calcium and calcium in the HAP lattice that impact structure: LRAP-K24S28(+P) had a distance consistent with an ideal helix (measured distance was 4.2 ± 0.3 Å) when lyophilized from solution with 0.007 mM Ca^{2+} in solution. When LRAP-K24S28(+P) was bound to HAP, a loss of helical structure was observed unless excess solution calcium (0.4 mM Ca^{2+}) was present. These observations suggest that the structural changes resulting from binding solution calcium modify the protein:surface interface. Given the observed structural change, a reasonable expectation would be different surface coverages in the presence or absence of Ca^{2+}, however, similar surface coverage by the protein was obtained. Since the observed structural change does not control the amount of protein binding, the structural change resulting from excess solution Ca^{2+} must serve another function, such as activating protein binding or mineral growth. Indeed, protein-protein interactions were observed to increase for LRAP(+P) in solution in the presence of excess solution Ca^{2+} (Le Norcy et al., 2011a), and these interactions may play an important role for the surface immobilized protein.

Although the majority of studies of amelogenin interactions with crystal surfaces have involved HAP (Moradian-Oldak et al., 1998a,b, 2002; Habelitz et al., 2006; Wang et al., 2007; Shaw and Ferris, 2008; Shaw et al., 2008; Kwak et al., 2009, 2011; Tarasevich et al., 2009; Le Norcy et al., 2011a,b; Masica et al., 2011; Uskokovic et al., 2011; Lu et al., 2013a,b), CAP is a more direct analog of enamel (Simmer and Fincham, 1995; Fincham et al., 1999; Margolis et al., 2006). The structure at LRAP-K24S28(+P) is also consistent with an ideal α-helix when bound to CAP (4.4 ± 0.3 Å), in contrast to HAP where the structure is shifted toward random coil (4.8 ± 0.4 Å). This is some of the first data suggesting that carbonation influences the structure of amelogenins, and therefore, could influence the resulting mineral growth.

The T21I-mutant is one of many naturally occurring, single-site mutations found in full-length amelogenin that results in enamel hypoplasia, with enamel features including smooth pits, variable thickness, mottled, and brown color (Ravassipour et al., 2000). That this significant loss of functional enamel results from a single-site mutation strongly suggests a change in structure, and changes in tertiary structure (protein-protein interactions) have been observed (Moradian-Oldak et al., 2000; Paine et al., 2002; Buchko et al., 2013). However, no structural change for the T21I-mutant was observed in LRAP-K24S28(+P), despite the proximity of the mutated residue to the K24S28 region. The mutation did result in the region being further from the surface and a simple interpretation for this observation is that the threonine in the native protein assists in holding the protein closer to the surface and replacement with a hydrophobic isoleucine destabilized this interaction. The distance from the surface for the T21I-mutation determined under standard conditions is similar to that found when excess Ca^{2+} was present, though it is unclear at this time if there is a mechanistic correlation between these two observations.

The functional importance of the structural flexibility in the K24S28 region is not clear and further crystal growth and structural studies will be necessary to tease out the mechanistic details. An equally important observation is that the structure doesn't completely switch conformations, i.e., under all conditions studied, there is still some helical character. This could merely be a result of the high entropic costs associated with switching structures when the protein is immobilized. Given the uniqueness of this structured region in LRAP, a more likely explanation is that it is a critical part of the functional design, possibly serving a regulatory role in enamel development. Only the continued *in vitro* investigation of the structural and functional properties of the amelogenin proteins will allow us to fully explore these mechanisms.

SUMMARY

The LRAP(+P):HAP interaction of the structurally flexible K24S28 region was evaluated as a function of ionic strength, calcium concentration, surface type, and protein mutation. Modest differences were observed in both structure and distance from the surface for this region of the protein. The most significant difference, relative to the standard condition, was observed with LRAP bound to HAP in the presence of excess Ca^{2+}, where the protein in this region transitioned from a looser α-helix to a nearly ideal α-helical structure and moved further from the surface. The dependence of LRAP structure (secondary, tertiary) on calcium concentration is mounting, and these studies have provided some of the first insights at the molecular level. Using a CAP surface also resulted in a more ideal helical structure, while the T21I-mutation resulted in moving the K24S28 region further from the surface. Collectively, these data provide continued evidence of the structural flexibility of the K24S28 region in amelogenins and further implicated it as a functionally important region.

ACKNOWLEDGMENTS

The authors thank Dr. Claude Yoder (Franklin and Marshall College) for supplying the carbonated apatite. This research was supported by NIH-NIDCR Grant DE-015347. The research was performed at the Pacific Northwest National Laboratory (PNNL), a facility operated by Battelle for the US Department of Energy.

REFERENCES

Aoba, T., and Moreno, E. C. (1987). The enamel fluid in the early secretory stage of porcine amelogenesis: chemical composition and saturation with respect to enamel mineral. *Calcif. Tissue Int.* 41, 86–94. doi: 10.1007/BF02555250

Bak, M., Rasmussen, J. T., and Nielsen, N. C. (2000). SIMPSON: a general simulation program for solid-state NMR spectroscopy. *J. Magn. Res.* 147, 296–330. doi: 10.1006/jmre.2000.2179

Bennett, A. E., Rienstra, C. M., Auger, M., Lakshmi, K. V., and Griffin, R. G. (1995). Heteronuclear decoupling in rotating solids. *J. Chem. Phys.* 103, 6951–6958. doi: 10.1063/1.470372

Bielecki, A., and Burum, D. P. (1995). Temperature-dependence of Pb-207 MAS spectra of solid lead nitrate - an accurate, sensitive thermometer for variable-temperature MAS. *J. Magn. Res. A* 116, 215–220. doi: 10.1006/jmra.1995.0010

Buchko, G. W., Lin, G., Tarsevich, B. J., and Shaw, W. J. (2013). A solution NMR investigation into the impaired self-assembly properties of two murine amelogenins containing the point mutations T21I or P41T. *Arch. Biochem. Biophys.* 537, 217–224. doi: 10.1016/j.abb.2013.07.015

Carpino, L. A., and Han, G. Y. (1972). 9-Fluorenylmethoxycarbonyl amino-protecting group. *J. Organ. Chem.* 37, 3404–3409. doi: 10.1021/jo00795a005

Delak, K., Harcup, C., Lakshminarayanan, R., Sun, Z., Fan, Y. W., Moradian-Oldak, J., et al. (2009). The tooth enamel protein, porcine amelogenin, is an intrinsically disordered protein with an extended molecular configuration in the monomeric form. *Biochemistry* 48, 2272–2281. doi: 10.1021/bi802175a

Drobny, G. P., Long, J. R., Karlsson, T., Shaw, W. J., Popham, J., Oyler, N., et al. (2003). Structural studies of biomaterials using double quantum solid state NMR spectroscopy. *Annu. Rev. Phys. Chem.* 54, 531–571. doi: 10.1146/annurev.physchem.54.011002.103903

Drobny, G. P., Long, J. R., Shaw, W. J., Cotten, M., and Stayton, P. S. (2002). Structure and dynamics of proteins adsorbed to biomaterial interfaces. *Encyclop. Nucl. Magn. Res.* 9, 458–468. doi: 10.1002/9780470034590.emrstm0540

Drobny, G. P., Stayton, P. S., Long, J. R., Louie, E. A., Karlsson, T., Popham, J. M., et al. (2006). "NMR Spectroscopy of Biological Solids," in *Structural Studies of Peptides on Biomaterial Surfaces Using Double-Quantum Solid-State Nuclear Magnetic Resonance Spectroscopy*, ed A. Ramamoorthy (New York, NY: CRC/Taylor & Francis Group).

Ebrahimpour, A., Johnsson, M., Richardson, C. F., and Nancollas, G. H. (1993). The characterization of hydroxyapatite preparations. *J. Coll. Int. Sci.* 159, 158–163. doi: 10.1006/jcis.1993.1307

Fincham, A. G., Moradian-Oldak, J., and Simmer, J. P. (1999). The structural biology of the developing dental enamel matrix. *J. Struct. Biol.* 136, 270–299.

Fincham, A. G., Moradian-Oldak, J., Simmer, J. P., Sarte, P., Lau, E. C., Diekwisch, T., et al. (1994). Self-assembly of a recombinant amelogenin protein generates supramolecular structures. *J. Struct. Biol.* 112, 103–109. doi: 10.1006/jsbi.1994.1011

Gibson, C. W., Golub, E., Ding, W. D., Shimokawa, H., Young, M., Termine, J., et al. (1991). Identification of the leucine-rich amelogenin peptide (LRAP) as the translation product of an alternatively spliced transcript. *Biochem. Biophys. Res. Commun.* 174, 1306–1312. doi: 10.1016/0006-291X(91)91564-S

Gibson, C. W., Li, Y., Daly, B., Suggs, C., Yuan, Z.-A., Fong, H., et al. (2008). The leucine-rich amelogenin peptide alters the amelogenin null enamel phenotype. *Cells Tissues Organs* 189, 169–174. doi: 10.1159/000151384

Goobes, G., Goobes, R., Shaw, W. J., Gibson, J. M., Long, J. R., Raghunathan, V., et al. (2007). The structure, dynamics and energetics of protein adsorption—lessons learned from adsorption of statherin to hydroxyapatite. *Magn. Res. Chem.* 45(Suppl.), S32–S47. doi: 10.1002/mrc.2123

Gullion, T., and Schaefer, J. (1989). Rotational-echo double-resonance NMR. *J. Magn. Res.* 81, 196–200.

Gullion, T., and Schaefer, J. (1991). Elimination of resonance offset effects in rotational-echo, double-resonance NMR. *J. Magn. Res.* 92, 439–442.

Habelitz, S., DenBesten, P. K., Marshall, S. J., Marshall, G. W., and Li, W. (2006). Self-assembly and effect on crystal growth of the leucine-rich amelogenin peptide. *Eur. J. Oral Sci.* 114, 315–319. doi: 10.1111/j.1600-0722.2006.00312.x

Kwak, S. Y., Green, S., Wiedemann-Bidlack, F. B., Beniash, E., Yamakoshi, Y., Simmer, J. P., et al. (2011). Regulation of calcium phosphate formation by amelogenins under physiological conditions. *Eur. J. Oral Sci.* 119(Suppl. 1), 103–111. doi: 10.1111/j.1600-0722.2011.00911.x

Kwak, S.-Y., Wiedemann-Bidlack, R. B., Beniash, E., Yamakoshi, Y., Simmer, J. P., Litman, A., et al. (2009). Role of 20-kDa amelogenin (P148) phosphorylation in calcium phosphate formation *in vitro*. *J. Biol. Chem.* 284, 18972–18979. doi: 10.1074/jbc.M109.020370

Le Norcy, E., Kwak, S. Y., Allaire, M., Fratzl, P., Yamakoshi, Y., Simmer, J. P., et al. (2011a). Effect of phosphorylation on the interaction of calcium with leucine-rich amelogenin peptide. *Eur. J. Oral Sci.* 119(Suppl. 1), 97–102. doi: 10.1111/j.1600-0722.2011.00900.x

Le Norcy, E., Kwak, S. Y., Wiedemann-Bidlack, F. B., Beniash, E., Yamakoshi, Y., Simmer, J. P., et al. (2011b). Leucine-rich amelogenin peptides regulate mineralization *in vitro*. *J. Dent. Res.* 90, 1091–1097. doi: 10.1177/0022034511411301

Le Norcy, E., Kwak, S. Y., Wiedemann-Bidlack, F. B., Beniash, E., Yamakoshi, Y., Simmer, J. P., et al. (2011c). Potential role of the amelogenin N-terminus in the regulation of calcium phosphate formation *in vitro*. *Cells Tissues Organs* 194, 188–193. doi: 10.1159/000324827

Le, T. Q., Gochin, M., Featherstone, J. D., Li, W., and DenBesten, P. K. (2006). Comparative calcium binding of leucine-rich amelogenin peptide and full-length amelogenin. *Eur. J. Oral Sci.* 114(Suppl. 1), 320–326. discussion: 327–329, 382. doi: 10.1111/j.1600-0722.2006.00313.x

Lu, J.-X., Xu, Y. S., Buchko, G. W., and Shaw, W. J. (2013a). Mineral association changes the secondary structure and dynamics of murine amelogenin. *J. Dent. Res.* 92, 1000–1004. doi: 10.1177/0022034513504929

Lu, J.-X., Xu, Y. S., and Shaw, W. J. (2013b). Phosphorylation and ionic strength alter the LRAP-HAP interface in the N-terminus. *Biochemistry* 52, 2196–2205. doi: 10.1021/bi400071a

Margolis, H. C., Beniash, E., and Fowler, C. E. (2006). Role of macromolecular assembly of enamel matrix proteins in enamel formation. *J. Dent. Res.* 85, 775–793. doi: 10.1177/154405910608500902

Masica, D. L., Gray, J. J., and Shaw, W. J. (2011). Partial high-resolution structure of phosphorylated and non-phosphorylated leucine-rich amelogenin protein adsorbed to hydroxyapatite. *J. Phys. Chem. C* 115, 13775–13785. doi: 10.1021/jp202965h

Moradian-Oldak, J. (2001). Amelogenins: assembly, processing and control of crystal morphology. *Matrix Biol.* 20, 293–305. doi: 10.1016/S0945-053X(01)00154-8

Moradian-Oldak, J., Bouropoulos, N., Wang, L., and Gharakhanian, N. (2002). Analysis of self-assembly and apatite binding properties of amelogenin protein lacking the hydrophilic C-terminal. *Matrix Biol.* 21, 197–205. doi: 10.1016/S0945-053X(01)00190-1

Moradian-Oldak, J., Leung, W., Tan, J., and Fincham, A. G. (1998a). Effect of apatite crystals on the activity of amelogenin degrading enzymes *in vitro*. *Connect. Tissue Res.* 39, 131–140; discussion: 141–139.

Moradian-Oldak, J., Tan, J., and Fincham, A. G. (1998b). Interaction of amelogenin with hydroxyapatite crystals: an adherence effect through amelogenin molecular self-association. *Biopolymers* 46, 225–238.

Moradian-Oldak, J., Paine, M. L., Lei, Y. P., Fincham, A. G., and Snead, M. L. (2000). Self-assembly properties of recombinant engineered amelogenin proteins analyzed by dynamic light scattering and atomic force microscopy. *J. Struct. Biol.* 131, 27–37. doi: 10.1006/jsbi.2000.4237

Moradian-Oldak, J., Simmer, J. P., Lau, E. C., Diekwisch, T., Slavkin, H. C., and Fincham, A. G. (1995). A review of the aggregation properties of a recombinant amelogenin. *Connect. Tissue Res.* 32, 125–130.

Moradian-Oldak, J., Simmer, J. P., Lau, E. C., Sarte, P. E., Slavkin, H. C., and Fincham, A. G. (1994). Detection of monodisperse aggregates of a recombinant amelogenin by dynamic light-scattering. *Biopolymers* 34, 1339–1347. doi: 10.1002/bip.360341006

Paine, M. L., Lei, P.-Y., Dickerson, K., and Snead, M. L. (2002). Altered amelogenin self-assembly based on mutations observed in human X-linked amelogeninsis imperfacta (AIH1). *J. Biol. Chem.* 277, 17112–17116. doi: 10.1074/jbc.M110473200

Ravassipour, D. B., Hart, P. S., Hart, T. C., Ritter, A. V., Yamauchi, M., Gibson, C., et al. (2000). Unique enamel phenotype associated with amelogenin gene (AMELX) codon 41 point mutation. *J. Dent. Res.* 79, 1476–1481. doi: 10.1177/00220345000790070801

Ravindranath, R. M. H., Devarajan, A., and Bringas, P. Jr. (2007). Enamel formation *in vitro* in mouse molar explants exposed to amelogenin polypeptides ATMP and LRAP on enamel development. *Arch. Oral Biol.* 52, 1161–1171. doi: 10.1016/j.archoralbio.2007.06.008

Shaw, W. J., Campbell, A. A., Paine, M. L., and Snead, M. L. (2004). The COOH terminus of the amelogenin, LRAP, is oriented next to the hydroxyapatite surface. *J. Biol. Chem.* 279, 40263–40266. doi: 10.1074/jbc.C400322200

Shaw, W. J., and Ferris, K. (2008). Structure, orientation, and dynamics of the C-terminal hexapeptide of LRAP determined using solid-state NMR. *J. Phys. Chem. B* 112, 16975–16981. doi: 10.1021/jp808012g

Shaw, W. J., Ferris, K., Tarasevich, B., and Larson, J. L. (2008). The structure and orientation of the C-terminus of LRAP. *Biophys. J.* 94, 3247–3257. doi: 10.1529/biophysj.107.119636

Simmer, J. P., and Fincham, A. G. (1995). Molecular mechanisms of dental enamel formation. *Crit. Rev. Oral Biol. Med.* 6, 84–108. doi: 10.1177/10454411950060020701

Stahl, J., Nakano, Y., Kim, S.-O., Gibson, C. W., Le, T., and DenBesten, P. (2013). Leucine rich amelogenin peptide alters ameloblast differentiation *in vivo*. *Matrix Biol.* 32, 432–442. doi: 10.1016/j.matbio.2013.05.004

Stayton, P., Drobny, G., Shaw, W., Long, J., and Gilbert, M. (2003). Molecular recognition at the protein-hydroxyapatite interface. *Crit. Rev. Oral Biol. Med.* 15, 370–376. doi: 10.1177/154411130301400507

Tarasevich, B. J., Lea, S., Bernt, W., Engelhard, M., and Shaw, W. J. (2009). Adsorption of amelogenin onto self-assembled and fluoroapatite surfaces. *J. Phys. Chem. B* 113, 1833–1842. doi: 10.1021/jp804548x

Tarasevich, B. J., Lea, S., and Shaw, W. J. (2010). The leucine rich amelogenin protein (LRAP) adsorbs as monomers or dimers onto surfaces. *J. Struct. Biol.* 169, 266–276. doi: 10.1016/j.jsb.2009.10.007

Tarasevich, B. J., Perez-Salas, U., Masica, D. L., Philo, J., Kienzle, P., Krueger, S., et al. (2013). Neutron reflectometry studies of the adsorbed structure of the amelogenin, LRAP. *J. Phys. Chem. B* 117, 3098–3109. doi: 10.1021/jp311936j

Tompa, P. (2002). Instrinsically unstructured proteins. *Trends Biochem. Sci.* 27. 527–533. doi: 10.1016/S0968-0004(02)02169-2

Uskokovic, V., Li, W., and Habelitz, S. (2011). Amelogenin as a promoter of nucleation and crystal growth of apatite. *J. Cryst. Growth* 316, 106–117. doi: 10.1016/j.jcrysgro.2010.12.005

Uversky, V. N. (2002). Natively unfolded proteins: a point where biology waits for physics. *Protein Sci.* 11, 739–756. doi: 10.1110/ps.4210102

Wang, L. J., Guan, X. Y., Du, C., Moradian-Oldak, J., and Nancollas, G. H. (2007). Amelogenin promotes the formation of elongated apatite microstructures in a controlled crystallization system. *J. Phys. Chem. C* 111, 6398–6404. doi: 10.1021/jp0675429

Wiejak, S., Masiukiewicz, E., and Rzeszotarska, B. (1999). A large scale synthesis of mono- and di-urethane derivatives of lysine. *Chem. Pharm. Bull.* 47, 1489–1490. doi: 10.1248/cpb.47.1489

Wishart, D. S., Bigam, C. G., Yao, J., Abildgaard, F., Dyson, H. J., Oldfield, E., et al. (1995). H-1, C-13 and N-15 chemical-shift referencing in biomolecular NMR. *J. Biomol. NMR* 6, 135–140. doi: 10.1007/BF00211777

Zhang, X., Ramirez, B. E., Liao, X., and Diekwisch, T. G. H. (2011). Amelogenin supramolecular assembly in nanospheres defined by a complex helix-coil-PPII helix 3D-structure. *PLoS ONE* 6:e24952. doi: 10.1371/journal.pone.0024952

Conflict of Interest Statement: The authors declare that the research was conducted in the absence of any commercial or financial relationships that could be construed as a potential conflict of interest.

Received: 17 May 2014; paper pending published: 02 June 2014; accepted: 17 June 2014; published online: 11 July 2014.

*Citation: Lu J-x, Burton SD, Xu YS, Buchko GW and Shaw WJ (2014) The flexible structure of the K24S28 region of Leucine-Rich Amelogenin Protein (LRAP) bound to apatites as a function of surface type, calcium, mutation, and ionic strength. Front. Physiol. **5**:254. doi: 10.3389/fphys.2014.00254*

This article was submitted to Craniofacial Biology, a section of the journal Frontiers in Physiology.

frontiers in PHYSIOLOGY

ORIGINAL RESEARCH ARTICLE
published: 11 November 2014
doi: 10.3389/fphys.2014.00430

The expanded amelogenin polyproline region preferentially binds to apatite versus carbonate and promotes apatite crystal elongation

Gokul Gopinathan[1†], Tianquan Jin[2†], Min Liu[3], Steve Li[1], Phimon Atsawasuwan[4], Maria-Therese Galang[4], Michael Allen[5], Xianghong Luan[1] and Thomas G. H. Diekwisch[1]*

[1] Oral Biology, University of Illinois at Chicago Brodie Laboratory for Craniofacial Genetics, University of Illinois at Chicago College of Dentistry, Chicago, IL, USA
[2] Biocytogen, One Innovation Drive, Worcester, MA, USA
[3] Department of Periodontology, Stomatological Hospital, Jilin University, Changchun, China
[4] University of Illinois at Chicago Department of Orthodontics, University of Illinois at Chicago College of Dentistry, Chicago, IL, USA
[5] Department of Medicine, University of Chicago, Chicago, IL, USA

Edited by:
Megan Pugach-Gordon, The Forsyth Insitute, USA

Reviewed by:
Michel Goldberg, Institut National de la Santé et de la Recherche Médicale and University Paris Descartes, France
Stefan Habelitz, University of California, San Francisco, USA

***Correspondence:**
Thomas G. H. Diekwisch, Department of Oral Biology, University of Illinois at Chicago College of Dentistry, 801 South Paulina Street, MC 690, Chicago IL 60612, USA
e-mail: tomdkw@uic.edu

† *These authors have contributed equally to this work.*

The transition from invertebrate calcium carbonate-based calcite and aragonite exo- and endoskeletons to the calcium phosphate-based vertebrate backbones and jaws composed of microscopic hydroxyapatite crystals is one of the great revolutions in the evolution of terrestrial organisms. To identify potential factors that might have played a role in such a transition, three key domains of the vertebrate tooth enamel protein amelogenin were probed for calcium mineral/protein interactions and their ability to promote calcium phosphate and calcium carbonate crystal growth. Under calcium phosphate crystal growth conditions, only the carboxy-terminus augmented polyproline repeat peptide, but not the N-terminal peptide nor the polyproline repeat peptide alone, promoted the formation of thin and parallel crystallites resembling those of bone and initial enamel. In contrast, under calcium carbonate crystal growth conditions, all three amelogenin-derived polypeptides caused calcium carbonate to form fused crystalline conglomerates. When examined for long-term crystal growth, polyproline repeat peptides of increasing length promoted the growth of shorter calcium carbonate crystals with broader basis, contrary to the positive correlation between polyproline repeat element length and apatite mineralization published earlier. To determine whether the positive correlation between polyproline repeat element length and apatite crystal growth versus the inverse correlation between polyproline repeat length and calcium carbonate crystal growth were related to the binding affinity of the polyproline domain to either apatite or carbonate, a parallel series of calcium carbonate and calcium phosphate/apatite protein binding studies was conducted. These studies demonstrated a remarkable binding affinity between the augmented amelogenin polyproline repeat region and calcium phosphates, and almost no binding to calcium carbonates. In contrast, the amelogenin N-terminus bound to both carbonate and apatite, but preferentially to calcium carbonate. Together, these studies highlight the specific binding affinity of the augmented amelogenin polyproline repeat region to calcium phosphates versus calcium carbonate, and its unique role in the growth of thin apatite crystals as they occur in vertebrate biominerals. Our data suggest that the rise of apatite-based biominerals in vertebrates might have been facilitated by a rapid evolution of specialized polyproline repeat proteins flanked by a charged domain, resulting in apatite crystals with reduced width, increased length, and tailored biomechanical properties.

Keywords: amelogenin, hydroxyapatite, calcium carbonate, polyproline repeat proteins, vertebrate evolution

INTRODUCTION

Biologically produced minerals are among the functionally most important and long-lasting components of living organisms: they provide strength and defense through the formation of endo– and exoskeletons and contribute the main structural components of the powerful dentate masticatory apparatus. Biominerals are also important for auditory perception (Tohno et al., 1997) and a sense of equilibrium (Pote and Ross, 1991). Pathological examples of biomineralization include calcified arteries, ectopic bone, and renal stones, to name just a few (Russell et al., 1986). Among the major mineral constituents of biominerals are carbonates, opal, ferric oxides, and magnetites, and phosphates (Lowenstam and Weiner, 1989). Biominerals are manufactured in many different fashions, through the help of organic matrix scaffolds or

in bulk, and by extracellular, intercellular, or intracellular mechanisms (Lowenstam, 1981). Protein scaffold-grown biominerals have emerged as some of the most prominent tissues in modern vertebrates, including bone, dentin, and enamel.

Commonly, two types of biomineralization proteins are distinguished: Framework macromolecules such as collagen, amelogenin and chitin (Lowenstam and Weiner, 1989) are considered organic matrix scaffolds for mineral deposition, while acidic phosphoproteins such as dentin matrix protein 1 and bone sialoprotein (George et al., 1993; Stubbs et al., 1997) are thought to act as nucleators for crystal growth. Many of the major biomineralization proteins are characterized by a high percentage of disordered residues, including dentin sialophosphoprotein (96/98%), dentin matrix protein 1 (96/96%), bone sialoprotein (83/87%), osteopontin (93/91%), amelogenin (65/70%), ameloblastin (75/88%), and enamelin (92/93%) (Kalmar et al., 2010). The tooth enamel protein amelogenin is a typical intrinsically disordered biomineralization protein as it controls the growth of apatite crystals for tooth enamel formation (Diekwisch et al., 1993; Delak et al., 2009). From a structural perspective, four distinct amelogenin domains are distinguished, the N-terminal tyrosine- and proline-rich TRAP molecule (mouse AA 1–45), the intermediary coil domain characterized by prominent histidine residues (mouse AA 46–117), the polyproline tri-peptide repeat region (mouse AA 118–164), and the glutamic acid enriched and hydrophilic C-terminus (mouse AA 165–180) (Zhang et al., 2011). A number of studies have confirmed the role of amelogenins in enamel crystal growth (Lagerström et al., 1991; Diekwisch et al., 1993; Gibson et al., 2001; Iijima and Moradian-Oldak, 2004), and the length of the amelogenin polyproline repeat region has been established as a potent regulator in the control of apatite crystal growth (Jin et al., 2009).

Apatites (Calciumhydroxyapatite, $Ca_{10}(PO_4)_6(OH)_2$) are the most common minerals in vertebrates, even though apatite minerals also occur in invertebrates, such as in the lingula shell (Iijima, 1991) and the crayfish mandible (Bentov et al., 2012). In contrast, calcium carbonates ($CaCO_3$) are the major forms of biominerals in invertebrates (Lowenstam and Weiner, 1989), and are only occasionally reported in vertebrates, e.g., in otoconia (Carlström et al., 1953; Kim et al., 2011). Nevertheless, most invertebrates including the fairly evolved echinoderms feature skeletons consisting of calcium carbonate plates and spines (Gilbert and Wilt, 2011), while beginning with calcium phosphate statoliths in hagfishes and lampreys (Carlström, 1963), most vertebrates rely on calcium phosphates in form of hydroxyapatite as the inorganic building block of bones and teeth (Pasteris et al., 2008). The first evidence of a vertebrate backbone composed of hydroxyapatite dates back more than 500 million years ago to the Cambrian and Ordovician period, and vertebrate columns based on apatite biominerals became an integral component of the vertebrate body plan throughout the highly successful emergence of vertebrates until today (Benton and Harper, 2009).

In the present study we have investigated the effect of polypeptides derived from the quintessential vertebrate tooth enamel biomineralization protein amelogenin on calcium carbonate, calcium phosphate and hydroxyapatite crystal growth and mineral binding. Among the amelogenin domains studied were the N-terminal helical region, the polyproline repeat region, and the polyproline repeat region augmented by the highly charged 13 amino acid long amelogenin C-terminus. To elucidate evolutionary trends, we then traced polyproline repeat regions among eukaryotic proteins, compared the effect of the amelogenin polyproline repeat region on calcium carbonate and calcium phosphate crystal growth, and provided an explanation for differences in crystal growth through differences in mineral binding affinity.

MATERIALS AND METHODS

PROLINE REPEAT ALIGNMENT

Genbank was searched using the mouse amelogenin and SM50 polyproline repeat region as query subjects. Positive hits were further searched for repeat regions and outcomes were summarized in **Figure 1**.

PROTEINS AND PEPTIDES USED IN THE PRESENT STUDY

The following amelogenin polypeptides were synthesized at the UIC Protein core facility (98% purity) and used in the present study: N33, MPLPPHPGSPGYINLSYEVLTPLKWY QSMIRQP; PXX, PMQPQSPLHP MQPLAPQPPL PPLFSMQP LS PIL; PXXC, PLHPMQPLAPQPPLPPLFSMQPLSPILPELPLEA WPATDKTKREEVD; PXX12, PMQPQPPVHPMQ; PXX24, PM QPQPPVHPMQPLPPQPPLPPMF; and PXX 33, PMQPQPPV HPMQPLPPQPPLPPMFPMQPLPPML.

CALCIUM CARBONATE AND CALCIUM PHOSPHATE NANOSCALE CRYSTAL GROWTH

Calcium phosphate and calcium carbonate crystal growth experiments were modified from previous studies (Beniash et al., 2005). Briefly, peptides and proteins were dissolved in DDW at a concentration of 4 mg/ml, adjusted to pH7.5–8.0 with 20 mM NH_4OH at 4°C and then incubated in a moisturized container with 10 mM $CaCl_2$ and either 6 mM $(NH_4)_2HPO_4$ or 6 mM $(NH_4)_2HPO_4$ at 37°C for 2 h. Subsequently, carbon coated copper grids were immersed into the solution for 1 min and quickly rinsed with DDW, blotted against filter paper, and air dried. Transmission electron microscopy was performed using a JEOL 1220 TEM.

CALCIUM CARBONATE MACROSCALE CRYSTAL GROWTH

Briefly, pH7.5–8.0 peptide/protein solutions similar to those described above (HAP Crystal Growth) were mixed with 20 mM $CaCl_2$ to the final concentration of 2 mg/ml peptide/protein and 2.5 mM $CaCl_2$. As a next step, 100µl of the protein/ $CaCl_2$ mixture on a 12 mm cover slip deposited in a 6-well plate was transferred into a sealed container containing 200 ml of 200 mM $(NH4)_2CO_3$. The entire container was then incubated at 37°C for 7 days, after which $CaCO_3$ crystals formed on the cover slip. Cover slips were thoroughly washed with DDW to remove salt, air dried, and then subjected to Hitachi SEM for observation.

PROTEIN/MINERAL BINDING ASSAY

Fourty µg of amelogenin proteins were incubated in 100 µl of calcium carbonate, calcium phosphate, or nano-hydroxyapatite solution (4µg/µl) at 37°C for 1 h. The pH of the mineral solution was adjusted to pH7.5 using glacial acetic acid or ammonium

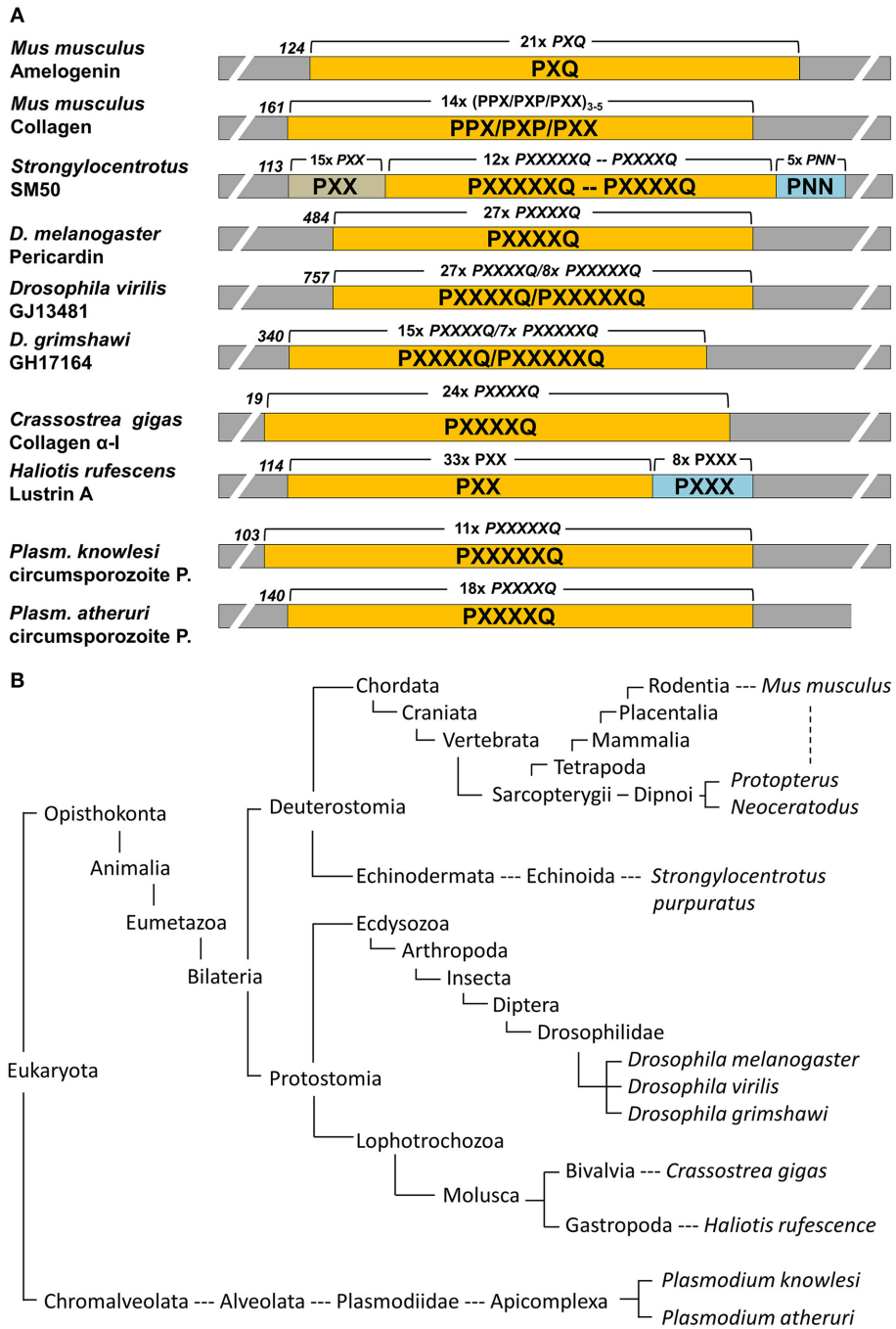

FIGURE 1 | Conservation of proline repeat elements among selected eukaryotic proteins as identified by BLAST searches. (A) illustrates the major proline repeat element composition, the N-terminal onset of the repeat region, and the number of repeats in selected eukaryotic repeat element containing proteins. P, proline; Q, glutamine; N, Asparagine; X, any amino acid. **(B)** Corresponding eukaryotic lineages to the repeat element containing proteins listed in **(A)**, with species including the Malaria parasite *Plasmodium*, well known moluscs like the Pacific oyster and the red abalone, insects such as the fruit fly *Drosophila*, the sea urchin as a representative echinoderm, and sarcopterygians ranging from lungfishes to humans. Note that this table only lists examples and is not meant to be comprehensive.

hydroxide. After 1 h incubation on a shaker, protein-HA complexes were washed with excessive amounts of 1xPBS, 3 x times at 10.000 x g to remove non-specific binding. Adsorbed protein from HA was released using 100 µl of RIPA lysis buffer. 30 µl of each sample protein were run on a 10% SDS-PAGE gel, transferred onto a PVDF membrane in a semi-dry blotting apparatus containing transfer buffer (25 mM tris-HCl, 40mM glycine, 10% methanol) for 45 min at 75 mA. The PVDF membrane

was blocked with 5% bovine serum albumin for 1 h at room temperature, incubated with a chicken anti-mouse amelogenin antibody or with a rabbit polyclonal antibody directed against the N-terminal mouse amelogenin fragment at a concentration of 1:2000 for 1 h. The membrane was washed with TBST three times for 10 min each and probed with a HRP-conjugated anti-chicken secondary antibody at a concentration of 1:10,000. HRP was detected using a chemiluminescent substrate (Supersignal West Pico Chemiluminescent Substrte, Pierce).

CRYSTAL MEASUREMENTS AND STATISTICAL ANALYSIS

All experiments were conducted in triplicate and crystal measurements were performed on printed electron micrographs from 10 randomly selected sample regions. Crystal dimensions per experimental group were recorded, and length and width average as well as standard deviation were calculated. Significance was determined using ANOVA and $p < 0.05$ was deemed significant.

RESULTS

POLYPROLINE REPEAT ELEMENTS OCCUR IN A BROAD RANGE OF EUKARYOTIC PROTEINS

Polyproline repeat element proteins were identified in a wide range of eukaryotic organisms, ranging from parasites to mammals (**Figure 1B**). Our analysis revealed long stretches of polyproline tripeptide repeats in mammalian amelogenins and collagens, in the echinoderm spicule protein SM50, and in the moluscan shell mineralization protein Lustrin A (**Figure 1A**). In addition, there were polyproline hexapeptide (6mer) or septapeptide (7mer) repeats in other portions of the SM50 spicule protein, in collagen homologes of the fruitfly *Drosophila* (pericardin) and the giant oyster *Crassostrea gigas*, as well as in the circumsporozoite proteins of the Malaria parasite *Plasmodium* (**Figure 1A**). According to BLAST searches, there was a 47% homology between SM50 and the *Drosophila* pericardin, a 46% homology between SM50 and the *Crassostrea* collagen, and a 43–53% homology between SM50 and the *Plasmodium* circumsporozoite protein.

IN CALCIUM PHOSPHATE CRYSTAL GROWTH STUDIES, THE POLYPROLINE REPEAT REGION PROMOTED THE FORMATION OF THIN CRYSTALLITES

In this set of experiments, the effects of three different portions of the amelogenin molecule on calcium carbonate and calcium phosphate crystal growth were compared (**Figure 2**). The N-terminal amelogenin fragment N33 caused calcium carbonate crystals to arrange in ring-shaped assemblies of hexagonal crystals, while the PXX repeat region peptide and the C-terminus augmented PXX fragment resulted in fused $CaCO_3$ crystal conglomerates (**Figures 2A–C**). The same protein fragments resulted in entirely different crystal shapes in conjunction with calcium phosphate crystal growth environments. Here the N-terminal amelogenin N33 caused the formation of fairly large and fused crystals, while crystal dimensions were somewhat shorter and thinner when using the PXX region alone, and only the PXX repeat peptide expanded by the charged C-terminal fragment resulted in short and thin calcium phosphate crystals (**Figures 2D–F,I,J**). There was some similarity between the crystals generated in the PXXC calcium phosphate crystal growth experiments (**Figure 2G**) and natural mouse enamel apatite crystals (**Figure 2H**), even though the spacing between the mouse enamel crystals was wider.

POLYPROLINE REPEAT PEPTIDES WITH INCREASING LENGTH RESULTED IN A COMPACTION OF CALCIUM CARBONATE CRYSTAL ASSEMBLY *IN VITRO*

Addition of polyproline designer peptides to the calcium carbonate crystallization solution resulted in the formation of needle-shaped calcium carbonate crystals arranged around a central core in a radial fashion (**Figure 3**). The PXX12 peptide yielded needles measuring $10.44 \pm 1.14\,\mu m$ in length and $1.10 \pm 0.22\,\mu m$ in thickness. The PXX24 peptides resulted in fused spicules with $7.23 \pm 1.81\,\mu m$ length and $1.91 \pm 0.30\,\mu m$ thickness. Addition of the PXX33 peptide resulted in the presence of cone-shaped processes consisting of fused individual crystallites and measuring $5.03 \pm 0.27\,\mu m$ in length and $2.88 \pm 0.82\,\mu m$ in thickness at the base. Samples without protein and samples containing albumin yielded cuboidal crystal shapes with smooth surfaces (**Figure 3**). Addition of amelogenin to the calcium carbonate crystallization mix resulted in cubes with rugged, deeply fissured surface structures (**Figure 3**). All three control conditions, no protein, BSA, and amelogenin, did not yield any needle-shaped crystal habits (**Figure 3**).

THE POLYPROLINE-RICH AMELOGENIN C-TERMINAL PEPTIDES STRONGLY BOUND TO THE CALCIUM PHOSPHATE AND HYDROXYAPATITE MINERAL AND NOT TO CALCIUM CARBONATE, WHILE THERE WAS LITTLE DIFFERENCE IN BINDING BETWEEN THE N-TERMINAL AMELOGENIN FRAGMENT AND THE THREE CALCIUM MINERALS STUDIED

The purpose of this experiment was to ask the question whether portions of the amelogenin molecule display preferential binding affinity to either apatite, calcium phosphate, or calcium carbonate mineral. In a first part of this experiment, the N-terminal N33 amelogenin peptide was incubated with calcium carbonate, calcium phosphate, and nanohydroxyapatite, and our binding assay revealed that N-terminal binding was approximately double as high between N33 and $CaCO_3$ as it was between N33 and the two calcium phosphates employed in this study (**Figure 4A**). The second experiment (**Figure 4B**) was conducted in parallel and revealed that the C-terminus augmented polyproline repeat peptide preferentially bound to calcium phosphate and the nanohydroxyapatite minerals, while there was only faint evidence of carbonate binding. Together, this study demonstrated that the long amelogenin polyproline repeat region augmented by the charged C-terminus strongly binds to calcium phosphate and nanohydroxyapatite, while the amelogenin N-terminus preferentially binds to calcium carbonate.

DISCUSSION

In the present study we asked the question how portions of the highly conserved amelogenin biomineralization molecule affect calcium phosphate and calcium carbonate crystal growth and whether this effect might be explained by the interaction between

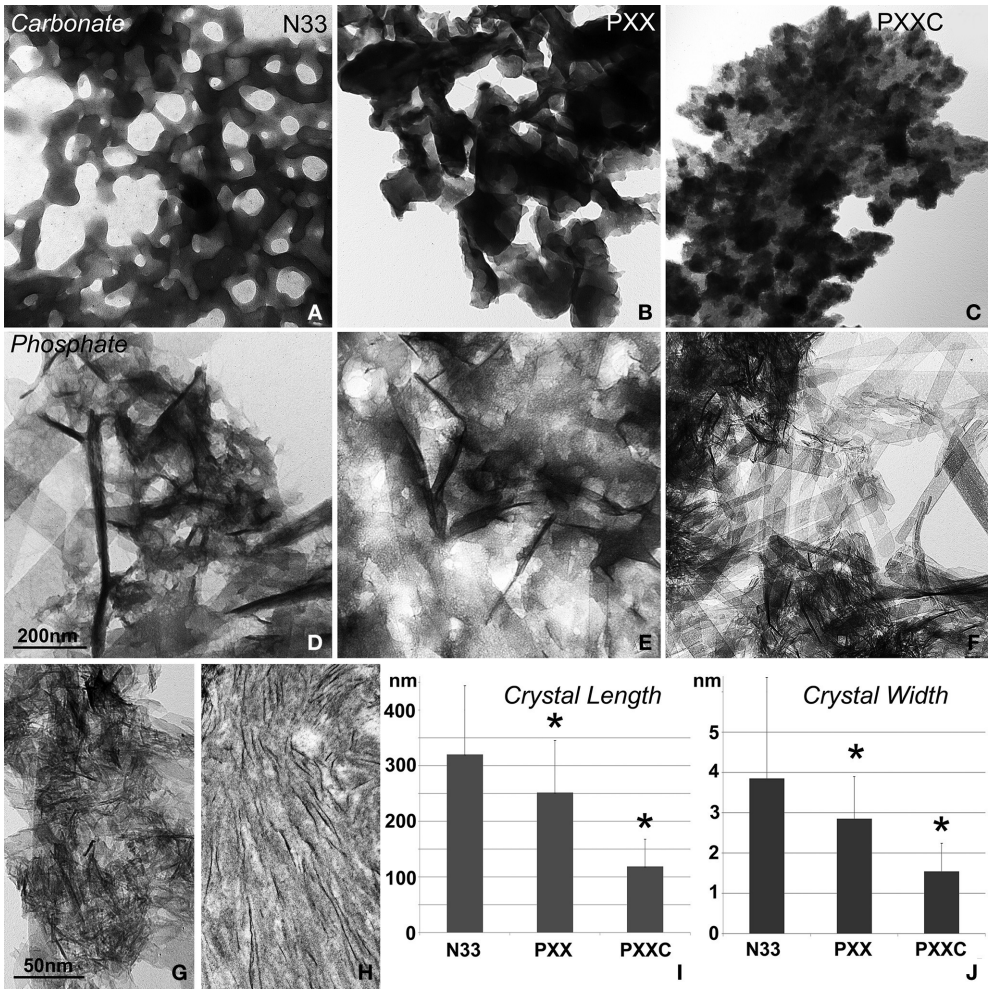

FIGURE 2 | Effect of amelogenin fragments on calcium carbonate and calcium apatite crystal growth. (A–C) demonstrates the effects of three different amelogenin fragments on carbonate crystal growth, including the N-terminal 33 amino acids (N33, **A**), the PXX repeat region alone (PXX, **B**), and the PXX region augmented by the hydrophilic C-terminus (PXXC, **C**). **(D–F)** is similar to **(A–C)**, but illustrates the effects of the same amelogenin fragments on calcium phosphate crystal growth, including the N-terminal 33 amino acids (N33, **D**), the PXX repeat region alone (PXX, **E**), and the PXX region augmented by the hydrophilic C-terminus (PXXC, **F**). **(G)** is a high magnification electron micrograph of the crystal shapes generated by the augmented PXX peptide and **(H)** is a similar micrograph of early stage mouse enamel crystals of 3 days postnatal mice. The measurements in **(I,J)** correspond to figures **(D–F)** and compare average apatite crystal length **(I,J)** width when crystals were grown in the presence of three different amelogenin-derived peptides, including N33, PXX, and PXXC. $*p < 0.05$.

amelogenin fragments and these two different calcium minerals. Amelogenin turned out to be an interesting study subject in the present inquiry because of its organization into distinct domains, its high level of conservation among individual domains, because of the presence of a distinct polyproline repeat domain, and in light of its presumed role in elongated crystal growth. Here we have tested the effect of amelogenin and some of its domains on both calcium carbonate and calcium phosphate mineral growth and binding to determine whether the interaction of amelogenin fragments with calcium phosphates when compared to calcium carbonates provided any unique insights into the evolutionary benefits of protein mediated calcium phosphate growth for vertebrate skeletal tissue function. Our study revealed that the amelogenin polyproline repeat region augmented by its hydrophilic C-terminus interacted primarily with calcium phosphates, and that this region promoted the growth of thin and individually distinct crystals, while the amelogenin N-terminus preferentially bound to calcium carbonates and inhibited C-axis crystal growth. Together, these findings provide unique insights into the protein dynamics that might have aided the evolutionary benefits of apatite-based skeletal tissues in vertebrates.

Our overview of polyproline repeat element containing proteins among eukaryotes gives testimony to the universal distribution of such proteins among eukaryotes, ranging from amelogenins to collagens, and from parasitic protists to most mammals. Some of these proteins are functionally related to biomineralization, such as amelogenins, collagens, SM50, and Lustrin A, while a group represented by the *Drosophila* pericardin proteins plays a role in heart development (Chartier et al., 2002), and others such as the circumsporozoite protein of various *Plasmodium* species

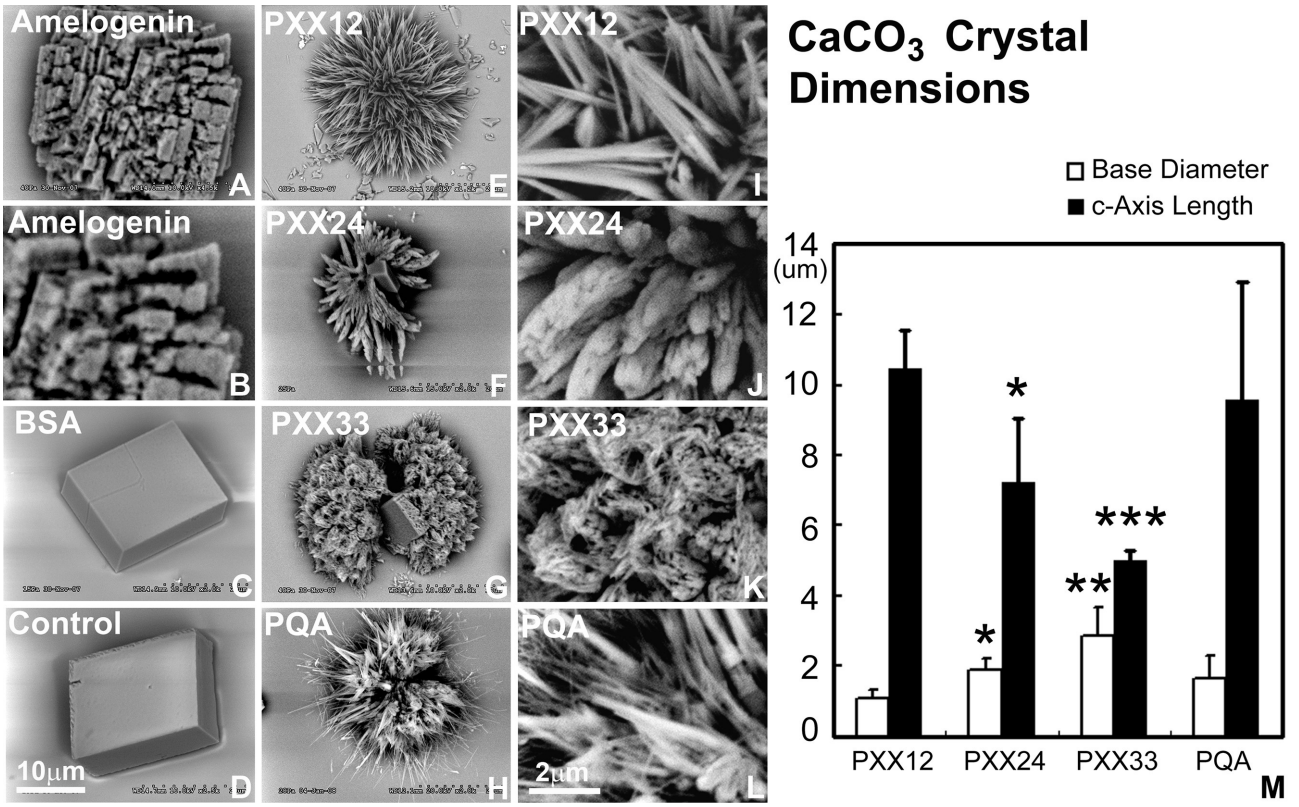

FIGURE 3 | Effect of polyproline repeat fragments of varying length on calcium carbonate crystal growth. Scanning electron micrographs shown here document the outcomes of calcium carbonate crystal growth studies in the presence of polyproline repeat fragments of varying lengths. **(A,B)** are calcium carbonate crystals grown in the presence of amelogenin, **(C)** using bovine serum albumin as a protein control, and **(D)** is without protein. In **(E–G)**, polyproline repeat peptides of varying length from 12 to 33mer were used, and **(H)** is a control in which the PXX repeat was replaced by a PQA repeat. **(B,I,J,K,I)** are scanning electron micrographs recorded at five time higher magnification (magnification bars in **D** and in **I**). M illustrates the decrease in c-axis length and the increase in base diameter with increasing polyproline repeat length (from PXX12 to PXX33 and PQA as a control on the x-axis and crystal dimensions on the y-axis). $*p < 0.05$, $**p < 0.01$, $***p < 0.001$.

are essential for the invasion of the parasite into the host organism (Plassmeyer et al., 2009). The broad distribution and multiple functions of polyproline repeat proteins suggest that the repeat region plays somewhat of a generic role that can be adapted to serve multiple functions (Adzhubei et al., 2013). However, a common element among such Polyproline-II repeat region containing proteins is their ability to form elongated fibril-type structures (Hall et al., 2014) and to interact with surfaces, either with other proteins (Adzhubei et al., 2013), or with polyphenols in saliva (Murray and Williamson, 1994), or with biological minerals such as apatites (Jin et al., 2009). These two qualities suggest that the amelogenin polyproline tri-peptide repeat region is likely engaged in interactions with the apatite surface, providing a semi-flexible elongated template for crystal growth. Our analysis also revealed that the polyproline peptide repeats were organized into either trimer, or hexamer/heptamer subunits, with tripeptide repeats as the rule in the two vertebrate proteins listed here. Subunit lengths of varying amino acid number are likely to affect the periodicity and surface exposure of critical amino acids for binding to the mineral or adjacent protein surface. Finally, the majority of the proline oligopeptide repeat regions contains a glutamine in the terminal repeat position, a feature that might be linked to the aggregation behavior of these proteins (Altschuler et al., 1997). The ability of polyglutamine proteins to aggregate is not only important for the generation of biomineralization templates (Jin et al., 2009), but also plays a role in the pathogenesis of neurodegenerative diseases, including Huntington's disease and Friedreich's ataxia (Shao and Diamond, 2007).

In our calcium phosphate crystal growth studies, the polyproline repeat region promoted the formation of thin crystallites, while the same proteins in calcium carbonate crystal growth conditions formed either ring-shaped assemblies of hexagonal crystals or fused $CaCO_3$ crystal conglomerates. These findings indicate that at least under the conditions described here, the ability to form needle-shaped crystals was unique to the interaction between calcium phosphates and the three amelogenin fragments employed in the present study. The occurrence of nanoscale needle-shaped and parallel organized crystals is predominantly a feature of vertebrate biominerals such as bone, dentin, and developing enamel (Fitton-Jackson and Randall, 1956; Diekwisch et al., 1995; He and George, 2004), even though invertebrates are entirely capable of promoting needle-shaped calcium carbonate spicules, albeit with relatively thicker diameters (Beniash et al., 1999). Our data also indicated that only the C-terminus

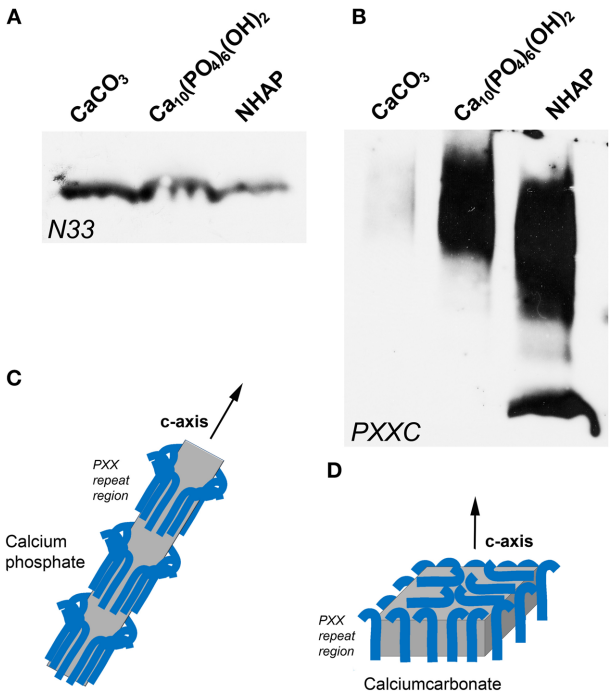

FIGURE 4 | Binding of amelogenin fragments to calcium minerals. **(A,B)** illustrate results from parallel experiments in which either an amelogenin N-terminal fragment (N33, **A**) or a C-terminus augmented amelogenin repeat fragment (PXXC, **B**) were incubated with three different calcium minerals, including calcium carbonate ($CaCO_3$), calcium phosphate, and nanohydroxyapatite (NHAP). **(C,D)** illustrates our explanation for the differences in calcium mineral crystal growth when subjected to different protein environments. Here we propose that polyproline repeat regions (blue hooks) as they occur in amelogenin bind to the a- and b- axis of calcium phosphate crystals and allow for the growth of long apatite crystal through expansion mostly in c-axis direction **(C)**. In contrast, proteins including polyproline peptides appear to affect calcium carbonate crystal growth equally in all directions, resulting in an overall compaction of the final crystal **(D)**.

augmented polyproline fragment promoted the growth of short, thin, and parallel nanoscale crystals, while both the amelogenin N-terminus and the polyproline region alone appeared to fuse individual crystals into thicker subunits. These results suggest that the amelogenin C-terminus is necessary for the immediate protein adhesion to the calcium phosphate crystal surface (Shaw et al., 2004) and the inhibition of a- and b- axis crystal growth in favor of c-axis directed crystal elongation (Diekwisch et al., 1993). Together, this set of data indicates that the combination of apatites with the augmented amelogenin carboxy-terminus results in the growth of minerals with stereotypical vertebrate biomineralization features such as small, short, and parallel crystal assemblies, while amelogenin fragments in combination with calcium carbonates generate bulk mineral clusters and fail to produce needle-shaped crystals.

We then asked whether the elongation of the polyproline region would affect calcium carbonate crystal growth in week-long growth studies to compare the effect on crystal elongation with our previously published apatite crystal growth studies using the same peptides (Jin et al., 2009). In opposite to the apatite mineralization outcomes (Jin et al., 2009), increased PXX polypeptide repeat length resulted in shorter calcium carbonate crystals with broader basis, suggesting that PXX repeat polypeptides affected calcium carbonate crystals in a different fashion than calcium apatite crystals. We attribute these differences in crystal growth patterns to possible differences in the interaction between the polyproline repeat region and different crystal facets, with polyproline repeat regions preferentially binding to a- and b- axis facets of apatite crystals and to all surfaces of carbonate crystals. In the larger context of typical vertebrate versus invertebrate biomineralization patterns, the different effects of polyproline repeat polypeptides on axial crystal growth in apatite and carbonate crystal morphologies corresponded with naturally occurring crystal shapes, i.e., long crystals in apatite minerals enamel and bone, and compact plates in the calcium carbonate minerals calcite, aragonite, and vaterite.

Our protein/mineral binding studies revealed that the polyproline-rich amelogenin carboxy-terminal fragments strongly bound to the calcium phosphate and hydroxyapatite mineral and not to calcium carbonate, while there was little difference in binding between the N-terminal amelogenin fragment and the three calcium minerals studied. This finding is significant in the context of previous studies that emphasized the importance of the amelogenin carboxy-terminus for apatite binding (Moradian-Oldak et al., 2002; Shaw et al., 2004; Sun et al., 2008; Pugach et al., 2010). However, also other portions of the amelogenin molecule are important for enamel formation, including the N-terminus (Dunglas et al., 2002). The relationship between the C-terminus and apatite binding was early on established by Moradian-Oldak et al. (2002), demonstrating that apatite binding of amelogenins lacking the C-terminus was significantly reduced, followed by a solid state NMR study in which the charged amelogenin C-terminal region was oriented next to the hydroxyapatite surface (Shaw et al., 2004). These findings were further corroborated by enamel protease cleavage experiments resulting in reduced amelogenin-apatite binding in amelogenins of decreasing length (Sun et al., 2008) and an enamel defect mouse model that overexpressed a transgene lacking the C-terminal 13 amino acids (Pugach et al., 2010). Finally, Zhu et al. pointed to the importance of the P70 proline as part of a series of central polyproline repeats for apatite binding and self-assembly, emphasizing the role of the proline repeats in the interaction between amelogenins and apatites (Zhu et al., 2011). Here we show that the charged carboxy-terminal amelogenin motif with its adjacent polyproline repeat region preferentially binds to apatite and calcium phosphates when compared to calcium carbonate, suggesting that the C-terminal polyproline/hydrophilic stretch has evolved as part of the vertebrate biomineralization machinery in control of apatite crystal growth. This interpretation adds to previous studies reporting a trend of increasing polyproline repeat length as a means to control apatite crystal dimension during vertebrate evolution (Bonass et al., 1994; Sire et al., 2005; Diekwisch et al., 2009; Jin et al., 2009). Varying the length of polyproline repeat stretches would affect the spacing between individual crystals within supramolecular amelogenin subunit compartments (Diekwisch et al., 1993) or in between nanosphere assemblies (Jin et al., 2009).

A number of possible reasons for the predominance of hydroxyapatites in vertebrate mineralized tissues have been proposed, including (i) the abundance of calcium and phosphorus in food sources, (ii) the sparing solubility and resulting relative stability of crystalline apatites, (iii) the ability of apatites to accept chemical substitutes, including carbonate substitutes, that greatly affect their physical and biomechanical properties (Pasteris et al., 2004), and (iv) mechanical advantages of apatites over carbonates, including advantages associated with increased hardness (Reid et al., 2012). Here we have introduced another, perhaps equally important reason for the evolutionary selection of apatite as the preferred vertebrate biomineral: its ability to be readily shaped by matrix proteins through the effect of repeat region assembly and the affinity of flanking charged domains to the lateral apatite surface, allowing for c-axis crystal growth and controlled inhibition of crystal width. This ability of the organic vertebrate protein matrix to shape calcium phosphate minerals into many parallel packed, individually separated, long and thin crystallites has become the biomechanical foundation for the strong yet flexible backbones and jaws of the vertebrate skeleton, ensuring survival and success in the late Cambrian/early Ordovician biosphere and until today.

ACKNOWLEDGMENTS

Studies were generously supported by NIDCR grant DE018900 to Thomas G. H. Diekwisch.

REFERENCES

Adzhubei, A. A., Sternberg, M. J., and Makarov, A. A. (2013). Polyproline-II helix in proteins: structure and function. *J. Mol. Biol.* 425, 2100–2132. doi: 10.1016/j.jmb.2013.03.018

Altschuler, E. L., Hud, N. V., Mazrimas, J. A., and Rupp, B. (1997). Random coil conformation for extended polyglutamine stretches in aqueous soluble monomeric peptides. *J. Pept. Res.* 50, 73–75. doi: 10.1111/j.1399-3011.1997.tb00622.x

Beniash, E., Addadi, L., and Weiner, S. (1999). Cellular control over spicule formation in sea urchin embryos: a structural approach. *J. Struct. Biol.* 125, 50–62. doi: 10.1006/jsbi.1998.4081

Beniash, E., Simmer, J. P., and Margolis, H. C. (2005). The effect of recombinant mouse amelogenins on the formation and organization of hydroxyapatite crystals *in vitro*. *J. Struct. Biol.* 149, 182–190. doi: 10.1016/j.jsb.2004.11.001

Benton, M. J., and Harper, H. A. T. (2009). *Introduction to Paleobiology and the Fossil Record*. Chichester: John Wiley & Sons Ltd.

Bentov, S., Zaslansky, P., Al-Sawalmih, A., Masic, A., Fratzl, P., Sagi, A., et al. (2012). Enamel-like apatite crown covering amorphous mineral in a crayfish mandible. *Nat. Commn.* 3:839. doi: 10.1038/ncomms1839

Bonass, W. A., Robinson, P. A., Kirkham, J., Shore, R. C., and Robinson, C. (1994). Molecular cloning and DNA sequence of rat amelogenin and a comparative analysis of mammalian amelogenin protein sequence divergence. *Biochem. Biophys. Res. Commun.* 198, 755–763. doi: 10.1006/bbrc.1994.1109

Carlström, D. (1963). A crystallographic study of vertebrate otoliths. *Biol. Bull.* 125, 441–463. doi: 10.2307/1539358

Carlström, D., Engström, H., and Hjorth, S. (1953). Electron microscopic and x-ray diffraction studies of statoconia. *Laryngoscope* 63, 1052–1057. doi: 10.1288/00005537-195311000-00002

Chartier, A., Zaffran, S., Astier, M., Sémériva, M., and Gratecos, D. (2002). Pericardin, a *Drosophila* type IV collagen-like protein is involved in the morphogenesis and maintenance of the heart epithelium during dorsal ectoderm closure. *Development* 129, 3241–3253.

Delak, K., Harcup, C., Lakshminarayanan, R., Sun, Z., Fan, Y., Moradian-Oldak, J., et al. (2009). The tooth enamel protein, porcine amelogenin, is an intrinsically disordered protein with an extended molecular configuration in the monomeric form. *Biochemistry* 48, 2272–2281. doi: 10.1021/bi802175a

Diekwisch, T., David, S., Bringas, P. Jr., Santos, V., and Slavkin, H. C. (1993). Antisense inhibition of AMEL translation demonstrates supramolecular controls for enamel HAP crystal growth during embryonic mouse molar development. *Development* 117, 471–482.

Diekwisch, T. G., Berman, B. J., Gentner, S., and Slavkin, H. C. (1995). Initial enamel crystals are not spatially associated with mineralized dentine. *Cell Tissue Res.* 279, 149–167. doi: 10.1007/BF00300701

Diekwisch, T. G., Jin, T., Wang, X., Ito, Y., Schmidt, M., Druzinsky, R., et al. (2009). Amelogenin evolution and tetrapod enamel structure. *Front. Oral Biol.* 13, 74–79. doi: 10.1159/000242395

Dunglas, C., Septier, D., Paine, M. L., Zhu, D. H., Snead, M. L., and Goldberg, M. (2002). Ultrastructure of forming enamel in mouse bearing a transgene that disrupts the amelogenin self-assembly domains. Calcif. *Tissue Int.* 71, 155–166. doi: 10.1007/s00223-001-2116-5

Fitton-Jackson, S., and Randall, J. T. (1956). The fine structure of bone. *Nature* 178, 798.

George, A., Sabsay, B., Simonian, P. A., and Veis, A. (1993). Characterization of a novel dentin matrix acidic phosphoprotein. Implications for induction of biomineralization. *J. Biol. Chem.* 268, 12624–12630.

Gibson, C. W., Yuan, Z. A., Hall, B., Longenecker, G., Chen, E., Thyagarajan, T., et al. (2001). Amelogenin-deficient mice display an amelogenesis imperfecta phenotype. *J. Biol. Chem.* 276, 31871–31875. doi: 10.1074/jbc.M104624200

Gilbert, P. U., and Wilt, F. H. (2011). Molecular aspects of biomineralization of the echinoderm endoskeleton. *Prog. Mol. Subcell. Biol.* 52, 199–223. doi: 10.1007/978-3-642-21230-7_7

Hall, M., Nylander, S., Jenkinson, H. F., and Persson, K. (2014). Structure of the C-terminal domain of AspA (antigen I/II-family) protein from Streptococcus pyogenes. *FEBS Open Bio* 4, 283–289. doi: 10.1016/j.fob.2014.02.012

He, G., and George, A. (2004). Dentin matrix protein 1 immobilized on type I collagen fibrils facilitates apatite deposition *in vitro*. *J. Biol. Chem.* 279, 11649–11656. doi: 10.1074/jbc.M309296200

Iijima, M., and Moradian-Oldak, J. (2004). Interactions of amelogenins with octacalcium phosphate crystal faces are dose dependent. *Calcif. Tissue Int.* 74, 522–531. doi: 10.1007/s00223-002-0011-3

Iijima, S. (1991). Helical microtubules of graphitic carbon. *Nature* 354, 56–58. doi: 10.1038/354056a0

Jin, T., Ito, Y., Luan, X., Dangaria, S., Walker, C., Allen, M., et al. (2009). Elongated polyproline motifs facilitate enamel evolution through matrix subunit compaction. *PLoS Biol.* 7:e1000262. doi: 10.1371/journal.pbio.1000262

Kalmar, L., Homola, D., Varga, G., and Tompa, P. (2010). Structural disorder in proteins brings order to crystal growth in biomineralization. *Bone* 51, 528–534. doi: 10.1016/j.bone.2012.05.009

Kim, E., Hyrc, K. L., Speck, J., Salles, F. T., Lundberg, Y. W., Goldberg, M. P., et al. (2011). Missense mutations in Otopetrin 1 affect subcellular localization and inhibition of purinergic signaling in vestibular supporting cells. *Mol. Cell. Neurosci.* 46, 655–661. doi: 10.1016/j.mcn.2011.01.005

Lagerström, M., Dahl, N., Nakahori, Y., Nakagome, Y., Bäckman, B., Landegren, U., et al. (1991). A deletion in the amelogenin gene (AMG) causes X-linked amelogenesis imperfecta (AIH1). *Genomics* 10, 971–975. doi: 10.1016/0888-7543(91)90187-J

Lowenstam, H. A. (1981). Minerals formed by organisms. *Science* 211, 1126–1131. doi: 10.1126/science.7008198

Lowenstam, H. A., and Weiner, S. (1989). *On Blomineralization*. San Diego, CA: Academic Press.

Moradian-Oldak, J., Bouropoulos, N., Wang, L., and Gharakhanian, N. (2002). Analysis of self-assembly and apatite binding properties of amelogenin proteins lacking the hydrophilic C-terminal. *Matrix Biol.* 21, 197–205. doi: 10.1016/S0945-053X(01)00190-1

Murray, N. J., and Williamson, M. P. (1994). Conformational study of a salivary proline-rich protein repeat sequence. *Eur. J. Biochem.* 219, 915–921. doi: 10.1111/j.1432-1033.1994.tb18573.x

Pasteris, J. D., Wopenka, B., Freeman, J. J., Rogers, K., Valsami-Jones, E., van der Houwen, J. A., et al. (2004). Lack of OH in nanocrystalline apatite as a function of degree of atomic order: implications for bone and biomaterials. *Biomaterials* 25, 229–238. doi: 10.1016/S0142-9612(03)00487-3

Pasteris, J. D., Wopenka, B., and Valsami-Jones, E. (2008). Bone and tooth mineralization: why apatite? *Element* 4, 97–104. doi: 10.2113/GSELEMENTS.4.2.97

Plassmeyer, M. L., Reiter, K., Shimp, R. L. Jr., Kotova, S., Smith, P. D., Hurt, D. E., et al. (2009). Structure of the *Plasmodium* falciparum circumsporozoite protein, a leading malaria vaccine candidate. *J. Biol. Chem.* 284, 26951–26963. doi: 10.1074/jbc.M109.013706

Pote, K. G., and Ross, M. D. (1991). Each otoconia polymorph has a protein unique to that polymorph. *Comp. Biochem. Physiol. B* 98, 287–295.

Pugach, M. K., Li, Y., Suggs, C., Wright, J. T., Aragon, M. A., Yuan, Z. A., et al. (2010). The amelogenin C-terminus is required for enamel development. *J. Dent. Res.* 89, 165–169. doi: 10.1177/0022034509358392

Reid, D. G., Mason, M. J., Chan, B. K., and Duer, M. J. (2012). Characterization of the phosphatic mineral of the barnacle Ibla cumingi at atomic level by solid-state nuclear magnetic resonance: comparison with other phosphatic biominerals. *J. R. Soc. Interface* 9, 1510–1516. doi: 10.1098/rsif.2011.0895

Russell, R. G., Caswell, A. M., Hearn, P. R., and Sharrard, R. M. (1986). Calcium in mineralized tissues and pathological calcification. *Br. Med. Bull.* 42, 435–446.

Shao, J., and Diamond, M. I. (2007). Polyglutamine diseases: emerging concepts in pathogenesis and therapy. *Hum. Mol. Genet.* 16 Spec No. 2, R115–R123. doi: 10.1093/hmg/ddm213

Shaw, W. J., Campbell, A. A., Paine, M. L., and Snead, M. L. (2004). The COOH terminus of the amelogenin, LRAP, is oriented next to the hydroxyapatite surface. *J. Biol. Chem.* 279, 40263–40266. doi: 10.1074/jbc.C400322200

Sire, J. Y., Delgado, S., Fromentin, D., and Girondot, M. (2005). Amelogenin: lessons from evolution. *Arch. Oral Biol.* 50, 205–212. doi: 10.1016/j.archoralbio.2004.09.004

Stubbs, J. T. 3rd., Mintz, K. P., Eanes, E. D., Torchia, D. A., and Fisher, L. W. (1997). Characterization of native and recombinant bone sialoprotein: delineation of the mineral-binding and cell adhesion domains and structural analysis of the RGD domain. *J. Bone Miner. Res.* 12, 1210–1222. doi: 10.1359/jbmr.1997.12.8.1210

Sun, Z., Fan, D., Fan, Y., Du, C., and Moradian-Oldak, J. (2008). Enamel proteases reduce amelogenin-apatite binding. *J. Dent. Res.* 87, 1133–1137. doi: 10.1177/154405910808701212

Tohno, Y., Utsumi, M., Tohno, S., Minami, T., Moriwake, Y., Yamada, M., et al. (1997). A constancy of mineral contents in human auditory ossicles. *Kaibogaku Zasshi* 72, 531–534.

Zhang, X., Ramirez, B. E., Liao, X., and Diekwisch, T. G. (2011). Amelogenin supramolecular assembly in nanospheres defined by a complex helix-coil-PPII helix 3D-structure. *PLoS ONE* 6:e24952. doi: 10.1371/journal.pone.0024952

Zhu, L., Uskoković, V., Le, T., DenBesten, P., Huang, Y., Habelitz, S., et al. (2011). Altered self-assembly and apatite binding of amelogenin induced by N-terminal proline mutation. *Arch. Oral Biol.* 56, 331–336. doi: 10.1016/j.archoralbio.2010.10.017

Conflict of Interest Statement: The authors declare that the research was conducted in the absence of any commercial or financial relationships that could be construed as a potential conflict of interest.

Received: 21 August 2014; paper pending published: 18 September 2014; accepted: 16 October 2014; published online: 11 November 2014.

*Citation: Gopinathan G, Jin T, Liu M, Li S, Atsawasuwan P, Galang M-T, Allen M, Luan X and Diekwisch TGH (2014) The expanded amelogenin polyproline region preferentially binds to apatite versus carbonate and promotes apatite crystal elongation. Front. Physiol. **5**:430. doi: 10.3389/fphys.2014.00430*

This article was submitted to Craniofacial Biology, a section of the journal Frontiers in Physiology.

frontiers in PHYSIOLOGY

ORIGINAL RESEARCH ARTICLE
published: 25 July 2014
doi: 10.3389/fphys.2014.00274

Analysis of co-assembly and co-localization of ameloblastin and amelogenin

Parichita Mazumder, Saumya Prajapati, Sowmya Bekshe Lokappa, Victoria Gallon and Janet Moradian-Oldak*

Division of Biomedical Sciences, Center for Craniofacial Molecular Biology, Herman Ostrow School of Dentistry, University of Southern California, Los Angeles, CA, USA

Edited by:
Bernhard Ganss, University of Toronto, Canada

Reviewed by:
Tom Diekwisch, University of Illinois at Chicago, USA
Javier Catón, King's College London, UK

****Correspondence:***
Janet Moradian-Oldak, Division of Biomedical Sciences, Center for Craniofacial Molecular Biology, Herman Ostrow School of Dentistry, University of Southern California, 2250 Alcazar St., Los Angeles, CA 90033, USA
e-mail: joldak@usc.edu

Epithelially-derived ameloblasts secrete extracellular matrix proteins including amelogenin, enamelin, and ameloblastin. Complex intermolecular interactions among these proteins are believed to be important in controlling enamel formation. Here we provide *in vitro* and *in vivo* evidence of co-assembly and co-localization of ameloblastin with amelogenin using both biophysical and immunohistochemical methods. We performed co-localization studies using immunofluorescence confocal microscopy with paraffin-embedded tissue sections from mandibular molars of mice at 1, 5, and 8 days of age. Commercially-available ameloblastin antibody (M300) against mouse ameloblastin residues 107–407 and an antibody against full-length recombinant mouse (rM179) amelogenin were used. Ameloblastin-M300 clearly reacted along the secretory face of ameloblasts from days 1–8. Quantitative co-localization was analyzed (QCA) in several configurations by choosing appropriate regions of interest (ROIs). Analysis of ROIs along the secretory face of ameloblasts revealed that at day 1, very high percentages of both the ameloblastin and amelogenin co-localized. At day 8 along the ameloblast cells the percentage of co-localization remained high for the ameloblastin whereas co-localization percentage was reduced for amelogenin. Analysis of the entire thickness on day 8 revealed no significant co-localization of amelogenin and ameloblastin. With the progress of amelogenesis and ameloblastin degradation, there was a segregation of ameloblastin and co-localization with the C-terminal region decreased. CD spectra indicated that structural changes in ameloblastin occurred upon addition of amelogenin. Our data suggest that amelogenin-ameloblastin complexes may be the functional entities at the early stage of enamel mineralization.

Keywords: ameloblastin, amelogenin, protein-protein co-assembly, confocal microscopy, quantitative co-localization analysis

INTRODUCTION

Tooth enamel, the hardest substance in the body, is formed by an evolutionarily highly conserved biomineralization process that is controlled by extracellular matrix proteins. During the secretory stage of enamel formation, the three major proteins secreted by ameloblasts are amelogenin (Amel) (Snead et al., 1985), ameloblastin (Ambn) (Krebsbach et al., 1996), and enamelin (Hu et al., 2001a,b; Hu and Yamakoshi, 2003). Proper mineralization of enamel depends upon the secretion of these proteins, as well as their being processed into smaller functional components and eventually degraded by proteinases such as enamelysin (matrix metalloproteinase 20, Mmp-20) and kallikrein 4 (Klk4) (Bartlett and Simmer, 1999). It was suggested that those proteins of enamel must have specific protein–protein interactions to assemble an organic matrix that is capable of undergoing mineral replacement and forming the highly ordered three-dimensional structure of the hydroxyapatite crystallites (Hu et al., 2001a; Bouropoulos and Moradian-Oldak, 2004; Bartlett et al., 2006; Fan et al., 2008; Iijima et al., 2010; Yang et al., 2011; Gallon et al., 2013). However, there is still a gap in our knowledge as how these enamel matrix components interact with one another to form an assembled matrix that initiate and orchestrate the events of mineralization (Paine et al., 2001; Yamakoshi et al., 2003; Ravindranath et al., 2004). We have recently reported cooperative function of amelogenin and enamelin as well as their interactions using both *in vitro* and *in vivo* strategies (Bouropoulos and Moradian-Oldak, 2004; Fan et al., 2011; Yang et al., 2011; Gallon et al., 2013).

Ameloblastin is a member of the secretory calcium-binding phosphoprotein (SCPP) family of proteins (Kawasaki and Weiss, 2003). It is a typical extracellular matrix (ECM) protein that may be involved in the regulation of adhesion, proliferation, and differentiation of ameloblasts (Fukumoto et al., 2004), and it seems to serve essential developmental functions of enamel. Support for this notion was provided by the finding that an enamel layer fails to appear on the teeth of mice that are genetically engineered to produce a truncated form of ameloblastin (exon 5 and 6 deleted) (Smith et al., 2009; Wazen et al., 2009). Inactivation of the ameloblastin gene leads not only to loss of production of the full-length protein by ameloblasts but also to a reduction in the expression levels of amelogenin with no apparent change in

the levels of other proteins (Fukumoto et al., 2004; Zalzal et al., 2008).

A potential mechanisms by which ameloblastin functions as an ECM protein in tooth enamel has been identified, including involvement in mineralization by means of calcium-binding sites at the C-terminus of ameloblastin (Yamakoshi et al., 2001; Hu et al., 2005; Kobayashi et al., 2007; Tamburstuen et al., 2010). Ameloblastin is rapidly processed after secretion. Full-length ameloblastin is only found adjacent to the non-secretary face of the Tomes' processes of the ameloblasts (Uchida et al., 1995; Hu et al., 1997; Murakami et al., 1997), while lower molecular weight proteins are present in the sheath space and in the rods of the superficial layer. The porcine N-terminal cleavage products (13, 15, 17 kDa) are stable and concentrate in the prism sheath. In contrast, the C-terminal cleavage products (40, 50 kDa) are successively cleaved into smaller peptides (8, 13, 15, 27, 29 kDa) and lost from the immature enamel soon after secretion (Uchida et al., 1998).

Our present study focuses on the co-localization of amelogenin and ameloblastin and their interactions. We propose that such interactions are important for the formation of highly organized enamel mineral and for maintaining its prismatic structure. We hypothesized that, by analyzing the spatial co-relation between ameloblastin and amelogenin in the enamel matrix using a well-established *in vivo* approach, complemented by investigating the interaction between full-length ameloblastin and amelogenin using *in vitro* experiments, we will gain new and important information on the roles played by ameloblastin-amelogenin complexes in normal dental enamel formation. We used immunofluorescence confocal microscopy with mouse mandibular first molars at differing postnatal ages (P1, P5, and P8) and two antibodies to ascertain when both ameloblastin and amelogenin are secreted into the ECM of enamel, as well as whether they are co-localized, which would support the possibility of their interaction *in vivo*. Commercially available antibody against 107–407 residues of mouse ameloblastin and an antibody against the full-length recombinant mouse (rM179) amelogenin were used in this procedure (Simmer et al., 1994). Direct *in vitro* evidence of structural changes in ameloblastin was observed upon addition of amelogenin using far-UV circular dichroism (CD) spectra.

MATERIALS AND METHODS

DESCRIPTION OF ANTIBODIES

Two primary antibodies were used in this study, (i) rabbit anti-ameloblastin (M300), commercially available antibody against the portion of mouse ameloblastin extending from residues 107–407 (**Figure 1A**, residues labeled with blue) (Santa-Cruz Biotechnology, Inc. Santa Cruz, California) and (ii) chicken anti-amelogenin generated against full-length mouse amelogenin (a gift from Prof M. Snead). For immunohistochemical staining two secondary antibodies were used (i) goat anti-rabbit conjugated with Texas Red and (ii) bovine anti-chicken conjugated with FITC (fluorescein isothiocyanate) (Santa-Cruz Biotechnology, Inc. Santa Cruz, California).

We checked whether there was any cross-reaction between antibodies and the proteins, by using Western blot with recombinant mouse amelogenin and ameloblastin (**Figures 1B,C**, lane 4-5). Samples were electrophoresed on 10 % polyacrylamide gel containing 0.1% sodium dodecyl sulfate (SDS-PAGE) under non-reducing conditions and then electrotransferred to polyvinylidene fluoride (PVDF) membranes (PALL, Life Sciences, BioTrace™ PVD 0.45 μm) in semi-dry transblotter (Bio-Rad Scientific Instruments) at 10 V for 45 min. After blocking with phosphate-buffered saline, 0.1% Tween 20 (PBST) (pH 7.4) with 5% non-fat milk for 2 h at 37°C, the membrane was washed five times with PBST. After washing, the membranes were treated with the primary antibody (M300, rabbit anti-ameloblastin) against

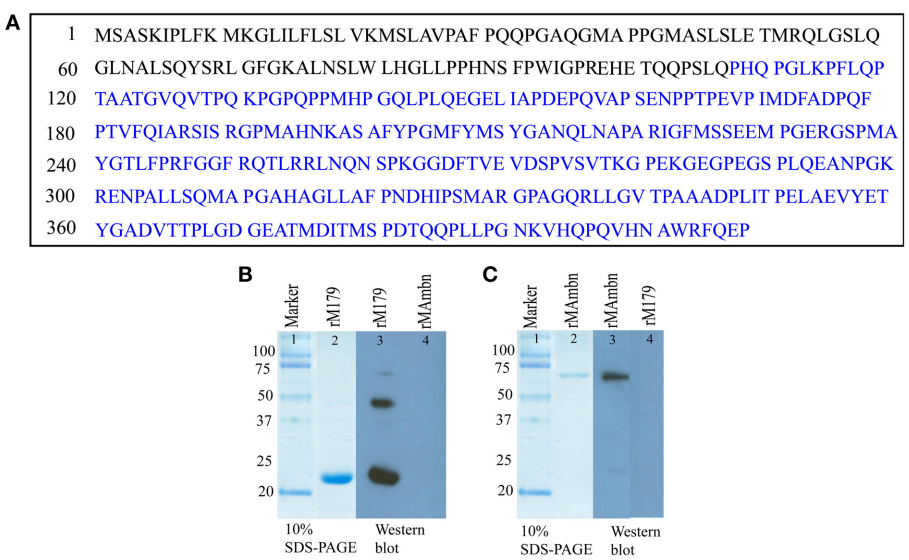

FIGURE 1 | (A) Sequence of full-length mouse ameloblastin (Gene ID: 11698), the epitope of anti-ameloblastin antibody M300 is indicated by blue color. Western blot analysis with **(B)** anti-amelogenin antibody (lane 3, 4) and **(C)** M300 antibody (lane 3, 4) to check cross reactivity of the antibodies with recombinant proteins.

mouse ameloblastin at a 1:1000 dilution overnight at 4°C. After five washes, the membranes were incubated for 2 h in anti-chicken (for amelogenin) and anti-rabbit (for ameloblastin) secondary antibody conjugated with horseradish peroxidase at an appropriate dilution (1:3000). After another wash, the membranes were incubated in Amersham™ ECL Western blotting detection reagents (GE healthcare). In lane 4 from **Figures 1B,C**, there was no protein band, demonstrating that the both ani-amelogenin and M300 antibody did not react with recombinant ameloblastin and amelogenin respectively.

PROTEIN EXPRESSION AND PURIFICATION

Preparation of the recombinant rM179 has been described elsewhere (Moradian-Oldak et al., 2000; Lakshminarayanan et al., 2010). The protein was further purified on a Jupiter C4 semi-preparative reversed phase column (10 × 250 mm, 5 μm) Varian Prostar HPLC system (ProStar/Dynamics 6, version 6.41, Varian, Palo Alto, CA). A linear gradient of 60% acetonitrile in 0.1% trifluoroacetic acid at a flow rate of 2 ml/min was used (**Figure 1B**, lane 2).

Recombinant porcine amelogenin (rP172) was expressed in *Escherichia coli* strain BL21-codon plus (DE3-RP, Agilent Technologies, Inc., Santa Clara, CA), precipitated by 20% ammonium sulfate and purified as previously described (Hu et al., 1996; Ryu et al., 1999). The precipitate was dissolved in 0.1% TFA and protein purification was accomplished on a reverse phase C4 column (10 × 250 mm, 5 μm) mounted on a Varian Prostar HPLC system (ProStar/Dynamics 6, version 6.41 Varian, Palo Alto, CA) and fractionated using a linear gradient of 60% acetonitrile at a flow rate of 1.5 mL/min.

Recombinant murine ameloblastin (rMAmbn) both phosphorylated and glycosylated (**Figure 1C**, lane 2) was prepared in a Drosophila melanogaster expression system using Schneider 2 cells (Invitrogen, CA) as previously described (Zeichner-David et al., 2006). The protein was purified by HPLC with a gradient of 20–80% B for 60 min (buffer B was 60% v/v aqueous acetonitrile in 0.1% v/v trifluoroacetic acid (TFA) and buffer A was 0.1% TFA) at a flow rate of 1.0 ml/min.

Sodium dodecyl sulfate–polyacrylamide gel electrophoresis (SDS–PAGE) was carried out in the presence of 0.1% SDS, using a 10% acrylamide gel (Laemmli, 1970) to characterize the proteins (**Figures 1B,C**). The gel was stained with Coomassie brilliant blue.

IMMUNOCHEMICAL ANALYSIS OF PROTEIN FROM ENAMEL EXTRACELLULAR MATRIX AT DAY 9

For immunochemical analyses, six 9-day-old (postnatal) mice were used. All mouse studies were conducted according to protocols approved by the USC Institutional Animal Care & Use Committee. The upper and lower molars were extracted from the alveolar bone. The enamel surface was then gently wiped to remove remnants of secretory ameloblasts. The sample was dissolved in 0.5 M acetic acid (four molar /100 μl) and dissolution is aided by grinding the samples in the acid with pestle and then total extracted protein was lyophilized. Samples were electrophoresed on 10 % polyacrylamide gel containing 0.1% sodium dodecyl sulfate (SDS-PAGE) under non-reducing conditions and then Western blot analysis was performed as described in previous Section using both anti-amelogenin and M300 primary antibody (**Figure 2**, lane 2, 3).

TISSUE PREPARATION

Mandibular processes of mice from postnatal days 1–8 (here the day of birth was termed postnatal day 0) were dissected and fixed in 4% paraformaldehyde in PBS at pH 7.4 for 24 h. Samples from day 5–8 were demineralized in 0.2% paraformaldehyde, 0.05% glutaraldehyde and 10% EDTA for ∼1–2 weeks (pH 8.0) at 4°C with rocking. The tissues were then processed for histological analysis and embedded in paraffin. Tissue sections of 7 μm thickness were cut from the wax blocks and mounted onto glass slides.

IMMUNOFLUORESCENCE LABELING

Tissue sections were subjected to an antigen retrieval step by incubation in 10 mM sodium citrate with 0.05% Tween 20 at pH 6.0 in a 60°C water bath overnight. The sections were allowed to cool in dH_2O before being rinsed in TBS and then incubated with 0.3% H_2O_2 for 15 min. After washing with TBS, sections were blocked with 1% bovine serum albumin (BSA) for 15 min before incubation overnight at room temperature with primary antibody. We have used 1:500 dilutions for anti-ameloblastin M300 and 1:1000 for anti-amelogenin (Section Description of Antibodies). For simultaneous immunofluorescence double-labeling mixture of both primary antibodies with above mentioned dilution were used. After another wash with TBS, sections were incubated with secondary antibody (for ameloblastin goat anti-rabbit-Texas Red and for amelogenin bovine anti-chicken-FITC with 1:100 dilution each) for 3 h at room temperature, before mounting with

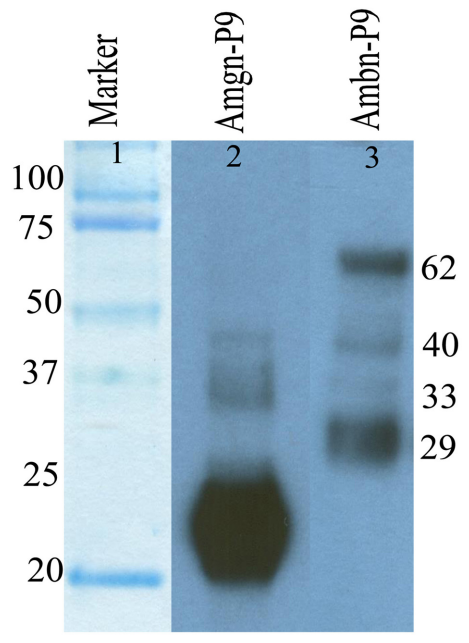

FIGURE 2 | Immunochemical detection of amelogenin (lane 2) and ameloblastin (lane 3) proteins and their degradation products present in enamel matrix from postnatal day 9 old (P9) mouse enamel.

Vectashield® Hard Set™ mounting medium with DAPI. Similar to primary antibody we have used mixture of both secondary antibodies for immunofluorescence double-staining. Several controls were performed to ascertain the specificity of the antibodies, which included incubating each primary antibody with both secondary antibodies, as well as each secondary antibody with both primary antibodies. The sections were visualized using a Leica TCS SP5 confocal microscope.

QUANTIFICATION OF CO-LOCALIZATION OF TWO ANTIGENS

Using the Leica Application Suite Advanced Fluorescence software (version 2.5.2.6939) confocal images were analyzed with a threshold of each channel at 30% and a background correction of 20%, and scatter grams were generated. Mander's colocalization coefficients were calculated to predict the contribution of each particular antigen to the areas with co-localization, using the following equations (Manders et al., 1993):

$$M_{red} = \frac{\sum_i R_{i,\ coloc}}{\sum_i R_i}; M_{green} = \frac{\sum_i G_{i,\ coloc}}{\sum_i G_i}$$

when, $R_{i,\ coloc} = R_i$ if $G_i > 0$; $G_{i,\ coloc} = G_i$ if $R_i > 0$, i.e., M_{red} is the sum of intensities of red pixels that have a green component divided by the total sum of red intensities.

CIRCULAR DICHROISM

CD measurements were carried out at 37°C on a JASCO J-715 spectropolarimeter between 190 and 260 nm in a quartz cell with a path length of 1 mm. Four spectra were accumulated for each sample, and the contribution of the buffer was always subtracted. Data are represented as mean residue ellipticities. Stock solution of rP172 (89% analogues to mouse amelogenin) was prepared in distilled water and rMAmbn was prepared in Tis-HCL pH 8.0. CD experiments were performed with 10 μM protein in 10 mM potassium phosphate buffer at pH7.4. CD spectra were normalized to the protein concentration and normalized spectra were deconvoluted using the CDSSTR algorithm and the Reference set 7 at Dichroweb (Lobley et al., 2002; Whitmore and Wallace, 2004). The values for helix1 and helix2 as well as sheet1 and sheet2 were added to obtain total helix and total sheet content (Sreerama et al., 1999).

RESULTS

DEGRADATION AND DISTRIBUTION OF MOUSE AMELOBLASTIN

We analyzed the degradation of mouse ameloblastin immunochemically using Western blot analysis (**Figure 2**, lane 3) with proteins extracted from 9 day old mouse enamel. In the enamel matrix sample, M300 antibody reacted with protein bands having molecular weights of near 62, 40, 33, and 29 kDa (**Figure 2**, lane 3). The largest 62 kDa band corresponds to the nascent ameloblastin and the others are presumably C-terminal ameloblastin processing products (Uchida et al., 1997, 1998; Brookes et al., 2001).

To observe the distribution of ameloblastion and its proteolytic products in enamel we have incubate tissue sections from day 1 (**Figure 3A**), 5 (**Figure 3B**) and 8 (**Figure 3C**) with anti-ameloblastin M300 antibody followed by immunofluorescence

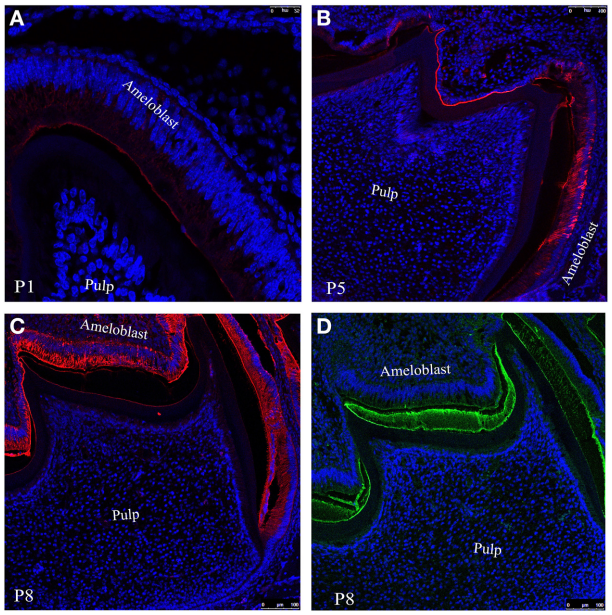

FIGURE 3 | Confocal images of mouse molar enamel showing immunofluorescence of ameloblastin at postnatal days (A) P1, (B) P5 and (C) P8. (D) Represents the immunofluorescence of amelogenin at P8. Nuclei are stained with DAPI (blue).

labeling with Texas red conjugated anti-rabbit secondary antibody (see Section Description of Antibodies and Immunofluorescence Labeling). Confocal image of the section at postnatal day 1(P1) indicated that M300 antibody stained the distal cytoplasm of ameloblasts, particularly in Tomes' processes and immature enamel near the secretory surfaces of pre-secretoty ameloblasts (**Figure 3A**). During the early maturation stage when the degradation of ameloblstin has already started, at day 5 (P5), they were present in the enamel epithelium and at the enamel surface (**Figure 3B**). At day 8 (P8), we observed that M300 reacted with the proteins which were accumulated in the juxtanuclear cytoplasm, the distal cytoplasm near the enamel surface, at the enamel surface and dentino-enamel junction (**Figure 3C**) (Lee et al., 1996).

The immunofluoresence study at P8 (**Figure 3C**) with M300 antibody gives us a clear picture of localization pattern of ameloblastin and its C-terminal processing products which were identified by immunochemical analysis (**Figure 2**, lane 3). **Figure 3D** shows the localization pattern of amelogenin and its processing products (**Figure 2**, lane 2) at day P8. The anti-amelogenin antibody stained evenly across the enamel layer (visualized by green color FITC conjugated secondary antibody).

THE CO-LOCALIZATION PATTERN OF Ambn AND Amgn IN MOUSE MANDIBULAR MOLARS

To visualize the co-localization of ameloblastin and amelogenin and for further confirmation of distribution of these two proteins in enamel extracellular matrix we acquired confocal images of tissue sections (simultaneously immunostained with two fluorophore mixture) at P1 (**Figure 4A**), P5 (**Figure 4B**) and P8

(**Figure 4C**). In **Figure 4** the regions which were yellow or orange in color represent the co-localization of both the protein. Next quantitative co-localization analysis (QCA) was performed using fluorescence software to quantify the percentage of co-localization of Ambn and Amgn at P1 and P8 (**Figures 5**, **6**) using selected region of these images (**Figure 4**, for P5 data not shown) with higher magnification.

QCA was conducted at day 1 using a selected co-localization region from **Figure 4A** (white square), which presented in **Figure 5A**. We have divided this co-localization region (yellow colored) into 14 small regions of interest (ROIs) and the direction of analyzed region of interest in **Figure 5** is indicated by pink arrow along the secretory face of the ameloblast (at the enamel surface) from the cervical loop to tip of the molar. Then Mander's co-localization coefficients were calculated to characterize the degree of overlap between two channels (**Figure 5B**, green for Amgn and **Figure 5C**, red for Ambn) in the image and to predict the contribution of each particular antigen to the

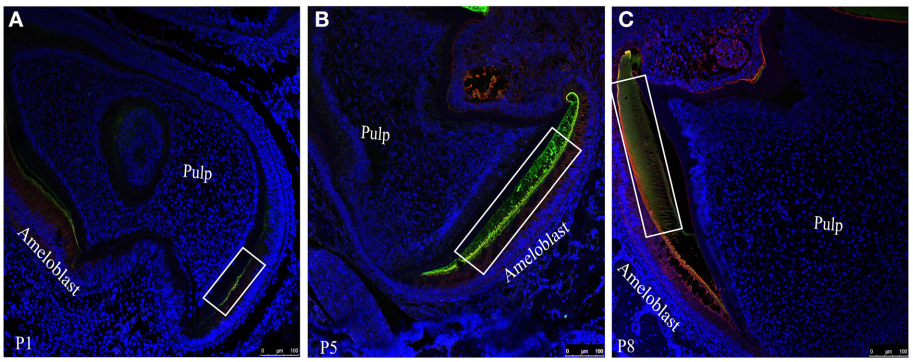

FIGURE 4 | Co-localization patterns (yellow color) of ameloblastin and amelogenin within the forming enamel layer of mouse mandibular molar sections at (A) P1, (B) P5 and (C) P8. Amelogenin and ameloblstin simultaneously co-labeled with FITC (green) and with TR (red) respectively.

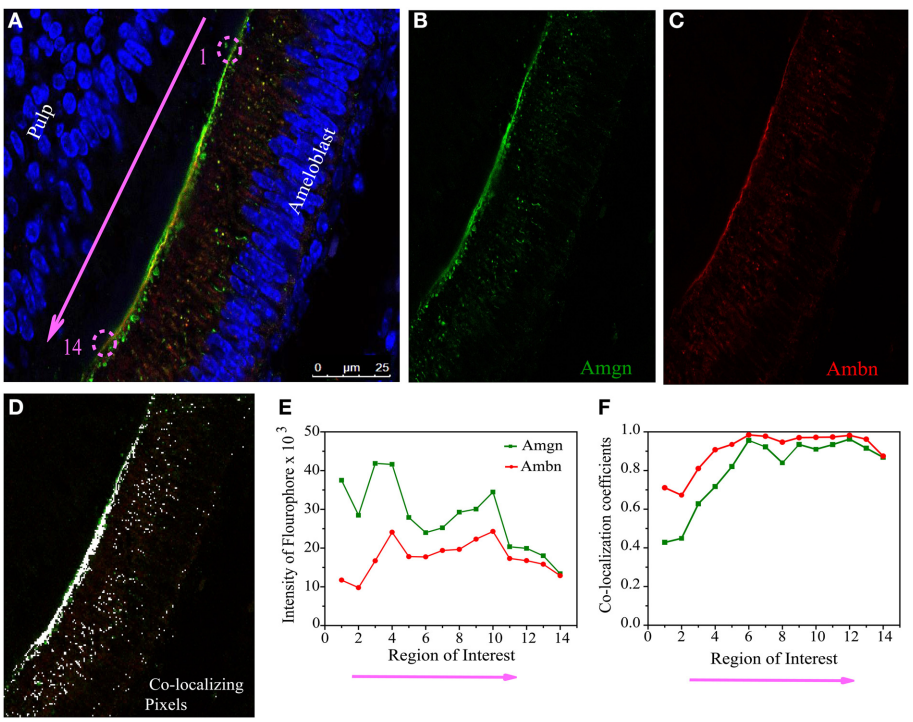

FIGURE 5 | Quantitative co-localization of ameloblastin and amelogenin in mouse molar enamel at P1. (A) Confocal image with higher magnification taken from the sample in **Figure 4A** (see square), considered for QCA analysis along the enamel surface (pink arrow). The individual channels detecting **(B)** only Amgn and **(C)** only Ambn signal. **(D)** Represent the pixels that have only co-localizing signal after threshold and background corrections of image **(A)**. **(E)** Graph of total intensity sum of each fluophore. **(F)** Plot of Mander's co-localization coefficient with respect to region of interest as shown in **(D)**. Each ROI dimension (5 × 5 µm). Note that ROI 1 to 14 in **(E,F)** correspond to the pink arrow in **(A)**.

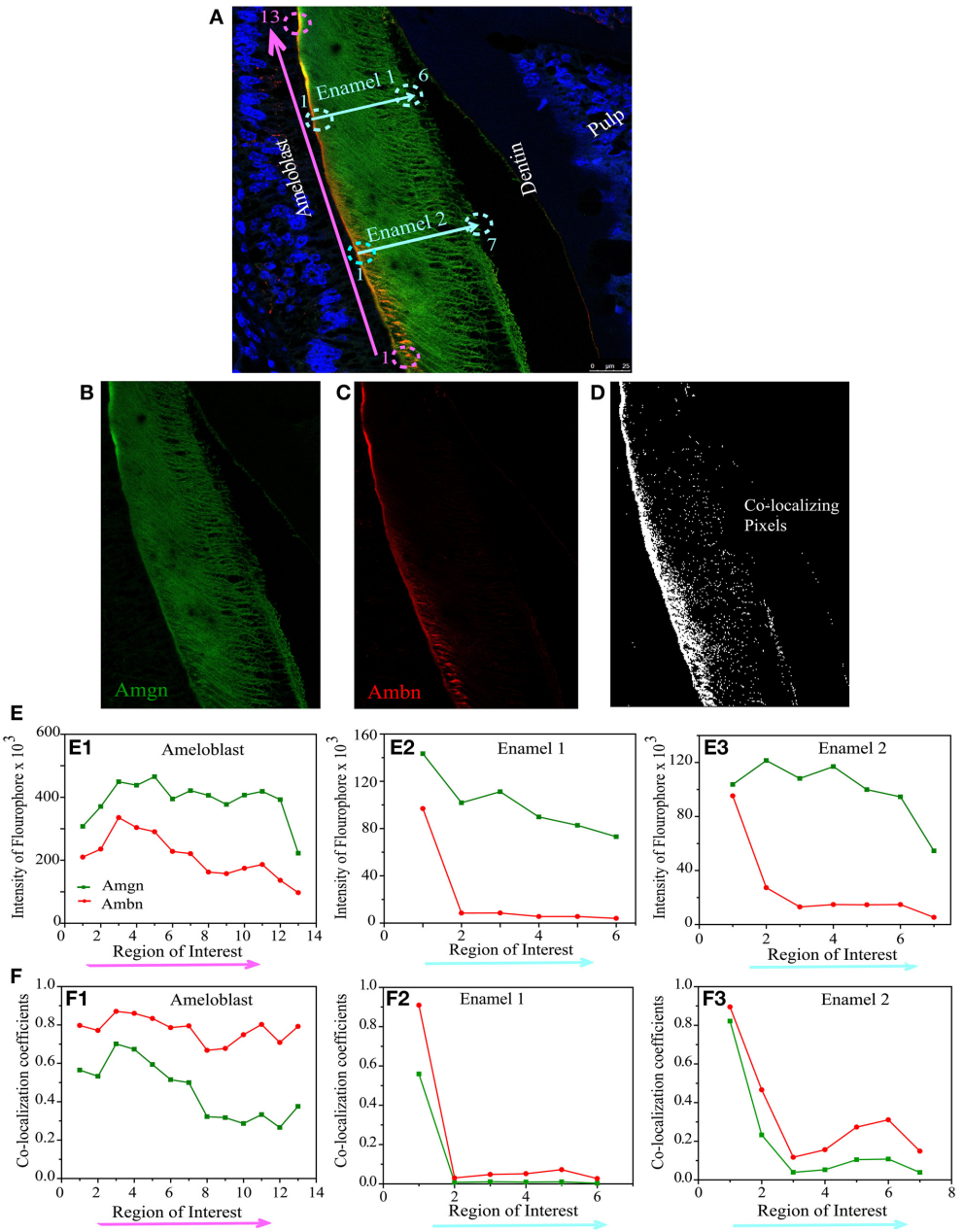

FIGURE 6 | Quantitative co-localization of ameloblastin and amelogenin in mouse molar enamel at P8. (A) Confocal image with higher magnification taken from the sample in **Figure 4C** (see square), considered for QCA analysis along the enamel surface (pink arrow) and enamel thickness (cyan arrows). The individual channels detecting **(B)** only Amgn and **(C)** only Ambn signal. **(D)** Represents co-localization pattern after analysis of image **(A)** with threshold and background correction of each channel. **(E)** Represents the intensity sum of each fluophore at each region of interest. **(F)** Plot of Mander's co-localization coefficient with respect to region of interest as shown in **(D)**. Each ROI dimension (10 × 10 μm). Note that **(E1,F1)** correspond to pink arrow in **(A)** and **(E2,F2)** correspond to cyan arrow in **(A)** (Enamel 1), and **(E3,F3)** correspond to cyan arrows (Enamel 2).

areas with co-localization, which is the number of pixels that have a co-localizing signal (**Figure 5D**, represented by white dots). First the values for signal intensity sum of the green channel (**Figure 5E**, green line), red channel (**Figure 5E**, red line) and the co-localization intensity (data not shown) were generated at each ROI. Then the co-localization intensity was divided by the signal intensity to obtain co-localization coefficients (**Figure 5F**), which measured the proportion of overlap of each channel with the other. As can be seen from the co-localization coefficient graph, at the initial stage of enamel development (P1), Amgn and Ambn co-localized near the secretory face of ameloblasts with almost the same proportion and high coefficient values (**Figure 5F**).

On day 8, QCA was performed with a section of **Figure 4C** (square or inset), represented in **Figure 6A**. At P8 the enamel

was more mature, we have calculated co-localization coefficients in two different configurations, one along the secretory face of the ameloblast from the cervical loop to tip of the molar (at the enamel surface indicated by pink arrow) and two along the thickness of the enamel layer from the enamel surface to dentino-enamel junction (indicated by cyan blue arrows as Enamel1 and Enamel2) (**Figure 6A**). The two individual channels of this confocal image were presented by **Figure 6B** (green channel for Amgn) and **Figure 6C** (red channel for Ambn) and the number of pixels that have a co-localizing signal in same image indicated by white dots in **Figure 6D**. We have calculated the total sum of green (**Figure 6E**, green line) and red (**Figure 6E**, red line) intensities along, (i) the ameloblast (**Figure 6E1**) and (ii) enamel thickness (**Figures 6E2,E3**). We observed that at day 8 the intensity difference between the two channels increased in both configurations (**Figures 6E1–E3**) relative to day 1 (**Figure 5E**). The co-localization coefficient plot at P8 indicated that Ambn co-localized with Amgn along the secretory face of ameloblasts, and their proportions of co-localization differed (**Figure 6F1**). There was a higher percentage of Ambn co-localizing with Amgn than Amgn co-localizing with Ambn. Along the enamel thickness moving award from the ameloblasts, no significant co-localization was observed (**Figures 6F2,F3**).

It appears that at an early stage both antigens (ameloblastin and amelogenin) are distributed in the same region with high spatial overlap, i.e., we can assume that they may be close enough to form co-assemblies, but with maturation ameloblastin has a high co-localization coefficient in comparison to amelogenin.

This trend can be clearly seen when the average of the co-localization coefficients for each age is calculated and plotted (**Figure 7A**). We have calculated the ratio of the total intensity sum of Ambn-red channel ($\sum_i R_i$) to the Amgn-green channel ($\sum_i G_i$) of each region of interest (**Figures 5E**, **6E**) along the enamel surface obtained from confocal images of day 1 and 8 mouse mandibular molars (**Figure 7B**). At an early developmental stage (day 1) we found that the ratio gradually reaches the value 1 when moving from the root to the tips of the tooth (**Figure 7B**, black line), which indicates that the proteins were secreted simultaneously and in similar proportions (calculated from QCA) from ameloblasts (Zalzal et al., 2008). With enamel maturation, at day 8 the intensity ratio decreases (**Figure 7B**, red line), indicating that at the maturation stage, ameloblastin and its proteolytic products (C-terminal large soluble polypeptides) (Lee et al., 1996; Uchida et al., 1997, 1998; Brookes et al., 2001) are gradually lost from the enamel surface.

Our co-localization studies suggested that amelogenin-ameloblastin complexes may be the functional entities at the early stage of enamel mineralization. In order to examine how amelogenin would affect ameloblastin's structure, we performed *in vitro* experiment, e.g., CD spectroscopy study with recombinant proteins.

CD SPECTROSCOPIC STUDY OF Ambn AND Amgn INTERACTION

CD spectra analysis of Ambn (10 μM) in the presence of equimolar Amgn revealed that Amgn induced changes in the secondary structure of Ambn (**Figure 8**). The CD spectrum of rMAmbn at 37 °C, with a negative minima around 208 nm and a small negative shoulder around 227 nm, is characteristic of an unordered structure (βII structure) (**Figure 8**, black solid line). Additionally, the spectra deconvolution shows rMAmbn contain intermixed alpha-helical (24%), beta-sheet (24%) and beta-turn (18%) regions with 34% unordered structure. The human recombinant full-length ameloblastin also exhibited βII like structural property at 37°C (Wald et al., 2011, 2013) and almost similar deconvolution pattern with less helical content and more beta character. With the addition of equimolar Amgn to Ambn, we observed an isoelliptic point appears at around 211 nm and a distinct change in CD bands. The intensity of the shoulder around 224 nm became more negative and at 192 nm a positive maxima was appeared. The spectral deconvolution exhibited the alpha-helical content increased to 51% and the beta-sheet, beta-turn and unordered forms decreased to 17, 12, and 14%, respectively. To avoid the interference of Amgn's structural changes on Ambn due to its self-association at high concentrations (>62.5 μM) (Lakshminarayanan et al., 2007), we used a very low concentration of Amgn (10 μM) and also we have

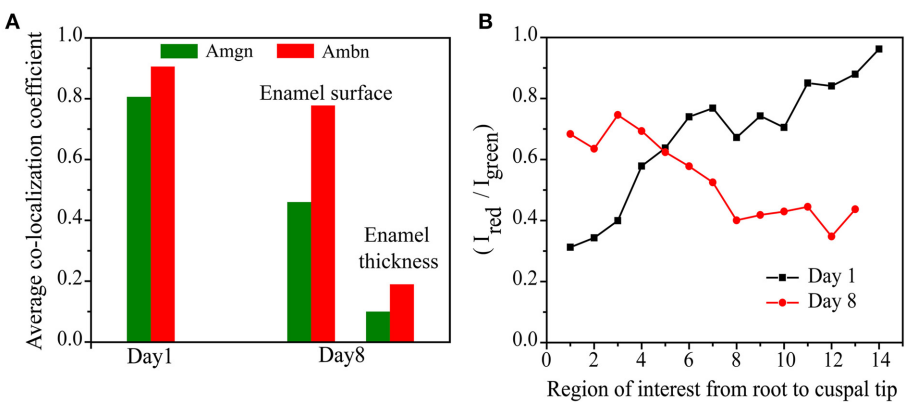

FIGURE 7 | Comparison of (A) the differences in the average co-localization coefficients of Amgn and Ambn at P1 and P8 and (B) intensity ratio of total sum of intensities of red to green channels of each region of interest along the enamel surface.

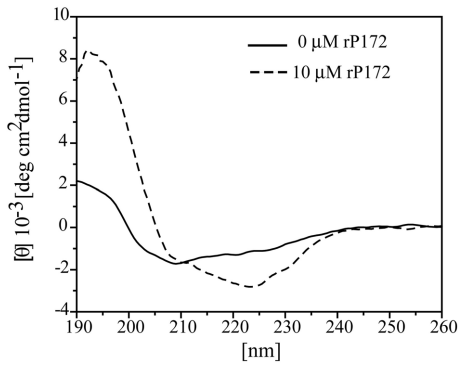

FIGURE 8 | Structural changes of ameloblastin (Ambn) in the presence of amelogenin (Amgn) provide evidence for their co-assembly. Far-UV circular dichroism (CD) spectra of 10 μM rMAmbn only (solid line) and in the presence of 10 μM rP172 (dashed line).

subtracted its contribution from the CD spectra of equimolar mixture of both the proteins. The structural changes in Ambn at this low Amgn concentration thus clearly indicated that the proteins formed hetero-assemblies.

DISCUSSION

Amelogenin and ameloblastin, the major enamel matrix proteins, are important for well-orchestrated enamel biomineralization (Snead et al., 1985; Krebsbach et al., 1996). They have synergistic roles in enamel development, as suggested by recent study showing that Amel $X^{-/-}$ /$Ambn^{-/-}$ mice have additional enamel defects not observed in either Amel $X^{-/-}$ or $Ambn^{-/-}$ mice (Hatakeyama et al., 2009). The co-distribution of amelogenin and ameloblastin in the majority of the secretory granules in Tomes' processes during appositional growth of the enamel layer may reflect a form of functional association between these two distinct proteins (Zalzal et al., 2008). There is *in vitro* evidence of interactions between amelogenin (tyrosyl-binding motif) and ameloblastin (Ravindranath et al., 2004). The same group further produced some indications that during early tooth development the murine ameloblastin 37 kDa isoform interacts with amelogenin (Ravindranath et al., 2007). However, there still remains a gap in our knowledge of how these proteins are distributed in the extracellular enamel matrix, what the contribution pattern of each particular protein is to the areas with co-localization during the different stages of tooth development, and also what structural changes occur when amelogenin and ameloblastin co-assemble.

In order to give clear insight into the putative cooperative function of ameloblastin and amelogenin we took advantage of quantitative co-localization techniques and performed a systematic analysis of the localization of ameloblastin with respect to amelogenin in the mouse mandibular molar. We performed an additional *in vitro* study using circular dichroism (CD) spectroscopy to show the structural changes in ameloblastin when it co-assembles with amelogenin. We concentrated on confocal images from mandibular first molars from postnatal mice from one to eight days old (here the day of birth was termed postnatal day 0). Previous research into the expression of ameloblastin and amelogenin by *in situ* hybridization using DNA biotinylated probes (Torres-Quintana et al., 2005) has indicated that mRNA expression of ameloblastin and amelogenin in mouse molars is first observed in pre-ameloblasts at the tip of the cusp at postnatal day 2 for ameloblastin and day 3 for amelogenin (the day of birth was considered as postnatal day 1) and that expression of both proteins was seen until amelogenin expression terminated in maturation-stage ameloblasts at postnatal day 10. In our present study we used samples up to postnatal day 8 to ensure that both amelogenin and ameloblastin will be present (**Figures 3A–D**). The present study showed that secretion of amelogenin and ameloblastin starts at the cuspal slopes of molars, as seen on postnatal day 1 (**Figures 3A**, **4A**, **5A**). We observed that secretion continues until at least postnatal day 8 (**Figures 3C**, **4C**, **6A**). This is in agreement with the study of mRNA expression of ameloblastin (Torres-Quintana et al., 2005) but amelogenin was observed here earlier than the first detection of mRNA expression of amelogenin in the previous study. This difference could be explained by individual difference between mice and their strains.

Quantitative co-localization analysis is potentially a powerful tool for studying extracellular matrix protein interactions, as spatially related proteins have a high probability of interacting. Moreover, significantly more data can be generated while eliminating bias and errors of visual interpretation (Costes et al., 2004). In a recent report (Gallon et al., 2013) we have used confocal microscopy to successfully determine co-localization between amelogenin and enamelin in enamel extracellular matrix.

We utilized the Mander's co-localization coefficients M1 and M2 as these coefficients are not dependent upon the intensities of the signals and can compare signal intensities for different fluorophores when their signal intensities differ (Manders et al., 1993). These coefficients give a measure of the amount of fluorescence of the co-localizing objects of the image relative to the total fluorescence. By plotting the co-localization co-efficients M_{green} and M_{red} of amelogenin or ameloblastin against the regions of interest, patterns of co-localization were revealed and comparisons were made. The use of an antibody against ameloblastin may allow us to detect the full-length protein as well as its proteolytic products containing that epitopes. Such products may include the equivalent to the reported rat ameloblastin proteolytic products (Uchida et al., 1997, 1998; Brookes et al., 2001). While the pattern of proteolysis of porcine ameloblastin is well documented (Chun et al., 2010), information regarding the rodent proteolytic pattern is limited. Here the 62, 40, 33, and 29 kDa products were detected by Western blot analysis of protein extracted from 9-day-old mice (**Figure 2**, lane 3). We followed the migration pattern of proteolytic products from the ameloblastin C-terminal in the ECM at day 8. It is notable that signals for amelogenin and/or ameloblastin were not so prominent within the ameloblasts. Following their secretion and processing by MMP-20, epitopes on both amelogenin and ameloblastin can be more available for interaction with the antibody in the ECM.

As seen in **Figure 7A**, the proportion of co-localization between ameloblastin and amelogenin varies with the postnatal age of the mouse. At early stages, when enamel is initially developing, the proteins co-localize with each other to a large degree

and in the same proportions (**Figure 5F**). Since we observe that the contribution of each antigen to the areas with co-localization is high, i.e., ameloblastin and amelogenin strongly overlap with each other at day 1, we interpret the data to suggest that at initial stages of enamel development they co-assemble. With enamel maturation this pattern changes. For a time, on day 8, the proportion of co-localizing ameloblastin remain greater than the proportion of co-localizing amelogenin, indicating there is now more "free" or non-co-localizing amelogenin than "free" ameloblastin. This also indicates that there is more amelogenin present in the extracellular matrix than ameloblastin at later stages, which is verified by plotting the intensity ratio with age (**Figure 7B**). These findings are in accordance with the published report that the C-terminal polypeptides of ameloblastin are successively cleaved into smaller peptides and lost from the extracellular matrix (Uchida et al., 1997, 1998) at maturation stage. Co-localization of amelogenin proteolytic products and ameloblastin N-terminal is possible and it is a subject of ongoing investigation (Mazumder et al., in preparation).

ACKNOWLEDGMENTS

The study was funded by NIH-NIDCR grants DE-020099 and DE-013414. We thank Prof. Malcolm Snead for kindly providing us antibody against amelogenin, Prof Margarita Zeichner-David for providing the Schneider 2 cells and Mrs. Lisha Chen for technical assistance.

REFERENCES

Bartlett, J. D., Ganss, B., Goldberg, M., Moradian-Oldak, J., Paine, M. L., Snead, M. L., et al. (2006). Protein-protein interactions of the developing enamel matrix. *Curr. Top. Dev. Biol.* 74, 57–115. doi: 10.1016/S0070-2153(06)74003-0

Bartlett, J. D., and Simmer, J. P. (1999). Proteinases in developing dental enamel. *Crit. Rev. Oral Biol. Med.* 10, 425–441. doi: 10.1177/10454411990100040101

Bouropoulos, N., and Moradian-Oldak, J. (2004). Induction of apatite by the cooperative effect of amelogenin and the 32-kDa enamelin. *J. Dent. Res.* 83, 278–282. doi: 10.1177/154405910408300402

Brookes, S. J., Kirkham, J., Shore, R. C., Wood, S. R., Slaby, I., and Robinson, C. (2001). Amelin extracellular processing and aggregation during rat incisor amelogenesis. *Arch. Oral Biol.* 46, 201–208. doi: 10.1016/S0003-9969(00)00121-7

Chun, Y. H. P., Yamakoshi, Y., Yamakoshi, F., Fukae, M., Hu, J. C. C., Bartlett, J. D., et al. (2010). Cleavage Site Specificity of MMP-20 for Secretory-stage Ameloblastin. *J. Dent. Res.* 89, 785–790. doi: 10.1177/0022034510366903

Costes, S. V., Daelemans, D., Cho, E. H., Dobbin, Z., Pavlakis, G., and Lockett, S. (2004). Automatic and quantitative measurement of protein-protein colocalization in live cells. *Biophys. J.* 86, 3993–4003. doi: 10.1529/biophysj.103.038422

Fan, D., Iijima, M., Bromley, K. M., Yang, X., Mathew, S., and Moradian-Oldak, J. (2011). The Cooperation of enamelin and amelogenin in controlling octacalcium phosphate crystal morphology. *Cells Tissues Organs* 194, 194–198. doi: 10.1159/000324208

Fan, D., Lakshminarayanan, R., and Moradian-Oldak, J. (2008). The 32 kDa enamelin undergoes conformational transitions upon calcium binding. *J. Struct. Biol.* 163, 109–115. doi: 10.1016/j.jsb.2008.04.007

Fukumoto, S., Kiba, T., Hall, B., Iehara, N., Nakamura, T., Longenecker, G., et al. (2004). Ameloblastin is a cell adhesion molecule required for maintaining the differentiation state of ameloblasts. *J. Cell Biol.* 167, 973–983. doi: 10.1083/jcb.200409077

Gallon, V., Chen, L., Yang, X., and Moradian-Oldak, J. (2013). Localization and quantitative co-localization of enamelin with amelogenin. *J. Struct. Biol.* 183, 239–249. doi: 10.1016/j.jsb.2013.03.014

Hatakeyama, J., Fukumoto, S., Nakamura, T., Haruyama, N., Suzuki, S., Hatakeyama, Y., et al. (2009). Synergistic roles of amelogenin and ameloblastin. *J. Dent. Res.* 88, 318–322. doi: 10.1177/0022034509334749

Hu, C. C., Bartlett, J. D., Zhang, C. H., Qian, Q., Ryu, O. H., and Simmer, J. P. (1996). Cloning, cDNA sequence, and alternative splicing of porcine amelogenin mRNAs. *J. Dent. Res.* 75, 1735–1741. doi: 10.1177/00220345960750100501

Hu, C. C., Fukae, M., Uchida, T., Qian, Q., Zhang, C. H., Ryu, O. H., et al. (1997). Sheathlin: cloning, cDNA/polypeptide sequences, and immunolocalization of porcine enamel sheath proteins. *J. Dent. Res.* 76, 648–657. doi: 10.1177/00220345970760020501

Hu, J. C. C., Sun, X. L., Zhang, C. H., and Simmer, J. P. (2001a). A comparison of enamelin and amelogenin expression in developing mouse molars. *Eur. J. Oral Sci.* 109, 125–132. doi: 10.1034/j.1600-0722.2001.00998.x

Hu, J. C. C., and Yamakoshi, Y. (2003). Enamelin and autosomal-dominant amelogenesis imperfecta. *Crit. Rev. Oral Biol. Med.* 14, 387–398. doi: 10.1177/154411130301400602

Hu, J. C. C., Yamakoshi, Y., Yamakoshi, F., Krebsbach, P. H., and Simmer, J. P. (2005). Proteomics and genetics of dental enamel. *Cells Tissues Organs* 181, 219–231. doi: 10.1159/000091383

Hu, J. C. C., Zhang, C. H., Yang, Y., Karrman-Mardh, C., Forsman-Semb, K., and Simmer, J. P. (2001b). Cloning and characterization of the mouse and human enamelin genes. *J. Dent. Res.* 80, 898–902. doi: 10.1177/00220345010800031001

Iijima, M., Fan, D., Bromley, K. M., Sun, Z., and Moradian-Oldak, J. (2010). Tooth enamel proteins enamelin and amelogenin cooperate to regulate the growth morphology of octacalcium phosphate crystals. *Crystal Growth Des.* 10, 4815–4822. doi: 10.1021/cg100696r

Kawasaki, K., and Weiss, K. M. (2003). Mineralized tissue and vertebrate evolution: the secretory calcium-binding phosphoprotein gene cluster. *Proc. Natl. Acad. Sci. U.S.A.* 100, 4060–4065. doi: 10.1073/pnas.0638023100

Kobayashi, K., Yamakoshi, Y., Hu, J. C. C., Gomi, K., Arai, T., Fukae, M., et al. (2007). Splicing determines the glycosylation state of ameloblastin. *J. Dent. Res.* 86, 962–967. doi: 10.1177/154405910708601009

Krebsbach, P. H., Lee, S. K., Matsuki, Y., Kozak, C. A., Yamada, R. M., and Yamada, Y. (1996). Full-length sequence, localization, and chromosomal mapping of ameloblastin - a novel tooth-specific gene. *J. Biol. Chem.* 271, 4431–4435. doi: 10.1074/jbc.271.8.4431

Laemmli, U. K. (1970). Cleavage of structural proteins during assembly of head of bacteriophage-T4. *Nature* 227, 680–685. doi: 10.1038/227680a0

Lakshminarayanan, R., Bromley, K. M., Lei, Y.-P., Snead, M. L., and Moradian-Oldak, J. (2010). Perturbed amelogenin secondary structure leads to uncontrolled aggregation in amelogenesis imperfecta mutant proteins. *J. Biol. Chem.* 285, 40593–40603. doi: 10.1074/jbc.M110.131136

Lakshminarayanan, R., Fan, D., Du, C., and Moradian-Oldak, J. (2007). The role of secondary structure in the entropically driven amelogenin self-assembly. *Biophys. J.* 93, 3664–3674. doi: 10.1529/biophysj.107.113936

Lee, S. K., Krebsbach, P. H., Matsuki, Y., Nanci, A., Yamada, K. M., and Yamada, Y. (1996). Ameloblastin expression in rat incisors and human tooth germs. *Int. J. Dev. Biol.* 40, 1141–1150.

Lobley, A., Whitmore, L., and Wallace, B. A. (2002). DICHROWEB: an interactive website for the analysis of protein secondary structure from circular dichroism spectra. *Bioinformatics* 18, 211–212. doi: 10.1093/bioinformatics/18.1.211

Manders, E. M. M., Verbeek, F. J., and Aten, J. A. (1993). Measurement of colocalization of objects in dual-color confocal images. *J. Microsc.* 169, 375–382. doi: 10.1111/j.1365-2818.1993.tb03313.x

Moradian-Oldak, J., Paine, M. L., Lei, Y. P., Fincham, A. G., and Snead, M. L. (2000). Self-assembly properties of recombinant engineered amelogenin proteins analyzed by dynamic light scattering and atomic force microscopy. *J. Struct. Biol.* 131, 27–37. doi: 10.1006/jsbi.2000.4237

Murakami, C., Dohi, N., Fukae, M., Tanabe, T., Yamakoshi, Y., Wakida, K., et al. (1997). Immunochemical and immunohistochemical study of the 27- and 29-kDa calcium-binding proteins and related proteins in the porcine tooth germ. *Histochem. Cell Biol.* 107, 485–494. doi: 10.1007/s004180050136

Paine, M. L., White, S. N., Luo, W., Fong, H., Sarikaya, M., and Snead, M. L. (2001). Regulated gene expression dictates enamel structure and tooth function. *Matrix Biol.* 20, 273–292. doi: 10.1016/S0945-053X(01)00153-6

Ravindranath, H. H., Chen, L. S., Zeichner-David, M., Ishima, R., and Ravindranath, R. M. H. (2004). Interaction between the enamel matrix proteins

amelogenin and ameloblastin. *Biochem. Biophys. Res. Commun.* 323, 1075–1083. doi: 10.1016/j.bbrc.2004.08.207

Ravindranath, R. M. H., Devarajan, A., and Uchida, T. (2007). Spatiotemporal expression of ameloblastin isoforms during murine tooth development. *J. Biol. Chem.* 282, 36370–36376. doi: 10.1074/jbc.M704731200

Ryu, O. H., Fincham, A. G., Hu, C. C., Zhang, C., Qian, Q., Bartlett, J. D., et al. (1999). Characterization of recombinant pig enamelysin activity and cleavage of recombinant pig and mouse amelogenins. *J. Dent. Res.* 78, 743–750. doi: 10.1177/00220345990780030601

Simmer, J. P., Lau, E. C., Hu, C. C., Aoba, T., Lacey, M., Nelson, D., et al. (1994). Isolation and characterization of a mouse amelogenin expressed in *escherichia coli*. *Calcif. Tissue Int.* 54, 312–319. doi: 10.1007/BF00295956

Smith, C. E., Wazen, R., Hu, Y. Y., Zalzal, S. F., Nanci, A., Simmer, J. P., et al. (2009). Consequences for enamel development and mineralization resulting from loss of function of ameloblastin or enamelin. *Eur. J. Oral Sci.* 117, 485–497. doi: 10.1111/j.1600-0722.2009.00666.x

Snead, M. L., Lau, E. C., Zeichner-David, M., Fincham, A. G., Woo, S. L. C., and Slavkin, H. C. (1985). DNA-sequence for cloned cDNA for murine amelogenin reveal the amino-acid sequence for enamel-specific protein. *Biochem. Biophys. Res. Commun.* 129, 812–818. doi: 10.1016/0006-291X(85)91964-3

Sreerama, N., Venyaminov, S. Y., and Woody, R. W. (1999). Estimation of the number of alpha-helical and beta-strand segments in proteins using circular dichroism spectroscopy. *Protein Sci.* 8, 370–380. doi: 10.1110/ps.8.2.370

Tamburstuen, M. V., Reppe, S., Spahr, A., Sabetrasekh, R., Kvalheim, G., Slaby, I., et al. (2010). Ameloblastin promotes bone growth by enhancing proliferation of progenitor cells and by stimulating immunoregulators. *Eur. J. Oral Sci.* 118, 451–459. doi: 10.1111/j.1600-0722.2010.00760.x

Torres-Quintana, M. A., Gaete, M., Hernandez, M., Farias, M., and Lobos, N. (2005). Ameloblastin and amelogenin expression in postnatal developing mouse molars. *J. Dent. Res.* 47, 27–34. doi: 10.2334/josnusd.47.27

Uchida, T., Fukae, M., Tanabe, T., Yamakoshi, Y., Satoda, T., Murakami, C., et al. (1995). Immunochemical and immunocytochemical study of a 15-kDa non-amelogenin and related proteins in the porcine immature enamel - proposal of a new group of enamel proteins sheath proteins. *Biomed. Res.* 16, 131–140.

Uchida, T., Murakami, C., Dohi, N., Wakida, K., Satoda, T., and Takahashi, O. (1997). Synthesis, secretion, degradation, and fate of ameloblastin during the matrix formation stage of the rat incisor as shown by immunocytochemistry and immunochemistry using region-specific antibodies. *J. Histochem. Cytochem.* 45, 1329–1340. doi: 10.1177/002215549704501002

Uchida, T., Murakami, C., Wakida, K., Dohi, N., Iwai, Y., Simmer, J. P., et al. (1998). Sheath proteins: Synthesis, secretion, degradation and fate in forming enamel. *Eur. J. Oral Sci.* 106, 308–314.

Wald, T., Bednarova, L., Osicka, R., Pachl, P., Sulc, M., Lyngstadaas, S. P., et al. (2011). Biophysical characterization of recombinant human ameloblastin. *Eur. J. Oral Sci.* 119, 261–269. doi: 10.1111/j.1600-0722.2011.00913.x

Wald, T., Osickova, A., Sulc, M., Benada, O., Semeradtova, A., Rezabkova, L., et al. (2013). Intrinsically disordered enamel matrix protein ameloblastin forms ribbon-like supramolecular structures via an N-terminal segment encoded by exon 5. *J. Biol. Chem.* 288, 22333–22345. doi: 10.1074/jbc.M113.456012

Wazen, R. M., Moffatt, P., Zalzal, S. F., Yamada, Y., and Nanci, A. (2009). A mouse model expressing a truncated form of ameloblastin exhibits dental and junctional epithelium defects. *Matrix Biol.* 28, 292–303. doi: 10.1016/j.matbio.2009.04.004

Whitmore, L., and Wallace, B. A. (2004). DICHROWEB, an online server for protein secondary structure analyses from circular dichroism spectroscopic data. *Nucleic Acids Res.* 32, W668–W673. doi: 10.1093/nar/gkh371

Yamakoshi, Y., Hu, J. C. C., Fukae, M., Tanabe, T., Oida, S., and Simmer, J. P. (2003). "Amelogenin and 32kDa enamelin protein-protein interactions," in *Biomineralization (BIOM2001): Formation, Diversity, Evolution and Application,* ed O. H. E. Kobayashi (Kanagawa: Tokai University Press), 338–342.

Yamakoshi, Y., Tanabe, T., Oida, S., Hu, C. C., Simmer, J. P., and Fukae, M. (2001). Calcium binding of enamel proteins and their derivatives with emphasis on the calcium-binding domain of porcine sheathlin. *Arch. Oral Biol.* 46, 1005–1014. doi: 10.1016/S0003-9969(01)00070-X

Yang, X., Fan, D., Mattew, S., and Moradian-Oldak, J. (2011). Amelogenin-enamelin association in phosphate-buffered saline. *Eur. J. Oral Sci.* 119, 351–356. doi: 10.1111/j.1600-0722.2011.00916.x

Zalzal, S. F., Smith, C. E., and Nanci, A. (2008). Ameloblastin and amelogenin share a common secretory pathway and are co-secreted during enamel formation. *Matrix Biol.* 27, 352–359. doi: 10.1016/j.matbio.2008.01.003

Zeichner-David, M., Chen, L. S., Hsu, Z. Y., Reyna, J., Caton, J., and Bringas, P. (2006). Amelogenin and ameloblastin show growth-factor like activity in periodontal ligament cells. *Eur. J. Oral Sci.* 114, 244–253. doi: 10.1111/j.1600-0722.2006.00322.x

Conflict of Interest Statement: The authors declare that the research was conducted in the absence of any commercial or financial relationships that could be construed as a potential conflict of interest.

Received: 22 May 2014; paper pending published: 12 June 2014; accepted: 07 July 2014; published online: 25 July 2014.

Citation: Mazumder P, Prajapati S, Lokappa SB, Gallon V and Moradian-Oldak J (2014) Analysis of co-assembly and co-localization of ameloblastin and amelogenin. Front. Physiol. ***5****:274. doi: 10.3389/fphys.2014.00274*

This article was submitted to Craniofacial Biology, a section of the journal Frontiers in Physiology.

frontiers in
PHYSIOLOGY

REVIEW ARTICLE
published: 10 September 2014
doi: 10.3389/fphys.2014.00339

Role of mineralization inhibitors in the regulation of hard tissue biomineralization: relevance to initial enamel formation and maturation

Henry C. Margolis[1,2]*, Seo-Young Kwak[1,2] and Hajime Yamazaki[1,2]

[1] *Department of Applied Oral Sciences, Center for Biomineralization, The Forsyth Institute, Cambridge, MA, USA*
[2] *Department of Developmental Biology, Harvard School of Dental Medicine, Boston, MA, USA*

Edited by:
Bernhard Ganss, University of Toronto, Canada

Reviewed by:
Yuji Mishina, University of Michigan, USA
Peter Proff, Regensburg University, Germany

****Correspondence:***
Henry C. Margolis, Department of Applied Oral Sciences, Center for Biomineralization, The Forsyth Institute, 245 First Street, Cambridge, MA 02142, USA
e-mail: hmargolis@forsyth.org

Vertebrate mineralized tissues, i.e., enamel, dentin, cementum, and bone, have unique hierarchical structures and chemical compositions. Although these tissues are similarly comprised of a crystalline calcium apatite mineral phase and a protein component, they differ with respect to crystal size and shape, level and distribution of trace mineral ions, the nature of the proteins present, and their relative proportions of mineral and protein components. Despite apparent differences, mineralized tissues are similarly derived by highly concerted extracellular processes involving matrix proteins, proteases, and mineral ion fluxes that collectively regulate the nucleation, growth and organization of forming mineral crystals. *Nature*, however, provides multiple ways to control the onset, rate, location, and organization of mineral deposits in developing mineralized tissues. Although our knowledge is quite limited in some of these areas, recent evidence suggests that hard tissue formation is, in part, controlled through the regulation of specific molecules that inhibit the mineralization process. This paper addresses the role of mineralization inhibitors in the regulation of biological mineralization with emphasis on the relevance of current findings to the process of amelogenesis. Mineralization inhibitors can also serve to maintain driving forces for calcium phosphate precipitation and prevent unwanted mineralization. Recent evidence shows that native phosphorylated amelogenins have the capacity to prevent mineralization through the stabilization of an amorphous calcium phosphate precursor phase, as observed *in vitro* and in developing teeth. Based on present findings, the authors propose that the transformation of initially formed amorphous mineral deposits to enamel crystals is an active process associated with the enzymatic processing of amelogenins. Such processing may serve to control both initial enamel crystal formation and subsequent maturation.

Keywords: amorphous calcium phosphate, biomineralization, dental enamel, inhibitors, mineral phase transformation

INTRODUCTION

Biomineralization is the process by a wide variety of living organisms, including mollusks, sponges and unicellular diatoms, for example, produce functional mineralized tissues (Mann, 2001). Vertebrate mineralized tissues, like dental enamel, dentin, cementum, and bone, fulfill specialized functions that reflect differences in their hierarchical organization and composition (Weiner, 1986). Although each of these tissues is comprised of a crystalline calcium apatite mineral phase and a protein component, they differ with respect to overall structure, crystal size and shape, level and distribution of trace mineral ions, the nature of the proteins present, and the relative proportions of mineral and protein components. Differences in structural organization and composition give rise to mineralized tissues with different physical and mechanical properties that are well-suited for their intended biological purpose (Birchall, 1989; Currey, 1999).

Although the mechanisms by which these mineralized tissues form are not fully understood, it is apparent that the unique structure of each mineralized tissue, including dental enamel, is the result of highly concerted cell and extracellular processes that regulate the on-set, growth rate, shape, location and arrangement of forming mineral crystals (Weiner, 1986). Evidence also suggests that critical aspects of hard tissue formation are controlled, in part, through the regulation of specific molecules that inhibit mineralization. This paper addresses the role of mineralization inhibitors in the regulation of biological mineralization and the potential relevance of such mechanisms in the process of dental enamel formation (amelogenesis).

FUNDAMENTAL ASPECTS OF VERTEBRATE MINERALIZED TISSUE FORMATION

EXTRACELLULAR PROTEIN MATRIX AND MINERALIZED TISSUE COMPOSITION

Biominerals are formed utilizing similar fundamental strategies, although there are unique differences that distinguish one tissue from another, especially dental enamel. Enamel, dentin and bone

are each derived from specialized cells; ameloblasts, odontoblasts and osteoblasts, respectively. These cells secrete an extracellular protein matrix that is predominantly comprised of a hydrophobic protein and smaller amounts of acidic hydrophilic molecules. In bone and dentin, the matrix is mostly collagen, while the major enamel matrix component (>90%) is amelogenin. It has been proposed that biomineralization is generally regulated through interactions between hydrophobic components, which provide a skeletal or space-filling structure (e.g., collagen in bone and dentin), and hydrophilic (acidic) molecules (e.g., phosphophoryn in dentin Veis et al., 1991; He et al., 2005) that regulate crystal nucleation and growth (Weiner, 1986; Addadi and Weiner, 1992). Considerable evidence shows that a highly-ordered preassembled collagen matrix serves as a template to guide subsequent mineralization, as we have previously discussed (Margolis et al., 2006). The initial collagenous matrix is mineral free and undergoes a series changes in structure and composition prior to mineralization (Weinstock and Leblond, 1973; Septier et al., 1998; Beniash et al., 2000), resulting in the formation of tissues that are 40–50% mineral and ∼35% organic by volume (Nikiforuk, 1985). The protein matrix of forming enamel is similarly comprised of a predominant hydrophobic protein (amelogenin) and two key minor protein components enamelin (hydrophilic and acidic) and ameloblastin (amphiphilic and acidic). The observations that the amelogenin-null mouse (Gibson et al., 2001) exhibits a marked enamel phenotype and that enamel does not form in the absence of enamelin (Hu et al., 2008; Smith et al., 2009) or ameloblastin (Fukumoto et al., 2004; Smith et al., 2009; Wazen et al., 2009) are in agreement with the proposed general requirement for hydrophobic-hydrophilic molecular interactions in biomineral formation.

Despite similarities in the hydrophobic/hydrophilic composition of developing extracellular bone, dentine and enamel matrices that lead to the formation of a similar mineral phase (i.e., a carbonated hydroxyapatite), mature enamel and the mechanism of its formation differ from those of dentine and bone. First, long thin ribbons of enamel mineral begin to form almost immediately after ameloblasts lay down the enamel matrix (Nylen et al., 1963; Arsenault and Robinson, 1989; Smith, 1998), indicating that mineralization does not take place within a pre-assembled enamel matrix template, as in the case of collagen-based tissues. These long thin mineral ribbons extend hundred of microns to the full thickness of the enamel layer that is laid down during the secretory stage of amelogenesis, although the mineral component occupies only 10–20% of the enamel volume, with the remaining volume occupied by the enamel matrix and water (Robinson et al., 1988; Fukae, 2002). During the maturation stage of amelogenesis (Robinson and Kirkham, 1985), the extracellular enamel matrix is almost completely removed by resident proteases and the initially formed mineral ribbons grow in width and thickness to form a dense mineralized tissue that is >95% mineral by weight, with only 1–2 weight % of remaining protein and a small amount of water. Hence, there is an inverse relationship between the protein and mineral content during enamel development (Robinson et al., 1979), as illustrated in **Figure 1**. Unlike that seen in bone and dentin, the enamel matrix is transient and the resulting enamel tissue is almost fully mineralized. The transient nature of the enamel matrix is uncommon in biomineralization (Weiner, 1986).

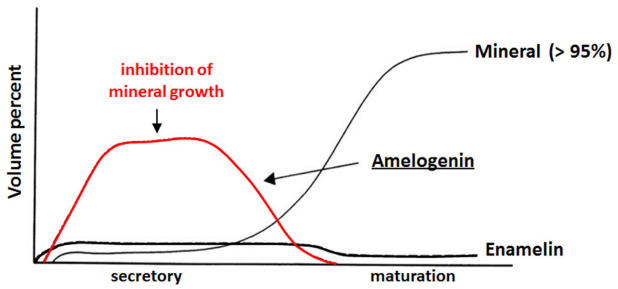

FIGURE 1 | Inverse relationship between protein and mineral content as a function of enamel development. Amelogenin is the major component (>90%) of the extracellular enamel matrix in the secretory stage. Adapted from a figure previously published by Mann (2001), with permission from Oxford University Press. This OUP material is for view only and cannot be reused.

CALCIUM PHOSPHATE FORMATION *IN VITRO* AND *IN VIVO*

The formation of a calcium phosphate mineral phase *in vitro* and *in vivo* requires a condition of supersaturation with respect to the forming phase. As shown in Equation 1 for hydroxyapatite (HA: $Ca_5OH(PO_4)_3$), a prototype for enamel, dentin and bone mineral, the degree of supersaturation (DS) can be defined as the ratio of the mean ionic activity product for a given mineral phase in solution to its thermodynamic solubility product constant (e.g., K_{SP-HA}) defined in the same manner, where "()" represent the activity of the enclosed ion [e.g., (Ca_f^{2+})]. The activity of an ion in solution is equal to the product of the concentration of the ion ($[x_i^Z]$) and an ion activity coefficient (a_i) that is a function of the ion size, charge, ionic strength and temperature. Such quantities can be calculated using ion-speciation software, as we have previously described (Moreno and Margolis, 1988). Supersaturation with respect to other calcium phosphate phases, such as octacalcium phosphate [OCP: $Ca_4H(PO_4)_3$] and dicalcium phosphate dihydrate (DCPD: $CaHPO_4{\cdot}2H_2O$), can be defined similarly as indicated in Equations (2) and (3), respectively. A minimum requirement for mineral formation *in vitro* or *in vivo* is the condition of supersaturation. As indicated by Equations 1–3, DS is a function of calcium, phosphate and hydrogen ion activities.

$$DS_{HA} = \left[\left(Ca_f^{2+}\right)^5\left(OH^-\right)\left(PO_4^{3-}\right)^3\right]^{1/9} \Big/ K_{SP-HA} \quad (1)$$

$$DS_{OCP} = \left[\left(Ca_f^{2+}\right)^4\left(H^+\right)\left(PO_4^{3-}\right)^3\right]^{1/8} \Big/ K_{SP-OCP} \quad (2)$$

$$DS_{DCPD} = \left[\left(Ca_f^{2+}\right)\left(HPO_4^{2-}\right)\right]^{1/2} \Big/ K_{SP-DCPD} \quad (3)$$

where, $(X_i^z) = a_i \times [X_i^z]$ and Ca_f^{2+} is *free* calcium.

Regarding the mineralization process, a given solution can be supersaturated with respect to more than one calcium phosphate phase at the same time. Due, in part, to kinetic factors

(for review, see Mann, 2001), however, the more soluble phase will form first and, through a series of *phase transformations*, convert to HA, which is the most thermodynamically stable calcium phosphate phase of the group. This phenomenon, called the *Ostwald-Lussac law of stages*, occurs in nature, as it does *in vitro* (Eanes, 2001). For example, it has been shown (Schroeder, 1969) that DCPD and OCP are the first mineral phases seen in forming dental calculus that subsequently convert to HA over time. Consistent with this observation and *Ostwald-Lussac law of stages*, at physiological pH (pH 7) and ionic strength (163 mM), HA has a relatively low solubility (expressed as the concentration of dissolved Ca^{2+}) of 0.11 mM, in comparison to OCP (1.42 mM) and DCPD (2.09 mM), as calculated (Moreno and Margolis, 1988). Such transformations may go through multiple phases before reaching the stable HA phase, depending on the free energy of activation (ΔG) associated with nucleation (n), growth (g), and phase transformation (t), as previously discussed and illustrated in **Figure 2** (Colfen and Mann, 2003).

Based on the discussion above, the role of *precursor* phases involved in HA and biomineral formation has received considerable attention. The calcium phosphate mineral phases discussed so far are crystalline in nature, as confirmed using spectroscopic (FT-IR, Raman) and diffraction (X-ray and electron diffraction) methods. However, it has been known for many years (for review, see Eanes, 2001) that amorphous calcium phosphate (ACP) is the first mineral phase to form upon mixing sufficiently high concentrations of calcium and phosphate. ACP is more soluble than the noted crystalline calcium phosphates and is the kinetically favored product (Meyer and Eanes, 1978), although it readily undergoes phase transformation to HA, as shown in **Figure 3**. The presence of ACP in vertebrate mineralized tissues (Posner and Betts, 1975) has been a topic of considerable debate (Termine and Posner, 1966; Boskey, 1997; Eanes, 2001; Weiner, 2006) because of its transient nature. However, recent evidence suggests that the transient nature of an amorphous mineral phase, that is, the formation of an amorphous mineral phase and its subsequent transformation to a crystalline solid, is a key element in biological mineral formation (Beniash et al., 1997; Weiner et al., 2005; Deshpande and Beniash, 2008; Kwak et al., 2009; Margolis and Beniash, 2010; Wiedemann-Bidlack et al., 2011). More recently, the importance of sequential steps involving ACP formation and transformation has been confirmed *in vitro* (Habraken et al., 2013), showing that the existence of pre-nucleation clusters that precede ACP formation lowers the energy barrier to nucleation and makes amorphous phases "accessible" under conditions that would favor the formation of more stable crystalline phases. Hence, it appears calcium phosphate formation *in vivo* and *in vitro* similarly proceed through a sequence of phase transformations, potentially involving: ACP → DCPD → OCP → HA. As will be discussed below, however, matrix molecules can dramatically influence the phase transformation process.

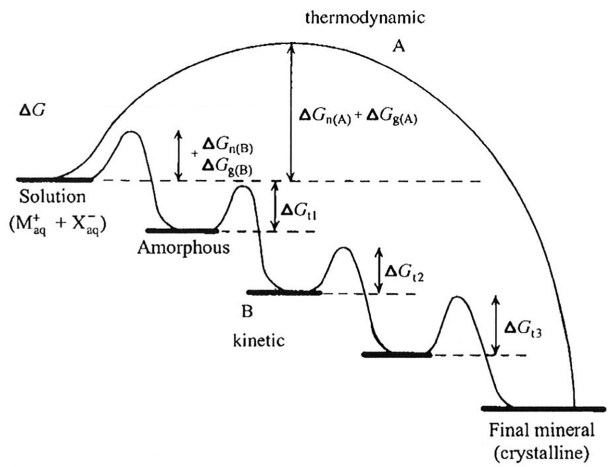

FIGURE 2 | Crystallization pathways under thermodynamic and kinetic control, illustrating that mineral formation may go through multiple phases (path B) before reaching the stable final crystalline product (e.g., HA), as discussed in the text, depending on the free energy of activation (ΔG) associated with nucleation (n), growth (g), and phase transformation (t). As shown, amorphous phases are frequently observed first under kinetically controlled conditions. This figure is from a publication (Colfen and Mann, 2003) in which this phenomenon is discussed in greater detail and is reproduced with permission. Copyright Wiley-VCH Verlag GmbH & Co. KGaA.

ROLE OF MINERALIZATION INHIBITORS IN BIOLOGICAL MINERALIZATION

STABILIZATION OF SUPERSATURATION *IN VIVO*

As illustrated in **Figure 3**, under conditions of relatively high supersaturation brought about by the rapid mixing of calcium and phosphate solutions, mineralization takes place spontaneously. This process involves the *homogeneous* nucleation and formation of precursor ACP nanoparticles, which subsequently transform to crystalline HA. In the absence of a buffer, this process causes a sharp decrease in pH due to the precipitation of a *basic* solid phase (**Figure 4**). In the presence of the full-length native amelogenin, P173, the solution pH does not drop and remains relatively constant for long periods of time, as illustrated in **Figure 4**, by preventing the bulk formation of HA crystals, as shown in **Figure 5** (Wiedemann-Bidlack et al., 2011). As can be seen in this TEM micrograph, P173 has the capacity to stabilize initially formed nanoparticles of ACP and prevent transformation to crystalline HA, as seen in the control (**Figure 3**). Of note, truncated native amelogenin, P148 that lacks the hydrophilic C-terminus was similarly found to be a potent stabilizer of ACP (Kwak et al., 2009). Hence, P173 and P148 are inhibitors of spontaneous HA crystal formation. In doing so, the supersaturation status of the experimental solution is also maintained, along with its inherent *stored* capacity to promote mineralization. Notably, native amelogenins like P173 and P148 contain a single phosphorylated site (serine-16) within the N-terminus (Margolis et al., 2006), as further discussed below.

The stabilization of biological fluids through the inhibition of HA crystal formation is well known and appears to fulfill biologically important functions. A prime example is human saliva that has been shown (Hay et al., 1982) to be supersaturated with respect to all known calcium phosphate phases. Evidence suggests that this condition of supersaturation is maintained by a family of salivary phosphoproteins, which have been shown to

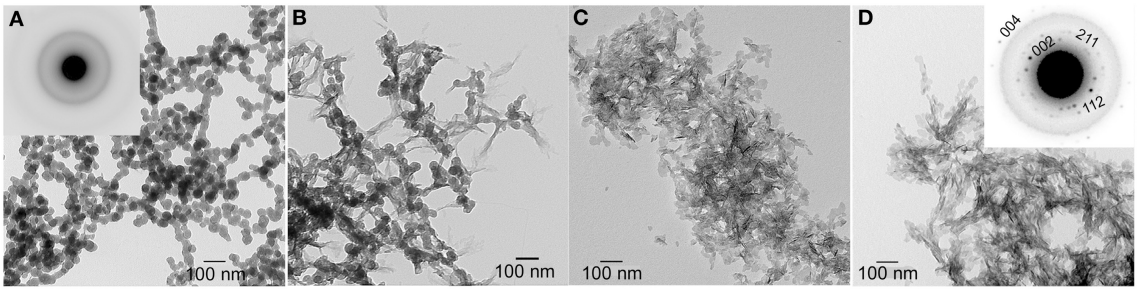

FIGURE 3 | TEM micrographs of calcium phosphate mineral products formed in the absence (control) of protein examined at selected times: 15 min (A), 45 min (B), 1–4 h (C), and 1 d (D). As shown at 15 min **(A)**, amorphous calcium phosphate (ACP) was initially formed based on the observed (inset) selected area electron diffraction (SAED) pattern. At 45 min, ACP phase transformation could be seen. After 1–4 h, randomly arranged plate-like apatitic crystals were found and confirmed by SAED analyses (**D**, inset). This image was reproduced from Kwak et al. (2009).

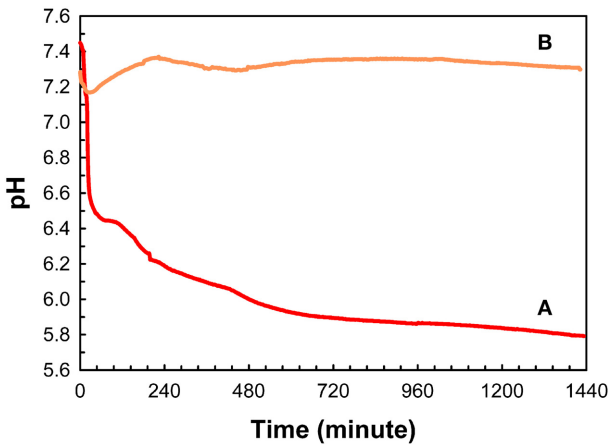

FIGURE 4 | Changes in pH as a function of time observed during mineralization experiments carried out in 60 μL sample volumes, in the absence (A) and presence of native full-length amelogenin, P173, at 2 mg/mL (B). This image was reproduced from Wiedemann-Bidlack et al. (2011).

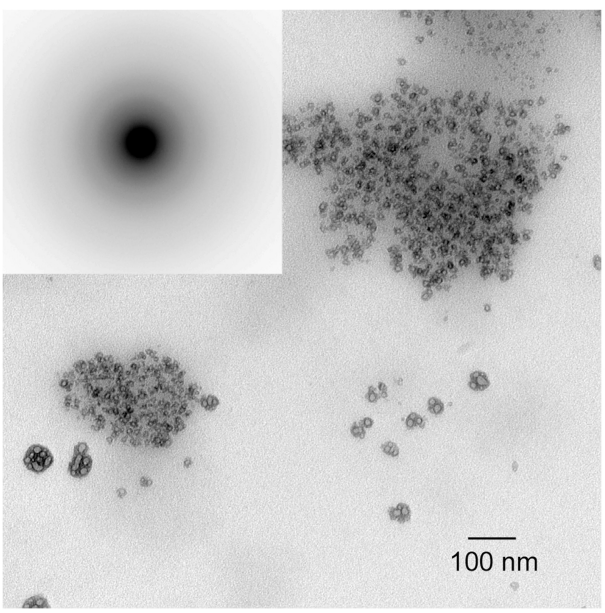

FIGURE 5 | TEM micrograph of calcium phosphate mineral products formed in the presence of native full-length amelogenin, P173, at 2 mg/mL. Only ACP was observed, even after 1 d, as confirmed by selected area electron diffraction (inset). This image was reproduced from Wiedemann-Bidlack et al. (2011).

be potent inhibitors of spontaneous calcium phosphate formation and seeded HA crystal growth *in vitro* (e.g., Hay et al., 1979). Under these conditions that persist in human saliva, calcium phosphate formation on hard and soft tissue surfaces in the oral cavity is prevented, as is the dissolution of tooth enamel in saliva. If saliva did not contain calcium and phosphate ions it would be *undersaturated* with respect to tooth enamel (i.e., with $DS_{EN} < 1$) and potentially promote the dissolution of enamel surfaces, albeit at a very slow rate. In fact, the observed spontaneous reversal of untreated early carious lesions (Koulourides et al., 1965; Dirks, 1966), where incipient lesions (i.e., white spots) take up mineral ions to become sound surfaces, can be attributed to the condition of saliva supersaturation. Hence, the prevention of unwanted mineral deposits in the oral cavity and the capacity of saliva to promote the repair (remineralization) of beginning enamel lesions is due to resident inhibitors of calcium phosphate formation that maintain saliva in its supersaturated state. Similarly, inhibitors of calcium oxalate formation have been identified in urine and are believed to play an important role in preventing the formation of kidney stones (e.g., Nene et al., 2013). Finally, it has been shown that spontaneous calcification of arteries and cartilage takes place in mice that lack the mineral binding matrix GLA protein, a known mineralization inhibitor. These latter observations, lead the authors of that study to conclude that the calcification of the extracellular matrix is a ubiquitous process that must be actively inhibited in soft tissues that do not normally mineralize (Luo et al., 1997).

REGULATION OF BIOMINERAL FORMATION

Mann (2001) summation that "*The chemical control of crystallization pathways that involve a sequence of kinetic inhibition and*

phase transformation can result in a high degree of selectivity in crystal structure and composition," is perhaps best illustrated in biology where numerous inhibitors of HA formation have been identified, including magnesium ion, carbonate, proteoglycans, polyphosphate and other phosphorylated molecules. In particular, inorganic pyrophosphate (PP_i) has been long recognized as a potent inhibitor of mineralization and as a potential regulator of biological mineralization. At micro-molar levels, PP_i inhibits the growth (Francis, 1969; Meyer and Nancollas, 1973; Meyer, 1984; Moreno et al., 1987) and dissolution (Fleisch et al., 1966; McGaughey and Stowell, 1977; McGaughey, 1983) of HA, as well as HA crystal formation from ACP (Termine et al., 1970; Robertson, 1973; Blumenthal et al., 1975). A study in our laboratory (Moreno et al., 1987) indicated that the inhibition of HA crystal growth results from PP_i adsorption to discrete growth sites on HA surfaces, in the same fashion that has been proposed to explain the inhibition of crystal growth by macromolecules (Moreno et al., 1979). Stabilization of ACP may similarly involve PP_i binding to ACP nanoparticles (Ofir et al., 2004).

Based on additional *in vitro* findings (Meyer, 1984) that suggest calcification cannot occur *in vivo* in the presence of physiological levels of PP_i, it was proposed (Meyer and Reddi, 1985) that pyrophosphatases regulate mineral deposition in bone and cartilage by hydrolyzing PP_i (to two molecules of orthophosphate) to eliminate its inhibitory activity. This overall concept has been supported by the elucidation (Ho et al., 2000) of the role of *progressive ankylosis* (*ank*) gene that encodes a transmembrane protein that appears to regulate calcification (and arthritis) by controlling both intracellular and extracellular levels of PP_i. Additional evidence has also been obtained showing that tissue non-specific alkaline phosphatase (TNAP) and plasma cell membrane glycoprotein-1 (PC-1) are key enzyme regulators of the extracellular PP_i concentrations required for controlled bone mineralization (Hessle et al., 2002). PC-1 is the major producer of the PP_i inhibitor, while TNAP can regulate the promotion of the onset of bone mineralization by hydrolyzing PP_i. Consistent with this idea, it has been demonstrated *in vitro* that upon the removal of PP_i from solution, either through adsorption or by HA surface-induced hydrolysis (Meyer, 1984; Litman and Margolis, unpublished findings), or by enzymatic degradation of PP_i, PP_i-stabilized calcium phosphate solutions rapidly form calcium phosphates.

With respect to amelogenesis, alkaline phosphatase (AP) has been found in secretory enamel, leading investigators to suggest that "dephosphorylation" of amelogenin (e.g., by AP) may play a role in regulating enamel formation (Brookes et al., 1998). Although this suggestion has not been fully substantiated *in vivo*, a study using cultured embryonic tooth germs showed that non-specific inhibition of phosphorylation by casein kinase impaired enamel formation (Torres-Quintana et al., 2000), lending support to the idea that phosphorylated enamel matrix proteins may play a role as mineralization inhibitors. More recently, it has been reported that TNAP is expressed by normal ameloblasts in a stage-specific manner, that is, at the point of transition from secretory to maturation stage (Yadav et al., 2012). In addition, AP was found to be highly expressed by the adjacent stratum intermedium of the developing enamel organ. Importantly, this latter study also showed that the TNAP knockout mice not only exhibited a phenotype similar to infantile hypophosphatasia, but also marked enamel defects, including reduced mineralization and disrupted rod and interrod structures. Hence, the reversal of mineralization inhibition, by PP_i hydrolysis or dephosphorylation, may represent a critical regulatory step in the formation of both developing bones and teeth.

Upon mineral growth, macromolecules found in bones and teeth can also effectively influence the *morphology* of calcium phosphate minerals through adsorption to specific crystal planes (e.g., Furedi-Milhofer et al., 1994; Flade et al., 2001). Of particular interest are observations that amelogenin (Iijima et al., 2001, 2002; Beniash et al., 2005), as well as other relevant biomineralization molecules like phosphophoryn (Burke et al., 2000) and glucose (Walsh et al., 1993), preferentially adsorb on (100), (010) faces of HA or OCP, suppressing their growth in a- and b-axis directions. Consequently, under these conditions, such crystals grow preferably along the long c-axis forming ribbon or needle-like structures resembling enamel crystals. As described in the next section, current evidence suggests that native amelogenins have the capacity to stabilize ACP, prevent unwanted crystallization, and ultimately guide the formation and organization of bundles of aligned enamel crystals during the secretory stage of enamel formation. The authors hypothesize, however, that the transformation of ACP to HA and the subsequent growth of HA crystals in thickness and width during maturation are the result of active regulation processes.

MECHANISM OF DENTAL ENAMEL FORMATION

Studies from our laboratory suggest that amelogenin mediates mineralization through a cooperative mechanism where mineralization and protein self-assembly occur simultaneously (Beniash et al., 2005). This conclusion is based on *in vitro* findings that show that the non-phosphorylated full-length recombinant mouse amelogenin, rM179, can guide the formation of well-aligned bundles of HA crystals *in vitro*, under experimental conditions designed to simultaneously induce amelogenin assembly and mineralization. Organized mineral formation was not observed when protein self-assembly was carried out prior to mineralization or when a truncated recombinant mouse amelogenin (rM166, lacking the hydrophilic C-terminus) was used. Similar results were subsequently obtained under cooperative assembly/mineralization conditions using recombinant full-length porcine amelogenin, rP172, which was also found to guide the formation of bundles of aligned HA crystals (Kwak et al., 2009). These latter experiments were monitored as a function of time to provide insight into the mechanism of amelogenin-mediated mineralization. These studies revealed that rP172 transiently stabilizes ACP nanoparticles (**Figure 6**), which were found to be significantly smaller than those seen in the control (**Figure 3**). As the reaction continued in the presence of rP172, an alignment of ACP nanoparticles was observed at ∼45 min. Arrays of needle-like crystals were then observed between 1–4 h. At 24 h, as shown, multiple bundles of well-aligned needle-like apatite crystals were seen that are similar to those found in the presence of rM179 (Beniash et al., 2005) and distinctly different

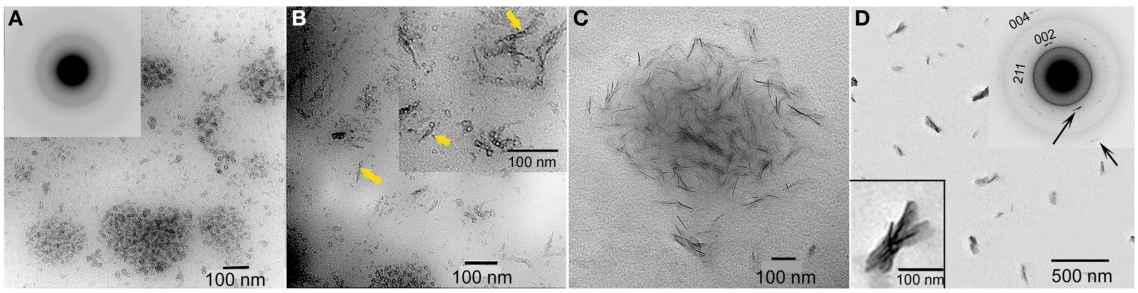

FIGURE 6 | TEM micrographs of calcium phosphate mineral products formed in the presence of 2 mg/ml recombinant full-length amelogenin, rP172, examined at selected times: 15 min (A), 45 min (B), 1–4 h (C), and 1 d (D). ACP particles seen at 15 min (**A**, inset) were found to align to form need-like particles (arrows) at 45 min **(B)**. After 1 d, based on selected area electron diffraction analyzes (**D**, inset), aligned bundles of needle-like apatitic crystals were formed. This image was reproduced from Kwak et al. (2009).

in comparison to the randomly arranged plate-like crystals found in the control (at 24 h, **Figure 3**). Truncated recombinant (non-phosphorylated) porcine amelogenin rP147 had relatively little effect on the mineralization process (Kwak et al., 2009), again indicating that the full-length amelogenin has a unique capacity to guide ordered mineralization. This unique capacity is attributed to the fact that full-length recombinant mouse (rM179) and porcine (rP172) amelogenin, as well as full-length native amelogenin (P173), undergo self-assembly to form hierarchical nanosphere (Fang et al., 2011, 2013) and chain-like (Wiedemann-Bidlack et al., 2007, 2011) structures, as a function of solution pH. Truncated amelogenins lacking the hydrophilic C-terminus do not form such organized structures. Notably, the single phosphate group in native amelogenins on serine-16 was found to have only a subtle influence on P173 assembly and structure, as determined by both conventional (Wiedemann-Bidlack et al., 2011) and cryo-TEM (Fang et al., 2013). However, small-angle X-ray scattering studies using phosphorylated and non-phosphorylated leucine-rich amelogenin peptides (LRAP, an alternative splice product that is comprised of the first 33 amino acids and the last 23 C-terminal amino acids of full-length (porcine) amelogenin) showed that phosphorylation of serine-16 had a significant effect on the folding of the peptide in solution (Le Norcy et al., 2011a). LRAP(+P) exhibited an unfolded structure, while LRAP(-P) exhibited a globular structure in solution. LRAP(+P), like P173, was also found to effectively stabilize ACP and inhibit HA formation *in vitro* (Le Norcy et al., 2011b). These influences on protein structure and folding may be of considerable functional importance, given the marked effect phosphorylation has on the capacity of native amelogenins to stabilize ACP and inhibit HA formation for extended periods of time, as further discussed below.

In recent years, two prominent theories of crystal growth—aptly named the classical and non-classical crystal growth theories, have received considerable attention, in part, through detailed investigations into the growth mechanisms of biominerals (Niederberger and Colfen, 2006). The classical mechanism for crystal growth is mineral ion mediated where mineral growth progresses through the successive accumulation of mineral ions to form a single crystal. The non-classical mechanism for crystal growth is mediated by initially formed nano-particles that subsequently assemble in an organized fashion to form what appear to be single crystals (so-called mesocrystals). Although it is often difficult to distinguish between these two mechanisms, early studies (Robinson et al., 1981; Robinson, 2007) have suggested that, during amelogenesis, enamel crystals form through the assembly of small amorphous mineral particles, although the amorphous nature of these particles was not verified experimentally. Since this initial proposal, however, data have been obtained that support the presence of ACP in the developing enamel matrix (Diekwisch, 1998; Bodier-Houlle et al., 2000). In a more recent study (Beniash et al., 2009), multiple independent techniques were used to carefully characterize the phase of the long thin parallel arrays of mineral deposits (e.g., as seen in **Figure 7**) that form during the secretory stage of amelogenesis that begin near the DEJ and extend to the enamel surface. Newly deposited mouse enamel, that is, in the outer enamel layers closer to the enamel surface and the ameloblast layer was found to be ACP, while older enamel, found in inner layers of enamel closer to DEJ contained apatitic crystals. Of particular importance, the newly deposited amorphous mineral and the older crystalline deposits had the same ribbon-like shape and organization in parallel arrays. These findings suggest that enamel mineral morphology and organization are established by the enamel matrix prior to the transformation of ACP to HA-like enamel crystals. These findings are also consistent with a proposed hypothesis that initial enamel crystals form from the assembly and fusion of amorphous calcium phosphate particles (e.g., Robinson, 2007). Transient amorphous mineral phases (i.e., ACP and amorphous calcium carbonate) have also been observed to be associated with a number of other biomineralization systems (Lowenstam and Weiner, 1985, 1989; Beniash et al., 1997; Wu et al., 1997; Levi-Kalisman et al., 2000; Aizenberg et al., 2002), including bone (Kim et al., 2005; Crane et al., 2006; Mahamid et al., 2008), leading to the proposal that the transformation of amorphous phases to crystalline materials is an important aspect of biological mineralization (Beniash et al., 1997; Weiner et al., 2005). Other molecules believed to be associated with the regulation of biomineralization, like highly phosphorylated osteopontin from milk (Gericke et al., 2005) and the N-terminal domain of dentin matrix protein 1 (Gajjeraman et al., 2007) have been shown to stabilize ACP.

POTENTIAL ROLE OF MINERALIZATION INHIBITORS IN DENTAL ENAMEL FORMATION

Based on current evidence, inhibition of mineralization by native amelogenins and its reversal *in vivo* may play critical roles in enamel formation. This conclusion is supported by data showing (1) an inverse relationship between protein and mineral content (**Figure 1**), and the notably high protein and low mineral content (10–20% by volume) of secretory stage enamel; (2) the capacity of native amelogenins to stabilize ACP and inhibit mineralization *in vitro*; (3) the apparent requirement for both proteases [i.e., matrix metalloproteinase 20 (MMP20) during the secretory stage Caterina et al., 2002 and kallikrein 4 (Klk4) during transition/maturation Hu et al., 2000; Simmer et al., 2009] and phosphatases (i.e., AP, as discussed above) for proper enamel formation; and (4) the rapid onset of mineral growth coinciding with loss of protein (**Figure 1**). These collective data suggest that during the secretory stage of enamel formation, enamel matrix proteins selectively guide ACP nanoparticle organization and transformation to thin ribbons of co-aligned HA crystals, while at the *same time* preventing unwanted bulk mineralization. Support for this scenario was recently provided by *in vitro* findings showing that under the proper kinetic conditions, controlled by variations in protein concentration, significantly lower concentrations of P173 can guide the transformation of initially stabilized ACP nanoparticles to ordered bundles of HA crystals that have similar morphology to initially formed enamel crystals (Kwak et al., 2014). In contrast to that seen with P173, however, P148 lacked the capacity to regulate ordered mineralization at reduced protein concentrations, although mineralization did take place. At higher concentrations, again, both P173 and P148 are potent stabilizers of ACP. Hence, upon its secretion, the parent phosphorylated full-length amelogenin P173 can initially prevent premature mineralization of HA crystals in forming enamel. However, full-length amelogenin undergoes proteolytic processing soon after secretion, resulting in a significant *decrease* in its concentration. In developing porcine enamel, the P173 content of secretory enamel was found to be only 7.4% of total amelogenin, a reduction in P173 by more than 90% (Wen et al., 1999). P173 was also found to be exclusively associated with newly formed enamel mineral (Uchida et al., 1991). In contrast to P173, the P148 content of the enamel matrix *increases* and becomes the predominant amelogenin cleavage product at 49.5% of total amelogenin (Wen et al., 1999). Based on these combined *in vitro* and *in vivo* findings, the authors propose that the onset of enamel crystal formation is regulated by a marked reduction (>10-fold) in P173 concentration to attain a critical lower level that has the potential to organize forming mineral deposits into oriented bundles of elongated HA crystals, as illustrated in a proposed model presented in **Figure 8**. At the same time, substantially higher concentrations of P148 (∼ 6–7 times higher than P173) that accumulate in the developing (porcine) enamel matrix serve an important role by preventing uncontrolled mineralization throughout the secretory stage of amelogenesis where the mineral volume is only 10–20% (Robinson et al., 1988; Fukae, 2002).

The noted proteolytic processing of amelogenin during the secretory stage of amelogenesis has been primarily attributed to MMP20 that is exclusively expressed during this initial stage of enamel formation. MMP20 has also been shown to be essential for proper enamel formation (Caterina et al., 2002). In its absence, the enamel layer is about one-half the normal thickness

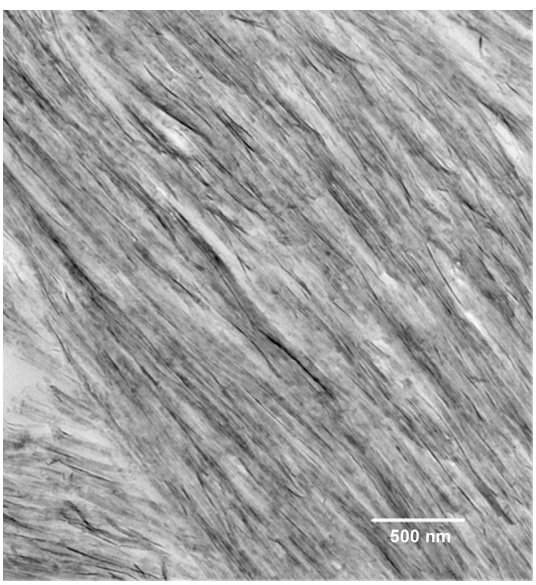

FIGURE 7 | Transmission electron microscopy micrograph of secretory stage mouse enamel showing parallel arrays of long thin ribbons of mineral.

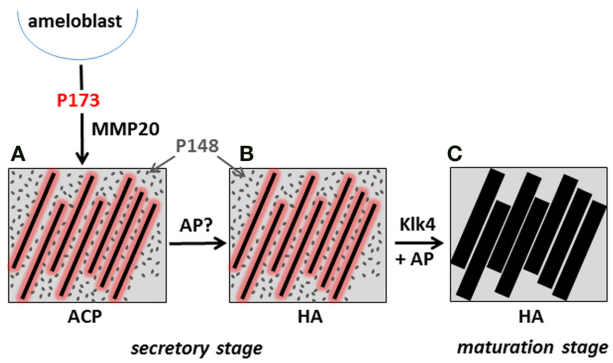

FIGURE 8 | Proposed model illustrating the potential role of P173 and P148 in dental enamel formation. The onset of the initial formation of linear arrays of ACP **(A)** during the secretory stage is brought about by the marked reduction of P173 by MMP20, reversing its inhibitory effect. Limited quantities of P173 (red) stabilize linear ACP arrays through direct interaction, as illustrated. The predominant P148 (gray) cleavage product plays a key role in preventing unwanted mineralization, while maintaining conditions of supersaturation. The linear arrays of ACP subsequently transform to apatitic crystals (Beniash et al., 2009) during the secretory stage **(B)**. During maturation, inhibition of bulk mineralization provided by P148 is eliminated by Klk4 proteolysis, along with small amounts of adsorbed P173 growth inhibitor, to initiate the lateral growth of initial enamel ribbons **(C)**. As noted in the text, AP may also play an essential role in regulating mineral formation in the secretory stage and mineral growth during the maturation stage by catalyzing amelogenin dephosphorylation.

and the decussating prism pattern of normal enamel is substantially disrupted. These latter findings verify that proteolytic processing of full-length amelogenin is required for proper enamel formation, consistent with our proposed model, that is based on the capacity of reduced levels of P173 to guide ordered HA crystal formation, while accumulating P148 levels maintain mineralization driving forces by preventing unwanted bulk mineralization. During maturation, Klk4 is predominantly expressed and is believed to be responsible for removing almost all of the remaining enamel matrix to allow the initial enamel crystals to grow in width and thickness (Hu et al., 2000). Hence, as illustrated in the presented model, we propose that the onset of mineralization during the secretory stage is brought about by the marked reduction of P173 content by MMP20, reversing its inhibitory effect. During maturation, inhibition of bulk mineralization provided by P148 is eliminated by Klk4 proteolysis, along with small amounts of adsorbed P173 growth inhibitor, to initiate the lateral growth of the secretory stage enamel ribbons. As noted above, AP may also play an essential role in regulating mineral formation in the secretory stage and mineral growth during the maturation stage by catalyzing amelogenin dephosphorylation and removing the noted mineralization inhibitory activity found to be associated with native amelogenins. The timing of the expression of key regulators of biomineralization during enamel formation is, therefore, of critical importance (e.g., Smith, 1998; Simmer et al., 2009). Additional studies addressing the potential roles of amelogenin proteolysis and de-phosphorylation in regulating initial enamel mineral formation and maturation are currently underway in our laboratory.

CONCLUSIONS

Mineralization inhibitors can play critical roles in regulating mineralized tissue formation, stability, and regeneration *in vivo*. With respect to dental enamel formation, mineralization events triggered by the proteolysis and/or de-phosphorylation of full-length native amelogenin during the secretory stage of amelogenesis may play an essential role in regulating enamel mineral formation and its hierarchical structure, while predominant amelogenin degradation products, like P148, serve to prevent uncontrolled mineral formation. During maturation, residual inhibition is removed via additional matrix processing, allowing initial enamel crystals to expand to form the highly dense enamel mineral layer.

ACKNOWLEDGMENT

This work is supported by NIDCR grant R01-DE023091 (Henry C. Margolis).

REFERENCES

Addadi, L., and Weiner, S. (1992). Control and design principles in biological mineralization. *Angew. Chem. Int. Ed.* 31, 153–169. doi: 10.1002/anie.199201531

Aizenberg, J., Lambert, G., Weiner, S., and Addadi, L. (2002). Factors involved in the formation of amorphous and crystalline calcium carbonate: a study of an ascidian skeleton. *J. Am. Chem. Soc.* 124, 32–39. doi: 10.1021/ja016990l

Arsenault, A. L., and Robinson, B. W. (1989). The Dentino-enamel junction: a structural and microanalytical study of early mineralization. *Calcif. Tissue Int.* 45, 111–121. doi: 10.1007/BF02561410

Beniash, E., Aizenberg, J., Addadi, L., and Weiner, S. (1997). Amorphous calcium carbonate transforms into calcite during sea urchin larval spicule growth. *Proc Biol Sci.* 264, 461–465.

Beniash, E., Metzler, R. A., Lam, R. S. K., and Gilbert, P. (2009). Transient amorphous calcium phosphate in forming enamel. *J. Struct. Biol.* 167, 95–95. doi: 10.1016/j.jsb.2009.04.002

Beniash, E., Simmer, J. P., and Margolis, H. C. (2005). The effect of recombinant mouse amelogenins on the formation and organization of hydroxyapatite crystals *in vitro*. *J. Struct. Biol.* 149, 182–190. doi: 10.1016/j.jsb.2004.11.001

Beniash, E., Traub, W., Veis, A., and Weiner, S. (2000). A transmission electron microscope study using vitrified ice sections of predentin: structural changes in the dentin collagenous matrix prior to mineralization. *J. Struct. Biol.* 132, 212–225. doi: 10.1006/jsbi.2000.4320

Birchall, J. D. (1989). "The importance of the study of biominerals to materials technology," in *Biomineralization: Chemical and Biochemical Perspectives. In Book the Importance of the Study of Biominerals to Materials Technology. In: Biomineralization: Chemical and Biochemical Perspectives,* eds S. Mann, J. Webb, and R. J. P. Williams (New York, NY: VCH Publishers), 491–509.

Blumenthal, N. C., Betts, F., and Posner, A. S. (1975). Nucleoside stabilization of amorphous calcium phosphate. *Mater. Res. Bull.* 10, 1055–1060. doi: 10.1016/0025-5408(75)90214-7

Bodier-Houlle, P., Steuer, P., Meyer, J. M., Bigeard, L., and Cuisinier, F. J. (2000). High-resolution electron-microscopic study of the relationship between human enamel and dentin crystals at the dentinoenamel junction. *Cell Tissue Res.* 301, 389–395. doi: 10.1007/s004410000241

Boskey, A. L. (1997). Amorphous calcium phosphate: the contention of bone. *J. Dent. Res.* 76, 1433–1436. doi: 10.1177/00220345970760080501

Brookes, S. J., Kirkham, J., Shore, R. C., Bonass, W. A., and Robinson, C. (1998). Enzyme compartmentalization during biphasic enamel matrix processing. *Connect. Tissue Res.* 39, 89–99. doi: 10.3109/03008209809023915

Burke, E. M., Guo, Y., Colon, L., Rahima, M., Veis, A., and Nancollas, G. H. (2000). Influence of polyaspartic acid and phosphophoryn on octacalcium phosphate growth kinetics. *Colloids Surf. B. Biointerfaces* 17, 49–57. doi: 10.1016/S0927-7765(99)00084-3

Caterina, J. J., Skobe, Z., Shi, J., Ding, Y. L., Simmer, J. P., Birkedal-Hansen, H., et al. (2002). Enamelysin (matrix metalloproteinase 20)-deficient mice display an amelogenesis imperfecta phenotype. *J. Biol. Chem.* 277, 49598–49604. doi: 10.1074/jbc.M209100200

Colfen, H., and Mann, S. (2003). Higher-order organization by mesoscale self-assembly and transformation of hybrid nanostructures. *Angew. Chem. Int. Ed Engl.* 42, 2350–2365. doi: 10.1002/anie.200200562

Crane, N. J., Popescu, V., Morris, M. D., Steenhuis, P., and Ignelzi, M. A. Jr. (2006). Raman spectroscopic evidence for octacalcium phosphate and other transient mineral species deposited during intramembranous mineralization. *Bone* 39, 434–442. doi: 10.1016/j.bone.2006.02.059

Currey, J. D. (1999). The design of mineralised hard tissues for their mechanical functions. *J. Exp. Biol.* 202, 3285–3294.

Deshpande, A. S., and Beniash, E. (2008). Bioinspired synthesis of mineralized collagen fibrils. *Cryst. Growth Des.* 8, 3084–3090. doi: 10.1021/cg800252f

Diekwisch, T. G. (1998). Subunit compartments of secretory stage enamel matrix. *Connect. Tissue Res.* 38, 101–111. discussion: 139–145. doi: 10.3109/03008209809017026

Dirks, O. B. (1966). Posteruptive changes in dental enamel. *J. Dent. Res.* 45, 503–510. doi: 10.1177/00220345660450031101

Eanes, E. D. (2001). "Amorphous calcium phosphate: in octacalcium phosphate; Monographs in oral science," in *Book Amorphous Calcium Phosphate: In Octacalcium Phosphate; Monographs in Oral Science,* eds L. C. Chow and E. D. Eanes (Basel: Karger), 130–147.

Fang, P. A., Conway, J. F., Margolis, H. C., Simmer, J. P., and Beniash, E. (2011). Hierarchical self-assembly of amelogenin and the regulation of biomineralization at the nanoscale. *Proc. Natl. Acad. Sci. U.S.A.* 108, 14097–14102. doi: 10.1073/pnas.1106228108

Fang, P. A., Margolis, H. C., Conway, J. F., Simmer, J. P., and Beniash, E. (2013). CryoTEM study of effects of phosphorylation on the hierarchical assembly of porcine amelogenin and its regulation of mineralization *in vitro*. *J. Struct. Biol.* 183, 250–257. doi: 10.1016/j.jsb.2013.05.011

Flade, K., Lau, C., Mertig, M., and Pompe, W. (2001). Osteocalcin-controlled dissolution-reprecipitation of calcium phosphate under biomimetic conditions. *Chem. Mater.* 13, 3596–3602. doi: 10.1021/cm011063z

Fleisch, H., Maerki, J., and Russell, R. G. G. (1966). Effect of pyrophosphate on dissolution of hydroxyapatite and its possible importance in calcium homeostasis *Proc. Soc. Exp. Biol. Med.* 122, 317–320. doi: 10.3181/00379727-122-31123

Francis, M. D. (1969). Inhibition of calcium hydroxyapatite crystal growth by polyphosphonates and polyphosphates. *Calcif. Tissue Res.* 3, 151–162. doi: 10.1007/BF02058658

Fukae, M. (2002). "Amelogenesis- three-dimensional structure of amelogenin micelles and their degradation by a cascade system," in *The Proceedings of International Symposium of Oral Science in Tsurumi University School of Dental Medicine* (Tsurumi).

Fukumoto, S., Kiba, T., Hall, B., Iehara, N., Nakamura, T., Longenecker, G., et al. (2004). Ameloblastin is a cell adhesion molecule required for maintaining the differentiation state of ameloblasts. *J. Cell Biol.* 167, 973–983. doi: 10.1083/jcb.200409077

Furedi-Milhofer, H., Moradian-Oldak, J., Weiner, S., Veis, A., Mintz, K. P., and Addadi, L. (1994). Interactions of matrix proteins from mineralized tissues with octacalcium phosphate. *Connect. Tissue Res.* 30, 251–264. doi: 10.3109/03008209409015041

Gajjeraman, S., Narayanan, K., Hao, J. J., Qin, C. L., and George, A. (2007). Matrix macromolecules in hard tissues control the nucleation and hierarchical assembly of hydroxyapatite. *J. Biol. Chem.* 282, 1193–1204. doi: 10.1074/jbc.M604732200

Gericke, A., Qin, C., Spevak, L., Fujimoto, Y., Butler, W. T., Sorensen, E. S., et al. (2005). Importance of phosphorylation for osteopontin regulation of biomineralization. *Calcif. Tissue Int.* 77, 45–54. doi: 10.1007/s00223-004-1288-1

Gibson, C. W., Yuan, Z. A., Hall, B., Longenecker, G., Chen, E. H., Thyagarajan, T., et al. (2001). Amelogenin-deficient mice display an amelogenesis imperfecta phenotype. *J. Biol. Chem.* 276, 31871–31875. doi: 10.1074/jbc.M104624200

Habraken, W., Tao, J. H., Brylka, L. J., Friedrich, H., Bertinetti, L., Schenk, A. S., et al. (2013). Ion-association complexes unite classical and non-classical theories for the biomimetic nucleation of calcium phosphate. *Nature* 4, 12. doi: 10.1038/ncomms2490

Hay, D. I., Moreno, E. C., and Schlesinger, D. H. (1979). Phosphoprotein inhibitor of calcium phosphate precipitation from human salivary secrections. *Inorg. Perspect. Biol. Med.* 2, 271–285.

Hay, D. I., Schluckebier, S. K., and Moreno, E. C. (1982). Equilibrium dialysis and ultrafiltration studies of calcium and phosphate binding by human salivary proteins. Implications for salivary supersaturation with respect to calcium phosphate salts.*Calcif. Tissue Int.* 34, 531–538. doi: 10.1007/BF02411299

He, G., Ramachandran, A., Dahl, T., George, S., Schultz, D., Cookson, D., et al. (2005). Phosphorylation of phosphophoryn is crucial for its function as a mediator of biomineralization. *J. Biol. Chem.* 280, 33109–33114. doi: 10.1074/jbc.M500159200

Hessle, L., Johnson, K. A., Anderson, H. C., Narisawa, S., Sali, A., Goding, J. W., et al. (2002). Tissue-nonspecific alkaline phosphatase and plasma cell membrane glycoprotein-1 are central antagonistic regulators of bone mineralization. *Proc. Natl. Acad. Sci. U.S.A.* 99, 9445–9449. doi: 10.1073/pnas.142063399

Ho, A. M., Johnson, M. D., and Kingsley, D. M. (2000). Role of the mouse ank gene in control of tissue calcification and arthritis. *Science* 289, 265–270. doi: 10.1126/science.289.5477.265

Hu, J. C. C., Hu, Y. Y., Smith, C. E., McKee, M. D., Wright, J. T., Yamakoshi, Y., et al. (2008). Enamel defects and ameloblast-specific expression in Enam knock-out/lacZ knock-in mice. *J. Biol. Chem.* 283, 10858–10871. doi: 10.1074/jbc.M710565200

Hu, J. C. C., Ryu, O. H., Chen, J. J., Uchida, T., Wakida, K., Murakami, C., et al. (2000). Localization of EMSP1 expression during tooth formation and cloning of mouse cDNA. *J. Dent. Res.* 79, 70–76. doi: 10.1177/00220345000790011301

Iijima, M., Moriwaki, Y., Takagi, T., and Moradian-Oldak, J. (2001). Effects of bovine amelogenins on the crystal morphology of octacalcium phosphate in a model system of tooth enamel formation. *J. Cryst. Growth* 222, 615–626. doi: 10.1016/S0022-0248(00)00984-2

Iijima, M., Moriwaki, Y., Wen, H. B., Fincham, A. G., and Moradian-Oldak, J. (2002). Elongated growth of octacalcium phosphate crystals in recombinant amelogenin gels under controlled ionic flow. *J. Dent. Res.* 81, 69–73. doi: 10.1177/154405910208100115

Kim, H. M., Himeno, T., Kokubo, T., and Nakamura, T. (2005). Process and kinetics of bonelike apatite formation on sintered hydroxyapatite in a simulated body fluid. *Biomaterials* 26, 4366–4373. doi: 10.1016/j.biomaterials.2004.11.022

Koulourides, T., Feagin, F., and Pigman, W. (1965). Remineralization of dental enamel by saliva *in vitro*. *Ann. N. Y. Acad. Sci.* 131, 751–757. doi: 10.1111/j.1749-6632.1965.tb34839.x

Kwak, S. Y., Kim, S., Yamakoshi, Y., Simmer, J. P., Beniash, E., and Margolis, H. C. (2014). Regulation of calcium phosphate formation by native amelogenins *in vitro*. *Connect. Tissue Res.* 55(S1), 21–24. doi: 10.3109/03008207.2014.923853

Kwak, S. Y., Wiedemann-Bidlack, F. B., Beniash, E., Yamakoshi, Y., Simmer, J. P., Litman, A., et al. (2009). Role of 20-kDa Amelogenin (P148) phosphorylation in calcium phosphate formation *in vitro*. *J. Biol. Chem.* 284, 18972–18979. doi: 10.1074/jbc.M109.020370

Le Norcy, E., Kwak, S. Y., Allaire, M., Fratzl, P., Yamakoshi, Y., Simmer, J. P., et al. (2011a). Effect of phosphorylation on the interaction of calcium with leucine-rich amelogenin peptide. *Eur. J. Oral Sci.* 119, 97–102. doi: 10.1111/j.1600-0722.2011.00900.x

Le Norcy, E., Kwak, S. Y., Wiedemann-Bidlack, F. B., Beniash, E., Yamakoshi, Y., Simmer, J. P., et al. (2011b). Leucine-rich amelogenin peptides regulate mineralization *in vitro*. *J. Dent. Res.* 90, 1091–1097. doi: 10.1177/0022034511411301

Levi-Kalisman, Y., Raz, S., Weiner, S., Addadi, L., and Sagi, I. (2000). X-Ray absorption spectroscopy studies on the structure of a biogenic amorphous calcium carbonate phase. *J. Chem. Soc. Dalton Trans.* 21, 3977–3982. doi: 10.1039/b003242p

Lowenstam, H. A., and Weiner, S. (1989). *On Biomineralization*. New York, NY: Oxford University Press.

Lowenstam, H. A., and Weiner, S. (1985). Transformation of amorphous calcium phosphate to crystalline dahllite in the radular teeth of chitons. *Science* 227, 51–53. doi: 10.1126/science.227.4682.51

Luo, G. B., Ducy, P., McKee, M. D., Pinero, G. J., Loyer, E., Behringer, R. R., et al. (1997). Spontaneous calcification of arteries and cartilage in mice lacking matrix GLA protein. *Nature* 386, 78–81. doi: 10.1038/386078a0

Mahamid, J., Sharir, A., Addadi, L., and Weiner, S. (2008). Amorphous calcium phosphate is a major component of the forming fin bones of zebrafish: indications for an amorphous precursor phase. *Proc. Natl. Acad. Sci. U.S.A.* 105, 12748–12753. doi: 10.1073/pnas.0803354105

Mann, S. (2001). "Chemical control of biomineralization," in *Biomineralization: Principles and Concepts in Bioinorganic Materials Chemistry*, ed S. Mann (Oxford: Oxford University Press), 58–62.

Margolis, H. C., and Beniash, E. (2010). "The role of amelogenin in dental enamel formation: a universal strategy for protein-mediated biomineralization," in *Amelogenins: Multifaceted Proteins for Dental and Bone Formation and Repair*, ed M. Goldberg (Bentham Science Publishers), 133–142.

Margolis, H. C., Beniash, E., and Fowler, C. E. (2006). Role of macromolecular assembly of enamel matrix proteins in enamel formation. *J. Dent. Res.* 85, 775–793. doi: 10.1177/154405910608500902

McGaughey, C. (1983). Binding of polyphosphates and phosphonates to hydroxyapatite, subsequent hydrolysis, phosphate exchange and effects on demineralization, mineralization and microcrystal aggregation *Caries Res.* 17, 229–241. doi: 10.1159/000260671

McGaughey, C., and Stowell, E. C. (1977). Effects of polyphosphates on the solubility and mineralization of HA: relevance to a rationale for anticaries activity. *J. Dent. Res.* 56, 579–587. doi: 10.1177/00220345770560060501

Meyer, J. L. (1984). Can biological calcification occur in the presence of pyrophosphate*?*. *Arch. Biochem. Biophys.* 231, 1–8. doi: 10.1016/0003-9861(84)90356-4

Meyer, J. L., and Eanes, E. D. (1978). Thermodynamic analysis of the amorphous to crystalline calcium phosphate transformation. *Calcif. Tissue Res.* 25, 59–68. doi: 10.1007/BF02010752

Meyer, J. L., and Nancollas, G. H. (1973). Influence of multidentate organic phosphonates on the crystal growth of hydroxyapatite. *Calcif. Tissue Res.* 13, 295–303. doi: 10.1007/BF02015419

Meyer, J. L., and Reddi, A. H. (1985). Changes in pyrophosphatase activity during the de novo mineralization associated with cartilage and bone formation. *Arch. Biochem. Biophys.* 242, 532–539. doi: 10.1016/0003-9861(85)90240-1

Moreno, E. C., Aoba, T., and Margolis, H. C. (1987). Pyrophosphate adsorption onto hydroxyapatite and its inhibition of crystal growth. *Compend. Suppl.* 8, S256–S266.

Moreno, E. C., and Margolis, H. C. (1988). Composition of human plaque fluids. *J. Dent. Res.* 67, 1181–1189. doi: 10.1177/00220345880670090701

Moreno, E. C., Varughese, K., and Hay, D. I. (1979). Effect of human salivary proteins on the precipitation kinetics of calcium phosphate. *Calcif. Tissue Int.* 28, 7–16. doi: 10.1007/BF02441212

Nene, S. S., Hunter, G. K., Goldberg, H. A., and Hutter, J. L. (2013). Reversible inhibition of calcium oxalate monohydrate growth by an osteopontin phosphopeptide. *Langmuir* 29, 6287–6295. doi: 10.1021/la400891b

Niederberger, M., and Colfen, H. (2006). Oriented attachment and mesocrystals: non-classical crystallization mechanisms based on nanoparticle assembly. *Phys. Chem. Chem. Phys.* 8, 3271–3287. doi: 10.1039/b604589h

Nikiforuk, G. (ed.). (1985). *In Understanding Dental Caries. 1. Etiology and Mechanisms Basic and Clinical Aspects*. Basel: Karger, 13–141.

Nylen, M. U., Omnell, K. A., and Eanes, E. D. (1963). Crystal growth in rat enamel. *J. Cell Biol.* 18, 109–123. doi: 10.1083/jcb.18.1.109

Ofir, P. B. Y., Govrin-Lippman, R., Garti, N., and Furedi-Milhofer, H. (2004). The influence of polyelectrolytes on the formation and phase transformation of amorphous calcium phosphate. *Cryst. Growth Des.* 4, 177–183. doi: 10.1021/cg034148g

Posner, A. S., and Betts, F. (1975). Synthetic amorphous calcium phosphate and its relation to bone mineral structure. *Acc. Chem. Res.* 8, 273–281. doi: 10.1021/ar50092a003

Robertson, W. G. (1973). Factors affecting the precipitation of calcium phosphate *in vitro Calcif. Tissue Res.* 11, 311–322. doi: 10.1007/BF02547230

Robinson, C. (2007). Self-oriented assembly of nano-apatite particles: a subunit mechanism for building biological mineral crystals. *J. Dent. Res.* 86, 677–679. doi: 10.1177/154405910708600801

Robinson, C., Briggs, H. D., Atkinson, P. J., and Weatherell, J. A. (1979). Matrix and mineral changes in developing enamel. *J. Dent. Res.* 58, 871–882. doi: 10.1177/00220345790580024101

Robinson, C., Fuchs, P., and Weatherell, J. A. (1981). The appearance of developing rat incisor enamel using a freeze fracturing technique. *J. Cryst. Growth*. 53, 160–165. doi: 10.1016/0022-0248(81)90062-2

Robinson, C., and Kirkham, J. (1985). "The dynamics of amelogenesis as revealed by protein compositional studies," in *The Chemistry and Biology of Mineralized Tissues. In Book The Dynamics of Amelogenesis as Revealed by Protein Compositional Studies. In: The Chemistry and Biology of Mineralized Tissues,* ed W. T. Butler (Birmingham, AL: Ebsco Media Inc.), 248–263.

Robinson, C., Kirkham, J., and Hallsworth, A. S. (1988). Volume distribution and concentration of protein, mineral and water in developing bovine enamel. *Arch. Oral Biol.* 33, 159–162. doi: 10.1016/0003-9969(88)90040-4

Schroeder, H. E. (ed.). (1969). *Formation and Inhibition of Dental Calculus.* Berne: Verlag Hans Huber, 119–122.

Septier, D., Hall, R. C., Lloyd, D., Embery, G., and Goldberg, M. (1998). Quantitative immunohistochemical evidence of a functional gradient of chondroitin 4-sulphate dermatan sulphate, developmentally regulated in the predentine of rat incisor. *Histochem. J.* 30, 275–284. doi: 10.1023/A:1003216024158

Simmer, J. P., Hu, Y. Y., Lertlam, R., Yamakoshi, Y., and Hu, J. C. C. (2009). Hypomaturation enamel defects in Klk4 knockout/LacZ knockin mice. *J. Biol. Chem.* 284, 19110–19121. doi: 10.1074/jbc.M109.013623

Smith, C. E. (1998). Cellular and chemical events during enamel maturation. *Crit. Rev. Oral Biol. Med.* 9, 128–161. doi: 10.1177/10454411980090020101

Smith, C. E., Wazen, R., Hu, Y. Y., Zalzal, S. F., Nanci, A., Simmer, J. P., et al. (2009). Consequences for enamel development and mineralization resulting from loss of function of ameloblastin or enamelin. *Eur. J. Oral Sci.* 117, 485–497. doi: 10.1111/j.1600-0722.2009.00666.x

Termine, J. D., and Posner, A. S. (1966). Infrared analysis of rat bone-age dependency of amorphous and crystalline mineral fractions. *Science* 153, 1523–1525. doi: 10.1126/science.153.3743.1523

Termine, J. D., Peckausk, R. A., and Posner, A. S. (1970). Calcium phosphate formation *in vitro*. II. Effects of environment on amorphous-crystalline transformation.*Arch. Biochem. Biophys.* 140, 318–325. doi: 10.1016/0003-9861(70)90072-X

Torres-Quintana, M. A., Lecolle, S., Septier, D., Palmier, B., Rani, S., MacDougall, M., et al. (2000). Inositol hexasulphate, a casein kinase inhibitor, alters enamel formation in cultured embryonic in embryonic mouse tooth germs. *J. Dent. Res.* 79, 1794–1801. doi: 10.1177/00220345000790101101

Uchida, T., Tanabe, T., Fukae, M., Shimizu, M., Yamada, M., Miake, K., et al. (1991). Immunochemical and immunohistochemical studies, using antisera against porcine 25 kDa amelogenin, 89 kDa enamelin and the 13-17 kDa nonamelogenins, on immature enamel of the pig and rat. *Histochemistry* 96, 129–138. doi: 10.1007/BF00315983

Veis, A., Sabsay, B., and Wu, C. B. (1991). Phosphoproteins as mediators of biomineralization. *ACS Symp. Ser.* 444, 1–12. doi: 10.1021/bk-1991-0444.ch001

Walsh, D., Kingston, J. L., Heywood, B. R., and Mann, S. (1993). Influence of monosaccharides and related molecules on the morphology of hydroxyapatite. *J. Cryst. Growth* 133, 1–12. doi: 10.1016/0022-0248(93)90097-G

Wazen, R. M., Moffatt, P., Zalzal, S. F., Yamada, Y., and Nanci, A. (2009). A mouse model expressing a truncated form of ameloblastin exhibits dental and junctional epithelium defects. *Matrix Biol.* 28, 292–303. doi: 10.1016/j.matbio.2009.04.004

Weiner, S. (1986). Organization of extracellularly mineralized tissues: a comparative study of biological crystal growth. *CRC Crit. Rev. Biochem.* 20, 365–408. doi: 10.3109/10409238609081998

Weiner, S. (2006). Transient precursor strategy in mineral formation of bone. *Bone* 39, 431–433. doi: 10.1016/j.bone.2006.02.058

Weiner, S., Sagi, I., and Addadi, L. (2005). Choosing the crystallization path less traveled. *Science* 309, 1027–1028. doi: 10.1126/science.1114920

Weinstock, M., and Leblond, C. P. (1973). Autoradiographic visualization of the deposition of a phosphoprotein at the mineralization front in the dentin of the rat incisor. *J. Cell Biol.* 56, 838–845. doi: 10.1083/jcb.56.3.838

Wen, H. B., Moradian-Oldak, J., Leung, W., Bringas, P., and Fincham, A. G. (1999). Microstructures of an amelogenin gel matrix. *J. Struct. Biol.* 126, 42–51. doi: 10.1006/jsbi.1999.4086

Wiedemann-Bidlack, F. B., Beniash, E., Yamakoshi, Y., Simmer, J. P., and Margolis, H. C. (2007). pH triggered self-assembly of native and recombinant amelogenins under physiological pH and temperature *in vitro*. *J. Struct. Biol.* 160, 57–69. doi: 10.1016/j.jsb.2007.06.007

Wiedemann-Bidlack, F. B., Kwak, S. Y., Beniash, E., Yamakoshi, Y., Simmer, J. P., and Margolis, H. C. (2011). Effects of phosphorylation on the self-assembly of native full-length porcine amelogenin and its regulation of calcium phosphate formation *in vitro*. *J. Struct. Biol.* 173, 250–260. doi: 10.1016/j.jsb.2010.11.006

Wu, L. N. Y., Genge, B. R., Dunkelberger, D. G., LeGeros, R. Z., Concannon, B., and Wuthier, R. E. (1997). Physicochemical characterization of the nucleational core of matrix vesicles. *J. Biol. Chem.* 272, 4404–4411. doi: 10.1074/jbc.272.7.4404

Yadav, M. C., de Oliveira, R. C., Foster, B. L., Fong, H., Cory, E., Narisawa, S., et al. (2012). Enzyme replacement prevents enamel defects in hypophosphatasia mice. *J. Bone Miner. Res.* 27, 1722–1734. doi: 10.1002/jbmr.1619

Conflict of Interest Statement: The authors declare that the research was conducted in the absence of any commercial or financial relationships that could be construed as a potential conflict of interest.

Received: 15 July 2014; paper pending published: 11 August 2014; accepted: 19 August 2014; published online: 10 September 2014.

*Citation: Margolis HC, Kwak S-Y and Yamazaki H (2014) Role of mineralization inhibitors in the regulation of hard tissue biomineralization: relevance to initial enamel formation and maturation. Front. Physiol. **5**:339. doi: 10.3389/fphys.2014.00339*

This article was submitted to Craniofacial Biology, a section of the journal Frontiers in Physiology.

frontiers in PHYSIOLOGY

ORIGINAL RESEARCH ARTICLE
published: 24 July 2014
doi: 10.3389/fphys.2014.00268

Preferential and selective degradation and removal of amelogenin adsorbed on hydroxyapatites by MMP20 and KLK4 *in vitro*

Li Zhu[1], Haichuan Liu[2], H. Ewa Witkowska[2], Yulei Huang[3], Kataro Tanimoto[4] and Wu Li[1]*

[1] *Department of Orofacial Sciences, School of Dentistry, University of California, San Francisco, San Francisco, CA, USA*
[2] *Department of Obstetrics, Gynecology and Reproductive Sciences, University of California, San Francisco, San Francisco, CA, USA*
[3] *Department of Oral Medicine, Guanghua School of Stomatology, Sun Yat-sen University, Guangdong, China*
[4] *Departments of Orthodontics and Craniofacial Developmental Biology, Hiroshima University Graduate School of Biomedical Sciences, Hiroshima, Japan*

Edited by:
Megan Pugach-Gordon, The Forsyth Insitute, USA

Reviewed by:
Tom Diekwisch, University of Illinois at Chicago, USA
John D. Bartlett, The Forsyth Institute, USA

****Correspondence:***
Wu Li, Department of Orofacial Sciences, School of Dentistry, University of California, San Francisco, Parnassus Avenue, San Francisco, CA 94143, USA
e-mail: wu.li@ucsf.edu

The hardest tooth enamel tissue develops from a soft layer of protein-rich matrix, predominated by amelogenin that is secreted by epithelial ameloblasts in the secretory stage of tooth enamel development. During enamel formation, a well-controlled progressive removal of matrix proteins by resident proteases, Matrix metalloproteinase 20 (MMP20), and kallikrein 4 (KLK4), will provide space for the apatite crystals to grow. To better understand the role of amelogenin degradation in enamel biomineralization, the present study was conducted to investigate how the adsorption of amelogenin to hydroxyapatite (HAP) crystals affects its degradation by enamel proteinases, MMP20 and KLK4. Equal quantities of amelogenins confirmed by protein assays before digestions, either adsorbed to HAP or in solution, were incubated with MMP20 or KLK4. The digested samples collected at different time points were analyzed by spectrophotometry, SDS-PAGE, high performance liquid chromatography (HPLC), and LC-MALDI MS/MS. We found that majority of amelogenin adsorbed on HAP was released into the surrounding solution by enzymatic processing (88% for MMP20 and 98% for KLK4). The results show that as compared with amelogenin in solution, the HAP-bound amelogenin was hydrolyzed by both MMP20 and KLK4 at significantly higher rates. Using LC-MALDI MS/MS, more accessible cleavage sites and hydrolytic fragments from MMP20/KLK4 digestion were identified for the amelogenin adsorbed on HAP crystals as compared to the amelogenin in solution. These results suggest that the adsorption of amelogenin to HAP results in their preferential and selective degradation and removal from HAP by MMP20 and KLK4 *in vitro*. Based on these findings, a new degradation model related to enamel crystal growth is proposed.

Keywords: amelogenin, tooth enamel, MMP20, KLK4, protein interactions, hydroxyapatites, biomineralization, proteolysis

INTRODUCTION

The superficial layer of a tooth is enamel, the hardest tissue known in vertebrates. The unique morphological structure and outstanding mechanical properties of the enamel make it different from other mineralized tissues in the body, such as bone, dentin, and cementum. Tooth enamel is comprised mainly of numerous hexagonal carbonated hydroxyapatite (HAP) crystals, organized into rod, and interrod structures with distinct mechanical properties (Ichijo et al., 1992; Plate and Hohling, 1994; Pergolizzi et al., 1995).

The enamel crystals are very thin (20–30 nm in diameter) but extremely long. Many investigators believe that these crystals span the entire thickness of tooth enamel, a distance up to 2.5 mm (Leblond and Warshawsky, 1979; Daculsi et al., 1984; Nanci et al., 1998). The unique morphology and organization of enamel crystals determine its excellent mechanical characteristics while also raise a persistent question of how these enamel crystals form in such a special shape. Solving this puzzle will advance our knowledge of the basic principle of amelogenin-mediated mineralization during enamel development, help us to better understand the fundamental mechanism of an enamel disease, amelogenesis imperfecta, and provide useful information for future acellular tooth enamel regeneration.

The hard enamel tissue develops from a soft protein-rich extracellular matrix secreted by epithelial ameloblasts during the secretory stage of enamel development. At later stages of enamel formation, a well-controlled progressive removal of matrix proteins by resident proteases will provide space for the apatite crystals to grow (Bartlett and Simmer, 1999).

The protein matrix of forming enamel is composed predominantly of amelogenins and its cleavage products (Termine et al., 1980; Fincham et al., 1999). Amelogenin protein is hydrophobic in nature except for its highly charged C-terminus. Amelogenins self-assemble into highly packed and

tightly associated nanospheres that interact with apatite crystals to provide the supportive framework for the growth of newly formed crystals with extremely thin and long structure (Robinson et al., 1998; Wen et al., 1999). This intercrystalline protein matrix also serves to prevent premature crystal–crystal fusion during the early stages of enamel formation (Moradian-Oldak et al., 2001).

It has been suggested that amelogenins are critical for the organization of the crystal pattern and regulation of enamel thickness. *In vitro* mineralization studies show that amelogenin can control crystal orientation and growth habit as well as facilitate aggregation of pre-formed hydroxyapatite crystals (Iijima et al., 2002). Mutation of amelogenin can cause amelogenesis imperfecta, a disorder of tooth enamel (Hart et al., 2002; Wright et al., 2003). The essential role of amelogenin in tooth enamel development is also confirmed by the amelogenin-null mice that exhibit defected amelogenesis phenotype with much thinner enamel layers (Gibson et al., 2001).

During enamel mineralization, the step-wise increase in mineral content is concomitant with progressive degradation of amelogenin in the enamel matrix. In particular, during the later stages, amelogenin proteins disappear rapidly and completely to facilitate crystal growth (Fukae and Shimizu, 1974). Matrix metalloproteinase 20 (MMP20) and kallikrein 4 (KLK4) are considered to be the two major amelogenin-processing enzymes during the early and late stages of enamel development, respectively (Bartlett et al., 1996; Bartlett and Simmer, 1999; Simmer and Hu, 2002). However, the relationship between apatite surface, enamel proteases, and enamel crystal growth remains yet to be explored. In this study, we focus on how the adsorption of amelogenin to HAP crystals affects its degradation by enamel proteinases, MMP20 and KLK4. We hypothesize that the binding of amelogenin to apatite may induce protein conformational change and subsequently affect the susceptibility of the adsorbed amelogenin to proteinases. The crystal-protein and protein-proteinase interactions are dynamically coordinated to regulate the mineral accretion. In the present study we have determined the effect of the apatite surface on enamel protease activity and amelogenin cleavage as a means to explain enamel crystal growth through proteolytic amelogenin degradation.

MATERIALS AND METHODS

SAMPLE PREPARATION OF PROTEINS BOUND TO HAP

Recombinant human amelogenin (rh174) and MMP20 were produced and purified as previously described (Li et al., 1999; Wang et al., 2006). Commercial recombinant human KLK4 was purchased from R&D Systems (Minneapolis, MN, USA). Hydroxyapatite (HAP) was synthesized according to the method reported by Nelson et al. and identified by X-ray diffraction as described in our previous publication (Zhu et al., 2009).

Amelogenin was incubated with HAP crystals at amount over the saturation binding ($875 \pm 37\,\mu g/m^2$) (Tanimoto et al., 2008a,b; Zhu et al., 2011). After 2 h incubation at room temperature with constant shaking, the protein-HAP complex was centrifuged at 5000 rpm for 5 min. The amount of protein bound was determined by measuring the change in concentration of protein solution before and after binding using Braford assay (BioRad, Hercules, CA).

REMOVAL OF AMELOGENIN FROM HAP BY MMP20 AND KLK4 DIGESTION

The digestion of HAP-bound amelogenin (0.2 mg) with MMP20 was performed with enzyme/substrate ratio of 1: 50 (W:W) in 100 μl of reaction buffer (50 mM Tris-HCl, 150 mM NaCl, 10 mM $CaCl_2$, 10 μM $ZnCl_2$, pH 7.5). At different time points after incubation on an orbital shaker at 37°C, the samples were boiled for 10 min to inactivate MMP20. After centrifugation at 5000 × rpm for 5 min, the supernatant was carefully and completely removed from the HAP sediment. The HAP was dissolved in 10 μl of 0.1% TFA and then reaction buffer was added to bring the volume up to final 100 μl and the pH to neutral. The amount of protein released from HAP during incubation and the amount retained on the mineral were quantitatively determined by UV detection at wavelength 220 nm. Control samples, including HAP-bound amelogenin only and HAP with addition of MMP20 only, were treated in the same manner. MMP20 was replenished at same amounts after 24 h of incubation. The experiments were conducted in triplicate, and the average OD values and standard deviations were calculated. The removal of adsorbed amelogenin by KLK4 was carried out in a buffer with 50 mM Tris-HCl at pH 7.5, 250 mM NaCl and 50 mM $CaCl_2$ under the similar conditions and analyzed by an identical methodology as described above.

COMPARATIVE DIGESTION OF HAP-BOUND AND HAP-FREE AMELOGENIN IN SOLUTION

Same amounts of HAP-bound and unbound amelogenin were digested with MMP20 and KLK4 at enzyme/substrate ratio of 1:50 in equal volumes of their corresponding reaction buffers in a time-course manner. The digestions were carried out at 37°C under continuous shaking. At each time point, 50 μl sample was withdrawn and the hydrolysis was stopped by boiling in a water bath for 10 min. The digested samples were then subjected to SDS-PAGE, reversed-phase high performance liquid chromatography (HPLC), and liquid chromatography matrix-assisted laser desorption ionization tandem mass spectrometry (LC-MALDI MS-MS).

In SDS-PAGE experiments, the digested samples (15 ul for MMP20 or 25 ul for KLK4) were mixed with SDS sample buffer, and resolved by using a 15% SDS-PAGE gel. Prior to HPLC separation, equal volume of 0.1% TFA was added to all the samples to dissolve HAP and release the retained proteins. The HPLC analyses were performed using a C4 column (Varian, Walnut Creek, CA, USA). A linear gradient from 0 to 95% acetonitrile (ACN) in 0.1% TFA was run over a period of 45 min at a flow-rate of 1 ml/min. Elution was monitored via absorbance at 214 nm. The peak areas (mAU/ml) of remaining substrate after hydrolysis were measured and compared.

After 36 h digestion, the samples were centrifuged at 5000 rpm for 5 min. The HAP pellets were dissolved in 50 μl of 0.1% TFA. Both proteolytic fragments still bound to the HAP and those released into the solution were identified by LC-MALDI MS/MS.

EFFECT OF BARE HAP ON MMP20 ACTIVITY

To determine whether HAP affects MMP20 activity, we added different amount of HAP into the 96-well plate that contained MMP20 and its substrate, a quenched fluorescent peptide

[Mca-Pro-Leu-Gly-Leu-Dap (Dnp)-Ala-Arg-NH_2; Bachem, CA, USA] in 200 μL of MMP20 reaction buffer. The digestion was conducted at the enzyme/susbtrate ratio of 1:100. We measured hydrolysis of the substrate by monitoring fluorescence every 5 min for 1 h at 37°C with 320 nm excitation and 405 nm emission.

RESULTS

MMP20 AND KLK4 DIGESTION PROGRESSIVELY AND EXTENSIVELY REMOVE AMELOGENIN FROM HAP

The amount of protein retained on HAP after digestion for various periods of time is illustrated in **Figure 1**. Both MMP20 and KLK4 hydrolysis could gradually remove the adsorbed amelogenin from HAP (**Figures 1A,C**) into the reaction buffer solution (**Figures 1B,D**). After 36 h of digestion by MMP20, only about 12% of amelogenin still remained on HAP. In comparison, the removal rate of adsorbed amelogenin was much faster by KLK4 digestion. Nearly 98% of amelogenin was released into the surrounding solution by merely 12-h processing. During the entire period of incubation with shaking, bound amelogenin could also be desorbed without digestion, but this loss appeared to be negligible compared to that observed in digested samples (**Figures 1A,C**). Because UV detection showed only a trace amount of MMP20 and KLK4 bound to HAP during digestion process, their effects on the measurement of amelogenin amount were not included from our analysis.

BINDING OF AMELOGENIN TO HAP ACCELERATED THE RATE OF MMP20 OR KLK4 HYDROLYSIS

The SDS-PAGE data showed that amelogenin bound to HAP was hydrolyzed by MMP20 faster than the proteins in solution (**Figure 2**). The amelogenin substrate on HAP progressively disappeared during the incubation. The intermediate digestion product at an apparent molecular weight of 23 kDa was further hydrolyzed by MMP20 into smaller fragments, which could not be detected by SDS-PAGE analysis. After 3 h of digestion, both the amelogenin at 25 kDa and derivative fragments at 23 kDa were almost completely degraded on HAP, but still partially remained in the samples without HAP.

Further validation and comparison were achieved through HPLC analysis to observe the loss of the 25 kDa protein peak and concomitant generation of peptide peaks. The results of HPLC demonstrated that the digestion of amelogenin on HAP or in solution immediately produced one product peak (labeled "23 kDa" in **Figure 3A**). The corresponding HPLC fraction of this peak was collected and analyzed by MALDI TOF MS. The measured mass (m/z = 18,616) suggested that the 23 kDa band seen on SDS-PAGE corresponded to amelogenin truncated at P^{164}/S (theoretical m/z = 18,615). The areas of individual peaks measured on HPLC traces before and after digestion were used

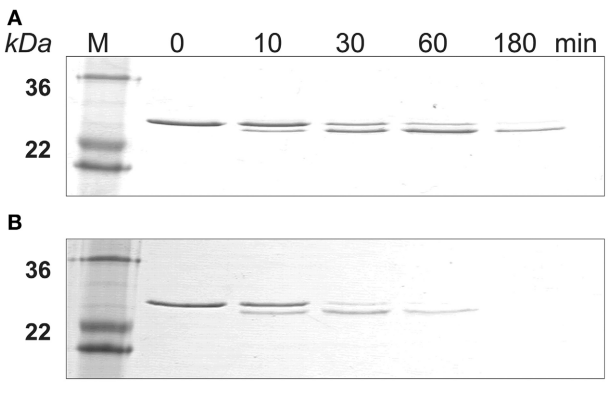

FIGURE 2 | MMP-20 digestion of amelogenin in solution and on HAP shown by SDS-PAGE. (A) Amelogenin digestion in solution. **(B)** MMP-20 hydrolysis of amelogenin adsorbed on HAP. M, standard molecular weight.

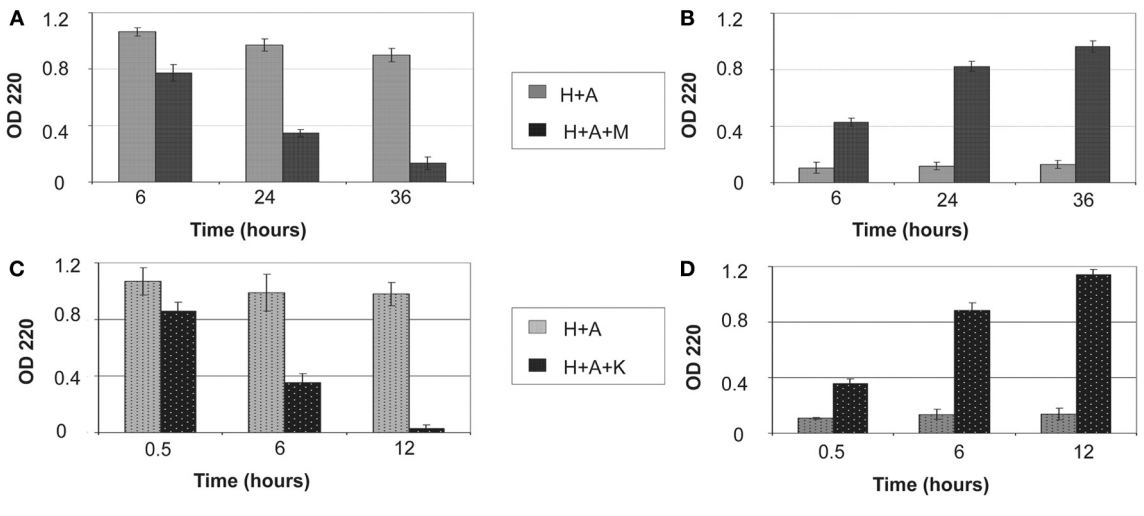

FIGURE 1 | Removal of bound amelogenin on HAP crystals by MMP-20 and KLK4 hydrolysis. (A) Protein amounts remained on crystals and **(B)** released into surrounding supernatant at different time points during MMP20 digestion; **(C)** Protein amounts remained on crystals and **(D)** released into surrounding supernatant at different time points during KLK4 digestion. **H+A,** HAP+rh174; **H+A+M**, HAP+rh174+MMP-20; **H+A+K**, HAP+rh174+KLK4.

to analyze the rate of hydrolysis. As shown in **Figure 3B**, the full-length amelogenin in solution was hydrolyzed significantly slower than the protein attached to the crystal surface. The same trend was observed for the 23 kDa proteolytic fragment, which was digested much slower in solution than in its HAP-bound form (**Figure 3C**). Interestingly, we note that the 23 kDa amelogenin fragment rapidly increases in the first hour of the digestion. This result indicates that MMP20 rapidly cleaves off amelogenin C-terminus, causing the accumulation of the truncated hydrophobic peptide in solution.

Similarly, SDS-PAGE data showed that KLK4 hydrolyzed amelogenin much faster on HAP than that in solution (**Figure 4**). At the end of 180 min of KLK4 hydrolysis, there is much less HAP-bound 25 kDa amelogenin remained as compared with amelogenin digested in solution.

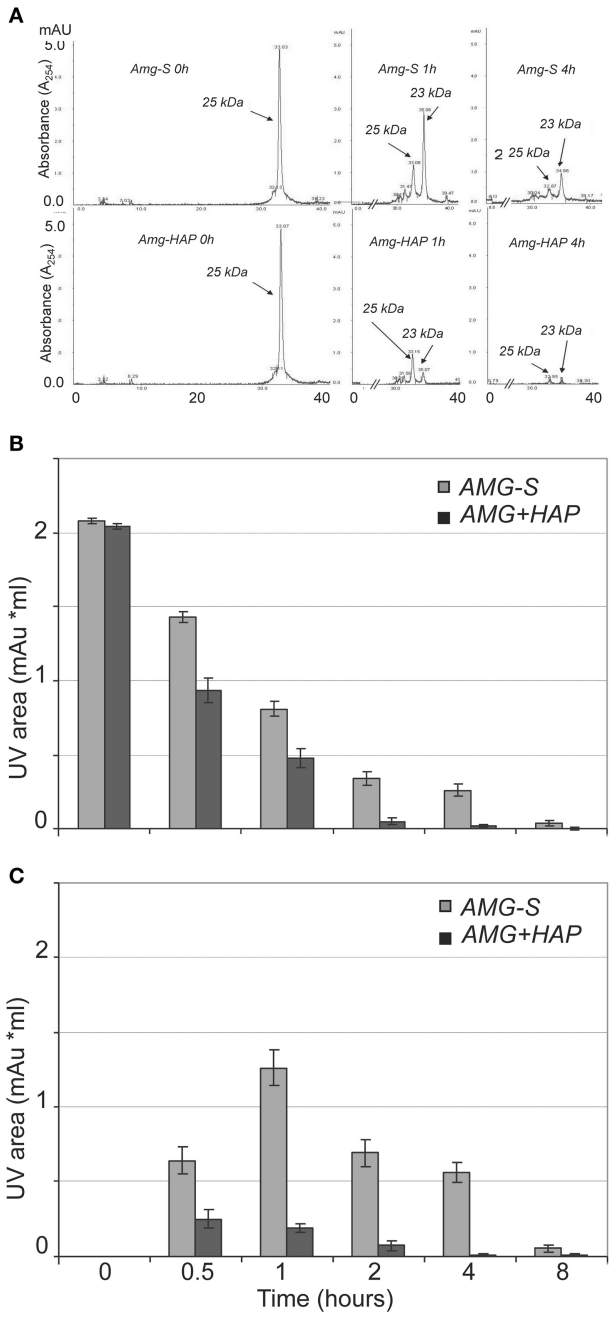

FIGURE 3 | MMP-20 hydrolysis of amelogenin in solution (AMG-S) and bound on HAP (AMG-HAP) were digested and quantified by HPLC. (A) HPLC peaks of 25 and 23 kDa amelgenins after 1 and 4 h of digestion. **(B)** Quantified UV areas of 25 kDa amelogenin substrate after digestion. **(C)** Quantified UV areas of 23 kDa amelogenin derivative during digestion.

BINDING OF AMELOGENIN TO HAP INCREASED THE ACCESSIBLE CLEAVAGE SITES FOR MMP20/KLK4

Previous *in vitro* proteolysis experiments have shown that unbound amelogenin is cleaved by MMP20 primarily at its N- and C-termini (Fincham et al., 1981; Tanimoto et al., 2008a,b). To detect whether the adsorption to HAP affects amelogenin cleavage pattern by proteases, samples digested in the presence or absence of HAP were analyzed by LC-MALDI MS/MS. **Table 1A** lists the cleavage sites of MMP20 and KLK4 in amelogenins adsorbed on HAP and in solution, identified by mass spectrometric analyses. Amelogenin residing on HAP was cleaved by MMP20 at 54 sites, out of which 30 appeared to be unique for the HAP-bound substrate (**Table 1B**). Similarly, KLK4 produced more cleavages within amelogenin bound to HAP (78 sites), in comparison to samples without HAP (53 sites) (**Table 1C**). These results suggested that HAP indeed influences the cleavage pattern of adsorbed amelogenin and the larger number of utilized cleavage sites might thus explain an enhanced proteolysis after the proteins adsorb to HAP. In addition, interaction with HAP may also expose additional cleavage sites within the central region, the most hydrophobic part in amelogenin (**Tables 1B,C**).

REDUCED MMP20 ACTIVITY BY BARE HAP

The quenched-peptide assay showed that the addition of bare HAP into the digestion reaction resulted in a significant decrease

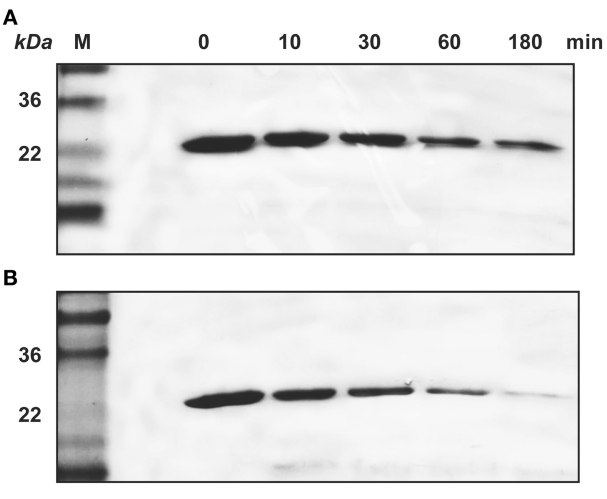

FIGURE 4 | KLK4 digestion of amelogenin in solution and on HAP shown by SDS-PAGE. (A) Amelogenin digestion in solution. **(B)** KLK4 hydrolysis of amelogenin adsorbed on HAP. M, standard molecular weight.

Table 1 | The numbers of cleavage sites generated by MMP-20 and KLK4 in amelogenins digested on HAP and in solution.

Proteinases	Numbers of cleavage sites	
	Amelogenin on HAP	Amelogenin in solution
(A)		
MMP20	55	25
KLK4	79	54
(B) CLEAVAGE SITES IN HUMAN AMELOGENIN FOR MMP20		
MPL*PPHPGHPGY/IN/F/S/YE/VLTP/LK/W/YQS*IRPPYP/S*Y*G*YEP*MGG*W/L*HH*Q*IIP*V*L*S*Q*QHPPTHT*LQPHHHIPVVP*A*Q*QP/VIPQQP*MMPVP*GQ/H/S*MTP*IQ/HHQPNLPPP*A/Q*QP/YQPQP/VQ*PQPHQP*MQPQPPVHP/MQ*P/L/PPQPPLPPMFP/MQ*PLPPMLP*DL/T/LEAWP/STDKTKREEVD		
(C) CLEAVAGE SITES IN HUMAN AMELOGENIN FOR KLK4		
MPLPPHPGHPG*Y/I*N/F/S*Y/E/V/LTP*L*K/W/Y/Q/S/IR/PPYPS/YGYEP/M/G/G/W/L/H/H/Q/IIPVLS/Q*QHPPT/H*T/L*Q*P*H/HHIP/VVP*A/QQP/VI/PQ/Q*PM*MPVPG*QH/S/MTP/IQ*H/H*QPN*LPPPA*QQPY*QPQP/VQPQPH*QP*M/QPQPP*VHP/M/Q*PL/PPQ*PPLPPM/FP/M/QP/L/PP/MLP/D/L/T*L/E/AW/PSTDKTK/REEVD		

*The / in **(B)** and **(C)** indicates the MMP20 or KLK4 cleavage sites identical in both amelogenins adsorbed on HAP and in solution. The * indicates the cleavage sites of MMP20 or KLK4 unique for amelogenins adsorbed on HAP.*

in the enzymatic activity of MMP20 in a dose-dependent manner (**Figure 5**).

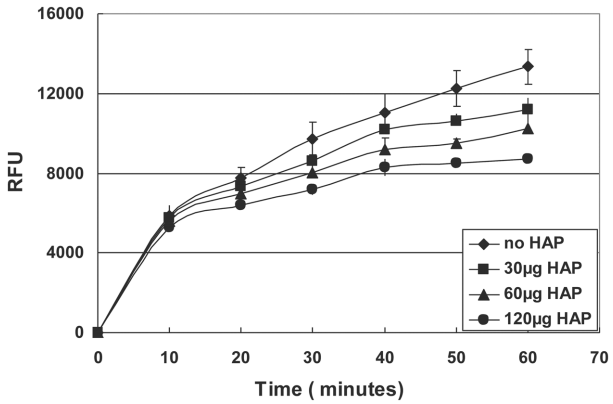

FIGURE 5 | Hydrolysis of quenched peptide by MMP20 in the presence of different amount of HAP.

DISCUSSION

The highly mineralized enamel crystals develop from a layer of enamel protein matrix that is predominated by amelogenins (>90%), which form special nanostructures to modulate crystal formation (Fincham and Moradian-Oldak, 1995; Fincham et al., 1999; Moradian-Oldak et al., 2001). The multilayer of amelogenin nanospheres in the matrix surrounding the thin and long crystals not only provide physical protection and mechanical support to these newly formed and extremely fragile crystals, but also modulate and inhibit their growth (Moradian-Oldak et al., 2001). During transition and maturation stages of enamel development, amelogenins are gradually processed by enamel proteinases, and mineralization simultaneously increases to form a fully mineralized enamel matrix (Fukae et al., 1998; Bartlett and Simmer, 1999; Li et al., 1999; Ryu et al., 1999, 2002; Simmer and Hu, 2002; Bartlett et al., 2003).

It has previously been evidenced that full-length amelogenin proteins strongly adsorb to apatite crystals and retard their further growth (Doi et al., 1984; Aoba and Moreno, 1987). Therefore, it is not difficult to understand that the removal of the proteins from matrix not only opens the space but also eliminates the possible inhibitory effects of amelogenin for enamel crystal growth. The question is which part of the matrix will be degraded and removed first, the proteins bound to crystals or unbound to appetite? If the amelogenins in the matrix (unbound to crystals) were digested faster or even at the same rates as those adhered to the crystal, the newly formed crystals with extreme thin and long structures would lose the protection and support. Consequently, they would be easy to collapse, break apart or fuse together. Therefore, the layers of amelogenin adsorbed on crystal surface need to be preferentially removed to open up the space for the growth of a new layer of crystals, while still having relatively intact surrounding protein matrix to support the thin and fragile nascent crystals.

The amelogenin-crystal interactions may contribute to this preferential degradation by proteinases. Proteins usually alter their conformation when bound to solid surfaces (Hlady and Buijs, 1996; Gray, 2004). In the recently published report by the Shaw group, they analyzed self-assembled amelogenin residing on single fluoroapatite (FAP) crystals, whose structures are the same as those of HAP crystals. They found that protein layer on the FAP surfaces were much thinner than the nanospheres originally present in solution. Their studies provide the strong evidence that amelogenin nanospheres undergo structural changes upon interacting with apatite surfaces (Tarasevich et al., 2009a,b). By using Fourier transform infrared (FTIR), the Beniash group also reported on the reduction in structural organization of amelogenin proteins upon their interactions with minerals at neutral pH (Beniash et al., 2012). In addition, it was shown that amelogenin nanospheres disassembled into oligomers and monomers when they adsorbed onto positively or negatively charged mica surfaces (Chen et al., 2012). The adsorption-induced conformational changes of the amelogenin and its assemblies can further alter their interactions with other enamel proteins, including proteinases (Smolarczyk et al., 2005; Sakiyama et al., 2006). The results of the present work clearly demonstrated that the binding of amelogenin to apatite crystals exerts significant effects on the proteolysis of the protein. Compared to the unbound proteins, the HAP-bound amelogenins were more rapidly hydrolyzed by both MMP20 and KLK4. Moreover, the additional proteinases-susceptible cleavage sites, primarily in the central region, were uncovered upon amelogenin binding to HAP. Previous studies suggested that the hydrophobic central region of amelogenins forms a dense core of nanosphere surrounded by the hydrophilic C-terminal tails in solution (Margolis et al., 2006). The buried central region is not readily accessible to the proteinases, and hence MMP20 hydrolysis of amelogenin occurs primarily at its termini. The

interactions of HAP and amelogenins result in the disassembly of nanospheres into monomers (Chen et al., 2012), which may effectively exposes the central region of the protein. As a result, more cleavage sites become accessible and a higher rate of hydrolysis was observed.

The present study identified that MMP20 and KLK4 hydrolyzed amelogenin in solution at 25 and 54 cleavage sites respectively. These numbers are significantly higher than those previously reported (Nagano et al., 2008, 2009). In addition, we detected seven MMP20-susceptible cleavage sites within the sequence of tyrosine rich amelogenin peptide (TRAP). Previous studies indicated that TRAP was not susceptible to MMP20 hydrolysis (Nagano et al., 2008, 2009). The differences in experiment results among laboratories may result from several reasons. First, as we aimed at investigating the complete enzymatic degradation of amelogenin, beyond the initial generation of large proteolytic fragments, we used relatively higher enzyme-to-substrate ratios, longer incubation time and also replenished enzyme after 24 h of incubation. Second, in order to maintain similar conditions when comparing digestion of amelogenin in solution and bound to HAP, all digestion reactions utilized constant and vigorous shaking to keep HAP particles suspended in solution. The shaking procedure is very critical in these experiments, because HAP easily forms big clumps, especially after amelogenin adsorption. In addition, we used both amelogenin and proteinases from human species that is different from other reported ones, which may be another reason for these different cleavage activities.

Proteins and peptides usually inhibit the crystal growth by blocking the attaching sites and they should be completely or partially detached to facilitate the further crystal growth (De Yoreo and Vekilov, 2003; De Yoreo et al., 2007; Friddle et al., 2010, 2011). Our proteolytic experiments (**Figure 1**) showed that MMP20 or KLK4 hydrolysis of amelogenin resulted in gradual loss of its binding affinity to HAP and nearly complete release of the protein from HAP. Furthermore, we found that KLK4 digested amelogenin more efficiently and more completely than MMP20, demonstrating its major role in the clearance of amelogenin from enamel matrix at the maturation stage.

A previous publication reported that HAP reduced amelogenin hydrolysis by MMP20 and KLK4 (Sun et al., 2010), which seems to contradict our current finding at the first glance. However, after further comparisons, we found that the difference was due to the different experimental systems and techniques used in these two studies. In Sun's study, HAP was the last component to be added into the reaction mixture containing amelogenin and proteinases. In contrast, in our system, amelogenin was first adsorbed onto HAP in a pre-binding step. We used the pre-binding procedure to saturate the HAP surfaces with amelogenins to mimic the physiological and developmental conditions *in vivo*. As we have known, in the secretory stage, enamel matrix contains a large amount of amelogenins and the majority of these amelogenins remain intact or are only partially hydrolyzed by proteinases (Smith et al., 1989). The amelogenin protein matrix surrounding the enamel crystals will interact with the surface of HAP, which would alter the conformation of the bound protein and in turn affect protein hydrolysis and crystal growth. The result that emerged from the experiments that utilized a pre-binding step prior to proteolysis indicated that the adsorption-induced changes of amelogenin hydrolysis should mainly result from the interactions between amelogenin and HAP crystal surfaces, rather than from the proteinase-crystal interactions as shown in our quenched peptide experiment (**Figure 5**).

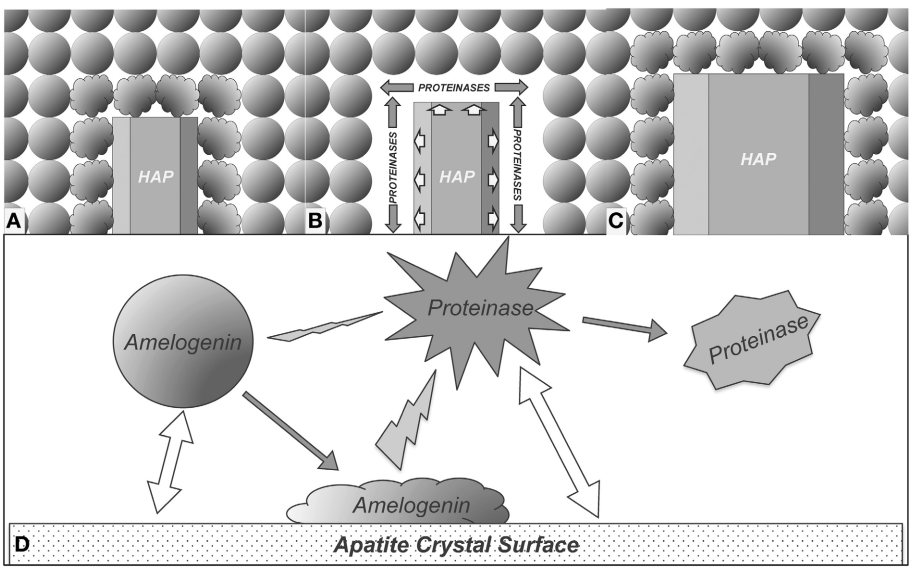

FIGURE 6 | Proposed model for enamel crystal growth guided by crystal-amelogenin-proteinase interactions. (A) HAP crystal interacts with amelogenins and causes their structural changes; **(B)** The structural changes of adsorbed amelogenins result in preferential amelogenin degradation on crystal surface; **(C)** Removal of the amelogenin on the crystal surface releases the space for HAP crystal growth; **(D)** Summary of the proposed model of enamel crystal growth guided by crystal-amelogenin-proteinase interactions. Amelogenin interactions with crystal surface change its conformation, which increases its susceptibility to proteinase. The direct effect of proteinase-crystal interactions will change the structure of proteinase, showing inhibitory effects.

In this experiment, different amounts of HAP were directly added into mixtures of MMP20 and its fluorescent substrate. The data showed dose-dependent inhibitory effects, indicating that the bare HAP can directly interact with MMP20 and inhibit its enzymatic activity.

Based on the results obtained from this study, we propose a model to explain how the enamel crystal growth is mediated by interactions among crystal, amelogenin, and proteinases. As shown in **Figure 6A**, the amelogenins secreted into enamel matrix first bind to the nascent HAP crystals and the adsorption of amelogenins onto the crystal surface results in conformational changes of the bound proteins. The conformational changes may expose more cleavage sites to proteinases. As a result, cleavage of amelogenins by MMP20 or KLK4 is enhanced (**Figure 6B**). The preferential removal of amelogenins from the crystal surface opens up the space surrounding the crystals for their further growth (**Figures 6C,D**). When the nascent crystals growing in this new space come into contact with the next layer of amelogenin nanospheres, yet another cycle of the interaction-mediated preferential removal of bound amelogenin and crystal growth is initiated. The cycle of *binding-growth-digestion* repeats until the HAP crystals grow to fill up the entire enamel space during tooth enamel development.

ACKNOWLEDGMENTS

This study was supported by National Institute of Health grant R01DE015821 and R01DE015821S1 to Wu Li. The UCSF SMMS Core Facility acknowledges the support of the Sandler Family Foundation and the Gordon & Betty Moore Family Foundation.

REFERENCES

Aoba, T., and Moreno, E. C. (1987). The enamel fluid in the early secretory stage of porcine amelogenesis: chemical composition and saturation with respect to enamel mineral. *Calcif. Tissue Int.* 41, 86–94. doi: 10.1007/BF02555250

Bartlett, J. D., and Simmer, J. P. (1999). Proteinases in developing dental enamel. *Crit. Rev. Oral Biol. Med.* 10, 425–441. doi: 10.1177/10454411990100040101

Bartlett, J. D., Simmer, J. P., Xue, J., Margolis, H. C., and Moreno, E. C. (1996). Molecular cloning and mRNA tissue distribution of a novel matrix metalloproteinase isolated from porcine enamel organ. *Gene* 183, 123–128. doi: 10.1016/S0378-1119(96)00525-2

Bartlett, J. D., Zhou, Z., Skobe, Z., Dobeck, J. M., and Tryggvason, K. (2003). Delayed tooth eruption in membrane type-1 matrix metalloproteinase deficient mice. *Connect. Tissue Res.* 44(Suppl. 1), 300–304. doi: 10.1080/713713624

Beniash, E., Simmer, J. P., and Margolis, H. C. (2012). Structural changes in amelogenin upon self-assembly and mineral interactions. *J. Dent. Res.* 91, 967–972. doi: 10.1177/0022034512457371

Chen, C. L., Bromley, K. M., Moradian-Oldak, J., and Deyoreo, J. J. (2012). *In situ* AFM study of amelogenin assembly and disassembly 2 dynamics on charged surfaces provides insights on matrix protein 3 self-assembly. *J. Am. Chem. Soc.* 134, 7–14. doi: 10.1021/ja206849c

Daculsi, G., Menanteau, J., Kerebel, L. M., and Mitre, D. (1984). Length and shape of enamel crystals. *Calcif. Tissue Int.* 36, 550–555. doi: 10.1007/BF02405364

De Yoreo, J., and Vekilov, P. (2003). "Principles of crystal nucleation and growth," in *Biomineralization, 1st Edn.*, eds P. M. Dove, J. J. De Yoreo, and S. Weiner (Washington, DC: Mineralogical Society of America), 57–93.

De Yoreo, J., Wierzbicki, A., and Dove, P. (2007). New insights into mechanisms of biomolecular control on growth of inorganic crystals. *Crys. Eng. Comm.* 9, 1144–1152. doi: 10.1039/b713006f

Doi, Y., Eanes, E. D., Shimokawa, H., and Termine, J. D. (1984). Inhibition of seeded growth of enamel apatite crystals by amelogenin and enamelin proteins *in vitro*. *J. Dent. Res.* 63, 98–105. doi: 10.1177/00220345840630021801

Fincham, A. G., Belcourt, A. B., Termine, J. D., Butler, W. T., and Cothran, W. C. (1981). Dental enamel matrix: sequences of two amelogenin polypeptides. *Biosci. Rep.* 1, 771–778. doi: 10.1007/BF01114799

Fincham, A. G., and Moradian-Oldak, J. (1995). Recent advances in amelogenin biochemistry. *Connect. Tissue Res.* 32, 119–124. doi: 10.3109/03008209509013713

Fincham, A. G., Moradian-Oldak, J., and Simmer, J. P. (1999). The structural biology of the developing dental enamel matrix. *J. Struct. Biol.* 126, 270–299. doi: 10.1006/jsbi.1999.4130

Friddle, R. W., Battle, K., Trubetskoy, V., Tao, J., Salter, E. A., Moradian-Oldak, J., et al. (2011). Single-molecule determination of the face-specific adsorption of Amelogenin's C-terminus on hydroxyapatite. *Angew. Chem. Int. Ed. Engl.* 50, 7541–7545. doi: 10.1002/anie.201100181

Friddle, R. W., Weaver, M. L., Qiu, S. R., Wierzbicki, A., Casey, W. H., and De Yoreo, J. J. (2010). Subnanometer atomic force microscopy of peptide-mineral interactions links clustering and competition to acceleration and catastrophe. *Proc. Natl. Acad. Sci. U.S.A.* 107, 11–15. doi: 10.1073/pnas.0908205107

Fukae, M., and Shimizu, M. (1974). Studies on the proteins of developing bovine enamel. *Arch. Oral Biol.* 19, 381–386. doi: 10.1016/0003-9969(74)90179-4

Fukae, M., Tanabe, T., Uchida, T., Lee, S. K., Ryu, O. H., Murakami, C., et al. (1998). Enamelysin (matrix metalloproteinase-20): localization in the developing tooth and effects of pH and calcium on amelogenin hydrolysis. *J. Dent. Res.* 77, 1580–1588. doi: 10.1177/00220345980770080501

Gibson, C. W., Yuan, Z. A., Hall, B., Longenecker, G., Chen, E., Thyagarajan, T., et al. (2001). Amelogenin-deficient mice display an amelogenesis imperfecta phenotype. *J. Biol. Chem.* 276, 31871–31875. doi: 10.1074/jbc.M104624200

Gray, J. J. (2004). The interaction of proteins with solid surfaces. *Curr. Opin. Struct. Biol.* 14, 110–115. doi: 10.1016/j.sbi.2003.12.001

Hart, P. S., Aldred, M. J., Crawford, P. J., Wright, N. J., Hart, T. C., and Wright, J. T. (2002). Amelogenesis imperfecta phenotype-genotype correlations with two amelogenin gene mutations. *Arch. Oral Biol.* 47, 261–265. doi: 10.1016/S0003-9969(02)00003-1

Hlady, V. V., and Buijs, J. (1996). Protein adsorption on solid surfaces. *Curr. Opin. Biotechnol.* 7, 72–77. doi: 10.1016/S0958-1669(96)80098-X

Ichijo, T., Yamashita, Y., and Terashima, T. (1992). Observations on the structural features and characteristics of biological apatite crystals. 2. Observation on the ultrastructure of human enamel crystals. *Bull. Tokyo Med. Dent. Univ.* 39, 71–80.

Iijima, M., Moriwaki, Y., Wen, H. B., Fincham, A. G., and Moradian-Oldak, J. (2002). Elongated growth of octacalcium phosphate crystals in recombinant amelogenin gels under controlled ionic flow. *J. Dent. Res.* 81, 69–73. doi: 10.1177/154405910208100115

Leblond, C. P., and Warshawsky, H. (1979). Dynamics of enamel formation in the rat incisor tooth. *J. Dent. Res.* 58, 950–975. doi: 10.1177/00220345790580024901

Li, W., Machule, D., Gao, C., and Denbesten, P. K. (1999). Activation of recombinant bovine matrix metalloproteinase-20 and its hydrolysis of two amelogenin oligopeptides. *Eur. J. Oral Sci.* 107, 352–359. doi: 10.1046/j.0909-8836.1999.eos107506.x

Margolis, H. C., Beniash, E., and Fowler, C. E. (2006). Role of macromolecular assembly of enamel matrix proteins in enamel formation. *J. Dent. Res.* 85, 775–793. doi: 10.1177/154405910608500902

Moradian-Oldak, J., Jimenez, I., Maltby, D., and Fincham, A. G. (2001). Controlled proteolysis of amelogenins reveals exposure of both carboxy- and amino-terminal regions. *Biopolymers* 58, 606–616. doi: 10.1002/1097-0282(200106)58:7%3C606::AID-BIP1034%3E3.0.CO;2-8

Nagano, T., Kakegawa, A., Gomi, K., Arai, T., and Simmer, J. (2008). "MMP-20 and KLK4 digestion of LRAP and TRAP," in *IADR/CADR 86th General* (Toronto, ON: Session).

Nagano, T., Kakegawa, A., Yamakoshi, Y., Tsuchiya, S., Hu, J. C., Gomi, K., et al. (2009). Mmp-20 and Klk4 cleavage site preferences for amelogenin sequences. *J. Dent. Res.* 88, 823–828. doi: 10.1177/0022034509342694

Nanci, A., Zalzal, S., Lavoie, P., Kunikata, M., Chen, W., Krebsbach, P. H., et al. (1998). Comparative immunochemical analyses of the developmental expression and distribution of ameloblastin and amelogenin in rat incisors. *J. Histochem. Cytochem.* 46, 911–934. doi: 10.1177/002215549804600806

Pergolizzi, S., Anastasi, G., Santoro, G., and Trimarchi, F. (1995). The shape of enamel crystals as seen with high resolution scanning electron microscope. *Ital. J. Anat. Embryol.* 100, 203–209.

Plate, U., and Hohling, H. J. (1994). Morphological and structural studies of early mineral formation in enamel of rat incisors by electron spectroscopic

imaging (ESI) and electron spectroscopic diffraction (ESD). *Cell Tissue Res.* 277, 151–158. doi: 10.1007/BF00303091

Robinson, C., Brookes, S. J., Shore, R. C., and Kirkham, J. (1998). The developing enamel matrix: nature and function. *Eur. J. Oral Sci.* 106(Suppl. 1), 282–291.

Ryu, O., Hu, J. C., Yamakoshi, Y., Villemain, J. L., Cao, X., Zhang, C., et al. (2002). Porcine kallikrein-4 activation, glycosylation, activity, and expression in prokaryotic and eukaryotic hosts. *Eur. J. Oral Sci.* 110, 358–365. doi: 10.1034/j.1600-0722.2002.21349.x

Ryu, O. H., Fincham, A. G., Hu, C. C., Zhang, C., Qian, Q., Bartlett, J. D., et al. (1999). Characterization of recombinant pig enamelysin activity and cleavage of recombinant pig and mouse amelogenins. *J. Dent. Res.* 78, 743–750. doi: 10.1177/00220345990780030601

Sakiyama, T., Aya, A., Embutsu, M., Imamura, K., and Nakanishi, K. (2006). Protease susceptibility of beta-lactoglobulin adsorbed on stainless steel surface as evidence of contribution of its specific segment to adsorption. *J. Biosci. Bioeng.* 101, 434–439. doi: 10.1263/jbb.101.434

Simmer, J. P., and Hu, J. C. (2002). Expression, structure, and function of enamel proteinases. *Connect. Tissue Res.* 43, 441–449. doi: 10.1080/713713530

Smith, C. E., Pompura, J. R., Borenstein, S., Fazel, A., and Nanci, A. (1989). Degradation and loss of matrix proteins from developing enamel. *Anat. Rec.* 224, 292–316. doi: 10.1002/ar.1092240219

Smolarczyk, K., Boncela, J., Szymanski, J., Gils, A., and Cierniewski, C. S. (2005). Fibrinogen contains cryptic PAI-1 binding sites that are exposed on binding to solid surfaces or limited proteolysis. *Arterioscler. Thromb. Vasc. Biol.* 25, 2679–2684. doi: 10.1161/01.ATV.0000189305.84297.8b

Sun, Z., Carpiaux, W., Fan, D., Fan, Y., Lakshminarayanan, R., and Moradian-Oldak, J. (2010). Apatite reduces amelogenin proteolysis by MMP-20 and KLK4 *in vitro*. *J. Dent. Res.* 89, 344–348. doi: 10.1177/0022034509360660

Tanimoto, K., Le, T., Zhu, L., Chen, J., Featherstone, J. D., Li, W., et al. (2008a). Effects of fluoride on the interactions between amelogenin and apatite crystals. *J. Dent. Res.* 87, 39–44. doi: 10.1177/154405910808700106

Tanimoto, K., Le, T., Zhu, L., Witkowska, H. E., Robinson, S., Hall, S., et al. (2008b). Reduced amelogenin-MMP20 interactions in amelogenesis imperfecta. *J. Dent. Res.* 87, 451–455. doi: 10.1177/154405910808700516

Tarasevich, B. J., Lea, S., Bernt, W., Engelhard, M. H., and Shaw, W. J. (2009b). Changes in the quaternary structure of amelogenin when adsorbed onto surfaces. *Biopolymers* 91, 103–107. doi: 10.1002/bip.21095

Tarasevich, B. J., Lea, S., Bernt, W., Engelhard, M., and Shaw, W. J. (2009a). Adsorption of amelogenin onto self-assembled and fluoroapatite surfaces. *J. Phys. Chem. B* 113, 1833–1842. doi: 10.1021/jp804548x

Termine, J. D., Eanes, E. D., and Conn, K. M. (1980). Phosphoprotein modulation of apatite crystallization. *Calcif. Tissue Int.* 31, 247–251. doi: 10.1007/BF02407188

Wang, S., Zhu, J., Zhang, Y., Li, L., Denbesten, P., and Li, W. (2006). On-column activation of bovine recombinant metalloproteinase 20. *Anal. Biochem.* 356, 291–293. doi: 10.1016/j.ab.2005.11.045

Wen, H. B., De Wijn, J. R., Van Blitterswijk, C. A., and De Groot, K. (1999). Incorporation of bovine serum albumin in calcium phosphate coating on titanium. *J Biomed Mater Res.* 46, 245–252.

Wright, J. T., Hart, P. S., Aldred, M. J., Seow, K., Crawford, P. J., Hong, S. P., et al. (2003). Relationship of phenotype and genotype in X-linked amelogenesis imperfecta. *Connect. Tissue Res.* 44(Suppl. 1), 72–78. doi: 10.1080/713713640

Zhu, L., Tanimoto, K., Le, T., Denbesten, P. K., and Li, W. (2009). Functional roles of prolines at amelogenin C terminal during tooth enamel formation. *Cells Tissues Organs* 189, 203–206. doi: 10.1159/000151376

Zhu, L., Uskoković, V., Le, T., Denbesten, P., Huang, Y., Habelitz, S., et al. (2011). Altered self-assembly and apatite binding of amelogenin induced by N-terminal proline mutation. *Arch. Oral Biol.* 56, 331–336. doi: 10.1016/j.archoralbio.2010.10.017

Conflict of Interest Statement: The authors declare that the research was conducted in the absence of any commercial or financial relationships that could be construed as a potential conflict of interest.

Received: 28 May 2014; paper pending published: 09 June 2014; accepted: 26 June 2014; published online: 24 July 2014.

*Citation: Zhu L, Liu H, Witkowska HE, Huang Y, Tanimoto K and Li W (2014) Preferential and selective degradation and removal of amelogenin adsorbed on hydroxyapatites by MMP20 and KLK4 in vitro. Front. Physiol. **5**:268. doi: 10.3389/fphys.2014.00268*

This article was submitted to Craniofacial Biology, a section of the journal Frontiers in Physiology.

frontiers in
PHYSIOLOGY

REVIEW ARTICLE
published: 04 July 2014
doi: 10.3389/fphys.2014.00240

Kallikrein-related peptidase-4 (KLK4): role in enamel formation and revelations from ablated mice

John D. Bartlett [1,2]* ***and James P. Simmer*** [3]

[1] *Harvard School of Dental Medicine, Boston, MA*
[2] *Department of Mineralized Tissue Biology, The Forsyth Institute, Cambridge, MA*
[3] *Department of Biological and Material Sciences, University of Michigan School of Dentistry, Ann Arbor, MI, USA*

Edited by:
Megan Pugach-Gordon, The Forsyth Insitute, USA

Reviewed by:
Tom Diekwisch, University of Illinois at Chicago, USA
Michael Paine, University of Southern California, USA

****Correspondence:***
John D. Bartlett, Harvard School of Dental Medicine; Department of Mineralized Tissue Biology, The Forsyth Institute, 245 First Street, Cambridge, MA 02142, USA
e-mail: jbartlett@forsyth.org

Enamel development occurs in stages. During the secretory stage, a soft protein rich enamel layer is produced that expands to reach its final thickness. During the maturation stage, proteins are removed and the enamel matures into the hardest substance in the body. KLK4 is expressed during the transition from secretory to the maturation stage and its expression continues throughout maturation. KLK4 is a glycosylated chymotrypsin-like serine protease that cleaves enamel matrix proteins prior to their export out of the hardening enamel layer. Mutations in *KLK4* can cause autosomal recessive, non-syndromic enamel malformations in humans and mice. *Klk4* ablated mice initially have normal-looking teeth with enamel of full thickness. However, the enamel is soft and protein-rich. Three findings are notable from *Klk4* ablated mice: first, enamel rods fall from the interrod enamel leaving behind empty holes where the enamel fractures near the underlying dentin surface. Second, the ∼10,000 crystallites that normally fuse to form a solid enamel rod fail to grow together in the ablated mice and can fall out of the rods. Third, and most striking, the crystallites grow substantially in width and thickness (a- and b-axis) in the ablated mice until they almost interlock. The crystallites grow in defined enamel rods, but interlocking is prevented presumably because too much protein remains. Conventional thought holds that enamel proteins bind specifically to the sides of enamel crystals to inhibit growth in width and thickness so that the thin, ribbon-like enamel crystallites grow predominantly in length. Results from *Klk4* ablated mice demonstrate that this convention requires updating. An alternative mechanism is proposed whereby enamel proteins serve to form a mold or support structure that shapes and orients the mineral ribbons as they grow in length. The remnants of this support structure must be removed by KLK4 so that the crystallites can interlock to form fully hardened enamel.

Keywords: enamel development, MMP20, amelogenin, ameloblastin, enamelin, enamel crystallites, enamel rods

INTRODUCTION

The enamel layer covers the crown of the tooth and is unique because it is an epithelially-derived calcified tissue and becomes the hardest substance in the body. Its hardness is between that of iron and carbon steel, but enamel has a higher elasticity (Newbrun and Pigman, 1960). Enamel hardness is a function of its high mineral content. Unlike bone and dentin (20–30% organic material by weight), fully formed enamel contains very little protein (less than 1% organic material) (Lefevre and Manly, 1938; Deakins and Volker, 1941). Enamel mineral is very similar to hydroxyapatite (HAP) [$Ca_5OH\ (PO_4)_3$], but also contains low percentages of carbonate, sodium, and magnesium. Therefore within the body, teeth are the most resistant to deterioration and have been examined extensively for anthropological studies.

But, what are the developmental and mechanistic processes that make enamel harder than the cementum formed along the tooth root, the dentin underlying the enamel layer, and the skeletal bones? The ameloblasts are a single cell layer that cover the developing enamel and are responsible for enamel composition. Enamel development (amelogenesis) can be broken down into three defined stages: secretory, transition and maturation. The stages are defined by the morphology and function of the ameloblasts. Dentin mineralizes first and pre-ameloblasts transform into secretory stage ameloblasts by elongating into tall columnar cells and by forming Tomes' processes at their apical ends nearest the forming enamel. The Tomes' process is a conical structure that points toward the forming enamel matrix. Enamel matrix proteins are primarily secreted from one side of the Tomes' process (secretory face) and all ameloblasts within a row secrete protein from the same side of their Tomes' processes. The first formed enamel ribbons grow between the dentin crystals perhaps by mineralizing around dentin proteins such as collagen. At their growing tips near the Tomes' process, secretory stage enamel ribbons are only about 1.5 nm thick and 15 nm wide (Daculsi and Kerebel, 1978; Cuisinier et al., 1992) and these ribbons are extended until they span the entire thickness of the enamel layer. Approximately 10,000 parallel mineral ribbons are present in each enamel rod (Daculsi et al., 1984). A rod is about 5 μm

in cross-sectional diameter (Skobe and Stern, 1980) and each is generated by a single ameloblast (Skobe, 1977). Enamel ribbons elongate at the mineralization front where enamel proteins are secreted (Ronnholm, 1962). As the ameloblasts secrete large amounts of enamel matrix proteins, they move away from the dentin surface so that the nascent enamel layer can thicken. The mineral ribbons crystallize into HAP within the rod and will grow progressively in c-axis length parallel to one another as the ameloblasts move progressively away from the dentin surface. The crystallites are surrounded with abundant proteins that prevent them from fusing into a solid rod. The secretory stage enamel is therefore protein rich and has a soft cheese-like consistency.

During the secretory stage, ameloblasts not only move away from the dentin as the enamel thickens, but they also move in groups that slide by one another and this movement culminates in the characteristic decussating enamel prism pattern observed in rodent incisors (Reith and Ross, 1973) or the entwined gnarled prism pattern seen in human molars (Boyde, 1989). Secretory stage ameloblasts secrete four different proteins into the enamel matrix. Three are "structural" proteins and one is a proteinase. The structural proteins are amelogenin (AMELX), ameloblastin (AMBN), enamelin (ENAM), and the proteinase is matrix metalloproteinase-20 (MMP20, enamelysin). Amelogenin comprises approximately 80–90% of the organic matter within the secretory stage enamel matrix and ameloblastin and enamelin comprise roughly 5 and 3–5%, respectively (Fincham et al., 1999; Hu et al., 2007). MMP20 is present in trace amounts. The precise function of these proteins remains unclear. However, human mutations in *AMELX* (Hu et al., 2012), *ENAM* (Rajpar et al., 2001), and *MMP20* (Kim et al., 2005; Ozdemir et al., 2005; Lee et al., 2010; Gasse et al., 2013) genes and mouse knockout models (Gibson et al., 2001; Caterina et al., 2002; Fukumoto et al., 2004; Masuya et al., 2005; Seedorf et al., 2007; Hu et al., 2008) have definitively demonstrated that each of these proteins are absolutely required for proper enamel formation. This conclusion is supported by the observation that the genes encoding secretory stage enamel proteins are consistently pseudogenized in vertebrates that have lost the ability to make teeth, or specifically dental enamel, during evolution (Meredith et al., 2009, 2011, 2013). By the end of the secretory stage the enamel layer has achieved its full thickness. It is not until the end of the maturation stage when the proteins are almost completely removed, that the enamel achieves its final hardened form.

As the ameloblasts enter the transition stage, they no longer move relative to each other. They retract their Tomes' processes and transition into shorter and fatter maturation stage cells and, at the enamel surface, start modulating between ruffle and smooth-ended cells (Smith, 1998). It is during the maturation stage that ameloblasts actively secrete kallikrein-related peptidase-4 (KLK4) to help remove the mass of previously secreted and partially hydrolyzed (by MMP20) matrix proteins from the enamel layer so that the crystallites can expand, coalesce and fuse with adjacent crystals (Simmer et al., 2009). This strengthens the enamel rods and forms the most highly mineralized substance in the body. Therefore, unlike cementum, dentin and bone, the proteins responsible for mineralization are removed from enamel so that the enamel can attain its final hardened form. Also, relative to the other mineralized tissues, the entwined rod and interrod enamel forms a more highly ordered 3D structure that is highly resistant to occlusal forces. The stages of enamel development and the developmental processes as the enamel forms are remarkably similar in different mammalian species (Weinmann et al., 1942; Robinson et al., 1988). Rodents have continuously erupting incisors so every developmental stage is always present in specific locations along the forming rodent incisor.

ENAMEL PROTEINASES

The proteinase expressed during the secretory through early maturation stage is MMP20 (Begue-Kirn et al., 1998) and the proteinase expressed from the transition through maturation stages is KLK4 (Hu et al., 2002). To date, these are the only two proteinases proven to be secreted into the enamel matrix (Bartlett, 2013). Both proteinases are present in small amounts during enamel development and each proteinase was separately cloned by performing PCR-based homology cloning (Bartlett et al., 1996; Simmer et al., 1998). KLK4 was originally named enamel matrix serine proteinase-1 (EMSP1) (Simmer et al., 1998), but its name was changed to KLK4 because the gene encoding KLK4 locates within the kallikrein gene cluster.

Human and mouse mutations in both *MMP20* (Caterina et al., 2002; Kim et al., 2005; Ozdemir et al., 2005; Lee et al., 2010; Gasse et al., 2013) and *KLK4* (Hart et al., 2004; Simmer et al., 2009; Wang et al., 2013) cause severe enamel malformations and therefore demonstrate that no other proteinase has an extensive overlapping function with either of these proteinases. If this were the case, no severe enamel phenotype would likely occur if the activity of MMP20 or KLK4 were compromised. Furthermore, accumulated porcine secretory stage enamel protein cleavage products have been extensively characterized and MMP20 specifically cleaves recombinant enamel proteins *in vitro* to generate the full spectrum of cleavages that occur *in vivo* (Ryu et al., 1999; Nagano et al., 2009). Others have proposed that MMP9 is present within secretory stage developing enamel (Feng et al., 2012). However, this claim is uncertain as MMP20 activity can explain all of the secretory stage amelogenin cleavages and MMP9 mutations cause metaphyseal anadysplasia, which is not associated with enamel defects (Lausch et al., 2009). Similarly, chymotrypsin C is associated with enamel formation (Lacruz et al., 2011). However, although loss of *CTRC* function is a risk factor for pancreatitis, an associated enamel phenotype has not been described (Zhou and Sahin-Toth, 2011). Signal-peptide-peptidase-like 2a (SPPL2A) is a membrane bound protease in lysosomes/late endosomes that is expressed by enamel epithelium during the secretory and maturation stages of amelogenesis. Spll2a null mice show defective enamel, highlighting the importance of intracellular degradation of enamel proteins reabsorbed by endocytosis (Bronckers et al., 2013). Although it is likely that several proteases degrade enamel proteins within ameloblast lysosomes, MMP20, and KLK4 remain the only proteinases that are known to be secreted into the enamel matrix (Bartlett, 2013).

DISCOVERY OF KLK4

In 1977 a protease was purified from pig enamel (Fukae et al., 1977) that was later demonstrated to be inhibited by serine proteinase inhibitors phenylmethylsulfonyl fluoride (PMSF) and

diisopropylfluoro phosphate (DIFP) (Shimizu et al., 1979). This protease was expressed during the early maturation stage when the enamel proteins are reabsorbed from the hardening enamel (Overall and Limeback, 1988). KLK4 was eventually cloned by PCR-based homology cloning from porcine cDNA with subsequent screening of a porcine cDNA library (Simmer et al., 1998). The porcine KLK4 preproenzyme is composed of 254 amino acids while the proenzyme has 230 residues and the active form has 224 amino acids (Simmer et al., 1998). The *KLK4* genes of both mouse and human have six exons the first of which is non-coding. The mouse *Klk4* gene is approximately 10 kb in size and locates in cytogenic region B2 on mouse chromosome 7 (Hu et al., 2000b). The human *KLK4* gene is approximately 7 kb in size and is located near the telomere of chromosome 19 (19q13.3–19q13.4) in a cluster of genes including the KLK family of serine proteases. Its gene exon/intron structure and protein domain structure is identical to that of the mouse (Hu et al., 2000b). Thus, because KLK4/EMSP1 was cloned after MMP20, it became the second proteinase identified by name that is secreted into the developing enamel matrix.

KLK4 TISSUE LOCALIZATION

KLK4 is a glycosylated, chymotrypsin-like serine protease that is expressed and secreted by transition to maturation stage ameloblasts (Hu et al., 2000a,b, 2002). KLK4 protein has not been isolated from any tissue other than from developing teeth (Ryu et al., 2002; Nagano et al., 2009). However, several studies have performed immunoassays or qPCR techniques to identify KLK4 in various tissues and many of these studies conflict with one another as to exactly where KLK4 is expressed (reviewed in Simmer et al., 2011b). To definitively identify where KLK4 is expressed, a gene targeted mouse strain was developed. These mice have a *LacZ* reporter gene with a mouse nuclear localization signal (NLS-βgal) inserted at the natural *Klk4* translation initiation site. Therefore, with these mice, locations of KLK4 expression were identified within tissues by using β-galactosidase histochemistry (Simmer et al., 2009). KLK4 was expressed highly in maturation stage ameloblasts (**Figure 1**) and low levels of KLK4 expression were observed in the striated ducts of the submandibular salivary gland and in small patches of prostate epithelia. Furthermore, in these *Klk4 LacZ* knock-in mice, no obvious morphological abnormalities were observed in any of the non-dental tissues examined suggesting that their normal development is not *Klk4* dependent (Simmer et al., 2011b). As is true for MMP20, it appears that the only essential, non-overlapping function of KLK4 is in enamel development.

KLK4 ACTIVATION

It is not known how KLK4 is activated *in vivo*. Removal of the KLK4 propeptide is essential for activation because it allows a salt linkage to form between the new N-terminus and the side chain of Asp194 and this is essential for enzyme activity (Scully et al., 1998; Debela et al., 2006). Unlike the other kallikrein-related peptidases, KLK4 has a Gln as the last residue of its propeptide and not an Arg or Lys which means that KLK4 cannot be activated by trypsin-like enzymes (Lundwall and Brattsand, 2008). KLK4 cannot activate itself, but can be activated by MMP20 and thermolysin *in vitro* (Ryu et al., 2002). However, KLK4 is active in *Mmp20* ablated mice (Yamakoshi et al., 2011) so MMP20 cannot be the sole KLK4 activator. Previously it was shown that dipeptidyl peptidase I (Cathepsin C, CTSC) activates KLK4 *in vitro* (Tye et al., 2009). In the enamel organ, CTSC is expressed at progressively increasing levels as development progresses to the early maturation stage when KLK4 begins its expression. Therefore, it remains a possibility that this cysteine aminopeptidase is the primary enzyme that activates KLK4.

KLK4 SUBSTRATE SPECIFICITY

KLK4 was assessed for its substrate specificity by using recombinant KLK4 to screen tetrapeptide positional scanning synthetic combinatorial libraries (PS-SCL) (Matsumura et al., 2005). The identified preferred P1–P4 positions were:

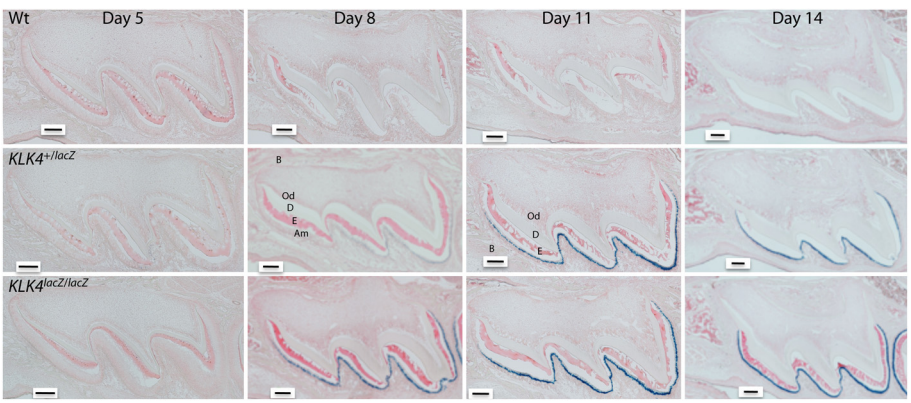

FIGURE 1 | Histochemical detection of β-galactosidase activity in maxillary first molars of wild-type (Wt) heterozygous (*Klk4*$^{+/lacZ}$) and homozygous (*Klk4*$^{lacZ/lacZ}$) mice at postnatal days 5, 8, 11, and 14. LacZ histochemistry shows nuclear localized β-galactosidase activity where KLK4 is normally expressed. At the 5-h incubation used, no endogenous (lysosomal) β-gal activity was observed and the Wt mice were negative. In mouse molars, a positive signal was only observed in transition and maturation ameloblasts. No expression was observed in odontoblasts. B, Bone; Od, odontoblasts; D, dentin; E, enamel; Am, ameloblasts. Scale bars = 100 μm. This figure was reprinted with permission (S. Karger AG, Basel) from Simmer et al. (2011a).

P1-Arg; P2-Gln/Leu/Val; P3-Gln/Ser/Val and P4-Ile/Val. The first report demonstrating that KLK4 cleaves amelogenin, used native porcine KLK4 incubated with recombinant pig amelogenin and this resulted in the generation of twelve cleavage products which were characterized by N-terminal sequencing (Ryu et al., 2002). It was subsequently demonstrated that the primary MMP20 N-terminal cleavage product, tyrosine-rich amelogenin polypeptide (TRAP), was further cleaved by KLK4 which was consistent with the notion that KLK4 cleaves enamel matrix proteins into small peptides to facilitate their export out of the enamel as the enamel hardens (Nagano et al., 2009). Porcine ameloblastin was stably expressed and secreted from HEK293-N cells and was purified for digestion by KLK4. The cleavage products were characterized by N-terminal sequencing and KLK4 was shown to cleave ameloblastin at nine different sites (Chun et al., 2010). The 32 kDa enamelin is presumed to be an MMP20 cleavage product and it is the only domain of the parent protein that accumulates in the deeper, more mature enamel layer. Native porcine KLK4 was incubated with native porcine 32 kDa enamelin and the digestion products were fractionated by reverse-phase high-performance liquid chromatography (RP-HPLC) and characterized by Edman sequencing, amino acid analysis, and mass spectrometry. KLK4 digestion of the 32-kDa enamelin generated nine major cleavage products (Yamakoshi et al., 2006). Therefore, KLK4 cleaves all the structural enamel matrix proteins that are known to be secreted into the enamel matrix. Recently, it was confirmed that MMP20 activates pro-KLK4 and strikingly, that active KLK4 cleaves and inactivates MMP20 (Yamakoshi et al., 2013). In effect, by activating KLK4, MMP20 inactivates itself. This mechanism of MMP20 inactivation is supported by evidence demonstrating that in *Klk4* ablated mice, MMP20 is active well into the maturation stage when MMP20 activity has normally ceased (Yamakoshi et al., 2011).

HUMAN *KLK4* MUTATIONS

Two different human *KLK4* mutations are known to cause autosomal recessive hypomaturation *amelogenesis imperfecta*. The first discovered is a nonsense mutation occurring upstream of the KLK4 catalytic domain (p.Trp153*). This tryptophan residue is completely conserved in mouse and pig KLK4 and expression of this mutated gene would result in a truncated protein lacking the final 101 amino acids which includes the catalytic triad (His71, Asp116, and Ser207). This homozygous mutation occurred in two female siblings and both their primary and permanent dentitions were similarly affected. The sibling's teeth were yellow-brown in color and were excessively sensitive to hot and cold. The enamel was normal in thickness, but radiographically showed only a slight increase in opacity over that of the underling dentin indicating a decreased enamel mineral content. This soft enamel fractured from the occlusal surfaces of the primary molars (Hart et al., 2004). No other phenotype resulted from this nonsense mutation in *KLK4*. The second human *KLK4* mutation was recently discovered by use of whole exome sequencing which identified a single nucleotide deletion (p.Gly82Alafs*87) in both alleles of a 9 year-old female. The frameshift was in the third of five coding exons so the mutant *KLK4* transcripts may have been degraded by nonsense-mediated decay. If translated, the mutant protein would lack the same catalytic triad that was also lacking in the first discovered *KLK4* mutation. As for the previously discovered KLK4 mutation, the enamel covering this proband's teeth appeared normal in size and shape, but was discolored yellow-brown and chipped on multiple teeth. This proband was also secondarily affected with dental caries (Wang et al., 2013). No other phenotype was observed due to the nucleotide deletion in *KLK4*. Therefore, in humans KLK4 is essential for enamel to achieve its final hardened form, and that just as for MMP20, the only non-overlapping function of KLK4 is in dental enamel development.

THE *KLK4 KNOCKOUT/LACZ* KNOCKIN MOUSE

As stated above under KLK4 tissue localization, gene targeting was used to generate a mouse strain carrying a null allele of *Klk4* that has a nuclear *LacZ* reporter gene inserted directly into the *Klk4* translation initiation site. Therefore, the *LacZ* code was positioned in the same genomic context as wild-type *Klk4* and so provided a sensitive tissue reporter for native *Klk4* expression (Simmer et al., 2009). Other than a tooth phenotype, the *Klk4* ablated mice were normal. The teeth were normal, the enamel attained normal thickness and no abnormalities were observed until the enamel reached the transition to early maturation stage of development. At this point, the normal export of enamel matrix proteins from the matrix back to the ameloblasts destined for lysosomal degradation was impeded. The enamel retained proteins that were normally removed and the soft, protein-rich enamel abraded from the mouse teeth (**Figures 2A–C**). This strongly supports the belief that KLK4 functions to cleave enamel matrix proteins to facilitate their export out of the hardening enamel (Simmer et al., 2009). Unexpectedly, the rod enamel sometimes pulled away from interrod enamel. This left holes in the interrod enamel that were once filled by enamel rods (**Figures 2D,E**) (Simmer et al., 2009, 2011a). Backscatter scanning electron microscopy revealed that the enamel layer of *Klk4* null mice is reasonably well-mineralized at the surface, but is progressively less mineralized with depth (Hu et al., 2011; Smith et al., 2011). This pattern suggests that extracellular degradation of enamel proteins by KLK4 facilitates the movement of proteins in the deeper enamel toward the surface for ameloblast endocytosis.

Another observation in the *Klk4* null mice was that the lack of KLK4 activity prevented the individual crystals within the rod from growing sufficiently in width and thickness so that they could interlock with adjacent crystals. Strikingly, bunches of crystals appeared to fall out of the rods and separate into individual crystals (**Figure 3**) similar in appearance to strands (crystals) of "uncooked angel hair spaghetti" falling out of a circular bundle (rod). Although the normal rod pattern was present in the *Klk4* ablated enamel, the ~10,000 crystallites within the rod failed to interlock properly and the crystallites fell from the rods (Simmer et al., 2009). Developmental analyses of *Klk4* null incisor enamel showed that percent mineral by weight increased almost identically to that occurring in wild-type mice until mid-maturation when a level of about 80% mineral by weight was attained. In contrast to wild-type enamel, the mineral content of the null mouse enamel remained unchanged as development progressed

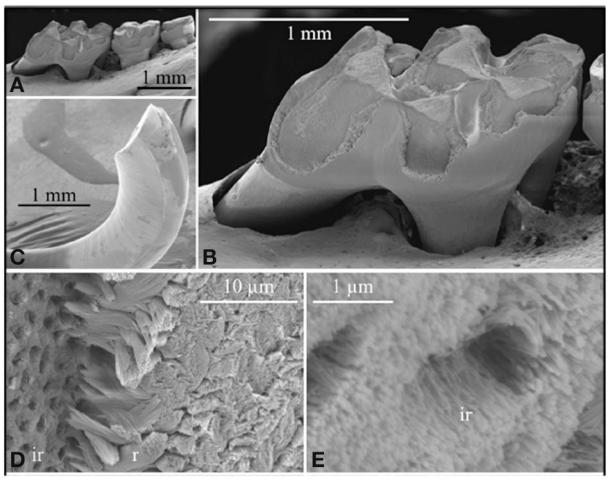

FIGURE 2 | Scanning electron micropscopy of the mandibular molars (A,B) and mandibular incisor (C–E) of a *Klk4* null mouse at 7 weeks. The enamel of all molars showed a significant loss of enamel from all working surfaces (buccal cusps, occlusal surface, and marginal ridges) **(A,B)**. Similarly, the enamel layer was abraded at the working (buccal) surface of the mandibular incisor at its tip **(C)**. Higher magnification of the chipped area near the tip of the incisor showed the break was in the enamel layer, close to, but not at the DEJ. The broken surface appears to be composed of interrod (ir) enamel with holes where enamel rods (r) had pulled out and separated **(D)** from the initial deposit of interrod enamel near the DEJ. The holes are too numerous to be made by odontoblastic processes penetrating the enamel (enamel spindles). The orientation of the crystallites on the walls of the holes is parallel to the direction of the tubular holes and to the crystallites between the holes **(E)**. This figure was originally published by the American Society for Biochemistry and Molecular Biology in Simmer et al. (2009).

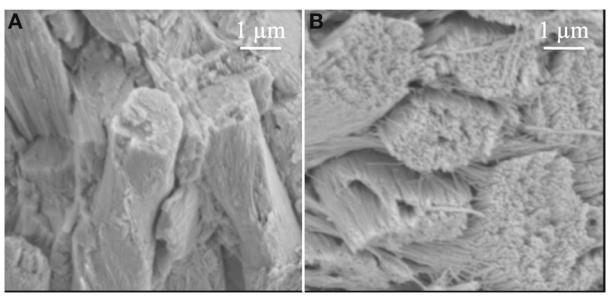

FIGURE 3 | Comparison of enamel rods from (A) wild-type and (B) *Klk4* null mice. Enamel rods in wild-type mice have tightly packed crystallites that lose some aspect of their individuality. Enamel rods in the *Klk4* null mice are composed of distinctly individual crystallites resembling angel hair spaghetti. Holes or vacancies in some rods give the impression that smaller bundles of crystallites broke at a slightly deeper level and slid out of the rod. This figure was originally published by the American Society for Biochemistry and Molecular Biology in Simmer et al. (2009).

through the maturation stage (Smith et al., 2011). This seminal finding indicated that enamel maturation advanced normally, even in the presence of abundant protein, but arrested when the residual protein physically blocked final crystal maturation by occupying the shrinking space between crystals. If amelogenins and/or the other proteins inhibited crystal maturation by selectively binding to the sides of enamel crystals, the inhibition would have occurred earlier and would have resulted in a more severe enamel phenotype. All-in-all, the *Klk4* knockin/knockout mouse has revealed surprises about enamel formation and has forced us to reexamine some of our more firmly held beliefs about how crystallites grow in width and thickness and interlock to form an enamel rod.

A MODIFIED THEORY OF ENAMEL DEVELOPMENT

During the secretory stage, proteins are secreted into the enamel matrix and are quickly cleaved by MMP20. Selected enamel protein cleavage products accumulate within the matrix and as new proteins are secreted they also are cleaved so that an abundance of MMP20 cleavage products are present throughout the enamel layer as the entire enamel layer grows away (thickens) from the dentin. Previously it was demonstrated that enamel mineral first forms as amorphous calcium phosphate (ACP) (Bodier-Houlle et al., 2000; Beniash et al., 2009). ACP has no defined structure. It can be thought of as "grains of sand" that require a mold if it is to have defined 3D structure. However, as described above, the enamel crystallites have a very specific shape. They grow into long thin ribbons. So it is postulated that the MMP20 cleavage products form a mold to define the shape of each crystallite ribbon so that the ACP can attain the proper shape prior to its conversion into HAP. Therefore, the nucleation event for mineral formation would occur within the protein mold so that the ACP will form a proper 3D ribbon structure prior to when it crystallizes into HAP. It is envisioned that the crystallite ribbon molds protect the crystallite ribbons, much as packaging material protects the contents of a box, as the enamel crystallites elongate from the dentin surface to the eventual outer surface of the enamel layer. This new theory (Simmer et al., 2012) represents a departure from previous beliefs that amelogenin by itself initiates enamel formation and from the thought that amelogenin inhibits crystallite growth in width and thickness (Bartlett and Simmer, 1999). In summary, results from the *Klk4* knockin/knockout mouse have led us to reevaluate our theories of enamel formation because we now have attained a better understanding of the importance of KLK4 activity and why it is so critical in enamel development.

ACKNOWLEDGMENTS

Research reported in this publication was supported by the National Institute of Dental and Craniofacial Research of the National Institutes of Health under award numbers RO1DE016276 (John D. Bartlett) and R01DE019775 (James P. Simmer).

REFERENCES

Bartlett, J. D. (2013). Dental enamel development: proteinases and their enamel matrix substrates. *ISRN Dent.* 2013, 684607. doi: 10.1155/2013/684607

Bartlett, J. D., and Simmer, J. P. (1999). Proteinases in developing dental enamel. *Crit. Rev. Oral Biol. Med.* 10, 425–441. doi: 10.1177/10454411990100040101

Bartlett, J. D., Simmer, J. P., Xue, J., Margolis, H. C., and Moreno, E. C. (1996). Molecular cloning and mRNA tissue distribution of a novel matrix metalloproteinase isolated from porcine enamel organ. *Gene* 183, 123–128. doi: 10.1016/S0378-1119(96)00525-2

Begue-Kirn, C., Krebsbach, P. H., Bartlett, J. D., and Butler, W. T. (1998). Dentin sialoprotein, dentin phosphoprotein, enamelysin and ameloblastin: tooth-specific molecules that are distinctively expressed during murine dental differentiation. *Eur. J. Oral Sci.* 106, 963–970. doi: 10.1046/j.0909-8836.1998.eos106510.x

Beniash, E., Metzler, R. A., Lam, R. S., and Gilbert, P. U. (2009). Transient amorphous calcium phosphate in forming enamel. *J. Struct. Biol.* 166, 133–143. doi: 10.1016/j.jsb.2009.02.001

Bodier-Houlle, P., Steuer, P., Meyer, J. M., Bigeard, L., and Cuisinier, F. J. (2000). High-resolution electron-microscopic study of the relationship between human enamel and dentin crystals at the dentinoenamel junction. *Cell Tissue Res.* 301, 389–395. doi: 10.1007/s004410000241

Boyde, A. (1989). "Enamel," in *Handbook of Microscopic Anatomy*, eds A. Oksche and L. Vollrath (Berlin: Springer-Verlag), 309–473.

Bronckers, A. L., Gueneli, N., Lullmann-Rauch, R., Schneppenheim, J., Moraru, A. P., Himmerkus, N., et al. (2013). The intramembrane protease SPPL2A is critical for tooth enamel formation. *J. Bone Miner. Res.* 28, 1622–1630. doi: 10.1002/jbmr.1895

Caterina, J. J., Skobe, Z., Shi, J., Ding, Y., Simmer, J. P., Birkedal-Hansen, H., et al. (2002). Enamelysin (matrix metalloproteinase 20)-deficient mice display an amelogenesis imperfecta phenotype. *J. Biol. Chem.* 277, 49598–49604. doi: 10.1074/jbc.M209100200

Chun, Y. H., Yamakoshi, Y., Yamakoshi, F., Fukae, M., Hu, J. C., Bartlett, J. D., et al. (2010). Cleavage site specificity of MMP-20 for secretory-stage ameloblastin. *J. Dent. Res.* 89, 785–790. doi: 10.1177/0022034510366903

Cuisinier, F. J., Steuer, P., Senger, B., Voegel, J. C., and Frank, R. M. (1992). Human amelogenesis. I: high resolution electron microscopy study of ribbon-like crystals. *Calcif. Tissue Int.* 51, 259–268. doi: 10.1007/BF00334485

Daculsi, G., and Kerebel, B. (1978). High-resolution electron microscope study of human enamel crystallites: size, shape, and growth. *J. Ultrastruct. Res.* 65, 163–172. doi: 10.1016/S0022-5320(78)90053-9

Daculsi, G., Menanteau, J., Kerebel, L. M., and Mitre, D. (1984). Length and shape of enamel crystals. *Calcif. Tissue Int.* 36, 550–555. doi: 10.1007/BF02405364

Deakins, M., and Volker, J. F. (1941). Amount of organic matter in enamel from several types of human teeth. *J. Dent. Res.* 20, 117–121. doi: 10.1177/00220345410200020201

Debela, M., Magdolen, V., Grimminger, V., Sommerhoff, C., Messerschmidt, A., Huber, R., et al. (2006). Crystal structures of human tissue kallikrein 4: activity modulation by a specific zinc binding site. *J. Mol. Biol.* 362, 1094–1107. doi: 10.1016/j.jmb.2006.08.003

Feng, J., Mcdaniel, J. S., Chuang, H. H., Huang, O., Rakian, A., Xu, X., et al. (2012). Binding of amelogenin to MMP-9 and their co-expression in developing mouse teeth. *J. Mol. Histol.* 43, 473–485. doi: 10.1007/s10735-012-9423-1

Fincham, A. G., Moradian-Oldak, J., and Simmer, J. P. (1999). The structural biology of the developing dental enamel matrix. *J. Struct. Biol.* 126, 270–299. doi: 10.1006/jsbi.1999.4130

Fukae, M., Tanabe, T., and Shimizu, M. (1977). Proteolytic enzyme activity in porcine immature enamel. *Tsurumi Shigaku* 3, 15–17.

Fukumoto, S., Kiba, T., Hall, B., Iehara, N., Nakamura, T., Longenecker, G., et al. (2004). Ameloblastin is a cell adhesion molecule required for maintaining the differentiation state of ameloblasts. *J. Cell Biol.* 167, 973–983. doi: 10.1083/jcb.200409077

Gasse, B., Karayigit, E., Mathieu, E., Jung, S., Garret, A., Huckert, M., et al. (2013). Homozygous and compound heterozygous MMP20 mutations in amelogenesis imperfecta. *J. Dent. Res.* 92, 598–603. doi: 10.1177/0022034513488393

Gibson, C. W., Yuan, Z. A., Hall, B., Longenecker, G., Chen, E., Thyagarajan, T., et al. (2001). Amelogenin-deficient mice display an amelogenesis imperfecta phenotype. *J. Biol. Chem.* 276, 31871–31875. doi: 10.1074/jbc.M104624200

Hart, P. S., Hart, T. C., Michalec, M. D., Ryu, O. H., Simmons, D., Hong, S., et al. (2004). Mutation in kallikrein 4 causes autosomal recessive hypomaturation amelogenesis imperfecta. *J. Med. Genet.* 41, 545–549. doi: 10.1136/jmg.2003.017657

Hu, J. C., Chan, H. C., Simmer, S. G., Seymen, F., Richardson, A. S., Hu, Y., et al. (2012). Amelogenesis imperfecta in two families with defined AMELX deletions in ARHGAP6. *PLoS ONE* 7:e52052. doi: 10.1371/journal.pone.0052052

Hu, J. C., Chun, Y. H., Al Hazzazzi, T., and Simmer, J. P. (2007). Enamel formation and amelogenesis imperfecta. *Cells Tissues Organs* 186, 78–85. doi: 10.1159/000102683

Hu, J. C., Hu, Y., Smith, C. E., McKee, M. D., Wright, J. T., Yamakoshi, Y., et al. (2008). Enamel defects and ameloblast-specific expression in Enam knock-out/lacz knock-in mice. *J. Biol. Chem.* 283, 10858–10871. doi: 10.1074/jbc.M710565200

Hu, J. C., Ryu, O. H., Chen, J. J., Uchida, T., Wakida, K., Murakami, C., et al. (2000a). Localization of EMSP1 expression during tooth formation and cloning of mouse cDNA. *J. Dent. Res.* 79, 70–76. doi: 10.1177/00220345000790011301

Hu, J. C., Zhang, C., Sun, X., Yang, Y., Cao, X., Ryu, O., et al. (2000b). Characterization of the mouse and human PRSS17 genes, their relationship to other serine proteases, and the expression of PRSS17 in developing mouse incisors. *Gene* 251, 1–8. doi: 10.1016/S0378-1119(00)00203-1

Hu, J. C., Sun, X., Zhang, C., Liu, S., Bartlett, J. D., and Simmer, J. P. (2002). Enamelysin and kallikrein-4 mRNA expression in developing mouse molars. *Eur. J. Oral Sci.* 110, 307–315. doi: 10.1034/j.1600-0722.2002.21301.x

Hu, Y., Hu, J. C., Smith, C. E., Bartlett, J. D., and Simmer, J. P. (2011). Kallikrein-related peptidase 4, matrix metalloproteinase 20, and the maturation of murine and porcine enamel. *Eur. J. Oral Sci.* 119(Suppl. 1), 217–225. doi: 10.1111/j.1600-0722.2011.00859.x

Kim, J. W., Simmer, J. P., Hart, T. C., Hart, P. S., Ramaswami, M. D., Bartlett, J. D., et al. (2005). MMP-20 mutation in autosomal recessive pigmented hypomaturation amelogenesis imperfecta. *J. Med. Genet.* 42, 271–275. doi: 10.1136/jmg.2004.024505

Lacruz, R. S., Smith, C. E., Smith, S. M., Hu, P., Bringas, P. Jr., Sahin-Toth, M., et al. (2011). Chymotrypsin C (caldecrin) is associated with enamel development. *J. Dent. Res.* 90, 1228–1233. doi: 10.1177/0022034511418231

Lausch, E., Keppler, R., Hilbert, K., Cormier-Daire, V., Nikkel, S., Nishimura, G., et al. (2009). Mutations in MMP9 and MMP13 determine the mode of inheritance and the clinical spectrum of metaphyseal anadysplasia. *Am. J. Hum. Genet.* 85, 168–178. doi: 10.1016/j.ajhg.2009.06.014

Lee, S. K., Seymen, F., Kang, H. Y., Lee, K. E., Gencay, K., Tuna, B., et al. (2010). MMP20 hemopexin domain mutation in amelogenesis imperfecta. *J. Dent. Res.* 89, 46–50. doi: 10.1177/0022034509352844

Lefevre, M. L., and Manly, R. S. (1938). Moisture, inorganic and organic contents of enamel and dentin from carious teeth. *J. Am. Dent. Assoc.* 24, 233–242.

Lundwall, A., and Brattsand, M. (2008). Kallikrein-related peptidases. *Cell. Mol. Life Sci.* 65, 2019–2038. doi: 10.1007/s00018-008-8024-3

Masuya, H., Shimizu, K., Sezutsu, H., Sakuraba, Y., Nagano, J., Shimizu, A., et al. (2005). Enamelin (Enam) is essential for amelogenesis: ENU-induced mouse mutants as models for different clinical subtypes of human amelogenesis imperfecta (AI). *Hum. Mol. Genet.* 14, 575–583. doi: 10.1093/hmg/ddi054

Matsumura, M., Bhatt, A. S., Andress, D., Clegg, N., Takayama, T. K., Craik, C. S., et al. (2005). Substrates of the prostate-specific serine protease prostase/KLK4 defined by positional-scanning peptide libraries. *Prostate* 62, 1–13. doi: 10.1002/pros.20101

Meredith, R. W., Gatesy, J., Cheng, J., and Springer, M. S. (2011). Pseudogenization of the tooth gene enamelysin (MMP20) in the common ancestor of extant baleen whales. *Proc. Biol. Sci.* 278, 993–1002. doi: 10.1098/rspb.2010.1280

Meredith, R. W., Gatesy, J., Murphy, W. J., Ryder, O. A., and Springer, M. S. (2009). Molecular decay of the tooth gene Enamelin (ENAM) mirrors the loss of enamel in the fossil record of placental mammals. *PLoS Genet.* 5:e1000634. doi: 10.1371/journal.pgen.1000634

Meredith, R. W., Gatesy, J., and Springer, M. S. (2013). Molecular decay of enamel matrix protein genes in turtles and other edentulous amniotes. *BMC Evol. Biol.* 13:20. doi: 10.1186/1471-2148-13-20

Nagano, T., Kakegawa, A., Yamakoshi, Y., Tsuchiya, S., Hu, J. C., Gomi, K., et al. (2009). Mmp-20 and Klk4 cleavage site preferences for amelogenin sequences. *J. Dent. Res.* 88, 823–828. doi: 10.1177/0022034509342694

Newbrun, E., and Pigman, W. (1960). The hardness of enamel and dentine. *Aust. Dent. J.* 5, 210–217. doi: 10.1111/j.1834-7819.1960.tb01939.x

Overall, C. M., and Limeback, H. (1988). Identification and characterization of enamel proteinases isolated from developing enamel. Amelogeninolytic serine proteinases are associated with enamel maturation in pig. *Biochem. J.* 256, 965–972.

Ozdemir, D., Hart, P. S., Ryu, O. H., Choi, S. J., Ozdemir-Karatas, M., Firatli, E., et al. (2005). MMP20 active-site mutation in hypomaturation amelogenesis imperfecta. *J. Dent. Res.* 84, 1031–1035. doi: 10.1177/154405910508401112

Rajpar, M. H., Harley, K., Laing, C., Davies, R. M., and Dixon, M. J. (2001). Mutation of the gene encoding the enamel-specific protein, enamelin, causes autosomal-dominant amelogenesis imperfecta. *Hum. Mol. Genet.* 10, 1673–1677. doi: 10.1093/hmg/10.16.1673

Reith, E. J., and Ross, M. H. (1973). Morphological evidence for the presence of contractile elements in secretory ameloblasts of the rat. *Arch. Oral Biol.* 18, 445–448. doi: 10.1016/0003-9969(73)90170-2

Robinson, C., Kirkham, J., Weatherell, J. A., Richards, A., Josephsen, K., and Fejerskov, O. (1988). Mineral and protein concentrations in enamel of

the developing permanent porcine dentition. *Caries Res.* 22, 321–326. doi: 10.1159/000261131

Ronnholm, E. (1962). An electron microscopic study of the amelogenesis in human teeth. I. The fine structure of the ameloblasts. *J. Ultrastruct. Res.* 6, 229–248. doi: 10.1016/S0022-5320(62)90055-2

Ryu, O., Hu, J. C., Yamakoshi, Y., Villemain, J. L., Cao, X., Zhang, C., et al. (2002). Porcine kallikrein-4 activation, glycosylation, activity, and expression in prokaryotic and eukaryotic hosts. *Eur. J. Oral Sci.* 110, 358–365. doi: 10.1034/j.1600-0722.2002.21349.x

Ryu, O. H., Fincham, A. G., Hu, C. C., Zhang, C., Qian, Q., Bartlett, J. D., et al. (1999). Characterization of recombinant pig enamelysin activity and cleavage of recombinant pig and mouse amelogenins. *J. Dent. Res.* 78, 743–750. doi: 10.1177/00220345990780030601

Scully, J. L., Bartlett, J. D., Chaparian, M. G., Fukae, M., Uchida, T., Xue, J., et al. (1998). Enamel matrix serine proteinase 1: stage-specific expression and molecular modeling. *Connect. Tissue Res.* 39, 111–122. doi: 10.3109/03008209809023917

Seedorf, H., Klaften, M., Eke, F., Fuchs, H., Seedorf, U., and Hrabe de Angelis, M. (2007). A mutation in the enamelin gene in a mouse model. *J. Dent. Res.* 86, 764–768. doi: 10.1177/154405910708600815

Shimizu, M., Tanabe, T., and Fukae, M. (1979). Proteolytic enzyme in porcine immature enamel. *J. Dent. Res.* 58, 782–789. doi: 10.1177/00220345790580023001

Simmer, J. P., Fukae, M., Tanabe, T., Yamakoshi, Y., Uchida, T., Xue, J., et al. (1998). Purification, characterization, and cloning of enamel matrix serine proteinase 1. *J. Dent. Res.* 77, 377–386. doi: 10.1177/00220345980770020601

Simmer, J. P., Hu, Y., Lertlam, R., Yamakoshi, Y., and Hu, J. C. (2009). Hypomaturation enamel defects in Klk4 Knockout/LacZ knockin mice. *J. Biol. Chem.* 284, 19110–19121. doi: 10.1074/jbc.M109.013623

Simmer, J. P., Hu, Y., Richardson, A. S., Bartlett, J. D., and Hu, J. C. (2011a). Why does enamel in Klk4-null mice break above the dentino-enamel junction? *Cells tissues organs.* 194, 211–215. doi: 10.1159/000324260

Simmer, J. P., Richardson, A. S., Smith, C. E., Hu, Y., and Hu, J. C. (2011b). Expression of kallikrein-related peptidase 4 in dental and non-dental tissues. *Eur. J. Oral Sci.* 119(Suppl. 1), 226–233. doi: 10.1111/j.1600-0722.2011.00834.x

Simmer, J. P., Richardson, A. S., Hu, Y. Y., Smith, C. E., and Ching-Chun Hu, J. (2012). A post-classical theory of enamel biomineralization. . . and why we need one. *Int. J. Oral Sci.* 4, 129–134. doi: 10.1038/ijos.2012.59

Skobe, Z. (1977). Enamel rod formation in the monkey observed by scanning electron microscopy. *Anat. Rec.* 187, 329–334. doi: 10.1002/ar.1091870305

Skobe, Z., and Stern, S. (1980). The pathway of enamel rods at the base of cusps of human teeth. *J. Dent. Res.* 59, 1026–1032. doi: 10.1177/00220345800590060401

Smith, C. E. (1998). Cellular and chemical events during enamel maturation. *Crit. Rev. Oral Biol. Med.* 9, 128–161. doi: 10.1177/10454411980090020101

Smith, C. E., Richardson, A. S., Hu, Y., Bartlett, J. D., Hu, J. C., and Simmer, J. P. (2011). Effect of kallikrein 4 loss on enamel mineralization: comparison with mice lacking matrix metalloproteinase 20. *J. Biol. Chem.* 286, 18149–18160. doi: 10.1074/jbc.M110.194258

Tye, C. E., Pham, C. T., Simmer, J. P., and Bartlett, J. D. (2009). DPPI may activate KLK4 during enamel formation. *J. Dent. Res.* 88, 323–327. doi: 10.1177/0022034509334240

Wang, S. K., Hu, Y., Simmer, J. P., Seymen, F., Estrella, N. M., Pal, S., et al. (2013). Novel KLK4 and MMP20 mutations discovered by whole-exome sequencing. *J. Dent. Res.* 92, 266–271. doi: 10.1177/0022034513475626

Weinmann, J. P., Wessinger, G. D., and Reed, G. (1942). Correlation of chemical and histological investigations on developing enamel. *J. Dent. Res.* 21, 171–182. doi: 10.1177/00220345420210020701

Yamakoshi, Y., Hu, J. C., Fukae, M., Yamakoshi, F., and Simmer, J. P. (2006). How do enamelysin and kallikrein 4 process the 32-kDa enamelin? *Eur. J. Oral Sci.* 114(Suppl. 1), 45–51. doi: 10.1111/j.1600-0722.2006.00281.x

Yamakoshi, Y., Richardson, A. S., Nunez, S. M., Yamakoshi, F., Milkovich, R. N., Hu, J. C., et al. (2011). Enamel proteins and proteases in Mmp20 and Klk4 null and double-null mice. *Eur. J. Oral Sci.* 119(Suppl. 1), 206–216. doi: 10.1111/j.1600-0722.2011.00866.x

Yamakoshi, Y., Simmer, J. P., Bartlett, J. D., Karakida, T., and Oida, S. (2013). MMP20 and KLK4 activation and inactivation interactions *in vitro*. *Arch. Oral Biol.* 58, 1569–1577. doi: 10.1016/j.archoralbio.2013.08.005

Zhou, J., and Sahin-Toth, M. (2011). Chymotrypsin C mutations in chronic pancreatitis. *J. Gastroenterol. Hepatol.* 26, 1238–1246. doi: 10.1111/j.1440-1746.2011.06791.x

Conflict of Interest Statement: The Associate Editor declares that, despite being affiliated to the same institution as one of the authors, John D. Bartlett, the review process was handled objectively and no conflict of interest exists. The authors declare that the research was conducted in the absence of any commercial or financial relationships that could be construed as a potential conflict of interest.

Received: 06 May 2014; paper pending published: 23 May 2014; accepted: 10 June 2014; published online: 04 July 2014.

Citation: Bartlett JD and Simmer JP (2014) Kallikrein-related peptidase-4 (KLK4): role in enamel formation and revelations from ablated mice. Front. Physiol. ***5****:240. doi: 10.3389/fphys.2014.00240*

This article was submitted to Craniofacial Biology, a section of the journal Frontiers in Physiology.

frontiers in PHYSIOLOGY

ORIGINAL RESEARCH ARTICLE
published: 19 March 2015
doi: 10.3389/fphys.2015.00057

Mapping residual organics and carbonate at grain boundaries and the amorphous interphase in mouse incisor enamel

Lyle M. Gordon and Derk Joester*

Department of Materials Science and Engineering, Northwestern University, Evanston, IL, USA

Edited by:
Bernhard Ganss, University of Toronto, Canada

Reviewed by:
Michel Goldberg, University Paris Descartes, France
Victor E. Arana-Chavez, University of São Paulo, Brazil

****Correspondence:***
Derk Joester, Department of Materials Science and Engineering, Northwestern University, 2220 Campus Drive, Evanston, IL 60208, USA
e-mail: d-joester@northwestern.edu

Dental enamel has evolved to resist the most grueling conditions of mechanical stress, fatigue, and wear. Adding insult to injury, it is exposed to the frequently corrosive environment of the oral cavity. While its hierarchical structure is unrivaled in its mechanical resilience, heterogeneity in the distribution of magnesium ions and the presence of Mg-substituted amorphous calcium phosphate (Mg-ACP) as an intergranular phase have recently been shown to increase the susceptibility of mouse enamel to acid attack. Herein we investigate the distribution of two important constituents of enamel, residual organic matter and inorganic carbonate. We find that organics, carbonate, and possibly water show distinct distribution patterns in the mouse enamel crystallites, at simple grain boundaries, and in the amorphous interphase at multiple grain boundaries. This has implications for the resistance to acid corrosion, mechanical properties, and the mechanism by which enamel crystals grow during amelogenesis.

Keywords: dental enamel, caries, atom probe tomography, chemical imaging, grain boundaries, interphases

INTRODUCTION

Enamel, the hardest tissue in vertebrates, is composed of 98 wt% hydroxylapatite (OHAp) along with 1–2 wt% organic molecules and water (Eastoe, 1960). During amelogenesis, ameloblasts first secrete a soft extracellular organic matrix comprised of water (∼50 wt%), mineral (∼30 wt%), and a number of proteins (∼20 wt%), including the amelogenins, ameloblastins, and enamelins, among others (Robinson et al., 1998). As the matrix becomes increasingly mineralized, it is simultaneously processed by proteolytic enzymes, degraded, and largely removed. Nevertheless, it is thought to play an important role in the chemical stabilization of an amorphous mineral precursor, the shaping and mechanical scaffolding of the precursor into a very long and thin ribbon, and the transformation of the precursor into the final crystalline material during enamel maturation (Beniash et al., 2009). Mature enamel is composed of crystallites of OHAp that are highly elongated parallel to the crystallographic *c*-axis and have polygonal cross sections with edge lengths of 20–50 nm in the *a*-*b*-plane. Tens of thousands of crystallites are bundled in rods with a diameter of 3–5 μm. Rods, in turn, are woven together in a complex three-dimensional pattern (**Figure 1**), with disordered interrod enamel filling the interstices. There are variations of specific aspects of this architecture that depend on the location of the enamel on the crown of a particular tooth, between teeth with different functional morphologies, and between the teeth of different species. Despite these, the similarities remaining are such that rodent teeth, in particular those of rats and mice, are well-established as model systems for amelogenesis and dental caries of human teeth (Bowen, 2013).

Thus, across the species, enamel has a complex composite inorganic-organic architecture with several levels of hierarchy from the nanometer to the millimeter scale (Palmer et al., 2008). Its remarkable hierarchical structure and the constituent organic matter are thought to be responsible for the substantial improvement of enamel mechanical properties, such as toughness, wear resistance, and fatigue life, compared to OHAp. This improvement is integral to enamel function, as pure OHAp would fail catastrophically under the typical forces seen during mastication (Baldassarri et al., 2008). However, enamel has an Achilles heel. It is susceptible to corrosion by acids. Net demineralization of enamel by acids produced in bacterial biofilms in the oral cavity leads to dental caries, the most prevalent infectious disease in humans. Caries severely affects physical and mental health, quality of life, and has major economic consequences (Robinson et al., 2000). It also disproportionately affects children and adults from less affluent backgrounds and in countries with less developed dental hygiene (World Health Organization Media Centre, 2012).

Despite decades of research on enamel, the complex nanoscale structure and chemistry of the tissue is still not fully understood. This has been a major roadblock in the development of accurate models for the mechanism by which carious lesions form, and has effectively prevented the development of early detection schemes, more effective prophylaxis, and minimally invasive therapies. It furthermore imposes limitations on modeling the mechanical properties of enamel and on our understanding of the mechanism by which crystals grow in forming enamel.

For instance, it has long been known that a number of physiologically relevant ions influence crystal growth during enamel maturation and that incorporation of such ions into the mineral

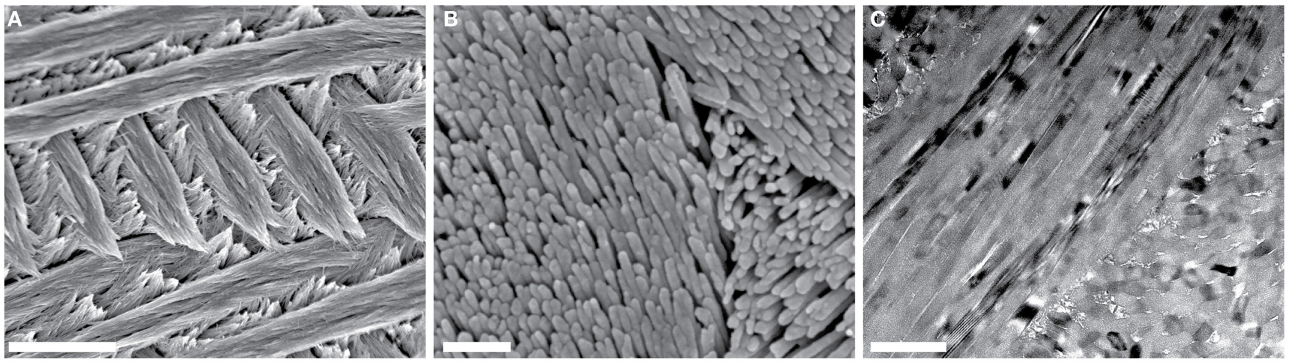

FIGURE 1 | Overview of mouse incisor enamel structure. (A,B) SEM images of a lactic acid-etched cross-section reveal decussating rods composed of thousands of high-aspect ratio hydroxylapatite nanowires. Scale bars in **(A,B)** correspond to 4 μm and 250 nm, respectively. **(C)** In this bright-field TEM image of a FIB-prepared thin section of the edge of one mouse enamel rod, parallel alignment of nanowires is apparent. Scale bar corresponds to 200 nm.

phase strongly affects the final structure and physico-chemical properties of enamel. Enamel crystallites consist of OHAp with the prototypical formula $Ca_{10}(PO_4)_6(OH)_2$. However, there is a substantial amount of vacancies, and apatites in general are very tolerant also of substitutional defects. For example, cations such as Na^+ and Mg^{2+} substitute for Ca^{2+} and anions such as Cl^- and F^- substitute for OH^- (Pan and Fleet, 2002). Carbonate ions (CO_3^{2-}) can replace either hydroxyl or phosphate ions, and are present at such high concentration in biogenic apatites that the latter are frequently referred to as carbonate-hydroxylapatites. The ions with the most substantial effects on the mineral are fluoride, magnesium, sodium, and carbonate ions. Except for fluoride, these substituents increase enamel solubility. However, we have little information regarding the distribution of these ions at length scales below tens of micrometers.

This is because the majority of our understanding is based on bulk compositional analysis, ion- and electron-probe microanalysis, and transmission electron microscopy (TEM). Although these tools have provided valuable information on the structure of enamel, they have a limited ability to probe compositional variations at the length scale of individual crystallites and the interfaces between them. We recently demonstrated that atom probe tomography (APT) is capable of providing this information (Gordon et al., 2015).

In APT, individual atoms or small clusters at the surface of a very sharp, needle shaped specimen are sequentially field-evaporated and -ionized. As the tip is stripped back atom-by-atom and layer-by-layer, each ion is projected onto a position-sensitive detector (**Figure 2**) (Kelly and Miller, 2007). The mass-to-charge ratio (m/z) and thus the chemical identity of each ion is determined by time-of-flight (TOF) mass-spectrometry using picosecond laser pulses to trigger evaporation events. The sequence and location of ions impinging on the detector enables reconstruction of the three dimensional structure of the sample. APT analyses volumes on the order of 10^5–10^6 nm^3, typically with sub-nanometer spatial resolution (Kelly and Miller, 2007). Traditionally applied to metals and certain semi-conductors, the development of ultraviolet-laser pulsing greatly increased the scope of the technique to include high resistivity materials and organics (Joester et al., 2012). APT has recently emerged as a technique to characterize hybrid organic/inorganic materials and interfaces, including for instance self-assembled monolayers, invertebrate teeth, and vertebrate bone, dentin, and enamel (Gault et al., 2010; Gordon and Joester, 2011; Gordon et al., 2012; Karlsson et al., 2014).

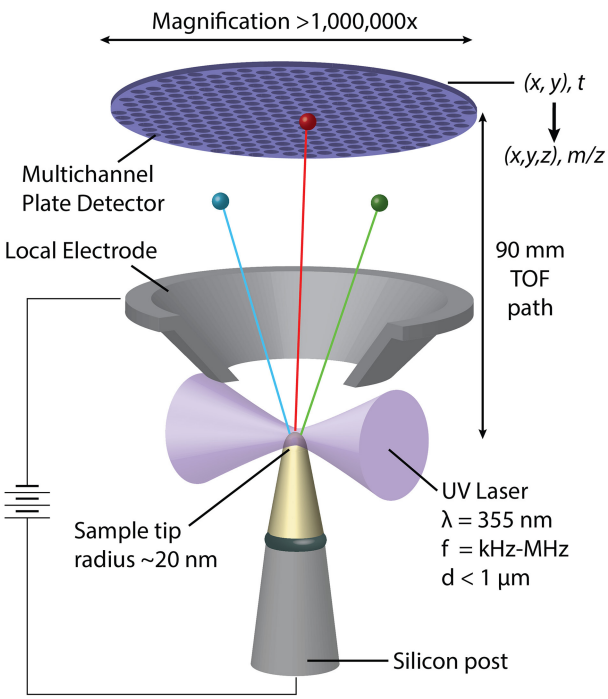

FIGURE 2 | Schematic representation of a pulsed-laser, local electrode atom probe (LEAP) tomograph. Following a UV-laser pulse, individual atoms or small clusters at the surface a sharp specimen tip field-evaporate and ionize. Accelerated toward the hollow-cone local electrode, each ion's time of flight is used to determine its mass/charge ratio (m/z) and thus its chemical identity. Where and in what order the ions hit the position sensitive detector depends on their original position in the sample.

We used APT to map the distribution of Mg^{2+} in regular, i.e., unpigmented, murine enamel, and found evidence for the presence of Mg-substituted amorphous calcium phosphate (Mg-ACP) as an intergranular phase (Gordon et al., 2015). We further discovered the importance of Mg^{2+} at grain boundaries and in Mg-ACP for the susceptibility of enamel to acid attack. The objectives of the present work were to identify the nanoscale distribution of organic carbon, primarily degradation products of the proteinaceous organic matrix in which the enamel crystallites grow, and inorganic carbon, i.e., carbonate, at enamel grain boundaries and within the amorphous intergranular phase. Both components are thought to strongly impact chemical and mechanical properties of enamel.

MATERIALS AND METHODS

CONSUMABLES

Epo-Tek 301 epoxy (Epoxy Technology, Billerica, MA); CarbiMet II SiC grinding paper, Microcut SiC grinding paper, Metadi supreme polycrystalline aqueous diamond polishing suspension, Masterprep Alumina suspension, Trident polishing cloth, Chemomet polishing cloth (Buehler, Lake Bluff, IL); Conductive Liquid Silver Paint (Ted Pella, Redding, CA). Super Glue Cyanoacrylate Adhesive (3M, St. Paul, MN).

INCISORS

Incisors were donated by Dr. A. Deymier-Black, Washington University, St Louis, MO.; Dr. C. Newcomb and Dr. S. Sur, Northwestern University. Lower (mandibular) incisors were excised from carcasses of animals euthanized in the context of other studies. After excision, incisors were gently cleaned, rinsed, and dried in air.

EMBEDDING, GRINDING, AND POLISHING

Dried incisors were embedded in Epo-Tek 301 epoxy and polymerized overnight at 25°C. Embedded samples were ground using progressively finer grits of Buehler SiC grinding paper (400, 600, 800, and 1200 grit). Ground samples were polished using 3 μm and 1.0 μm polycrystalline aqueous diamond polishing suspensions on a Buehler Trident polishing cloth. After a final polishing step using 0.05 μm Al_2O_3 suspension on a Buehler Chemomet polishing cloth, samples were rinsed with water and dried under flowing argon gas.

QUALITATIVE ACID ETCHING

Freshly polished, epoxy-embedded enamel cross-sections were etched for 1 min at 25°C in 250 mM aqueous lactic acid adjusted to pH 4.0 with NaOH.

COATING

For SEM imaging, samples were secured to an aluminum stub with cyanoacrylate adhesive, coated with ∼5 nm of Pt with an Ion Beam Sputter Deposition and Etching System (IBS/e, South Bay Technologies, San Clemente, CA) operating at a base pressure of $< 10^{-4}$ Pa and working pressure of 10^{-2} Pa Ar, with two ion guns operating at 8 kV and 3 mA per gun. The coating was grounded to the stub with conductive liquid silver paint.

SCANNING ELECTRON MICROSCOPY

SEM was performed with an FEI Helios Nanolab (Hillsboro, OR) operating at 5 keV with 0.1–0.7 nA probe current.

TRANSMISSION ELECTRON MICROSCOPY SAMPLE PREPARATION

Transmission electron microscopy (TEM) lamellae were prepared from a polished mouse incisor cross section following established procedures with a DualBeam scanning electron microscope (SEM) and focused ion beam (FIB) instrument (Helios NanoLab, FEI, Hillsboro, OR) (Giannuzzi and Stevie, 1999). A strap of platinum (FIB-Pt) was deposited over a region of interest using the ion beam (30 kV, 93 pA) to locally decompose an organometallic precursor gas, (trimethyl)methylcyclopentadienyl-platinum [$(CH_3)_3Pt(CpCH_3)$]. A trench was then milled out (30 kV, 6.5 nA) on either side of a 2 μm wide slice of material. The slice of material was cut free (30 kV, 2.8 nA) from the substrate on three sides leaving only a small connecting bridge. An *in situ* tungsten nanomanipulator probe (Omniprobe) was attached to the free side of the substrate using FIB-Pt (30 kV, 93 pA). The remaining connection to the substrate was milled away (30 kV, 93 pA) and the probe was retracted with the sample. The sample was then welded to a copper TEM half-grid (Omniprobe) using FIB-Pt and the connection to the probe was milled away (30 kV, 93 pA). The lamella was successively thinned to ∼100 nm at 30 kV (93 pA) at a 1–2° angle grazing incidence milling condition. The sample was then thinned to ∼60–80 nm by low angle milling (∼7°) at 5 kV and 2 kV (28 pA); this step also removed the majority of any amorphized/gallium-implanted surface layers.

TRANSMISSION ELECTRON MICROSCOPY

TEM was performed with a Hitachi H-7700 (Hitachi High-Technologies Science America, Northridge, CA) operating at 120 kV.

ATOM PROBE TOMOGRAPHY SAMPLE PREPARATION

Samples for APT were prepared using the dual-beam SEM/FIB instrument (Helios Nanolab, FEI, Hillsboro, Oregon) using established protocols (Miller et al., 2005, 2007; Thompson et al., 2007). A rectangular strap of FIB-Pt was deposited over a region of interest ($2 \times 25\ \mu m^2$) on polished cross-sections. A wedge of material below the Pt strap was cut out on three sides. The wedge was attached to an *in-situ* nano-manipulator (Omniprobe, Dallas, TX) using FIB-Pt before cutting the final edge free. Segments 1–2 μm wide were cut from the wedge and sequentially affixed to the tops of Si posts in an array (Cameca Scientific Instruments, Madison, WI) with FIB-Pt. Each tip was shaped and sharpened using annular milling patterns of increasingly smaller inner and outer diameters. The majority of the amorphized surface region and implanted gallium in the tip surface was removed by milling at 2 kV, 0.4 nA.

ATOM PROBE TOMOGRAPHY

Atom probe tomographic analyses were conducted in a Cameca local-electrode atom-probe tomograph (LEAP 4000XSi, Cameca, Madison, WI) using a pulsed laser ($\lambda = 355$ nm, 200–250 kHz, 50–150 pJ per pulse). The DC potential on a microtip during APT was controlled to maintain an evaporation rate of 0.0025 or 0.005 ions per laser pulse. The base temperature of the microtip was

maintained at 40 K and the ambient vacuum pressure was below 10^{-8} Pa. Peak ranges were defined as the entire visible peak and background subtraction was performed using built in routines in Cameca integrated visualization and analysis software (IVAS).

Three-dimensional reconstruction of APT data was performed using IVAS based on published algorithms, assuming a hemispherical tip shape (Bas et al., 1995; Miller, 2000). Standard reconstruction parameters, field factor ($k_f = 3.3$) and image compression factor ($\xi = 1.33$) were used with an electric field-dependent tip radius (r). The average evaporation field (F_e) of the enamel apatite ($14\,V{\cdot}nm^{-1}$) was determined from SEM and/or TEM images of microtips after APT analysis. Average atomic volumes for the reconstruction were calculated based on the hydroxylapatite crystal structure (Hughes et al., 1989).

For compositional analysis of apatite crystallites the cores of the grains were manually isolated with multiple rectangular prism regions of interest to exclude the grain boundaries and multiple grain junctions. Twenty nine APT data sets from 11 mandibular incisors of 6 mice were collected and analyzed.

RESULTS AND DISCUSSION

SPECTRAL ANALYSIS AND GLOBAL COMPOSITION

We prepared samples of inner enamel (IE) and outer enamel (OE) from mouse (*Mus musculus)* incisors as described previously (Gordon et al., 2015). Samples for APT were prepared from ground and polished sections by standard focused ion beam (FIB) milling techniques (Thompson et al., 2007). Atom probe spectra (**Figure 3**) show the typical features of OHAp (Gordon et al., 2012, 2015). Atomic and molecular ions containing Ca, P, and O give rise to a series of peaks of high abundance. Small inorganic cations that are known constituents of enamel, including Mg^{2+} and Na^{+}, are present at low abundance. A small amount of fluoride is detected as F^{+} and CaF^{+}. This fluoride is likely introduced because of low levels of fluoride in the typical rodent diet.

In addition, spectral features that differentiate enamel from synthetic OHAp were identified. The majority of these correspond to atomic and molecular ions comprised of a combination of one or more of the elements C, H, N, and O (**Table 1**). Due to the low mass resolving power of the atom probe we cannot unambiguously identify the chemical composition of a number of these ions. For example, at m/z = 28, we would expect to see CO^{+}, CH_2N^{+}, and $C_2H_4^{+}$. We think that the latter two possibilities are less likely because in H-containing species one typically sees a series of ions corresponding to a parent ion and between zero and a maximum number of hydrogens. However, peaks corresponding to $CH_{0–2}N^{+}$ and $C_2H_{0–3}^{+}$ are not found in enamel spectra. While similar arguments can be made in identifying the most likely candidates for many CHNO-containing ions in the spectra, we cannot be certain. As a result, it is not generally possible to determine the chemical identity of the organic molecules present. Indeed, the CHNO-containing ions detected in atom probe spectra of enamel resemble those observed in spectra of bone and dentin (Gordon et al., 2012), where the predominant source is collagen, and chiton teeth, where the organic matrix primarily consists of the polysaccharide chitin (Gordon and Joester, 2011).

An additional complication is that carbonate ions are a known constituent of enamel. Carbonate also gives rise to C^{2+} and CO_x^{+} ($x = 0, 1, 2$) ions in atom probe spectra (McMurray et al., 2011; Gordon et al., 2012, 2015). However, any nitrogen present most likely originates from organic molecules, for instance proteins that are degraded during enamel maturation. The C/N molar ratio of the known proteins in the enamel organic matrix is in the range from 3.5 to 3.8; that of amelogenin, its most abundant constituent, is 3.76. Assuming that proteolytic degradation of the organic matrix does not change the C/N ratio, we can therefore estimate how much of the total organic mass observed in AP spectra is protein based on the amount of nitrogen observed.

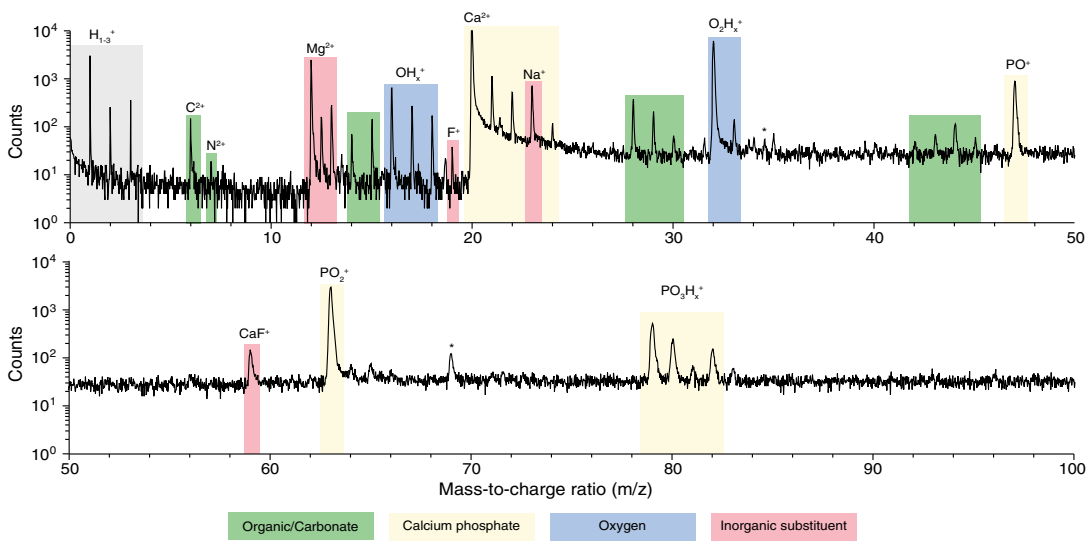

FIGURE 3 | Atom probe mass spectra. From APT analysis of isolated organic-rich region at grain edge in mouse inner enamel. Atomic and molecular fragments corresponding to calcium phosphates (mineral), organic molecules, inorganic substituents, and fluoride species, are highlighted. Trace amount of FIB-implanted Ga (*) were also detected.

There is only one peak, at m/z = 7, which we can unambiguously identify as N^{2+}. We can rule out interference from CH_2^{2+} because there is no evidence of CH^{2+} (m/z = 6.5) or CH_3^{2+} ions. While we think it likely that N^+ and NH^+ contribute to the peaks at m/z = 14 and 15, we expect at least some contribution from CH_2^+ and CH_3^+ also. We therefore calculate a lower bound of $5{\cdot}10^{-4}$ wt% N and $2{\cdot}10^{-3}$ wt% total organic carbon (TOC) using only the count of N^{2+} ions. Using all the potential N-containing peaks (**Table 1**) provides an estimate of the upper bound (0.04 wt% N and 0.15 wt% TOC in OE, **Table 2**). Note that even the upper bound for TOC is considerably below the bulk average (∼1 wt%) (Eastoe, 1960). This may be due to the higher concentration of organics at the periphery of rods and in interrod enamel (Habelitz et al., 2001).

SPATIAL DISTRIBUTION OF MINOR ENAMEL CONSTITUENTS

In three-dimensional reconstructions of mouse enamel (**Figure 4**), the cross sections of faceted nanowires are readily apparent from the distribution of minor ions such as Mg^{2+} that are present at grain boundaries (Gordon et al., 2015). Grain boundaries are the largely flat interfaces between two adjacent enamel crystallites; grain edges, or more generally, multiple grain boundaries exist where three or more crystallites meet. We previously found that at multiple boundaries, and probably also at simple grain boundaries, an intergranular phase exists that we identified as Mg-substituted amorphous calcium phosphate (Mg-ACP, 0.5–6 wt% Mg^{2+}) (Gordon et al., 2015).

Inspection of 3D reconstructions reveals CHNO-containing ions are present at concentrations significantly above the background level at some, but not all multiple grain boundaries and at much lower level throughout the bulk of the grains (**Figure 4**). There is no evidence of enrichment at simple grain boundaries. It is important to note that while for any given ion identified in atom probe spectra, we can perform a background correction for compositional analysis, it is not possible to decide which of the ions rendered in reconstructions correspond to background. Reconstructions, especially those of low abundance constituents thus appear noisy. Analysis of the nearest neighbor distances (Figure S1) between CHNO-containing ions in OHAp crystallites indicates they are distributed randomly in space (indistinguishable from simulated randomized data). If these ions were fragments of larger organic molecules, we would expect them to

Table 1 | Detected CHNO-containing ions and relative abundance.

Ion	m/z	Mole fraction (at %)	Ion	m/z	Mole fraction (at %)
C^{2+}	6	0.01	**CO^+**, $C_2H_4^+$	28	0.1
N^{2+}	7	0.01	**CHO^+**, $C_2H_5^+$	29	0.1
C^+	12	0.1	**CH_2O^+**, NO, $C_2H_6^+$	30	0.07
CH^+	13	0.06	**CNO^+**, $C_2H_2O^+$, $C_3H_6^+$	42	0.02
N^+, CH_2^+, CO^{2+}	14	0.03	**$CHNO^+$**, $C_2H_3O^+$, $C_3H_7^+$	43	0.03
NH^+, CH_3^+	15	0.06	**CO_2^+**, CH_2NO^+, $C_3H_8^+$	44	0.1
			CO_2H^+	45	0.08

Ions in bold face fonts indicate the identity used for mass spectral decomposition (last column of composition table).

Table 2 | Enamel Composition.

Constituent	Mass fraction (wt%)			
	Outer enamel, whole sample	OE crystallites $N = 6$	Inner enamel, whole sample	IE crystallites $N = 7$
Ca	50.46 ± 0.06	47 ± 6	37.76 ± 0.06	34 ± 2
P	15.9 ± 0.2	17 ± 3	21.7 ± 0.2	24 ± 1
O	31.6 ± 0.3	33 ± 3	38.0 ± 0.2	40 ± 1
H	0.231 ± 0.003	0.3 ± 0.03	0.159 ± 0.002	0.2 ± 0.03
Na	0.020 ± 0.001	0.5 ± 0.1	0.590 ± 0.003	0.5 ± 0.1
Mg	0.266 ± 0.003	0.04 ± 0.02	0.332 ± 0.004	0.07 ± 0.04
F	0.189 ± 0.008	0.5 ± 0.3	0.44 ± 0.01	0.5 ± 0.2
Cl	0.128 ± 0.003	0.2 ± 0.06	0.12 ± 0.002	0.2 ± 0.06
N_{min} . . . N_{max}	$5{\cdot}10^{-4}$ . . . 0.02	–	$8{\cdot}10^{-4}$ . . . 0.04	–
TC = TOC + TIC	0.116 ± 0.004	0.1 ± 0.03	0.151 ± 0.004	0.1 ± 0.05
TOC_{min} . . . TOC_{max}	0.002 . . . 0.08	–	$3{\cdot}10^{-3}$ . . . 0.15	–
TIC_{min} . . . TIC_{max}	0.098 . . . 0.02	–	0.197 . . . 0.05	–

TC, total carbon; TOC, total organic carbon was estimated based on N_{max} and the C/N molar ratio of amelogenin (3.76). TIC, total inorganic carbon was estimated as the difference between TC and TOC. Outer and inner enamel whole sample data are each from one tip reported with error based on counting statistics. The composition of N crystallites is reported as mean ± standard deviation.

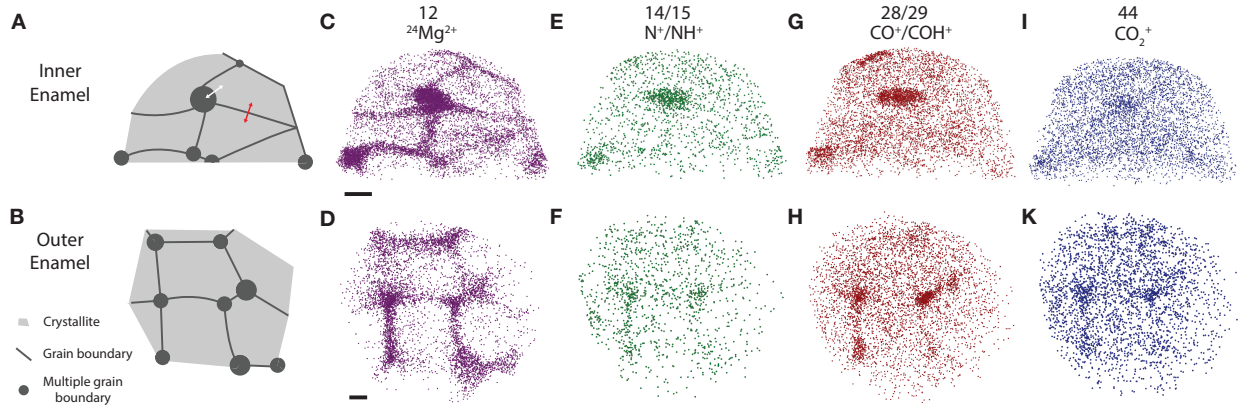

FIGURE 4 | APT reconstructions. (A,B) Schematic drawing of grain boundaries between mouse enamel crystallites, **(C,D)** $^{24}Mg^{2+}$, **(E,F)** N^+, **(G,H)** CO^+, **(I,K)** CO_2^+ ion positions in mouse inner and outer enamel. Scale bars correspond to 10 nm. Composition profiles (**Figure 5**) are determined by averaging concentrations in the direction normal to a grain boundary, as indicated by the red arrow. Proximity histograms (**Figure 5**) report average concentrations relative to an isosurface, approximately indicated by white arrow, but integrated over the entire surface. Reconstructions are oriented such that the view direction is parallel to the long axis of the nanowires, i.e., along the [00.1] zone axis.

cluster. We therefore conclude that there are no organic molecules in the crystallites.

For a quantitative analysis of the distribution of organic matter, we computed one-dimensional concentration profiles (**Figures 5A–E**) across grain boundaries that were identified on base of the Mg^{2+} distribution. Inspection confirmed the qualitative observation that, unlike Mg^{2+}, CHNO-containing ions are not enriched above background at grain boundaries, indicating that neither residual protein, other organics, or carbonate ions are present at higher concentration than in the bulk of the crystallite. As expected, the Ca and O concentration along with the total number of detected ions does not change significantly across the grain boundaries (**Figures 5A–B**, S2), indicating that there the reconstructions are not affected by trajectory aberrations at the grain boundary (Vurpillot et al., 2000). Given the low absolute concentration of N-containing ions, and the relatively high background, it is likely that the there is in fact no organic material in the bulk or at simple grain boundaries at all.

Based on the absence of organic carbon within the enamel crystallites and at simple grain boundaries, we determined the mass fraction of inorganic carbon (carbonate) within the crystallites. For crystallites in mouse IE and OE, we find 0.1 wt% C (**Table 2**), corresponding to ∼0.5 wt% CO_3^{2-}. For crystalline OHAp this corresponds to 1.2% substitution of CO_3^{2-} on OH^- or PO_4^{3-} apatite lattice sites. This value is considerably lower than the bulk average of ∼3–5 wt% CO_3^{2-}, or 6–10% substitution (Terpstra and Driessens, 1986). It is currently not clear whether this is due to a systematic underestimation of carbonate by APT, or whether carbonate concentrations in enamel are heterogeneous. It is conceivable that carbonate is enriched at the periphery of rods and in the interrod enamel, similar to residual organics.

The composition of the intergranular phase at multiple grain boundaries was quantified by way of an isoconcentration surface (isosurface) that encloses a volume wherein the concentration of a given ion is higher than a threshold (here: 0.5 at% Mg^{2+}). Proximity histograms (proxigrams, **Figures 5F–K**) report the average mole fraction of ions as a function of distance to this isoconcentration surface (Hellman et al., 2000). Such proxigrams indicate enrichment of CHNO-containing ions (1–3 wt%), and therefore carbonate and residual protein, in the intergranular phase. The concentration of carbonate and organic matter at the interface between the crystallites and the intergranular phase is graded over ∼3 nm, similar to the concentration of Mg^{2+}.

Interestingly, the total concentration of hydrogen also increases from the surface of the crystallite to the interior of the Mg-ACP precipitate. Hydrogen is a ubiquitous contaminant of vacuum chambers made from metals and typically appears in reconstructions as a more or less uniform background. The strong correlation between Mg^{2+}, N-, and H-containing ions is atypical and likely corresponds to actual hydrogen present in the sample. Hydrogen can in principle originate from hydroxyl ions, organic matter, and water. An excess of hydroxyl ions would require a mechanism to balance the charge. There is evidence of elevated sodium concentration (∼1 wt% at the interphase compared to ∼0.5 wt% in the bulk, Figure S3) that could be acting to balance the charge. We therefore think that the increase in hydrogen comes from hydroxyl ions, water or organics, or a combination thereof.

In summary, we conclude that essentially all of the residual organic matter, some carbonate, and possibly some water are present in the Mg-ACP intergranular phase at multiple grain boundaries. Outside the intergranular phase at multiple grain boundaries, the carbonate concentration seems to be homogeneous, and organic matter is most likely absent. This has important consequences for the susceptibility of enamel to acid corrosion that leads to caries lesions, for the mechanical properties of enamel, and provides some information

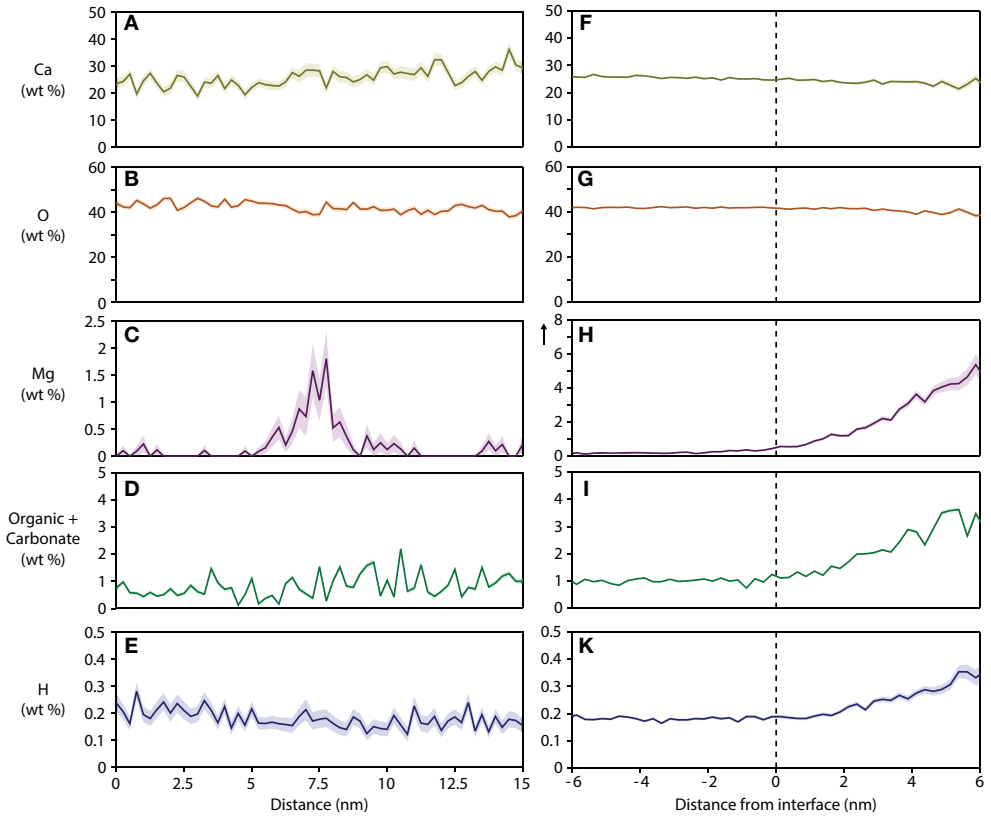

FIGURE 5 | Concentration profiles and proximity histograms. Representative concentration profiles across grain boundaries **(A–E)** and proximity histograms of an organic-rich intergranular region **(F–K)** in mouse inner enamel. Note that in proxigrams, distance is plotted relative to the position of the isosurface (0.5 at% Mg), i.e. the interface between the OHAp nanowire and the precipitate. The vertical arrow in plot **(H)** indicates an extended y-axis compared to the corresponding plot **(C)**.

regarding the growth of OHAp crystallites during enamel maturation.

IMPLICATIONS FOR ACID CORROSION OF MOUSE ENAMEL

We have previously shown that grain boundaries in rodent enamel are much more susceptible to acid dissolution than the bulk of the crystallites (Gordon et al., 2015). This leads to highly anisotropic etching and may contribute to the development of subsurface carious lesions. While carbonate and Mg^{2+} are both present at low levels in the bulk of the mouse enamel crystallites, where they are expected to increase solubility (Legfros et al., 1996; Gordon et al., 2015), the high Mg^{2+} content and presence of Mg-ACP at grain boundaries renders these even more soluble. We expect that this effect is exacerbated by the elevated organic and carbonate content of the amorphous interphase. The presence of water would likely allow for more rapid transport of protons into and removal of dissolved ions out of enamel, further weakening its resistance against acid attack. On the other hand, a hydrated amorphous interphase would likely serve as a conduit for rapid diffusion of calcium, phosphate, and fluoride into enamel during re-mineralization from saliva. In fact, the existence of aqueous nanochannels in enamel has been suggested based on transport properties (Featherstone et al., 1979). While the amorphous interphase, at least in atom probe reconstructions, does not appear to be a pore *per se*, it is conceivable that it facilitates diffusive transport processes to a similar degree.

IMPLICATIONS FOR ENAMEL MECHANICAL PROPERTIES

The interfaces between crystallites are of great importance for the mechanical and wear properties of enamel at the nanoscale (He and Swain, 2008; Ang et al., 2010; Arsecularatne and Hoffman, 2012; Yilmaz et al., 2013). A model in which a thin and "soft" organic (mono) layer surrounds each crystallite has been found to fit the experimental data quite well. In contrast to this model, we find organic material only at boundaries of three or more crystallites. However, each crystallite has a "rind" which is high in Mg^{2+}, and may indeed be surrounded by a thin intergranular film of Mg-ACP. In this context it is important to note that not all grain boundaries are alike in the sense that the amount and the maximal concentration of Mg^{2+} differ markedly; this may be a function of the specific properties of the grain boundary (angle of misorientation, crystallographic planes). Furthermore, the intergranular phase at multiple grain boundaries is clearly graded and likely has different properties. In ceramics, amorphous intergranular films have been shown to have a dramatic impact on the mechanical properties (Clarke, 1987). Mechanical

models of enamel will need to be adjusted to reflect these new insights.

IMPLICATIONS FOR CRYSTAL GROWTH DURING ENAMEL MATURATION

The distribution of Mg^{2+}, carbonate ions, organics, and water appears to be markedly different in the bulk of the crystallites, at simple grain boundaries, and in the intergranular phase at multiple grain boundaries. That of Mg^{2+} matches expectations for a species that has low solubility in the crystalline OHAp. During crystal growth from solution, Mg^{2+} would therefore accumulate in the solution ahead of the moving interface. Where the growth fronts of two or more adjacent crystallites meet, Mg^{2+} concentrations in solution would further increase. Some of this Mg^{2+} would be incorporated at grain boundaries. However, if the Mg^{2+} concentration is sufficiently high in the aqueous phase, precipitation of Mg-ACP rather than further growth of OHAp could lead to the formation of the intergranular phase. For carbonate ions, the only difference is that there seems to be no accumulation at simple grain boundaries. This is unusual because it implies that unlike Mg^{2+}, it cannot be accommodated there, or that it is sequestered to multiple grain boundaries by a yet unknown mechanism. Organic matter is different in the sense that there seems to be no appreciable incorporation in the crystallites or at simple grain boundaries. This is an interesting finding because proteins of the organic matrix are known to bind to crystalline OHAp *in vitro* and indeed their function is thought to include control over crystal growth (Wallwork et al., 2001). In many other systems, proteins that bind strongly to crystals are occluded during growth (Pokroy et al., 2004; Li et al., 2011). It is possible that the presence of Mg^{2+} in solution modifies their affinity for OHAp, or that proteolytic processing reduces it to the point where they are not incorporated. In any case, the pattern of incorporation of Mg^{2+}, organics, and carbonate, and in particular the graded composition of the intergranular phase indicates that the concentrations of these minority constituents in the aqueous phase keeps rising during enamel maturation. This is an important consideration for the design and interpretation of *in vitro* experiments. While we did not find any indication for a direct interaction of residual organics with Mg^{2+} (Gordon et al., 2015), it is possible, even likely that there are specific interactions between organic matter and Mg^{2+}, Mg^{2+} and water, or other combinations that play an important role in the formation and the properties of the amorphous intergranular phase.

Note that we interpret our findings here in the context of classical crystal growth from supersaturated solution. Several lines of evidence, however, suggest that initial mineral particles, and possibly even the thin mineral ribbons observed in newly formed, early secretory stage enamel, are comprised of ACP (Landis and Navarro, 1983; Diekwisch et al., 1995; Beniash et al., 2009). ACP therefore is an amorphous precursor phase, similar to those observed in a variety of other systems (Weiner and Addadi, 2011). Typically, amorphous phases are much more accommodating of impurities than crystalline phases. Based on our data, this is true also for ACP, where the amount of Mg^{2+}, organics, carbonate, and water is much higher and more variable than in crystalline OHAp. There are in principle three ways for the precursor to transform into the final phase. Dissolution of the more soluble amorphous mineral and re-precipitation of the less soluble crystallites is consistent with the model we discuss above. If the amorphous phase is not a solid, but a dense liquid as observed in protein crystallization (Vekilov, 2004) and suggested for a number of biomineralizing systems (Wallace et al., 2013), the same argument applies. It is much more difficult to reconcile a solid-state phase transformation with the distribution of impurities we observe in mature enamel. This is because impurities trapped in the amorphous precursor at a higher concentration than in the final crystal would have to move away from the crystal growth front; given the low diffusivity of most ions and organic molecules in the solid state at physiological temperatures, this seems kinetically disfavored. We did observe, however, rapid diffusion of fluoride in the amorphous intergranular phase and at grain boundaries at ambient conditions (Gordon et al., 2015), such that it is maybe too early to rule out a solid-state transformation. In addition, more complex mechanisms, such as a mixed mode transformation that involves attachment of amorphous particles at the crystalline interface and concomitant growth and coarsening through the liquid phase remain possible.

CONCLUSIONS

We have shown here that APT allows us to map residual organic matter, carbonate ions, and possibly water to specific nanoscale interfaces and interphases in mouse enamel. We find that all impurities are elevated in the amorphous intergranular phase, Mg-ACP, that is present at multiple grain boundaries, but that the distribution within OHAp crystallites and at simple grain boundaries is specific to the impurity. Based on this distribution we suggest that multiple grain boundaries are particularly sensitive to acid corrosion and are thus expected to play an important role in the development of carious lesions. We furthermore find that individual crystallites are not surrounded by a monolayer of organic matter. Instead, we propose that Mg^{2+} segregation to the grain boundaries and/or an intergranular film of Mg-ACP may be responsible for those aspects of the mechanical performance of enamel that were previously ascribed to the presence of organic matter. Finally, the nanoscale distribution of trace ions, organic, and inorganic carbon in fully mineralized mouse enamel is consistent with crystallization from the amorphous precursor by dissolution and re-precipitation; a solid transformation remains a second possibility. Further work is required to improve our ability to distinguish between organic and inorganic carbon, and to account for the considerable heterogeneity of enamel, for instance the boundaries of enamel rods and interrod enamel. We think that given the fundamental similarities between murine and human enamel, it is likely that many of these findings also apply to the latter. This remains to be proven, however.

ACKNOWLEDGMENTS

The National Science Foundation (NSF DMR-0805313, DMR-1106208, and DMR-1341391), the Northwestern University Materials Research Center (NSF-MRSEC DMR-1121262), the International Institute for Nanotechnology, the Institute for Sustainability and Energy at Northwestern (ISEN), the Petroleum Research Fund of the ACS, and the Canadian National Sciences

and Engineering Research Council, through a graduate fellowship to LG, in part supported this work. This work made use of the Northwestern University Center for Atom Probe Tomography (NUCAPT) supported by NSF-MRI (DMR-0420532) and ONR-DURIP (N00014-0400798, N00014-0610539, N00014-0910781), the Optical Microscopy and Metallography Facility, and the Northwestern University Atomic and Nanoscale Characterization and Experimental Center (NU*ANCE*) Electron Probe Instrumentation Center (EPIC) supported by NSF-NSEC (EEC-0118025/003), NSF-MRSEC (DMR-1121262), the Keck Foundation, the State of Illinois, and Northwestern University.

SUPPLEMENTARY MATERIAL

The Supplementary Material for this article can be found online at: http://www.frontiersin.org/journal/10.3389/fphys.2015.00057/abstract

REFERENCES

Ang, S. F., Bortel, E. L., Swain, M. V., Klocke, A., and Schneider, G. A. (2010). Size-dependent elastic/inelastic behavior of enamel over millimeter and nanometer length scales. *Biomaterials* 31, 1955–1963. doi: 10.1016/j.biomaterials.2009.11.045

Arsecularatne, J., and Hoffman, M. (2012). Ceramic-like wear behaviour of human dental enamel. *J. Mech. Behav. Biomed. Mater.* 8, 47–57. doi: 10.1016/j.jmbbm.2011.12.002

Baldassarri, M., Margolis, H., and Beniash, E. (2008). Compositional determinants of mechanical properties of enamel. *J. Dent. Res.* 87, 645–649. doi: 10.1177/154405910808700711

Bas, P., Bostel, A., Deconihout, B., and Blavette, D. (1995). A general protocol for the reconstruction of 3D atom probe data. *Appl. Surf. Sci.* 87, 298–304. doi: 10.1016/0169-4332(94)00561-3

Beniash, E., Metzler, R. A., Lam, R. S., and Gilbert, P. (2009). Transient amorphous calcium phosphate in forming enamel. *J. Struct. Biol.* 166, 133–143. doi: 10.1016/j.jsb.2009.02.001

Bowen, W. H. (2013). Rodent model in caries research. *Odontology* 101, 9–14. doi: 10.1007/s10266-012-0091-0

Clarke, D. R. (1987). On the equilibrium thickness of intergranular glass phases in ceramic materials. *J. Am. Ceram. Soc.* 70, 15–22. doi: 10.1111/j.1151-2916.1987.tb04846.x

Diekwisch, T. G., Berman, B. J., Gentner, S., and Slavkin, H. C. (1995). Initial enamel crystals are not spatially associated with mineralized dentine. *Cell Tissue Res.* 279, 149–167. doi: 10.1007/BF00300701

Eastoe, J. E. (1960). Organic matrix of tooth enamel. *Nature* 187, 411–412. doi: 10.1038/187411b0

Featherstone, J., Duncan, J., and Cutress, T. (1979). A mechanism for dental caries based on chemical processes and diffusion phenomena during *in-vitro* caries simulation on human tooth enamel. *Arch. Oral Biol.* 24, 101–112. doi: 10.1016/0003-9969(79)90057-8

Gault, B., Yang, W., Ratinac, K. R., Zheng, R., Braet, F., and Ringer, S. P. (2010). Atom probe microscopy of self-assembled monolayers: preliminary results. *Langmuir* 26, 5291–5294. doi: 10.1021/la904459k

Giannuzzi, L. A., and Stevie, F. A. (1999). A review of focused ion beam milling techniques for TEM specimen preparation. *Micron* 30, 197–204. doi: 10.1016/S0968-4328(99)00005-0

Gordon, L. M., and Joester, D. (2011). Nanoscale chemical tomography of buried organic-inorganic interfaces in the chiton tooth. *Nature* 469, 194–197. doi: 10.1038/nature09686

Gordon, L. M., Cohen, M. J., MacRenaris, K. W., Pasteris, J. D., Takele, S., and Joester, D. (2015). Amorphous intergranular phases control the properties of tooth enamel. *Science* 347 746–750. doi: 10.1126/science.1258950

Gordon, L. M., Tran, L., and Joester, D. (2012). Atom probe tomography of apatites and bone-type mineralized tissues. *ACS Nano* 6, 10667–10675. doi: 10.1021/nn3049957

Habelitz, S., Marshall, S., Marshall, G. Jr., and Balooch, M. (2001). Mechanical properties of human dental enamel on the nanometre scale. *Arch. Oral Biol.* 46, 173–183. doi: 10.1016/S0003-9969(00)00089-3

He, L. H., and Swain, M. V. (2008). Understanding the mechanical behaviour of human enamel from its structural and compositional characteristics. *J. Mech. Behav. Biomed. Mater.* 1, 18–29. doi: 10.1016/j.jmbbm.2007.05.001

Hellman, O. C., Vandenbroucke, J. A., Rüsing, J., Isheim, D., and Seidman, D. N. (2000). Analysis of three-dimensional atom-probe data by the proximity histogram. *Microsc. Microanal.* 6, 437–444. doi: 10.1007/s100050010051

Hughes, J. M., Cameron, M., and Crowley, K. D. (1989). Structural variations in natural F, OH, and Cl apatites. *Am. Mineral.* 74, 870–876.

Joester, D., Hillier, A., Zhang, Y., and Prosa, T. J. (2012). Organic materials and organic/inorganic heterostructures in atom probe tomography. *Micros. Today* 20, 26–31. doi: 10.1017/S1551929512000260

Karlsson, J., Sundell, G., Thuvander, M., and Andersson, M. (2014). Atomically resolved tissue integration. *Nano Lett.* 14, 4220–4223. doi: 10.1021/nl501564f

Kelly, T. F., and Miller, M. K. (2007). Invited review article: atom probe tomography. *Rev. Sci. Instrum.* 78, 031101. doi: 10.1063/1.2709758

Landis, W. J., and Navarro, M. (1983). Correlated physicochemical and age changes in embryonic bovine enamel. *Calcif. Tissue Int.* 35, 48–55. doi: 10.1007/BF02405006

Legfros, R., Sakae, T., Bautista, C., Retino, M., and LeGeros, J. (1996). Magnesium and carbonate in enamel and synthetic apatites. *Adv. Dent. Res.* 10, 225–231. doi: 10.1177/08959374960100021801

Li, H., Xin, H. L., Kunitake, M. E., Keene, E. C., Muller, D. A., and Estroff, L. A. (2011). Calcite prisms from mollusk shells (Atrina Rigida): swiss−cheese−like organic–inorganic single−crystal composites. *Adv. Funct. Mater.* 21, 2028–2034. doi: 10.1002/adfm.201002709

McMurray, S., Gorman, B., and Diercks, D. (2011). TEM and atom probe investigation of calcium carbonate precipitation in seawater. *Microsc. Microanal.* 17, 758–759. doi: 10.1017/S1431927611004661

Miller, M. K. (2000). *Atom Probe Tomography: Analysis at the Atomic Level.* New York, NY: Springer.

Miller, M. K., Russell, K. F., and Thompson, G. B. (2005). Strategies for fabricating atom probe specimens with a dual beam FIB. *Ultramicroscopy* 102, 287–298. doi: 10.1016/j.ultramic.2004.10.011

Miller, M. K., Russell, K. F., Thompson, K., Alvis, R., and Larson, D. J. (2007). Review of atom probe FIB-based specimen preparation methods. *Microsc. Microanal.* 13, 428–436. doi: 10.1017/S1431927607070845

Palmer, L. C., Newcomb, C. J., Kaltz, S. R., Spoerke, E. D., and Stupp, S. I. (2008). Biomimetic systems for hydroxyapatite mineralization inspired by bone and enamel. *Chem. Rev.* 108, 4754–4783. doi: 10.1021/cr8004422

Pan, Y., and Fleet, M. E. (2002). Compositions of the apatite-group minerals: substitution mechanisms and controlling factors. *Rev. Mineral. Geochem.* 48, 13–49. doi: 10.2138/rmg.2002.48.2

Pokroy, B., Quintana, J. P., El'ad, N. C., Berner, A., and Zolotoyabko, E. (2004). Anisotropic lattice distortions in biogenic aragonite. *Nat. Mater.* 3, 900–902. doi: 10.1038/nmat1263

Robinson, C., Brookes, S. J., Shore, R. C., and Kirkham, J. (1998). The developing enamel matrix: nature and function. *Eur. J. Oral Sci.* 106, 282–291. doi: 10.1111/j.1600-0722.1998.tb02188.x

Robinson, C., Shore, R., Brookes, S., Strafford, S., Wood, S., and Kirkham, J. (2000). The chemistry of enamel caries. *Crit. Rev. Oral Biol. Med.* 11, 481. doi: 10.1177/10454411000110040601

Terpstra, R., and Driessens, F. (1986). Magnesium in tooth enamel and synthetic apatites. *Calcif. Tissue Int.* 39, 348–354. doi: 10.1007/BF02555203

Thompson, K. F., Lawrence, D. F., Larson, D. J., Olson, J. D., Kelly, T. F., and Gorman, B. (2007). *In situ* site-specific specimen preparation for atom probe tomography. *Ultramicroscopy* 107, 131–139. doi: 10.1016/j.ultramic.2006.06.008

Vekilov, P. G. (2004). Dense liquid precursor for the nucleation of ordered solid phases from solution. *Cryst. Growth Des.* 4, 671–685. doi: 10.1021/cg049977w

Vurpillot, F., Bostel, A., and Blavette, D. (2000). Trajectory overlaps and local magnification in three-dimensional atom probe. *Appl. Phys. Lett.* 76, 3127–3129. doi: 10.1063/1.126545

Wallace, A. F., Hedges, L. O., Fernandez-Martinez, A., Raiteri, P., Gale, J. D., Waychunas, G. A., et al. (2013). Microscopic evidence for liquid-liquid separation in supersaturated CaCO3 solutions. *Science* 341, 885–889. doi: 10.1126/science.1230915

Wallwork, M. L., Kirkham, J., Zhang, J., Smith, D. A., Brookes, S. J., Shore, R. C., et al. (2001). Binding of matrix proteins to developing enamel crystals: an atomic force microscopy study. *Langmuir* 17, 2508–2513. doi: 10.1021/la001281r

Weiner, S., and Addadi, L. (2011). Crystallization pathways in biomineralization. *Annu. Rev. Mater. Res.* 41, 21–40. doi: 10.1146/annurev-matsci-062910-095803

World Health Organization Media Centre. (2012). "*Oral Health,*" *Fact Sheet*. Geneva: World Health Organization Media Centre.

Yilmaz, E. D., Bechtle, S., Özcoban, H., and Schreyer, A., Schneider, G. A. (2013). Fracture behavior of hydroxyapatite nanofibers in dental enamel under micropillar compression. *Scr. Mater.* 68, 404–407. doi: 10.1016/j.scriptamat.2012.11.007

Conflict of Interest Statement: The authors declare that the research was conducted in the absence of any commercial or financial relationships that could be construed as a potential conflict of interest.

Received: 17 September 2014; accepted: 13 February 2015; published online: 19 March 2015.

Citation: Gordon LM and Joester D (2015) Mapping residual organics and carbonate at grain boundaries and the amorphous interphase in mouse incisor enamel. Front. Physiol. ***6****:57. doi: 10.3389/fphys.2015.00057*

This article was submitted to Craniofacial Biology, a section of the journal Frontiers in Physiology.

frontiers in PHYSIOLOGY

ORIGINAL RESEARCH ARTICLE
published: 10 October 2014
doi: 10.3389/fphys.2014.00395

Helium ion microscopy of enamel crystallites and extracellular tooth enamel matrix

Felicitas B. Bidlack[1,2]*, Chuong Huynh[3], Jeffrey Marshman[3] and Bernhard Goetze[3]

[1] *Department of Mineralized Tissue Biology, Forsyth Institute, Cambridge, MA, USA*
[2] *Department of Developmental Biology, Harvard School of Dental Medicine, Boston, MA, USA*
[3] *Carl Zeiss Microscopy LLC, One Corporation Way, Peabody, MA, USA*

Edited by:
Bernhard Ganss, University of Toronto, Canada

Reviewed by:
Harald Osmundsen, University of Oslo, Norway
Janet Moradian-Oldak, University of Southern California, USA

****Correspondence:***
Felicitas B. Bidlack, Department of Mineralized Tissue Biology, Forsyth Institute, 245 First Street, Cambridge, MA 02142, USA
e-mail: fbidlack@forsyth.org

An unresolved problem in tooth enamel studies has been to analyze simultaneously and with sufficient spatial resolution both mineral and organic phases in their three dimensional (3D) organization in a given specimen. This study aims to address this need using high-resolution imaging to analyze the 3D structural organization of the enamel matrix, especially amelogenin, in relation to forming enamel crystals. Chemically fixed hemi-mandibles from wild type mice were embedded in LR White acrylic resin, polished and briefly etched to expose the organic matrix in developing tooth enamel. Full-length amelogenin was labeled with specific antibodies and 10 nm immuno-gold. This allowed us to use and compare two different high-resolution imaging techniques for the analysis of uncoated samples. Helium ion microscopy (HIM) was applied to study the spatial organization of organic and mineral structures, while field emission scanning electron microscopy (FE-SEM) in various modes, including backscattered electron detection, allowed us to discern the gold-labeled proteins. Wild type enamel in late secretory to early maturation stage reveals adjacent to ameloblasts a lengthwise parallel alignment of the enamel matrix proteins, including full-length amelogenin proteins, which then transitions into a more heterogeneous appearance with increasing distance from the mineralization front. The matrix adjacent to crystal bundles forms a smooth and lacey sheath, whereas between enamel prisms it is organized into spherical components that are interspersed with rod-shaped protein. These findings highlight first, that the heterogeneous organization of the enamel matrix can be visualized in mineralized en bloc samples. Second, our results illustrate that the combination of these techniques is a powerful approach to elucidate the 3D structural organization of organic matrix molecules in mineralizing tissue in nanometer resolution.

Keywords: tooth enamel, matrix organization, amelogenin, immuno-gold labeling, helium ion microscopy, high-resolution microscopy

INTRODUCTION

A major hurdle for our understating of tooth enamel formation has been to analyze simultaneously protein and mineral phase in developing teeth. This is because tooth enamel is a composite material consisting of proteins and calcium phosphate crystallites that are extremely small and needle shaped. With a thickness that is only a few nanometers (Daculsi et al., 1984) the crystallites are far below the resolution limit of light microscopy, the technique of choice for conventional histology and immunohistochemistry analyses. However, the increasing mineral content in later stages of enamel development prevents the thin sectioning and the use of these classical histology methods to visualize the proteins in the un-demineralized specimen. The specimen has to be demineralized to allow for the preparation of thin sections followed by labeling or staining, and analysis using light microscopy. Electron microscopy is classically the technique of choice to study the formation and arrangement of the mineral phase. In early stages of enamel formation the mineral content of the enamel is still low enough to allow for ultra-thin sectioning and labeling with immuno-gold, if desired, and the use of transmission electron microscopy (TEM) analyses, including selected area electron diffraction to identify the mineral phase. Using this approach, it has been shown that enamel mineral formation starts as amorphous calcium phosphate (ACP) (Beniash et al., 2009). Thus, the protein matrix guides ACP maturation to form the correct shape of hydroxyapatite-like (HAP) crystallites (Moradian-Oldak, 2012). At later stages of enamel formation, the higher mineral content prevents the preparation of ultra-thin sections for TEM analyses. Scanning electron microscopy (SEM) is then frequently used to study the appearance of tooth surfaces, or to analyze polished and etched sections of the tooth to learn about the thickness and degree of mineralization of the enamel layer, as well as its microstructure. SEM analyses of fractured tooth surfaces give a spatial impression of enamel microstructure without prior etching.

Of the three structural tooth enamel matrix proteins amelogenin, ameloblastin, and enamelin, it is amelogenin that constitutes, with about 90 weight percent, the bulk of the organic matrix (Fincham et al., 1999). Although amelogenin is required for proper enamel formation, it is reabsorbed into the secreting ameloblast cells. The organic enamel matrix is therefore ephemeral and changes in composition and structural organization dynamically throughout enamel formation.

Since the formation and arrangement of enamel crystallites is protein-guided, it is desirable to analyze simultaneously in a given specimen both mineral and organic phases to better understand their interactions and spatial organization. One method with sufficient analytical resolution to visualize both the small crystallites and specifically labeled proteins is the use of TEM for the detection of immunogold-labeled proteins in ultra-thin sections of mineralized tissue. However, this technique cannot visualize the three dimensional structural organization of protein and mineral phase (Nanci et al., 1994; Diekwisch et al., 1995). Other high-resolution techniques such as atomic force microscopy, freeze fracture techniques, or cryo-TEM have delivered valuable new insights (Robinson et al., 1981; Beniash et al., 2005; He et al., 2008) but do not allow for the distinction between different matrix proteins in the organic phase. This poses a critical problem because the highly ordered composite protein-mineral structure results from key interactions between matrix proteins, growing crystals, and changes in the mineralizing matrix. These protein-protein and protein-mineral interactions regulate the final morphology and arrangement of hydroxyapatite-like crystals and, as a consequence, the mechanical properties of the resulting mature mineralized tissue (Margolis et al., 2006; Beniash, 2011; Moradian-Oldak, 2012).

This study pioneers the use of a new imaging technique, helium ion microscopy (HIM), to study enamel and addresses the need to analyze simultaneously the spatial organization of matrix proteins and crystallites *in situ* to advance our understanding of tooth enamel formation (Hill et al., 2012; Notte and Goetze, 2014). HIM has, as a novel imaging technique, recently received a lot of attention because it allows for imaging at nanometer resolution with outstanding depth of field. HIM enables us to look in a new way at a wide array of sample preparations since there are no constraints, as in TEM or light microscopy, on sample concentrations, thickness of the sample, or the opacity of the substrate. In many respects, the sample preparation for HIM and SEM are very similar. However, as discussed below, there are important differences between these two techniques such as the mechanisms of contrast generation and image formation. So far, HIM has mostly been applied in material sciences. This paper presents a comparison between FE-SEM and HIM imaging of developing tooth enamel and introduces HIM as a method of in situ analyses of biomineralization samples. Specifically, we used this high resolution imaging approach to test the hypothesis that the 3D structural organization of the enamel matrix is different in direct vicinity to bundles of forming crystallites compared to the matrix filled space between these crystallite bundles. The identification of differences in matrix organization lays the groundwork for further studies to identify the distribution of the structural proteins of the enamel matrix and their cleavage products.

MATERIALS AND METHODS

SAMPLE PREPARATION

All procedures for obtaining the samples followed the Forsyth IACUC approved protocol. Mouse wild type (C57BL/6) hemimandibles and hemi-maxillae were fixed in 4% zinc formalin for 24 h at room temperature, rinsed in water and dehydrated through a graded ethanol series followed by gradual ethanol substitution with LR White acrylic resin (Electron Microscopy Sciences, Hatfield, PA). The samples were polymerized at 60°C for 24 h and, after cooling to room temperature, polished in a parasagittal plane to expose the area of interest within the tooth enamel. Etching of the polished surface for 15 s in 0.1 M phosphoric acid (Sigma Aldrich) exposed the enamel matrix between and around forming enamel crystal bundles. After air-drying, samples were mounted on electron microscopy stubs and viewed in HIM and FE-SEM.

Tooth enamel at various stages of development was used for the imaging, starting with early secretory enamel, including late secretory, transition stage, and maturation stage enamel. These different stages of enamel development are very well defined and characterized (Smith et al., 2011) in relation to external landmarks and distance measurements from the cervical loop. These reference points were adapted from the work of Smith and Nanci (1989), as adapted by Lacruz et al. (2012) and are visible also in embedded samples. This procedure ensured that precisely defined and comparable enamel regions and mineralization stages were analyzed.

Immunohistochemistry

Commercially available primary antibodies were used to label the C-terminus of the full-length amelogenin molecule (Abcam ab59705). The primary antibody for the full-length amelogenin was applied at a 1:1000 dilution and then identified using a goat anti-rabbit IgG conjugated to 10 nm immuno-gold secondary antibody labeling (Aurion, obtained through Electron Microscopy Sciences, Hatfield, PA, USA). Specifically, the embedded, polished and etched samples were transferred into phosphate buffered saline (1× PBS), rinsed twice for 2 min, then treated with 2% sodiumborohydrate solution for a total of 90 min at room temperature with four solution changes, followed by five rinses in 1× PBS of 2 min each and 20 min in 4% goat serum at RT. The primary antibody was applied in 4% goat serum overnight at 4°C. The sample was rinsed twice for 5 min in 1× PBS before the secondary antibody was applied at 1:25 dilution for 2 h at RT followed by 4 h at 4°C. The sample was then washed five times for 5 min in 1× PBS, followed by five 2-min rinses in distilled water and air-dried. Negative controls were processed the same way, except that the addition of primary antibody was omitted during incubation with 4% goat serum overnight at 4°C. It has been shown previously that the goat anti-rabbit IgG conjugated immunogold label does not bind unspecifically to mineral or enamel matrix protein (Du et al., 2009).

IMAGING

All samples were imaged without any coating. SEM was performed on a Zeiss Merlin FE-SEM at Zeiss LLC., headquarters in Peabody, MA, and a Zeiss Ultra Plus FE-SEM at the Harvard

Center for Nanoscale Structures. With both instruments, samples were viewed at a working distance of 3–4 mm, a voltage of 1 kV, and 50–52 pA probe current.

For HIM either the Zeiss Orion® helium ion microscope located at MIT or the instrument at the Zeiss headquarters in Peabody was used and samples were viewed at 9–11 mm working distance and flood gun settings optimized for each sample.

The ion beam for imaging is generated in the HIM by introducing helium ions to a cryogenically cooled tungsten tip, a crystalline metal wire that is chemically etched to form a very pointy tip, the shape of a pyramid (**Figure 1**). The shape of the tip is refined through field evaporation of atoms from the tip, which results in atomically sharp edges and only a few atoms protruding from the tip. For operation, only three atoms forming a trimer are used as emitting source and this process is thus referred to as building the trimer. When properly aligned, the helium ions interact with the emitting tungsten tip such that only the emission from one atom, seen as the brightest one of the trimer, is used for imaging. Changing the gas pressure modifies the beam current. The beam path and the shape of the beam envelope are schematically illustrated in **Figure 2**. The deBroglie wavelength of the accelerated helium ions is about 100 times smaller than the corresponding voltage dependent wavelength of electrons used in SEM. Compared to the Schottky FEG electron source in field emission scanning electron microscopes (FE-SEM), the source brightness in HIM is about 30 times higher (Bell, 2009). These factors, and the small energy spread of the HIM source, contribute to the superb sub-nanometer spatial resolution and great contrast in HIM images of uncoated specimens and provide different information than SEM. In comparisons between HIM and SEM imaging, it has been shown that the interactions of helium ions with the sample material during imaging are confined to a very small volume at the sample surface (Bell, 2009). This beam-sample interaction in the HIM is similar to the effect of SEM imaging at very low voltage.

However, different from SEM imaging, and illustrated in **Figure 3**, only a positive net charge is created by the helium ion beam at the very top surface layer because they readily obtain electrons and thus become neutralized when passing into bulk matter. A low-energy electron flood beam in the Orion HIM neutralizes this positive charge. Both energy as well as duration of the flooding with the neutralizing beam can be adjusted and performed either after each line or after each frame when the sample is scanned. During imaging with the helium beam, the flood gun is blanked, while during neutralizing of charges the helium beam is blanked and the secondary electron detector is biased negatively, thus preventing saturation. This imaging approach allows for the analysis of insolating samples, such as biological samples, at nanometer resolution and without application of conductive

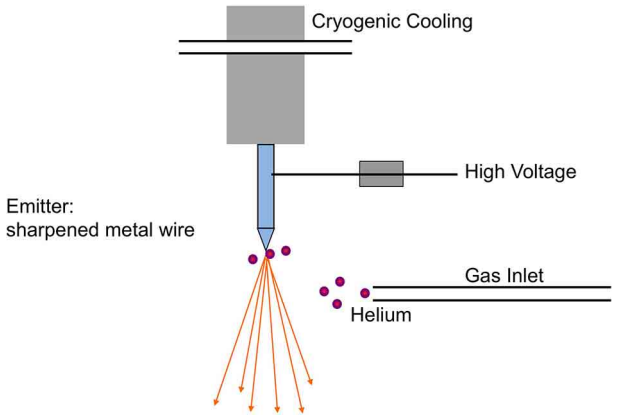

FIGURE 1 | Schematic of the field emission source in the helium ion microscope. The crystalline metal wire tip, chemically etched to form a very pointy tip, is cooled to about 80 K and located in a high vacuum chamber, which is filled with helium gas during operation. The helium atoms are ionized in the high electric field at the end of the wire tip and accelerated to form the helium ion beam with an appropriate voltage between the emitting tip and an extractor. Illustration simplified from Hill et al. (2012).

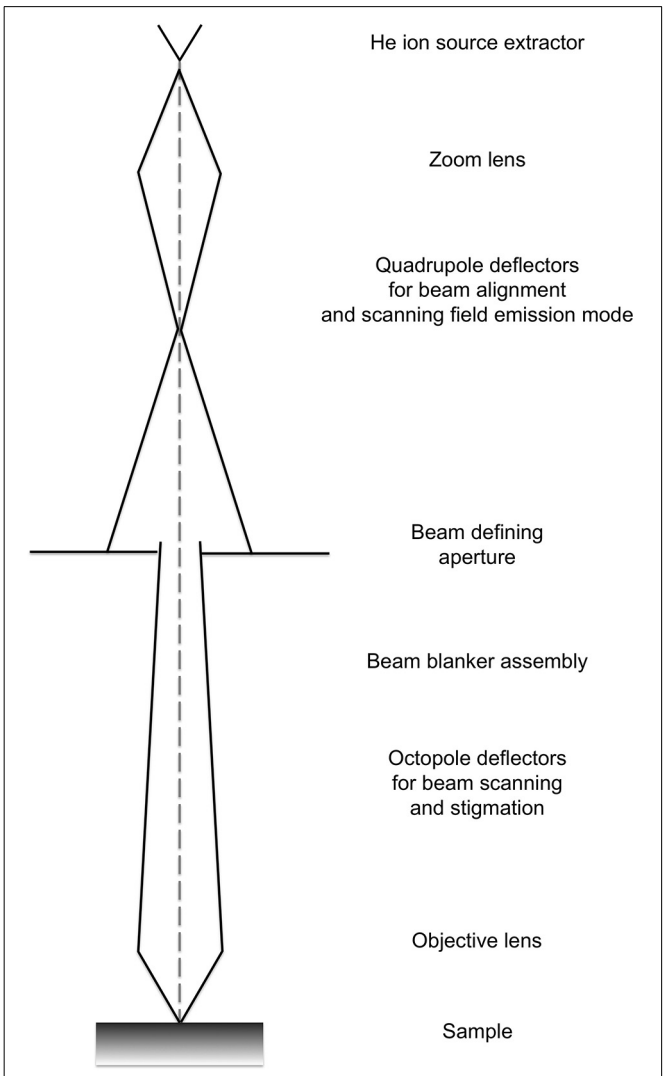

FIGURE 2 | Schematic showing the typical beam envelope and principal components of a helium ion microscope column. Illustration modified from the comprehensive description of helium ion microscopy (Hill et al., 2012).

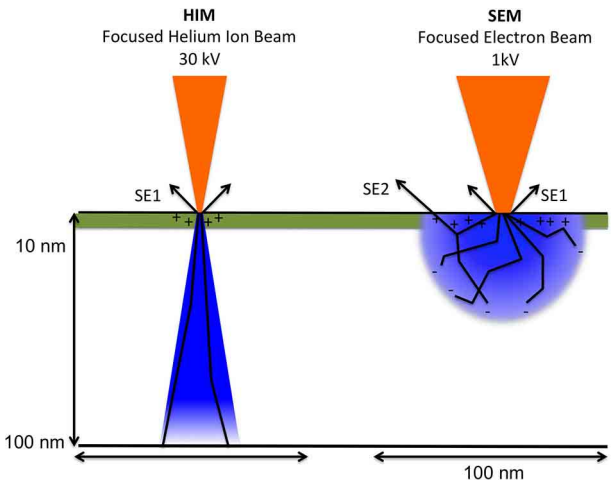

FIGURE 3 | Schematic comparing between helium ion beam and electron beam and charge distribution upon beam-sample interaction. The volume of sample interaction, depicted in blue, represents the volume affected by the incident ion or electron beam. It depends on the atomic composition of the sample (Z number), as well as the energy and angle of the incident beam. Arrows labeled SE1indicate secondary electrons created by the primary beam. SE2: secondary electrons created from back scattered electrons. The escape depth of secondary electrons is indicated in green. Illustration based on the comprehensive description of helium ion microscopy (Hill et al., 2012) and the most recent description of advances in HIM imaging (Notte and Goetze, 2014).

coating. Furthermore, the helium beam has, compared to the electron beam, very little angular deflection upon entering the sample due to the high mass of helium ions compared to electrons. Since electrons are much lighter they experience much higher deflection angles after entering the bulk sample.

The surface sensitivity of HIM also mandates that the surface of a given sample be free of contamination with hydrocarbons that can result from sample preparation steps such as a final rinse of the sample with methanol to evaporate water, or from using canned air often used in SEM sample preparation to blow off the sample surface. Also, if a given sample is to be analyzed by different techniques in a workflow, HIM analyses should precede SEM analyses because the interactions between electron beam and sample in the SEM can result in beam damage and surface alteration, especially when uncoated organic samples are viewed. As a consequence, the generation of hydrocarbons on the sample surface generates a layer of atoms that interact with the helium beam. The sample appears as if out of focus, or as if covered by a blanket, it could be described as the "table cloth effect."

Despite apparent similarity in sample preparation between SEM and HIM, such as mounting the sample on the same metal stubs and viewing desiccated samples under high vacuum, the differences between these two techniques provide different images of the same sample and different kinds of information.

RESULTS

HELIUM ION MICROSCOPY

HIM imaging is extremely sensitive to contamination of the sample surface with hydrocarbons, which result in loss of contrast and depth of field. This surface and contamination sensitivity requires that methods of sample preparation be optimized for HIM. For example, a final rinse of the sample in methanol to accelerate water evaporation after a final washing step, or the use of canned air to blow a sample dry, can result in a layer of hydrocarbons resembling a table cloth on the surface that prevent the detection of any surface details, but no such effect is seen in SEM analyses. Protocols for sample preparation and storage have been optimized for HIM to ensure clean and contamination free sample surfaces. Samples viewed in SEM and HIM for comparison were always prepared and stored exactly the same way.

As seen in **Figure 4**, HIM provides exceptional depth of field and resolution. The low magnification imaging of mature mouse incisor enamel shows that the technique provides good contrast and allows for the discernment of crystallites within enamel prisms at low magnifications and in overview images with a field of view of 30 μm (**Figure 4A**). At high magnification, with field of view of 3 μm, single enamel crystallites are crisp and clearly seen in all of their different orientations and throughout the depth of field (**Figure 4B**).

Imaging of early maturation stage and transition stage enamel provides a good opportunity to test whether organic matter provides enough contrast and can be discerned from calcium phosphate crystallites. **Figure 5** illustrates this point and shows remnants of the organic matrix between enamel prisms. Both mineral and organic matter are seen with very good depth of field, the organic material appears smooth and adjacent crystallites seem embedded in it.

Examples for HIM imaging of late secretory stage enamel are shown in **Figure 6**. **Figure 6A** gives an overview at 9 μm field of view and shows bundles of crystallites embedded in the organic matrix (arrows). The typical rodent decussation pattern, with single layers of prisms being oriented perpendicular to each other is visible. The organic material directly adjacent to the prism perimeter has a lacey appearance (marked ##). At higher magnification, a field of view of 3 μm, shown in **Figure 6B** illustrates the different appearance of the matrix in direct vicinity to crystallite bundles compared to the organic matrix between prisms.

To identify the organic material, we have also analyzed samples with 10 nm immuno-gold labeled amelogenin. However, because immuno-gold particles are covered with protein in the form of the secondary antibody, they have the same contrast as the protein matrix surrounding them. So, using the primary detector in HIM, the immuno-gold label was not detected. That this was not due to the absence of labeling signal was verified by analyzing the same sample and sample area in back scattered electron mode in FE-SEM, where the immuno-gold label can be clearly seen, as described below. Therefore, a backscattered electron detector is required in the HIM to detect this kind of signal. At the time of these analyses, however, the instruments available did not have this set up.

FIELD EMISSION SCANNING ELECTRON MICROSCOPY (FE-SEM)

A comparison between HIM and FE-SEM analyses of secretory stage enamel is shown in **Figure 7** and highlights the differences between these two imaging techniques: the much greater

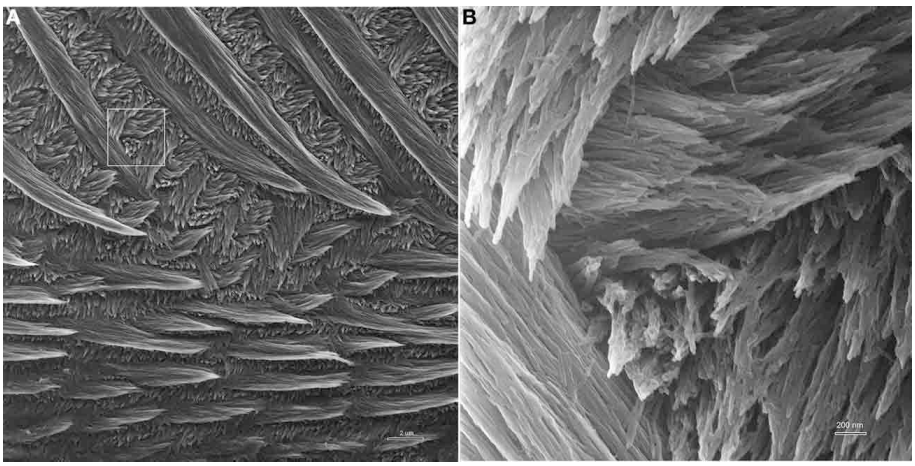

FIGURE 4 | Helium ion micrograph of maturation stage mouse incisor enamel, polished and etched in parasagittal plane. The sample is uncoated. **(A)** View over enamel prism organization close to the labial tooth surface. The excellent contrast and resolution permit, despite low magnification, the discernment of enamel crystallites within the prisms. Scale bar 2 µm. The area indicated in A is magnified in **(B)** and illustrates the excellent resolution and depth of field of helium ion microscopy at higher magnification where single crystallites can clearly be distinguished.

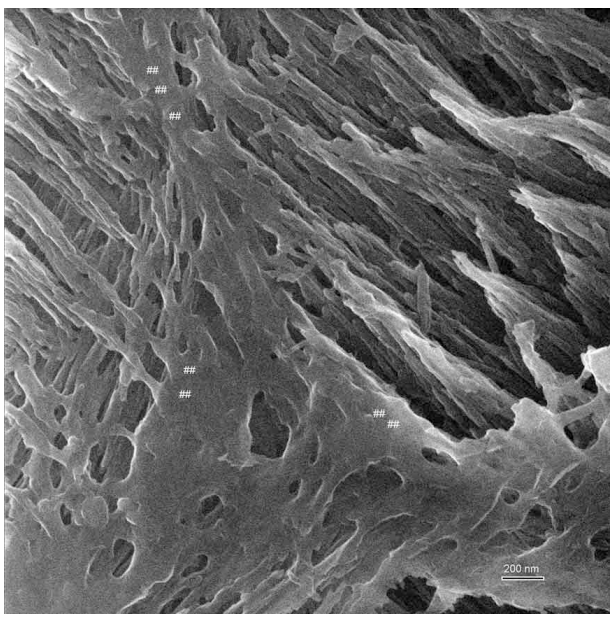

FIGURE 5 | Helium ion micrograph of an uncoated sample of mouse incisor enamel in early maturation stage, polished and etched in parasagittal plane. The imaged area shows enamel crystallites extending in their long axis in different directions and planes as they belong to different enamel prisms. The great depth of field reveals on the left side of the image crystallites in the foreground extending between upper left to lower right. At a further depth but imaged at equal resolution and contrast intensity, crystallites extend between lower left and upper right. Between the prisms appears smooth organic material (marked ##). Scale bar 200 nm.

depth of field in HIM imaging combined with helium ion beam-sample interactions that remain very much on the sample surface, on the one hand, and the deeper reaching electron beam-sample interactions in FE-SEM, on the other hand. As a result, organic material in the same stage of enamel development and in equally prepared samples has a different appearance, and provides different information when analyzed in HIM compared to FE-SEM. **Figures 7A,B** reveal in FE-SEM analysis structural details of the organic matrix surface that are not discernible in HIM (**Figures 7C,D**). **Figures 7B,D** show details of **Figures 7A,C** in higher magnification. The mineral phase of forming prisms has been removed in the etching process thus exposing the organic matrix surrounding the forming prism. Although the HIM images reveal the network-like organization of organics delimiting the prism space (**Figures 7C,D**), the matrix between prisms appears smooth and no structural details can be clearly discerned. FE-SEM, in contrast, has much less depth of field and the space accommodating the forming prisms appears as a black hole. Yet, the structure of the organic matrix is much clearer and details can be discerned. For example, just as in HIM, the organic matrix forming the wall, as it were, of the prism spaces is smooth and similar to lace as indicated (marked as ##). Interestingly, the matrix between the forming prisms has a completely different organization and a variety of shapes and structures can be seen. Abundant spherical structures of up to about 100 nm diameter can be discerned (**Figure 7A** arrow heads), as well as rod like features of several hundred nanometer length and less than 100 nm diameter are visible (**Figure 7B** open arrows).

Using immunogold labeling of the C-terminal end of amelogenin, the full-length amelogenin or the cleaved C-terminus can be identified, and the enamel matrix organization upon secretion by secretory stage ameloblasts is visible in FE-SEM (**Figure 8**). The parallel alignment of elongated, rod shaped structures is seen using the in-lens detector (**Figure 8A**) and identified by the backscattered electron signal of the immuno-gold label as seen in **Figure 8B**, with the control shown in **Figure 8C**. The parallel alignment of the labeled protein aggregates is apparent and seems to sit on a zig-zag shaped line that divides the area of parallel rods from an underlying area of different organization.

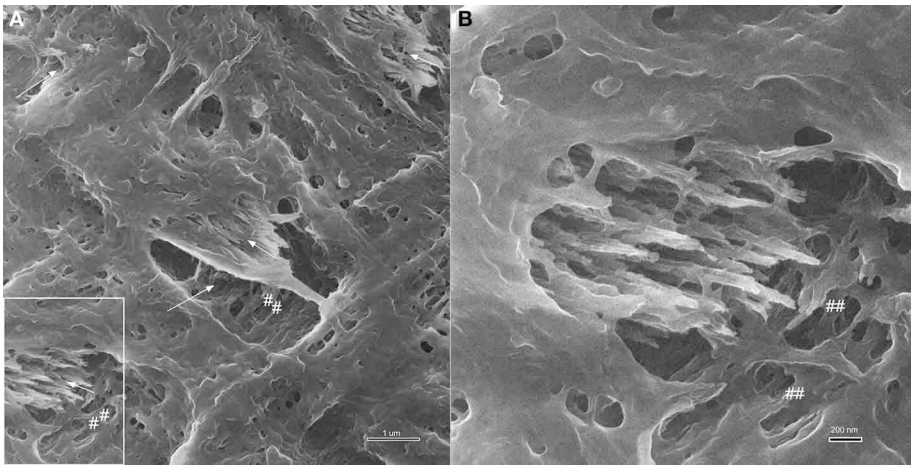

FIGURE 6 | Helium ion micrographs of mouse incisor enamel in late secretory stage with crystallites (arrows) embedded in organic matrix. **(A)** Overview image, 9 μm field of view. Crystallites are in bundles and arranged in typical rodent decussation pattern (arrows). Organic material directly adjacent to the prism perimeter has a lacey appearance (marked as ##). Area indicated in **(A)** imaged at higher magnification in **(B)** with a field of view of 3 μm to illustrate the different appearance of the matrix in direct vicinity to crystallite bundles compared to the organic matrix between prisms.

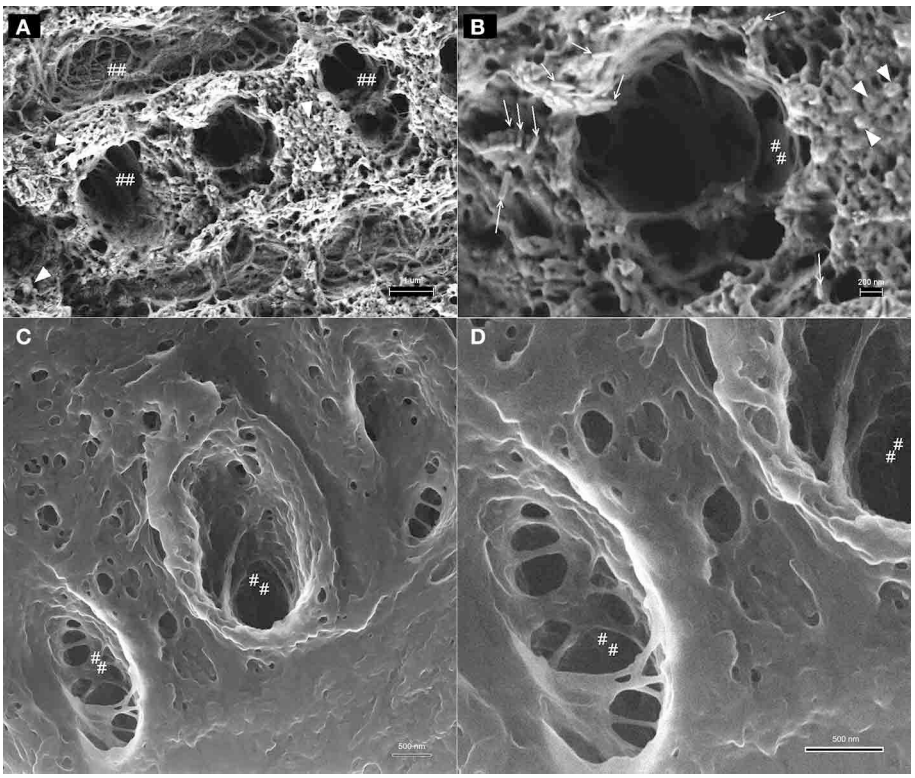

FIGURE 7 | Comparison between imaging in FE-SEM and HIM imaging of organic matrix in secretory stage mouse enamel. The mineral phase of forming prisms has been removed by etching thus exposing the organic matrix. **(A,B)** FE-SEM images show the variable structure of the organic matrix, the spaces accommodating the forming prisms appear as a black hole, however, due to limited depth of field. Organic matrix forming the wall, as it were, of the prism spaces is smooth and similar to lace as indicated (marked as ##). Spherical structures of up to ∼100 nm diameter are abundant between forming prisms (arrow heads) and rod like features of several hundred nanometer length and less than 100 nm diameter can be discerned (open arrows). **(C,D):** HIM images reveal with great depth of field the network-like organization of organics delimiting the prism space. The matrix between prisms appears smooth and no structural details can be clearly discerned.

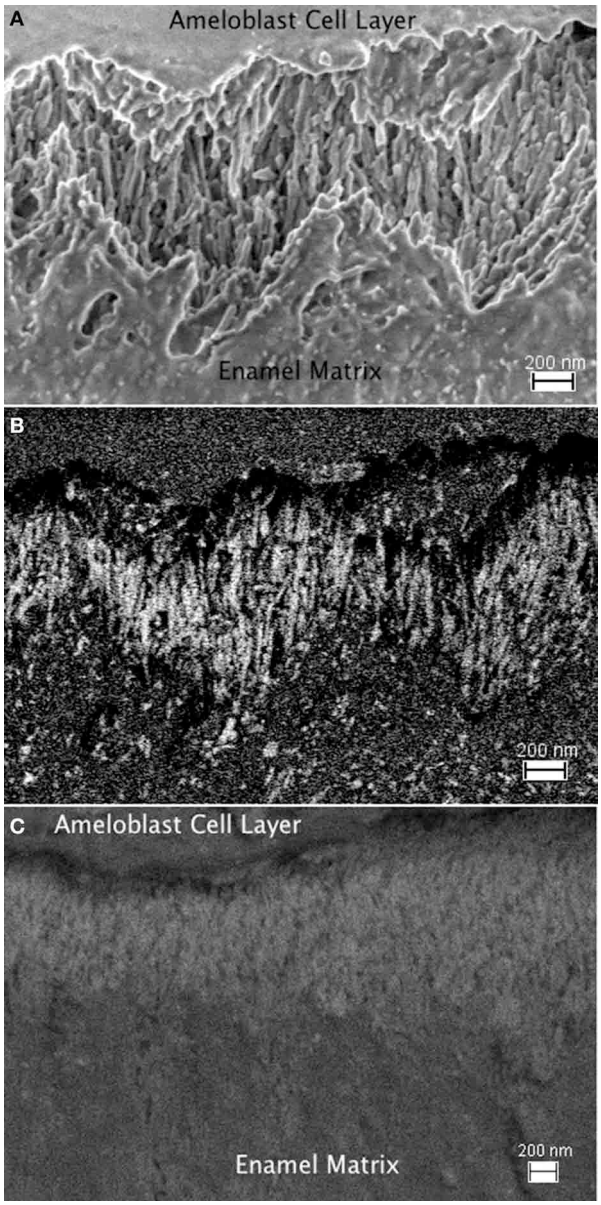

FIGURE 8 | FE-SEM imagines of enamel matrix organization upon secretion by secretory stage ameloblasts. (A): The parallel alignment of elongated, rod shaped structures is seen using the in-lens detector. The interface between ameloblast cell layer and secreted matrix is in the top part of the image, the mineralizing matrix is in the bottom part. The time since secretion increases with the distance from the ameloblasts. **(B)** Back scattered electron signal of the same sample area to identify the immuno-gold labeled full-length amelogenin. The electron density of the gold particles results in their bright white appearance. A zig-zag shaped line divides the area of parallel aligned matrix structure from an underlying area of different organization in the lower part of the image with earlier secreted enamel matrix. This zig-zag line follows the shape of the Tomes process of the ameloblasts, which extend from the upper part into the imaged area. **(C)** Control sample imaged in back scattered electron mode. The absence of gold labeling results in a lack of high contrast due to absence of a backscattered signal from gold particles. This implies that in the absence of the primary antibody labeling the C-terminal end of the amelogenin, the immuno-gold particles do not bind nonspecifically, or preferentially to mineral or enamel matrix proteins.

This zig-zag line follows the shape of the Tomes' process of the ameloblasts. The arrangement of rod-shaped structures at the mineralization front, between the ameloblast cell layer (on top of the image area) and the secretory stage enamel matrix is shown in high magnification in **Figure 9**, where 10 nm sized particles can be discerned using the in-lens detector (**Figure 9A**) and the backscattered electron detector (**Figure 9B**).

DISCUSSION

In the study of tooth enamel formation there exists a divide between *in vitro* studies and the use of animal models and *in situ* analyses of enamel formation. This is partly due to the technical challenges of analyzing the formation of very small calcium phosphate crystals in an organic matrix. This study is an attempt to address this problem by using high-resolution imaging techniques such as HIM and FE-SEM to investigate the relationship between calcium phosphate crystallites and structural organization of the organic matrix *in situ* and in various stages of enamel development.

The most abundant of the three structural enamel matrix proteins, amelogenin, is required for proper enamel formation, but is reabsorbed into the secreting ameloblast cells (Bartlett, 2013). The organic enamel matrix is therefore ephemeral and changes dynamically throughout enamel formation (Simmer et al., 2012). Amelogenin has only one phosphorylation at Ser16 and no other post-translational modifications (Takagi et al., 1984; Fincham and Moradian-Oldak, 1995). Because it has only one posttranslational modification, amelogenin has been successfully expressed in bacteria and, due to its high abundance, can be purified from immature pig teeth. These advantages have afforded *in vitro* studies with sufficient quantities of purified protein, which sets amelogenin apart from the other two enamel matrix proteins ameloblastin and enamelin. A wealth of *in vitro* studies has focused on the self-assembly behavior of amelogenin under a range of conditions, recently reviewed by Moradian-Oldak (2012). Amelogenin forms a gel-like self-assembly structure under physiological conditions of pH, temperature, and concentration (Mechanic et al., 1967; Katz et al., 1969; Wiedemann-Bidlack et al., 2007). Therefore, amelogenin is most frequently studied *in vitro* under non-physiological conditions where nanospheres are observed that, under certain conditions further assemble to form elongated structures (Du et al., 2005; Bromley et al., 2011; Chen et al., 2011; Wiedemann-Bidlack et al., 2011). However, recent evidence indicates that the often described amelogenin nanospheres are not stable in the presence of calcium and/or phosphate ions or when mineralization is initiated (Tarasevich et al., 2009a).

New insights from *in vitro* studies about the interaction of amelogenin with mineral and calcium phosphate crystal surfaces and previous models of enamel formation have provided a basis for expanded, or updated models of enamel mineralization and the role of amelogenin (Robinson et al., 2003; Robinson, 2007; Tarasevich et al., 2009b; Beniash et al., 2012; Moradian-Oldak, 2012). Recent models propose that amelogenin nanospheres (Du et al., 2005), dimers (Martinez-Avila et al., 2012), or barrel structures (Fang et al., 2013) aggregate into linear arrays, comparable to strings of pearls, and form a template that induces apatite

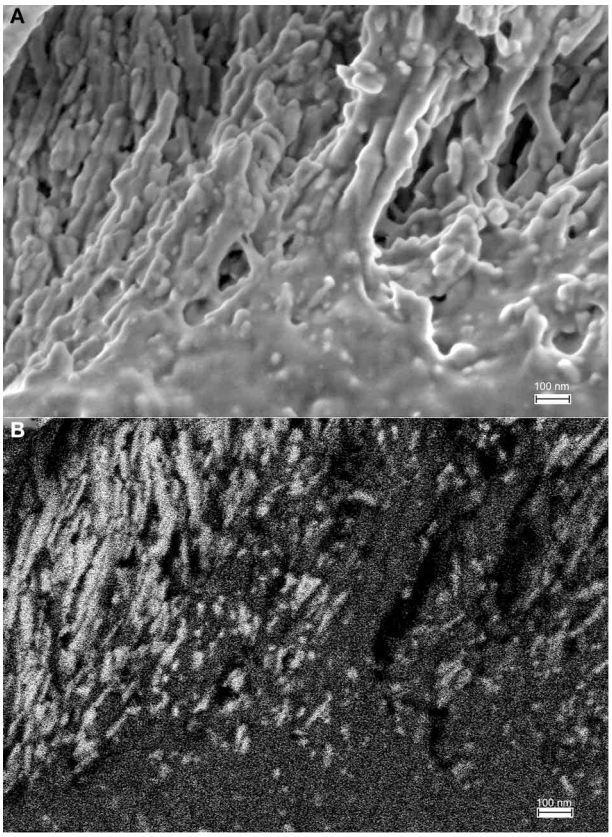

FIGURE 9 | Rod-shaped structures at the mineralization front, between the ameloblast cell layer (on top of the image area) and the secretory stage enamel matrix is shown in high magnification. (A) Field of view 1.816 μm imaged using the in-lens detector, 10 nm sized particles can be discerned. **(B)** Backscattered electron image of the same sample area showing the immuno-gold labeled amelogenin in bright white due to the high electron density of gold particles.

formation. The role of inducing apatite formation and guiding crystal arrangement has been suggested for amelogenin by various authors, and has been modified to propose that native full-length amelogenin stabilizes ACP phases, whereas upon cleavage this stabilizing quality is lost and the amorphous mineral transforms into crystalline hydroxyl apatite (Beniash et al., 2009; Yang et al., 2010; Kwak et al., 2011; Moradian-Oldak, 2012).

Combining what is known about the dynamic nature of the enamel matrix *in situ* and *in vitro* findings of changing amelogenin self-assembly and molecular structure in the presence of mineral, one would expect that the enamel matrix appearance varies according to location and at interfaces with crystallites. To refine our models and concepts of enamel formation requires the analysis of mineralizing enamel *in situ* and the application of high-resolution imaging techniques that provide nanometer resolution. The data presented here demonstrate that HIM imaging, especially in combination with FE-SEM, is a very promising approach to achieve this goal. Taking advantage of the much smaller wavelength of helium ions compared to electrons and a small convergence angle of the helium ions on the sample, as explained briefly above in Methods (**Figure 3**), an outstanding depth of field is achieved in HIM imaging as seen in **Figures 4–6**. These images also illustrate quite well the advantage of charge neutralization available in HIM imaging through the use of a flood gun. Although all of the analyzed samples are uncoated biological samples embedded in acrylic resin and thus completely insulating material, there is no charge build up in HIM imaging, which is on the contrary notorious in electron microscopy of this sample type. Especially the very thin crystallites that protrude from the sample in various directions, seen in mature enamel depicted in **Figure 3** and early maturation stage enamel in **Figure 4**, can be imaged at very high resolution in HIM without developing charges and appear equally crisp in all planes. The problem of charges developing in electron microscopy can be addressed using imaging under variable pressure conditions albeit at the significant expense of analytical resolution. Although it seems apparent in these figures that the needle shaped morphology is indicative of enamel crystallites, the unequivocal distinction between protein and mineral, and ideally mineral phase identification, requires additional sample analysis. Conventionally, mineral phase identification is performed using selected area diffraction analyses in (TEM) of ultra thin sections. However, using an electron backscattered diffraction system (ESBD) offers an alternative approach for mineral phase identification on en bloc samples with polished surface. Unfortunately, this kind of detector was not available on the microscopes used in this study.

The much greater depth of field in HIM imaging combined with helium ion beam-sample interactions that remain very much on the sample surface, on the one hand, and the deeper reaching electron beam-sample interactions in FE-SEM (**Figure 3**), on the other hand, explain the different imaging results illustrated in **Figure 7**. Using FE-SEM, structural details and organization of the organic material are revealed in the same stage of enamel development, but in equally prepared samples (**Figures 7A,B**) these features cannot be discerned using HIM (**Figures 7C,D**).

For this study we have used immunohistochemistry in conjunction with high-resolution microscopy to only identify amelogenin (**Figures 8A–C**, **9**) and explore the usefulness of HIM in comparison to FE-SEM for the detection of immuno-gold labels. However, it is known that ameloblastin and enamelin are also present at the mineralization front (Gallon et al., 2013; Mazumder et al., 2014) and required for enamel formation (Fukumoto et al., 2004; Hu et al., 2008; Bartlett, 2013). It is therefore important to keep in mind that the presented data do not preclude the presence of these matrix proteins in newly secreted matrix and enamel prisms formation.

The data presented here demonstrate that HIM imaging, especially in combination with FE-SEM, is a very promising approach to further our understanding of enamel matrix organization and enamel mineralization *in situ*. The use of these two high-resolution imaging techniques together on a given sample provides complementary information on the structural three dimensional organization of the mineralizing enamel matrix and its relation to crystallite formation.

ACKNOWLEDGMENTS

We are grateful for insightful discussions and great departmental support provided by Drs. John D. Bartlett and Megan Pugach. This work was funded by NIH grant 1R03DE021765-01A1.

REFERENCES

Bartlett, J. D. (2013). Dental enamel development: proteinases and their enamel matrix substrates. *ISRN Dent.* 2013:684607. doi: 10.1155/2013/684607

Bell, D. C. (2009). Contrast mechanisms and image formation in helium ion microscopy. *Microsc. Microanal.* 15, 147–153. doi: 10.1017/S1431927609090138

Beniash, E. (2011). Biominerals–hierarchical nanocomposites: the example of bone. *Wiley Interdiscip. Rev. Nanomed. Nanobiotechnol.* 3, 47–69. doi: 10.1002/wnan.105

Beniash, E., Metzler, R. A., Lam, R. S., and Gilbert, P. U. (2009). Transient amorphous calcium phosphate in forming enamel. *J. Struct. Biol.* 166, 133–143. doi: 10.1016/j.jsb.2009.02.001

Beniash, E., Simmer, J. P., and Margolis, H. C. (2005). The effect of recombinant mouse amelogenins on the formation and organization of hydroxyapatite crystals *in vitro*. *J. Struct. Biol.* 149, 182–190. doi: 10.1016/j.jsb.2004.11.001

Beniash, E., Simmer, J. P., and Margolis, H. C. (2012). Structural changes in amelogenin upon self-assembly and mineral interactions. *J. Dent. Res.* 91, 967–972. doi: 10.1177/0022034512457371

Bromley, K. M., Kiss, A. S., Lokappa, S. B., Lakshminarayanan, R., Fan, D., Ndao, M., et al. (2011). Dissecting amelogenin protein nanospheres: characterization of metastable oligomers. *J. Biol. Chem.* 286, 34643–34653. doi: 10.1074/jbc.M111.250928

Chen, C. L., Bromley, K. M., Moradian-Oldak, J., and Deyoreo, J. J. (2011). In situ AFM study of amelogenin assembly and disassembly dynamics on charged surfaces provides insights on matrix protein self-assembly. *J. Am. Chem. Soc.* 133, 17406–17413. doi: 10.1021/ja206849c

Daculsi, G., Menanteau, J., Kerebel, L. M., and Mitre, D. (1984). Length and shape of enamel crystals. *Calcif. Tissue Int.* 36, 550–555. doi: 10.1007/BF02405364

Diekwisch, T. G., Berman, B. J., Gentner, S., and Slavkin, H. C. (1995). Initial enamel crystals are not spatially associated with mineralized dentine. *Cell Tissue Res.* 279, 149–167. doi: 10.1007/BF00300701

Du, C., Falini, G., Fermani, S., Abbott, C., and Moradian-Oldak, J. (2005). Supramolecular assembly of amelogenin nanospheres into birefringent microribbons. *Science* 307, 1450–1454. doi: 10.1126/science.1105675

Du, C., Fan, D., Sun, Z., Fan, Y., Lakshminarayanan, R., and Moradian-Oldak, J. (2009). Immunogold labeling of amelogenin in developing porcine enamel revealed by field emission scanning electron microscopy. *Cells Tissues Organs* 189, 207–211. doi: 10.1159/000151385

Fang, P. A., Margolis, H. C., Conway, J. F., Simmer, J. P., and Beniash, E. (2013). CryoTEM study of effects of phosphorylation on the hierarchical assembly of porcine amelogenin and its regulation of mineralization *in vitro*. *J. Struct. Biol.* 183, 250–257. doi: 10.1016/j.jsb.2013.05.011

Fincham, A. G., and Moradian-Oldak, J. (1995). Recent advances in amelogenin biochemistry. *Connect. Tissue Res.* 32, 119–124. doi: 10.3109/03008209509013713

Fincham, A. G., Moradian-Oldak, J., and Simmer, J. P. (1999). The structural biology of the developing dental enamel matrix. *J. Struct. Biol.* 126, 270–299. doi: 10.1006/jsbi.1999.4130

Fukumoto, S., Kiba, T., Hall, B., Iehara, N., Nakamura, T., Longenecker, G., et al. (2004). Ameloblastin is a cell adhesion molecule required for maintaining the differentiation state of ameloblasts. *J. Cell Biol.* 167, 973–983. doi: 10.1083/jcb.200409077

Gallon, V., Chen, L., Yang, X., and Moradian-Oldak, J. (2013). Localization and quantitative co-localization of enamelin with amelogenin. *J. Struct. Biol.* 183, 239–249. doi: 10.1016/j.jsb.2013.03.014

He, X., Li, W., and Habelitz, S. (2008). The cooperative self-assembly of 25 and 23kDa amelogenins. *J. Struct. Biol.* 164, 314–321. doi: 10.1016/j.jsb.2008.09.005

Hill, R., Notte, J. A., and Scipioni, L. (2012). "Scanning Helium Ion Microscopy," in *Advances in Imaging and Electron Physics*, Vol. 170, ed P. H. Hawkes (Amsterdam, London, Waltham, San Diego: Elsevier Inc.), 65–148. doi: 10.1016/B978-0-12-394396-5.00002-6

Hu, J. C., Hu, Y., Smith, C. E., Mckee, M. D., Wright, J. T., Yamakoshi, Y., et al. (2008). Enamel defects and ameloblast-specific expression in Enam knock-out/lacz knock-in mice. *J. Biol. Chem.* 283, 10858–10871. doi: 10.1074/jbc.M710565200

Katz, E. P., Seyer, J., Levine, P. T., and Glimcher, M. J. (1969). The comparative biochemistry of the organic matrix of developing enamel–II. Ultracentrifugal and electrophoretic characterization of proteins soluble at neutral pH. *Arch. Oral Biol.* 14, 533–539. doi: 10.1016/0003-9969(69)90146-0

Kwak, S. Y., Green, S., Wiedemann-Bidlack, F. B., Beniash, E., Yamakoshi, Y., Simmer, J. P., et al. (2011). Regulation of calcium phosphate formation by amelogenins under physiological conditions. *Eur. J. Oral. Sci.* 119 Suppl. 1, 103–111. doi: 10.1111/j.1600-0722.2011.00911.x

Lacruz, R. S., Smith, C. E., Moffatt, P., Chang, E. H., Bromage, T. G., Bringas, P. Jr., et al. (2012). Requirements for ion and solute transport, and pH regulation during enamel maturation. *J. Cell. Physiol.* 227, 1776–1785. doi: 10.1002/jcp.22911

Margolis, H. C., Beniash, E., and Fowler, C. E. (2006). Role of macromolecular assembly of enamel matrix proteins in enamel formation. *J. Dent. Res.* 85, 775–793. doi: 10.1177/154405910608500902

Martinez-Avila, O., Wu, S., Kim, S. J., Cheng, Y., Khan, F., Samudrala, R., et al. (2012). Self-assembly of filamentous amelogenin requires calcium and phosphate: from dimers via nanoribbons to fibrils. *Biomacromolecules* 13, 3494–3502. doi: 10.1021/bm300942c

Mazumder, P., Prajapati, S., Lokappa, S. B., Gallon, V., and Moradian-Oldak, J. (2014). Analysis of co-assembly and co-localization of ameloblastin and amelogenin. *Front. Physiol.* 5:274. doi: 10.3389/fphys.2014.00274

Mechanic, G. L., Katz, E. P., and Glimcher, M. J. (1967). The Sephadex gel filtration characteristics of the neutral soluble proteins of embryonic bovine enamel. *Biochim. Biophys. Acta* 133, 97–113. doi: 10.1016/0005-2795(67)90042-6

Moradian-Oldak, J. (2012). Protein-mediated enamel mineralization. *Front Biosci. (Landmark Ed.)* 17, 1996–2023. doi: 10.2741/4034

Nanci, A., Kawaguchi, H., and Kogaya, Y. (1994). Ultrastructural studies and immunolocalization of enamel proteins in rodent secretory stage ameloblasts processed by various cryofixation methods. *Anat. Rec.* 238, 425–436. doi: 10.1002/ar.1092380402

Notte, J., and Goetze, B. (2014). "Imaging with the helium ion microscope," in *Surface Analysis and Techniques in Biology,* ed V. S. Smentkowski (Switzerland: Springer International Publishing), 171–195. doi: 10.1007/978-3-319-01360-2_7

Robinson, C. (2007). Self-oriented assembly of nano-apatite particles: a subunit mechanism for building biological mineral crystals. *J. Dent. Res.* 86, 677–679. doi: 10.1177/154405910708600801

Robinson, C., Fuchs, P., and Weatherall, J. A. (1981). The appearance of developing rat incisor enamel using a freeze fracture technique. *J. Cryst. Growth* 53, 160–165. doi: 10.1016/0022-0248(81)90062-2

Robinson, C., Shore, R. C., Wood, S. R., Brookes, S. J., Smith, D. A., Wright, J. T., et al. (2003). Subunit structures in hydroxyapatite crystal development in enamel: implications for amelogenesis imperfecta. *Connect Tissue Res.* 44 Suppl. 1, 65–71. doi: 10.1080/03008200390152115

Simmer, J. P., Richardson, A. S., Hu, Y. Y., Smith, C. E., and Ching-Chun Hu, J. (2012). A post-classical theory of enamel biomineralization. . . and why we need one. *Int. J. Oral. Sci.* 4, 129–134. doi: 10.1038/ijos.2012.59

Smith, C. E., Hu, Y., Richardson, A. S., Bartlett, J. D., Hu, J. C., and Simmer, J. P. (2011). Relationships between protein and mineral during enamel development in normal and genetically altered mice. *Eur. J. Oral. Sci.* 119 Suppl. 1, 125–135. doi: 10.1111/j.1600-0722.2011.00871.x

Smith, C. E., and Nanci, A. (1989). A method for sampling the stages of amelogenesis on mandibular rat incisors using the molars as a reference for dissection. *Anat. Rec.* 225, 257–266. doi: 10.1002/ar.1092250312

Takagi, T., Suzuki, M., Baba, T., Minegishi, K., and Sasaki, S. (1984). Complete amino acid sequence of amelogenin in developing bovine enamel. *Biochem. Biophys. Res. Commun.* 121, 592–597. doi: 10.1016/0006-291X(84)90223-7

Tarasevich, B. J., Lea, S., Bernt, W., Engelhard, M. H., and Shaw, W. J. (2009b). Changes in the quaternary structure of amelogenin when adsorbed onto surfaces. *Biopolymers* 91, 103–107. doi: 10.1002/bip.21095

Tarasevich, B. J., Lea, S., Bernt, W., Engelhard, M., and Shaw, W. J. (2009a). Adsorption of amelogenin onto self-assembled and fluoroapatite surfaces. *J. Phys. Chem. B* 113, 1833–1842. doi: 10.1021/jp804548x

Wiedemann-Bidlack, F. B., Beniash, E., Yamakoshi, Y., Simmer, J. P., and Margolis, H. C. (2007). pH triggered self-assembly of native and recombinant

amelogenins under physiological pH and temperature *in vitro*. *J. Struct. Biol.* 160, 57–69. doi: 10.1016/j.jsb.2007.06.007

Wiedemann-Bidlack, F. B., Kwak, S. Y., Beniash, E., Yamakoshi, Y., Simmer, J. P., and Margolis, H. C. (2011). Effects of phosphorylation on the self-assembly of native full-length porcine amelogenin and its regulation of calcium phosphate formation *in vitro*. *J. Struct. Biol.* 173, 250–260. doi: 10.1016/j.jsb.2010.11.006

Yang, X., Wang, L., Qin, Y., Sun, Z., Henneman, Z. J., Moradian-Oldak, J., et al. (2010). How amelogenin orchestrates the organization of hierarchical elongated microstructures of apatite. *J. Phys. Chem. B* 114, 2293–2300. doi: 10.1021/jp910219s

Conflict of Interest Statement: The authors declare that the research was conducted in the absence of any commercial or financial relationships that could be construed as a potential conflict of interest.

Received: 15 July 2014; accepted: 23 September 2014; published online: 10 October 2014.

Citation: Bidlack FB, Huynh C, Marshman J and Goetze B (2014) Helium ion microscopy of enamel crystallites and extracellular tooth enamel matrix. Front. Physiol. ***5****:395. doi: 10.3389/fphys.2014.00395*

This article was submitted to Craniofacial Biology, a section of the journal Frontiers in Physiology.

frontiers in PHYSIOLOGY

ORIGINAL RESEARCH ARTICLE
published: 05 September 2014
doi: 10.3389/fphys.2014.00333

Remineralization and repair of enamel surface by biomimetic Zn-carbonate hydroxyapatite containing toothpaste: a comparative *in vivo* study

Marco Lelli[1†], Angelo Putignano[2†], Marco Marchetti[1], Ismaela Foltran[1], Francesco Mangani[3], Maurizio Procaccini[2], Norberto Roveri[1] and Giovanna Orsini[2]*

[1] *Department of Chemistry "G. Ciamician," Alma Mater Studiorum, University of Bologna, Bologna, Italy*
[2] *Department of Clinical Sciences and Stomatology, Polytechnic University of Marche, Ancona, Italy*
[3] *Department of Translational Medicine, Tor Vergata University of Rome, Rome, Italy*

Edited by:
Bernhard Ganss, University of Toronto, Canada

Reviewed by:
Thimios Mitsiadis, University of Zurich, Switzerland
Simone Grandini, University of Siena, Italy

***Correspondence:**
Giovanna Orsini, Polytechnic University of Marche, Via Tronto 10, 60126 Ancona, Italy
e-mail: g.orsini@univpm.it; giovorsini@yahoo.com

† These authors have contributed equally to this work.

Consumption of acidic foods and drinks and other factors that cause enamel wear are responsible for the daily enamel loss and degradation. Use of some toothpastes that have been showed to possess different properties of remineralisation and/or repair of the enamel surface may help to protect tooth enamel. The aim of this study was to evaluate whether the use of toothpaste containing Zn-carbonate hydroxyapatite (CHA) nanostructured microcrystals may exert remineralization/repair effects of the enamel surface. Two groups of patients, aged between 18 and 75 years, used a Zn-CHA nanocrystals-based toothpaste (experimental group) and a potassium nitrate/sodium fluoride toothpaste (active control group) for 8 weeks. At the end of this period, extractions were performed in five subjects per study group. Negative controls consisted of two subjects treated with non-specified fluoride toothpaste. Teeth were processed for morphological and chemical-physic superficial characterizations by means of Scanning Electronic Microscopy with Elementary analysis, X-Ray Diffraction analysis and Infrared analysis. In this study, the use of a Zn-CHA nanocrystals toothpaste led to a remineralization/repair of the enamel surface, by deposition of a hydroxyapatite-rich coating. On the other hand, the use of both a nitrate potassium/sodium fluoride and non-specified fluoride toothpastes did not appreciably change the enamel surface. In conclusion, this study demonstrates that the toothpaste containing Zn-CHA nanostructured microcrystals, differently from nitrate potassium/sodium fluoride and non-specified fluoride toothpastes, may promote enamel superficial repair by means of the formation of a protective biomimetic CHA coating.

Keywords: enamel, toothpaste, Zn-carbonate hydroxyapatite nanocrystals, fluoride, repair, remineralization

INTRODUCTION

Enamel loss as a part of tooth wear has become a common problem in everyday dental practice, which can be caused by erosion (Hooper et al., 2003), attrition and abrasion, being often associated with dentine hypersensitivity (DH) in different teeth (Absi et al., 1987; Addy, 1990; Addy et al., 2007; Addy and West, 2013). The predicted percentage of adults presenting severe tooth wear has increases with age from 3% at the age of 20 years to 17% at the age of 70 years (Van't Spijker et al., 2009).

Erosion is currently believed to be the major factor involved in tooth wear, and has been defined as the dissolution of teeth natural hydroxyapatite by either extrinsic or intrinsic acids, which are not originated from bacteria (Scheutzel, 1996; Zero and Lussi, 2000). Attrition describes the wear of teeth at sites of direct contact between teeth, which can be associated with occlusal function and may be exaggerated by parafunctional habits such as bruxism (Smith and Knight, 1984). Abrasion describes the wear of teeth caused by objects, including toothbrush, abrasive toothpastes as well as a variety of habits like pipe smoking (Dababneh et al., 1999). The combined action of all the above mentioned mechanisms may occur frequently, resulting in the dentine exposure, which might lead to the development of DH by means of the most widely accepted hydrodynamic theory proposed by Brannström (Brannström, 1963; Hefferren, 1976; Groeneveld et al., 1990; Drisko, 2007).

Among the numerous treatment regimens that have been recommended over these years, particular attention has been focused on toothpastes containing potassium salts (Markowitz et al., 1991; Nagata et al., 1994; Peacock and Orchardson, 1995; Orchardson and Gillam, 2000; Poulsen et al., 2006; Bellamy et al., 2009) and, more recently, on a new toothpaste formulation containing zinc (Zn)-substituted carbonate-hydroxyapatite (CHA) nanostructured microcrystals (from now on called Zn-CHA toothpaste), which has been shown to produce *in vitro* remineralization of the altered enamel surfaces and to be effective in closing dentinal tubules (Kuroiwa et al., 1994; Rimondini et al., 2007; Lee et al., 2008; Roveri et al., 2008, 2009a). Indeed, a clinical randomized trial has shown the efficacy of CHA-based toothpastes

in reducing DH, after 4 and 8 weeks. In particular, this study demonstrated that Zn-CHA toothpaste compared with potassium nitrate/fluoride toothpaste (KNO_3/NaF, active control) showed a significant improvement in airblast test scores (mean percentage of reduction 46.0 vs. 29.4% in controls) and subjective test scores (47.5 vs. 28.1%, respectively), with both differences being significant already after 4 weeks (Orsini et al., 2010).

However, this latter trial presented two major limitations consisting in: (a) the true efficacy of both toothpastes could not be assessed, since no morphological analyses were carried out on the dental surfaces; (b) no negative control such as a fluoride toothpaste (Holland et al., 1997) was used. Therefore, the aim of the present study was to investigate (1) whether the *in vitro* action of Zn-CHA toothpaste, based on the gradual remineralizing/repairing action of the dental surface by means of the deposition of a biomimetic CHA coating (Rimondini et al., 2007; Roveri et al., 2009a) could be confirmed also *in vivo,* and (2) whether the Zn-CHA toothpaste and the KNO_3/NaF toothpaste may lead to stable morphological changes of the dental surface. These aims will be assessed by comparing the enamel surface of teeth treated *in vivo* for 8 weeks with: (I) Zn-CHA toothpaste (experimental group); (II) KNO_3/NaF toothpaste (active control group); (III) fluoride toothpaste (negative control group).

MATERIALS AND METHODS

STUDY DESIGN AND POPULATION

This study was carried out as the conclusive part of a previously published randomized trial conducted at the Department of Clinical Sciences and Stomatology of the Polytechnic University of Marche, Ancona, Italy (registered in the Australian New Zealand Clinical Trials Registry with the number: 00362190). According to Silverman et al. (1996) inclusion criteria were: hypersensitive area on facial surfaces of the teeth (incisors, cuspids, bicuspids and first molars with exposed cervical dentine), with at least two teeth scoring one or more at the air blast sensitivity test; good periodontal health (no probing depth >4 mm) with no other conditions which might explain their apparent DH; good physical health; age between 18 and 75 years; provision of written informed consent. Exclusion criteria were: chipped teeth, defective restorations, fractured undisplaced cuspids, deep dental caries or large restorations showing pulpal response, deep periodontal pockets, orthodontic appliances, dentures, or bridgework that would interfere with the evaluation of hypersensitivity; periodontal surgery within the previous 6 months; ongoing treatment with antibiotics and/or anti-inflammatory drugs; ongoing treatment for tooth hypersensitivity; pregnancy or lactation (Singal et al., 2005); acute myocardial infarction within the past 6 months, use of a pace-maker, uncontrolled metabolic diseases, major psychiatric disorder, heavy smoking and alcohol or drug abuse.

Eligible subjects were randomized to receive either the new toothpaste formulation (experimental group), containing biomimetic nanocrystals of Zn-substituted CHA, assembled in microparticles (Zn-CHA toothpaste, BioRepair® Plus, Coswell S.p.A., Funo, Bologna, Italy) or a commercially available desensitizing toothpaste (active control group), containing 5% KNO_3/NaF with 1450 ppm fluoride (KNO_3/NaF toothpaste, Sensodyne ProNamel™, GlaxoSmithKline Consumer Healthcare, Brentford, U.K.). The final protocol was approved by the Ethical Committee of the Polytechnic University of Marche, Ancona, Italy.

The clinical examination of the subjects was performed at baseline, after 4 weeks and after 8 weeks (end of the follow-up). During the visits, a minimum of two and up to four hypersensitive teeth was assessed using the most common and validated stimuli tests: tactile test, airblast test, cold water test and subjective test (Tarbet et al., 1979; Holland et al., 1997; Singal et al., 2005; Orsini et al., 2010).

Among the patients that completed the study, five subjects in the experimental group and five subjects in the active control group were selected for the present study because they needed extractions of sound teeth for orthodontic or prosthetic reasons. The extractions were performed after the end of the follow-up (8 weeks). At this time, two further subjects that needed extractions and brushed their teeth using a non-specified fluoride toothpaste were also included (fluoride toothpaste, negative control group).

ANALYSIS OF Zn-SUBSTITUTED CARBONATE-HYDROXYAPATITE (CHA) NANOCRYSTALS AND CHA MICROCLUSTERS CONTAINED IN THE EXPERIMENTAL TOOTHPASTE

Plate-acicular shaped CHA nanocrystals, about 70-100 nm in size, were synthesized according to a modification of the method previously reported and patented (Gazzaniga et al., 2006). CHA nanocrystals have been allowed, after synthesis, to grow in the reaction mixture under stirring up to the formation of nanostructured clusters having dimensions ranging from about 0.5 to 3.0 μm, according to the patented methodology. Then, the stirring was suspended allowing the deposition of CHA nanostructured microclusters isolated by filtration of the solution, repeatedly washed with water, and freeze-dried (Roveri et al., 2009b). CHA nanocrystals as well as the formed microclusters were analyzed by means of SEM, TEM, XRD, FT-IR. Specimens of human enamel served as controls.

MORPHOLOGICAL CHARACTERIZATION

Scanning Electron Microscopy (SEM) observations were carried out by means of a SEM, Carl-Zeiss EVO, 40 XVP (Oberkoche, Germany) equipped with energy dispersive detector (EDAX) Inca 250 (Oxford, UK), using secondary electrons at 25 Kv and different magnifications. Specimens were mounted on aluminum stubs with a carbon tape and covered by a 10 nm thick carbon coating, using a coating unit.

Transmission Electron Microscopy (TEM) investigations were carried out by means of a Philips CM 100 (Eindhoven, The Netherland) instrument. The powdered samples were ultrasonically dispersed in ultra pure water and then a few droplets of the slurry deposited on holey-carbon foils were mounted on conventional copper micro grids. This latter morphological characterization was realized only on CHA nanocrystals and CHA nanostructured microclusters contained in the Zn-CHA experimental toothpaste.

X RAY DIFFRACTION ANALYSIS (XRD)

X-ray diffraction powder patterns were collected using an Analytical X'Pert Pro (Eindhoven, The Netherland) equipped with X'Celerator detector powder diffractometer using Cu Kα radiation generated at 40 kV and 40 mA. The instrument was configured with a 1° divergence and 0.2 mm receiving slits (X'PERT Guide, 2004).

The samples were prepared using the front-loading of standard aluminum sample holders, which are 1 mm deep, 20 mm high and 15 mm wide. The crystallinity degree was evaluated according to the following formula: crystallinity = (X/Y) 100 where X = net area of diffracted peaks, and Y = net area of diffracted peaks + background area.

INFRARED MICROSCOPY SPECTRAL ANALYSIS (FT-IR)

FT-IR spectra were recorded on a Thermo Nicolet 380 FT-IR spectrometer (Illinois, USA) equipped with a commercial ATR accessory. The infrared spectra were registered from 4000 to 400 cm^{-1} at 2 cm^{-1} resolution using a Bruker IFS 66v/S spectrometer using KBr pellets. Spectra were collected by averaging 32 scans at 4 cm^{-1} resolution.

RESULTS

CARBONATE-HYDROXYAPATITE (CHA) NANOCRYSTALS AND CHA MICROCLUSTERS CHARACTERIZATION

Figure 1 shows scanning and transmission electron micrographs of synthetic biomimetic CHA nanocrystals, with characteristic plate-like features and acicular morphology, and the aggregated CHA nanostructured microclusters.

The XRD of synthetic biomimetic CHA nanocrystals, showing the broadened diffraction maxima of an apatite single phase, is reported in **Figure 2A**. This pattern is compared with the XRD collected from the synthetic biomimetic CHA nanostructured microclusters used for preparing the Zn-CHA toothpaste (**Figure 2B**) and the XRD of human tooth enamel (**Figure 2C**). There are evident similarities between **Figures 2A,B**, whereas **Figure 2C** shows the highest degree of crystallinity, proper of the natural enamel. The FT-IR spectra of synthesized CHA nanostructured microclusters and human enamel apatite are reported in **Figures 3A,B**, respectively. In both these spectra, it is possible to find characteristic bands at 1032 - 1104 cm^{-1}, due to the phosphate group. The absorption band at 1472 cm^{-1} is related to the carbonate group substitution of the phosphate one, while the shoulder at 1550 cm^{-1} can be attributed to the carbonate group substituting the hydroxyl group in the apatite structure.

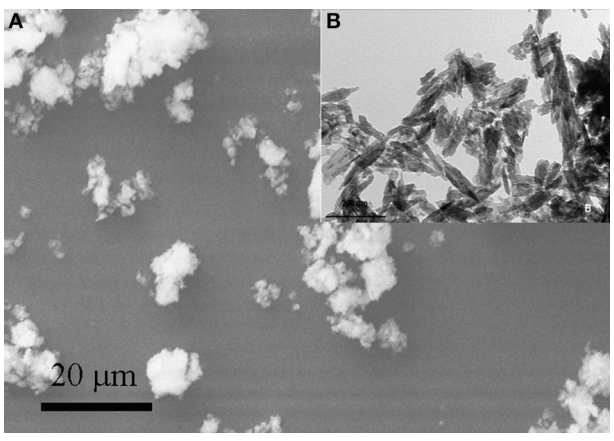

FIGURE 1 | Scanning electron micrograph of synthetic biomimetic CHA nanocrystals forming microclasters (A), and the inset showing the transmission electron micrograph of CHA nanocrystals with characteristic acicular morphology (B).

ENAMEL SURFACE ANALYSIS

A total of 12 teeth (one for each subject) were evaluated: five teeth extracted from subjects of the experimental group after the protocolled use of the Zn-CHA toothpaste, five teeth from subjects of the active control group after the protocolled use of KNO_3/NaF toothpaste, two teeth from subjects that did not participate to the protocol (that brushed their teeth with a non-specified fluoride toothpaste, negative control). No complications after the extractions were observed in all the subjects enrolled in the present morphological *in vivo* investigation.

Figure 4A shows a scanning electron micrograph of the enamel surface of a tooth treated with Zn-CHA toothpaste. In this micrograph, two different enamel superficial morphologies are evident: homogeneous smooth surface areas (black circle),

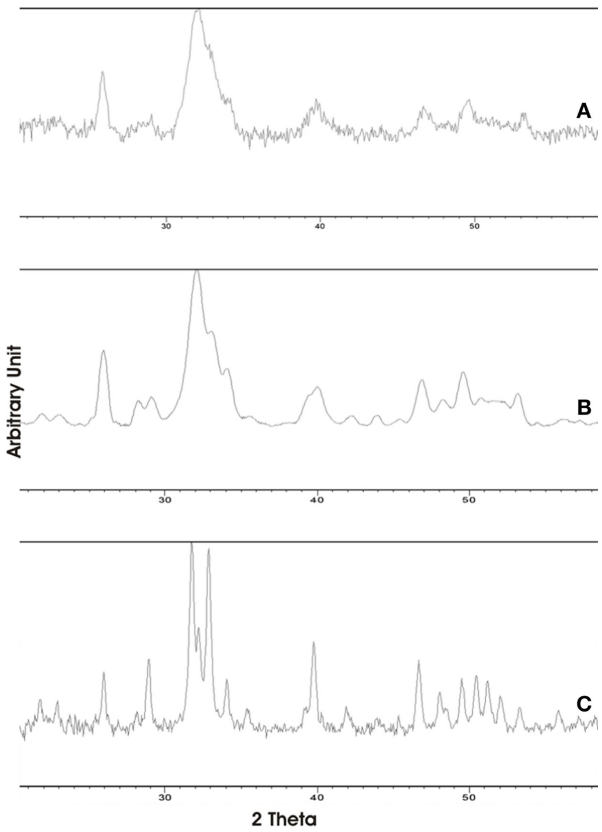

FIGURE 2 | X-ray diffraction patterns collected for synthetic biomimetic CHA nanocrystals (A), CHA nanostructured microcrystals (B), and human tooth enamel (C).

characterized by scraped surfaces, and areas of thin depositions (white circle). **Figures 4B,C** report the elementary analysis results obtained by EDAX probe pointed on surface areas labeled by black and white circles, respectively. No evidence of silica and fluoride can be observed, only the presence of calcium (C) and phosphorus (P). The Ca/P molar ratio results, calculated from **Figures 4B,C**, are 1.67 and 1.63, respectively.

Figure 5A shows the scanning electron micrograph of the enamel surface of a tooth treated using KNO_3/NaF toothpaste (positive control), in which two different areas can be discerned. In the first central area (white circle), there is a deposition of a phase mainly composed by silica and sodium, as shown in the elementary analysis results obtained by EDAX probe (**Figure 5B**). The presence of fluoride has not been detected. The elementary analysis results obtained by EDAX probe of the other area (black circle) (**Figure 5C**) reveal a Ca/P molar ratio of 1.9, which is the characteristic value of the native enamel hydroxyapatite (Wirsing et al., 1974; Hoyer et al., 1984).

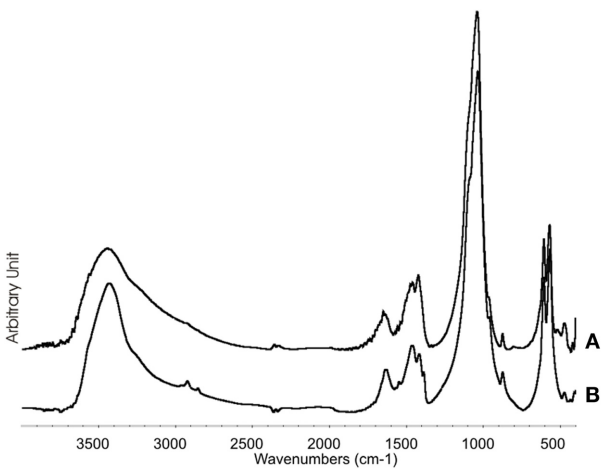

FIGURE 3 | FT-IR Synthetic biomimetic CHA nanostructured microclusters (A), and natural enamel (B).

The enamel surface of a tooth representing the negative control, brushed with a non-specified fluoride toothpaste shows a zone of enamel loss (**Figure 6**).

Figure 7A shows the broadened X-Ray diffraction maxima of the synthetic biomimetic CHA microclusters of the Zn-CHA experimental toothpaste. This XRD pattern can be compared with the ones obtained from enamel slabs of teeth treated using Zn-CHA toothpaste, KNO_3/NaF toothpaste and fluoride toothpaste, reported in **Figures 7B–D**, respectively. The XRD pattern obtained from enamel surfaces treated using Zn-CHA toothpaste (**Figure 7B**) is similar to the one obtained from Zn-CHA nanostructured microclusters (**Figure 7A**), thus revealing its deposition on the enamel surface.

On the other hand, the XRD pattern recorded on the enamel surfaces obtained from teeth treated using KNO_3/NaF toothpaste (**Figure 7C**) appear slightly less sharpened than those obtained from the surface of enamel treated using the fluoride toothpaste (**Figure 7D**). **Figure 8A** shows the FT-IR absorption pattern of the enamel surface of teeth treated with Zn-CHA toothpaste, which is similar to the one of the enamel HA (Roveri et al., 2009b).

The analysis of the FT-IR absorption phosphate bands at about 1030 - 1090 cm^{-1} shows the different degree of crystallinity relative to the different enamel samples analyzed. In fact, the adsorption bands reported in **Figure 8A** demonstrate a low degree of resolution of the phosphate peak in the enamel treated using the CHA-based toothpaste. On the other hand, the FT-IR absorption pattern obtained in the enamel treated using the KNO_3/NaF toothpaste (**Figure 8B**) reveals the presence of a peak at 3573 cm^{-1}, which is characteristic of the substitution of hydroxyl groups with fluoride ions, into the hydroxyapatite structure (Wang et al., 2009). This peak is also visible in the FT-IR absorption pattern obtained in the spectrum of enamel *in vivo* treated with the fluoride toothpaste (**Figure 8C**).

DISCUSSION

Hydroxyapatite, in enamel and in bone, is responsible for the mechanical behavior of the calcified tissues. Unlike bone, when the enamel hydroxyapatite is dissolved or abraded, it cannot spontaneously remineralize, because enamel contains no cells

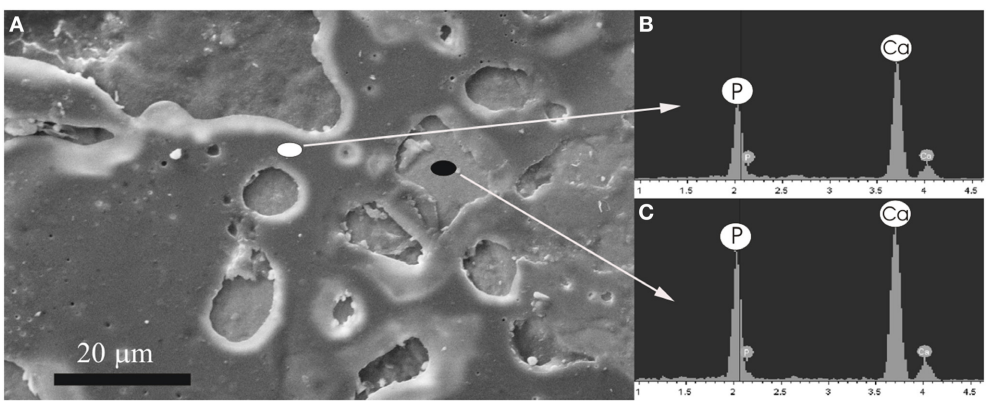

FIGURE 4 | Scanning electron micrograph of the enamel surface of a tooth *in vivo* treated using the Zn-CHA toothpaste (A), EDAX results using a probe pointed in the area labeled by the white circle (B), EDAX results using a probe pointed in the area labeled by the black circle (C).

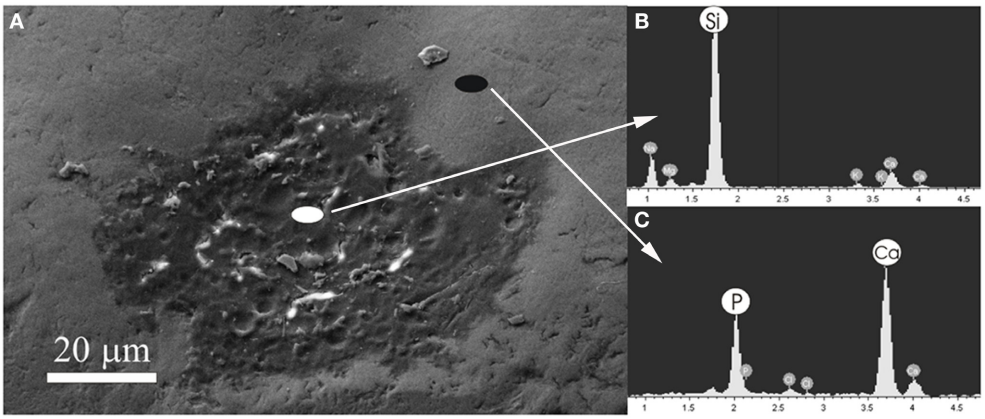

FIGURE 5 | Scanning electron micrograph of the enamel surface of a tooth *in vivo* treated using the KNO_3/NaF toothpaste (A), EDAX with probe pointed in the area labeled by the white circle (B), EDAX with probe pointed in the area labeled by the black circle (C).

(Roveri et al., 2009a). Biomimetic carbonate hydroxyapatite (CHA) nanocrystals have been synthesized with a stoichiometric Ca/P molar ratio of about 1.7 ± 0.1, containing 4 ± 1 wt% of carbonate ions, prevalently replacing phosphate groups, while 1% of Ca^{2+} ions are substituted by Zn^{2+}. The nanostructured Zn-CHA microcrystals, prepared in laboratory according to the patented methodology, represent the active component of the experimental Zn-CHA toothpaste. The micrometric dimension of the crystal clusters allows avoiding any suspicion about the *in vivo* utilization of nano-dimensioned particles. Nevertheless, the nanostructured surface of the microclusters is responsible for the high surface area that is crucial for their chemical reactivity.

Synthesized biomimetic CHA nanocrystals and human enamel apatite not only contain a similar carbonate amount, but also have been shown to promote carbonate substitution to the phosphate and/or hydroxyl group, which is very similar to the synthetic and biological CHA nanocrystals. The synthetic experimental CHA nanocrystals have a plate-like morphology and a structure very close to that of the enamel, dentine and bone hydroxyapatite, and exhibiting very similar FT-IR spectra, even if enamel spectrum shows the highest degree of crystallinity according to previous findings (Teaford, 1988).

In summary, in the present work, the surface of teeth treated *in vivo* for 8 weeks with: (i) Zn-CHA toothpaste (experimental group); (ii) KNO_3/NaF toothpaste (active control group); (iii) fluoride toothpaste (negative control group) have been compared, by means of SEM-EDAX investigation, XRD, and FT-IR.

SEM-EDAX, XRD, and FT-IR observations showed that, after the *in vivo* treatment using the Zn- CHA toothpaste, an appreciable formation of a biomimetic CHA coating was present on the enamel surface. On the other hand, not any mineral deposition, in spite of silica, has been observed after the *in vivo* treatment using both a KNO_3/NaF toothpaste and non-specified fluoride toothpaste. The *in vivo* treatment with these two latter toothpastes changes the structure of enamel natural hydroxyapatite crystals, increasing their degree of crystallinity (XRD investigation), by means of the partial substitution of hydroxyl groups with fluoride ions (FT-IR investigation). Indeed, the phosphate band in the enamel surface after treatment with KNO_3/NaF or a non-specified fluoride toothpaste appears highly solved respect to the one of the phosphate group reported in **Figure 8A**, thus demonstrating the high degree of crystallinity of these enamel surfaces.

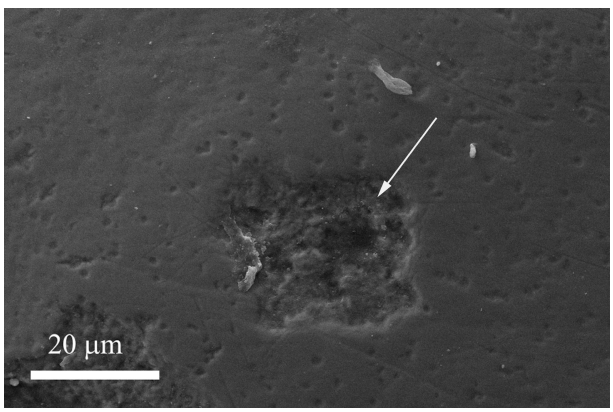

FIGURE 6 | Scanning electron micrograph of the enamel surface treated using a non-specified fluoride toothpaste, showing a zone of enamel loss (arrow).

On the other hand, the remineralizing/repairing effect of the enamel surface treated using synthetic nanostructured CHA microcrystals is consistent with a mineral biomimetic apatitic deposition, which does not alter the chemical-physic properties of the enamel. The biomimetic CHA coating can appear of different thickness, probably due to the underside different enamel surface morphology, which can change in function of the degree of enamel damage. However, the EDAX analysis reveals that the Ca/P molar ratio of CHA crystals (about 1.7) is homogeneously constant on the enamel surface. This finding assures a uniform enamel protection against the enamel wear and loss phenomena, thus preventing dentine exposure.

Results of the first clinical randomized trial by Orsini et al. (2010) have already demonstrated the efficacy of Zn-CHA toothpastes in reducing DH. Moreover, a further very recent

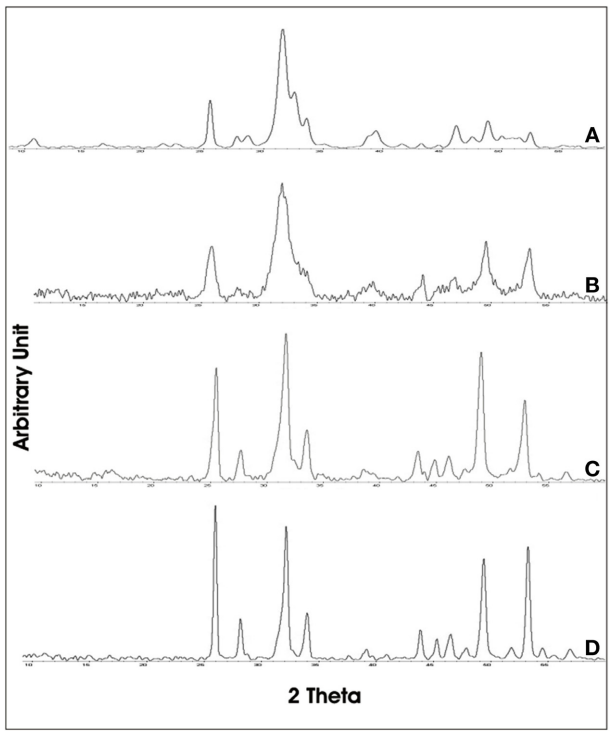

FIGURE 7 | DRX pattern of the enamel after the *in vivo* treatment using the following. (A) synthetic biomimetic CHA nanostructured microclusters, **(B)** Zn-CHA toothpaste, **(C)** KNO3/NaF toothpaste, **(D)** Fluoride toothpaste.

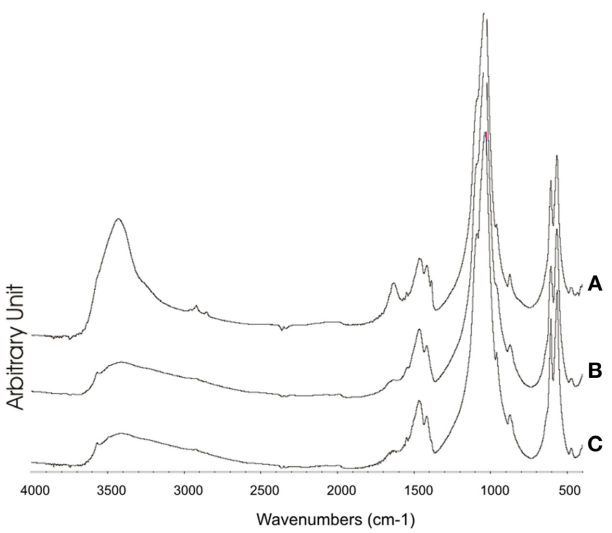

FIGURE 8 | FT-IR of the enamel surface after treatment using. (A) Zn-CHA containing toothpaste, **(B)** KNO_3/NaF toothpaste, **(C)** Fluoride toothpaste.

randomized trial by the same authors showed that this effect could be exerted after only 3 days of treatment (Orsini et al., 2013).

The results of this *in vivo* morphological and chemical-physic study might in part explain the beneficial effect of Zn-CHA toothpastes in reducing DH, since the deposition of a synthetic nanostructured CHA microcrystals-rich coating could lead to a remineralizing/repairing effect of the enamel surface, in the teeth treated using Zn-CHA toothpaste. Therefore, the principal finding of this study is that: (1) the remineralizing mechanism of the nanostructured CHA microcrystals, largely documented by previous *in vitro* reports (Roveri et al., 2008, 2009a) can be also confirmed *in vivo*. Moreover, it can be suggested that this synthetic CHA deposition mainly occurs on the enamel areas characterized by enamel loss and/or damage (probably due to erosion effects), thus being considered as a real enamel repair (see **Figure 4**).

In contrast, (2) the use of a toothpaste containing KNO_3/NaF may form only a deposition, consisting of silica, as an abrasive phase on the enamel surface, which, however, does not remineralize the damaged enamel area, but it is generally deposed in correspondence of natural concavities proper of the natural tooth morphology (see **Figure 5**). Furthermore, no deposition on the enamel surfaces has been observed after treatment using the fluoride and the KNO_3/NaF toothpastes (see **Figure 6**), which may lead only to a partial substitution of the hydroxyl groups with fluoride ions in the native enamel hydroxyapatite.

The CHA formed coating is generally insoluble in physiological mouth pH, but it may undergo to solubilization when, for instance, a bacterial biofilm covers the teeth and its products decrease the pH value. During the CHA coating solubilization, Ca ions, phosphates, and Zn ions are released, allowing the Zn to exploit a strong antibacterial effect, which interferes with the plaque formation, thus preventing further solubilization processes of the newly deposed Zn-CHA coating. Therefore, it may be suggested that the coating formed by Zn- CHA toothpastes may exploit not only a remineralizing effect of the dental surface, but also a beneficial effect toward bacterial plaque attacks.

The main limitation of this work is that the *in vivo* remineralizing effect exploited by the Zn-CHA toothpaste was morphologically demonstrated only on the enamel surfaces, since the analyzed extracted teeth did not present areas of dentine exposition. Therefore, further studies will be carried out *in vivo* to analyse whether a stable biomimetic CHA deposition (Roveri et al., 2009a) and a repairing mechanism can be demonstrated also in dentinal surfaces.

In conclusion, the present study shows that only the use of a toothpaste containing Zn-substituted CHA nanocrystals can produce a biomimetic coating on the enamel surface, thus mimicking the composition, structure, morphology and surface reactivity of the biological enamel hydroxyapatite.

ACKNOWLEDGMENTS

We thank the Universities of Bologna and Polytechnic of Marche (funds for selected research topics), the Chemical Center s.r.l. (for technical support and instrumental facilities), the Inter University Consortium for Research on Chemistry of Metals in Biological Systems (C.I.R.C.M.S.B) and RBAP114AMK, RINAME Project, "Rete integrata per la nano medicina" (funds for selected research topics) Coswell S.P.A., Funo, Bologna, Italy is acknowledged for providing toothpastes.

REFERENCES

X'PERT Guide. (2004). *X'Pert High Score Plus 2.0a.* Almelo: Panalytical B.V.

Absi, E. G., Addy, M., and Adams, D. (1987). Dentine hypersensitivity. A study of the patency of dentinal tubules in sensitive and non-sensitive cervical dentine. *J. Clin. Periodontol.* 14, 280–284. doi: 10.1111/j.1600-051X.1987.tb01533.x

Addy, M. (1990). Etiology and clinical implications of dentine hypersensitivity. *Dent. Clin. North Am.* 34, 503–514.

Addy, M., and West, N. X. (2013). The role of toothpaste in the aetiology and treatment of dentine hypersensitivity. *Monogr. Oral Sci.* 23, 75–87. doi: 10.1159/000350477

Addy, M., West, N. X., Barlow, A., and Smith, S. (2007). Dentine hypersensitivity: is there both stimulus and placebo responses in clinical trials? *Int. J. Dent. Hyg.* 5, 53–59. doi: 10.1111/j.1601-5037.2007.00228.x

Bellamy, P. G., Khera, N., Day, T. N., Barker, M. L., and Mussett, A. J. (2009). A randomized clinical trial to compare plaque inhibition of a sodium fluoride/potassium nitrate dentifrice versus a stabilized stannous fluoride/sodium hexametaphosphate dentifrice. *J. Contemp. Dent. Pract.* 10, 1–9.

Brannström, M. (1963). "A hydrodynamic mechanism in the transmission of pain producing stimuli through dentine," in *Sensory Mechanisms in Dentine*, ed D. J. Anderson (Oxford: Pergamon Press), 73–79.

Dababneh, R. H., Khouri, A. T., and Addy, M. (1999). Dentine hypersensitivity – an enigma? a review of terminology, epidemiology, mechanisms, aetiology and management. *Br. Dent. J.* 187, 606–611.

Drisko, C. (2007). Oral hygiene and periodontal considerations in preventing and managing dentine hypersensitivity. *Int. Dent. J.* 57, 399–410. doi: 10.1111/j.1875-595X.2007.tb00167.x

Gazzaniga, G., Roveri, N., Rimondini, L., Palazzo, B., Iafisco, M., and Gualandi, P. (2006). *Biologically Active Nanoparticles of a Carbonate-Substituted Hydroxyapatite Process for Their Preparation and Compositions Incorporating the Same*. Patent:WO2007137606. Available online at: http://www.google.com/patents/WO2007137606A1?cl=en&hl=it

Groeneveld, A., Van, E. A. A., and Backer, D. O. (1990). Fluoride in caries prevention: is the effect pre- or post-eruptive? *J. Dent. Res.* 69, 751–755.

Hefferren, J. J. (1976). Radioactive dentine abrasion. *J. Dent. Res.* 55, 563–573.

Holland, G. R., Narhi, M. N., Addy, M., Gangarosa, L., and Orchardson, R. (1997). Guidelines for the design and conduct of clinical trials on dentine hypersensitivity. *J. Clin. Periodontol.* 24, 808–813.

Hooper, S., West, N. X., Pickles, M. J., Joiner, A., Newcombe, R. G., and Addy, M. (2003). Investigation of erosion and abrasion on enamel and dentine: a model *in situ* using toothpastes of different abrasivity. *J. Clin. Periodontol.* 30, 802–808. doi: 10.1034/j.1600-051X.2003.00367.x

Hoyer, I., Gaengler, P., and Bimberg, R. (1984). *In vivo* remineralization of human enamel and dental calculus formation. *J. Dent. Res.* 63, 1136–1139.

Kuroiwa, M., Kodaka, T., Kuroiwa, M., and Abe, M. (1994). Dentin hypersensitivity. Occlusion of dentinal tubules by brushing with and without an abrasive dentifrice. *J. Periodontol.* 65, 291–296.

Lee, S. Y., Kwon, H. K., and Kim, B. I. (2008). Effect of dentinal tubule occlusion by dentifrice containing nano-carbonate apatite. *J. Oral Rehabil.* 35, 847–853. doi: 10.1111/j.1365-2842.2008.01876.x

Markowitz, K., Bilotto, G., and Kim, S. (1991). Decreasing intradental nerve activity in the cat with potassium and divalent cations. *Arch. Oral Biol.* 36, 1–7.

Nagata, T., Ishida, H., Shinohara, H., Nishikawa, S., Kasahara, S., Wakano, Y., et al. (1994). Clinical evaluation of a potassium nitrate dentifrice for the treatment of dentinal hypersensitivity. *J. Clin. Periodontol.* 21, 217–221.

Orchardson, R., and Gillam, D. G. (2000). The efficacy of potassium salts as agents for treating dentin hypersensitivity. *J. Orofac. Pain* 14, 9–19.

Orsini, G., Procaccini, M., Manzoli, L., Giuliodori, F., Lorenzini, A., and Putignano, A. (2010). A double-blind randomized-controlled trial comparing the desensitizing efficacy of a new dentifrice containing carbonate/hydroxyapatite nanocrystals and a sodium fluoride/potassium nitrate dentifrice. *J. Clin. Periodontol.* 37, 510–517. doi: 10.1111/j.1600-051X.2010.01558.x

Orsini, G., Procaccini, M., Manzoli, L., Sparabombe, S., Tiriduzzi, P., Bambini, F., et al. (2013). A 3-day randomized clinical trial to investigate the desensitizing properties of three dentifrices. *J. Periodontol.* 84, e65–e73. doi: 10.1902/jop.2013.120697

Peacock, J. M., and Orchardson, R. (1995). Effects of potassium ions on action potential conduction in A- and C-fibers of rat spinal nerves. *J. Dent. Res.* 74, 634–641.

Poulsen, S., Errboe, M., Lescay Mevil, Y., and Glenny, A. M. (2006). Potassium containing toothpastes for dentine hypersensitivity. *Cochrane Database Syst. Rev.* 3, CD001476. doi: 10.1002/14651858

Rimondini, L., Palazzo, B., Iafisco, M., Canegallo, L., Demarosi, F., Merlo, M., et al. (2007). The remineralizing effect of carbonate-hydroxyapatite nanocrystals on dentine. *Mater. Sci. Forum* 539–543, 602–605. doi: 10.4028/www.scientific.net/MSF.539-543.602

Roveri, N., Battistella, E., Foltran, I., Foresti, E., Iafasco, M., Lelli, M., et al. (2008). Synthetic biomimetic carbonate-hydroxyapatite nanocrystals for enamel remineralization. *Adv. Mater. Res.* 47–50, 821–824. doi: 10.4028/www.scientific.net/AMR.47-50.821

Roveri, N., Battistella, E., Bianchi, C. L., Foltran, I., Foresti, E., Iafasco, M., et al. (2009a). Surface enamel remineralization: biomimetic apatite nanocrystals and fluoride ions different effects. *J. Nanomater.* 2009, 1–9. doi: 10.1155/2009/746383

Roveri, N., Foresti, E., Lelli, M., and Lesci, I. G. (2009b). Recent advancements in preventing teeth health hazard: the daily use of hydroxyapatite instead of fluoride. *Rec. Patents Biomed. Eng.* 2, 197–215. doi: 10.2174/18747647109020 30197

Scheutzel, P. (1996). Etiology of dental erosion intrinsic factors. *Eur. J. Oral Sci.* 104, 178–190.

Silverman, G., Berman, E., Hanna, C. B., Salvato, A., Fratarcangelo, P., Bartizek, R. D., et al. (1996). Assessing the efficacy of three dentifrices in the treatment of dentinal hypersensitivity. *J. Am. Dent. Assoc.* 127, 191–201.

Singal, P., Gupta, R., and Pandit, N. (2005). 2% Sodium fluoride-iontophoresis compared to a commercially available desensitizing agent. *J. Periodontol.* 76, 351–357. doi: 10.1902/jop.2005.76.3.351

Smith, B. G. N., and Knight, J. K. (1984). A comparison of patterns of toothwear with the etiological factors. *Br. Dent. J.* 157, 16–19.

Tarbet, W. J., Silverman, G., and Stolman, J. M. (1979). An evaluation of two methods for the quantitation of dentinal hypersen-sitivity. *J. Am. Dent. Assoc.* 98, 914–918.

Teaford, M. F. (1988). A review of a dental microwear and diet in modern mammals. *Scan. Microsc.* 2, 1149–1166.

Van't Spijker, A., Rodriguez, J. M., Kreulen, C. M., Bronkhorst, E. M., Bartlett, D. W., and Creugers, N. H. (2009). Prevalence of tooth wear in adults. *Int. J. Prosthodont.* 22, 35–42.

Wang, J., Chao, Y., Wan, Q., Yan, K., and Meng, Y. (2009). Fluoridated hydroxyapatite/titanium dioxide nanocomposite coating fabricated by a modified electrochemical deposition. *J. Mater. Science Mater. Med.* 20, 1047–1055. doi: 10.1007/s10856-008-3673-1

Wirsing, A., Judd, G., and Ansell, G. S. (1974). Electron probe microanalysis of human enamel microstructure. *J. Dent. Res.* 53, 491–494.

Zero, D. T., and Lussi, A. (2000). "Etiology of enamel erosion: intrinsic and extrinsic factors," in *Tooth Wear and Sensitivity*, eds M. Addy, G. Embery, W. M. Edgar, and R. Orchardson (London: Martin Dunitz), 121–140.

Conflict of Interest Statement: The authors declare that the research was conducted in the absence of any commercial or financial relationships that could be construed as a potential conflict of interest.

Received: 15 July 2014; paper pending published: 27 July 2014; accepted: 13 August 2014; published online: 05 September 2014.

Citation: Lelli M, Putignano A, Marchetti M, Foltran I, Mangani F, Procaccini M, Roveri N and Orsini G (2014) Remineralization and repair of enamel surface by biomimetic Zn-carbonate hydroxyapatite containing toothpaste: a comparative in vivo study. Front. Physiol. ***5****:333. doi: 10.3389/fphys.2014.00333*

This article was submitted to Craniofacial Biology, a section of the journal Frontiers in Physiology.

Advantages of publishing in Frontiers

OPEN ACCESS
Articles are free to read, for greatest visibility

COLLABORATIVE PEER-REVIEW
Designed to be rigorous – yet also collaborative, fair and constructive

FAST PUBLICATION
Average 85 days from submission to publication (across all journals)

COPYRIGHT TO AUTHORS
No limit to article distribution and re-use

TRANSPARENT
Editors and reviewers acknowledged by name on published articles

SUPPORT
By our Swiss-based editorial team

IMPACT METRICS
Advanced metrics track your article's impact

GLOBAL SPREAD
5'100'000+ monthly article views and downloads

LOOP RESEARCH NETWORK
Our network increases readership for your article

Frontiers
EPFL Innovation Park, Building I • 1015 Lausanne • Switzerland
Tel +41 21 510 17 00 • Fax +41 21 510 17 01 • info@frontiersin.org
www.frontiersin.org

Find us on